Design and Development of Magneto Rheological Fluid Base Damper

A Thesis submitted to Gujarat Technological University

For the Award of

Doctor of Philosophy

in

Mechanical Engineering

By

Sapramer Hamirbhai Rewabhai

Enrollment No. : 119997119011

Under supervision of

Dr. G. D. Acharya

GUJARAT TECHNOLOGICAL UNIVERSITY

AHMEDABAD

June 2017

DECLARATION

I declare that the thesis entitled **"Design and Development of Magneto Rheological Fluid Base Damper"** submitted by me for the degree of Doctor of Philosophy, is the record of research work carried out by me during the period from **October 2011** to **December 2016** under the supervision of **Dr. G. D. Acharya**, Principal, Atmiya Engineering College of Science and Technology, Rajkot and this has not formed the basis for the award of any degree, diploma, associate ship and fellowship, titles in this or any other University or other institution of higher learning.

I further declare that the material obtained from other sources has been duly acknowledged in the thesis. I shall be solely responsible for any plagiarism or other irregularities, if noticed in the thesis.

Signature of the Research Scholar: _____ Date: 20/06/2017

Name of Research Scholar: **Sapramer Hamirbhai Rewabhai**

Place: Ahmedabad.

CERTIFICATE

I certify that the work incorporated in the thesis titled as **Design and Development of Magneto Rheological Fluid Base Damper** submitted by Mr. **Sapramer Hamirbhai Rewabhai** was carried out by the candidate under my supervision/guidance. To the best of my knowledge: (i) the candidate has not submitted the same research work to any other institution for any degree/diploma, Associateship, Fellowship or other similar titles (ii) the thesis submitted is a record of original research work done by the Research Scholar during the period of study under my supervision, and (iii) the thesis represents independent research work on the part of the Research Scholar.

Signature of Supervisor: Date: 20/06/2017

Name of Supervisor: Dr. G. D. Acharya

Place: Ahmedabad.

Originality Report Certificate

It is certified that PhD Thesis titled **Design and Development of Magneto Rheological Fluid Base Damper** submitted by Mr. Sapramer Hamirbhai Rewabhai has been examined by us. We undertake the following:

a. Thesis has significant new work / knowledge as compared already published or are under consideration to be published elsewhere. No sentence, equation, diagram, table, paragraph or section has been copied verbatim from previous work unless it is placed under quotation marks and duly referenced.

b. The work presented is original and own work of the author (i.e. there is no plagiarism). No ideas, processes, results or words of others have been presented as Author own work.

c. There is no fabrication of data or results which have been compiled / analyzed.

d. There is no falsification by manipulating research materials, equipment or processes, or changing or omitting data or results such that the research is not accurately represented in the research record.

e. The thesis has been checked using **https://turnitin.com** (copy of originality report attached) and found within limits as per GTU Plagiarism Policy and instructions issued from time to time (i.e. permitted similarity index <=25%).

Signature of Research Scholar: …….. Date: 20/06/2017

Name of Research Scholar: **Sapramer Hamirbhai Rewabhai**

Place: Ahmedabad

Signature of Supervisor: …….. Date: 20/06/2017

Name of Supervisor: **Dr. G. D. Acharya**

Place: Ahmedabad

Copy of Originality Report

HRS

ORIGINALITY REPORT

%15	%14	%9	%8
SIMILARITY INDEX	INTERNET SOURCES	PUBLICATIONS	STUDENT PAPERS

PRIMARY SOURCES

1	doras.dcu.ie Internet Source	%5
2	cee.uiuc.edu Internet Source	%4
3	Submitted to Rajarambapu Institute of Technology Student Paper	%2
4	wanderlodgegurus.com Internet Source	%1
5	www.sportdevices.com Internet Source	%1
6	www.coursehero.com Internet Source	%1
7	www.springer.com Internet Source	%1
8	www.devileye.net Internet Source	%1
9	Submitted to University of Newcastle Student Paper	%1

EXCLUDE QUOTES	ON	EXCLUDE MATCHES	< 1%
EXCLUDE BIBLIOGRAPHY	ON		

turnitin

Digital Receipt

This receipt acknowledges that Turnitin received your paper. Below you will find the receipt information regarding your submission.

The first page of your submissions is displayed below.

Submission author:	Shantilal Shah Engineering College…
Assignment title:	Final Report_209
Submission title:	HRS
File name:	209_HRS_PhD_THESIS_17-01-17…
File size:	8.1M
Page count:	155
Word count:	40,769
Character count:	200,304
Submission date:	17-Jan-2017 05:32PM
Submission ID:	756043440

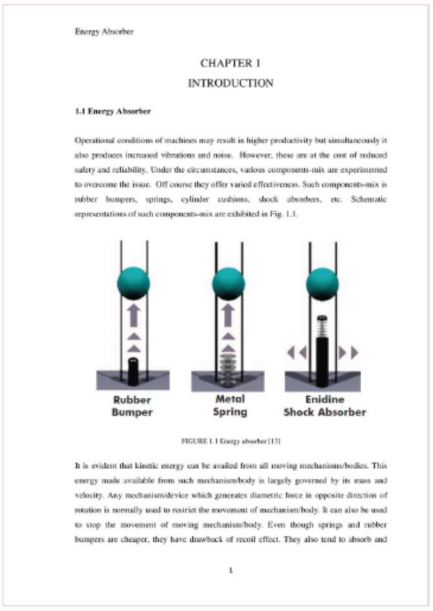

Energy Absorber

CHAPTER 1

INTRODUCTION

1.1 Energy Absorber

Operational conditions of machines may result in higher productivity but simultaneously it also produces increased vibrations and noise. However, these are at the cost of reduced safety and reliability. Under the circumstances, various components-mix are experimented to overcome the issue. Off course they offer varied effectiveness. Such components-mix is rubber bumpers, springs, cylinder cushions, shock absorbers, etc. Schematic representations of such components-mix are exhibited in Fig. 1.1.

FIGURE 1.1 Energy absorber [13]

It is evident that kinetic energy can be availed from all moving mechanisms/bodies. This energy made available from such mechanism/body is largely governed by its mass and velocity. Any mechanism/device which generates diametric force in opposite direction of rotation is normally used to restrict the movement of mechanism/body. It can also be used to stop the movement of moving mechanism/body. Even though springs and rubber bumpers are cheaper, they have drawback of recoil effect. They also tend to absorb and

1

Ph. D. THESIS Non-Exclusive License to GUJARAT TECHNOLOGICAL UNIVERSITY

In consideration of being a Ph. D. Research Scholar at GTU and in the interests of the facilitation of research at GTU and elsewhere, I, **Sapramer Hamirbhai Rewabhai** having Enrollment No. **119997119011** hereby grant a non-exclusive, royalty free and perpetual license to GTU on the following terms:

a) GTU is permitted to archive, reproduce and distribute my thesis, in whole or in part, and/or my abstract, in whole or in part (referred to collectively as the "Work") anywhere in the world, for non-commercial purposes, in all forms of media;

b) GTU is permitted to authorize, sub-lease, sub-contract or procure any of the acts mentioned in paragraph (a);

c) GTU is authorized to submit the Work at any National / International Library, under the authority of their "Thesis Non-Exclusive License";

d) The Universal Copyright Notice (©) shall appear on all copies made under the authority of this license;

e) I undertake to submit my thesis, through my University, to any Library and Archives. Any abstract submitted with the thesis will be considered to form part of the thesis.

f) I represent that my thesis is my original work, does not infringe any rights of others, including privacy rights, and that I have the right to make the grant conferred by this non-exclusive license.

g) If third party copyrighted material was included in my thesis for which, under the terms of the Copyright Act, written permission from the copyright owners is required, I have

obtained such permission from the copyright owners to do the acts mentioned in paragraph (a) above for the full term of copyright protection.

h) I retain copyright ownership and moral rights in my thesis, and may deal with the copyright in my thesis, in any way consistent with rights granted by me to my University in this non-exclusive license.

i) I further promise to inform any person to whom I may hereafter assign or license my copyright in my thesis of the rights granted by me to my University in this non-exclusive license.

j) I am aware of and agree to accept the conditions and regulations of PhD including all policy matters related to authorship and plagiarism.

Signature of Research Scholar:……... Date: 20/06/2017

Name of Research Scholar: **Sapramer Hamirbhai Rewabhai**

Place: Ahmedabad

Signature of Supervisor: …….. Date: 20/06/2017

Name of Supervisor: **Dr. G. D. Acharya**

Place: Ahmedabad

Seal:

Thesis Approval Form

The viva-voce of the Ph.D. Thesis submitted by Shri **Sapramer Hamirbhai Rewabhai** (Enrollment No. **119997119011**) entitled **Design and Development of Magneto Rheological Fluid Base Damper** was conducted on **Tuesday - 20/06/2017**, (day and date) at Gujarat Technological University.

(Please tick any one of the following option)

☐ We recommend that he be awarded the Ph.D. degree.

☐ We recommend that the *viva-voce* be re-conducted after incorporating the following suggestions.

(briefly specify the modifications suggested by the panel)

☐ The performance of the candidate was unsatisfactory. We recommend that he should not be awarded the Ph.D. degree.

(The panel must give justifications for rejecting the research work)

---------- ----------

Name and Signature of Supervisor with Seal External Examiner -1 Name and Signature

---------- ----------

External Examiner -2 Name and Signature External Examiner -3 Name and Signature

ABSTRACT

Over the past three decades, a great deal of interest has been generated regarding the use of structural protective systems to mitigate the effects of dynamic environmental hazards, such as vibration, on mechanical engineering structures and automobile sectors for human comfort, earthquakes and strong wind, on civil engineering structures. These systems usually employ supplemental damping devices to increase the energy dissipation capability of the protected structure. One of the most promising new devices proposed for structural protection is magnetorheological (MR) fluid dampers.

MR fluids possess rheological properties, which can be changed in a controlled way. These rheological changes are reversible and dependent on the strength of an excitation magnetic field. MR fluids have potentially beneficial applications when placed in various applied loading (shear, valve and squeeze) modes.

Magnetorheological dampers, or as they are more commonly called, MR dampers, are being developed for a wide variety of applications where controllable damping is desired. MR fluid dampers have the capability of changing their effective damping force depending on the current input to the damper. These applications include dampers for automobiles, heavy trucks, prosthetic limbs, gun recoil systems, bicycles, and possibly others related to mechanical discipline like brake, clutch etc.

Magnetorheological (MR) fluid dampers having very good mechanical simplicity, high dynamic range, low power requirements, large force capacity, and robust ness, this class of devices has been shown to mesh well with application demands and constraints to offer an attractive means of protecting infrastructure systems.

This work issues the design and analysis of the linear magnetorheological damper. Basic information concerning the characteristics of the typical magnetorheological fluid and the damper incorporating it, were presented with the detail description of the applied fluid developed in our premises. With reference to the computations, the prototype damper was designed, manufactured and tested under different operating conditions. Performed calculations were verified with the experimental results and their accuracy was evaluated. The conclusions and observations from the research were compiled in the summary.

Acknowledgement

I am very much thankful to respected Sirs, Dr. G. D. Acharya, Dr. S. P. Bhatnagar, Dr. V. D. Dhiman and Dr. M. G. Bhatt for their continuous encouragement, guidance and tremendous support. The studies described in this thesis were performed at Physics department, Shree M. K. Bhavnagar University, Bhavnagar. While conducting this research project I received support from many people in one way or another, without whose support, this thesis would not have been completed in its present form. It is my pleasure to take this opportunity to thank all of you. I would like to apologize to those I do not mention by name here; however, I highly valued your kind support.

I am also oblige to Mr. A. M. Talsania, Dr. Desale, Mr. V. G. Kurgasthala and Mr. Chandrakant Vora for their untiring effort and guidance for the present work. I am equally obliging to the staff members of my institution, Government Polytechnic, Bhavnagar for their positive approach and continuous support. Further, I would like to express my great thanks to Comissionerate of Technical Education, Gujarat state, for allowing me to do the research work.

Last but not least, my parents and my family members Nayna, Varun, Dhruv… … … I have no word to say…

And above of all, to the supreme power who is the originator of all these occurrences, we call as GOD for my entire life.

Hamir Sapramer

Date: 20/06/2017

Table of Contents

List of Abbreviations

AC	:	Alternating Current
ANOVA	:	Analysis of Variance
CV	:	Coefficient of Variation
CVD	:	Chemical Vapor Deposition
DOE	:	Design of Experiment
DOF	:	Degree of Freedom
ER	:	Electro Rheological
HP	:	Horse Power
IC	:	Internal Combustion
ISO	:	International Standardizations for Organization
IUT	:	In-Use-Thickening
LVDT	:	Linear Variable Differential Transformer
MR	:	Magneto Rheological
MRF	:	Magneto Rheological Fluid
RPM	:	Revolution per Minuit
RSM	:	Response Surface Methodology
SD	:	Standard Deviation
SDOF	:	Single-Degree-Of-Freedom
TVS	:	Transient Voltage Suppressor

List of Figures

List of Tables

List of Appendices

CHAPTER 1
INTRODUCTION

1.1 Energy Absorber

Operational conditions of machines may result in higher productivity but simultaneously it also produces increased vibrations and noise. However, these are at the cost of reduced safety and reliability. Under the circumstances, various components-mix are experimented to overcome the issue. Off course they offer varied effectiveness. Such components-mix is rubber bumpers, springs, cylinder cushions, shock absorbers, etc. Schematic representations of such components-mix are exhibited in Fig. 1.1.

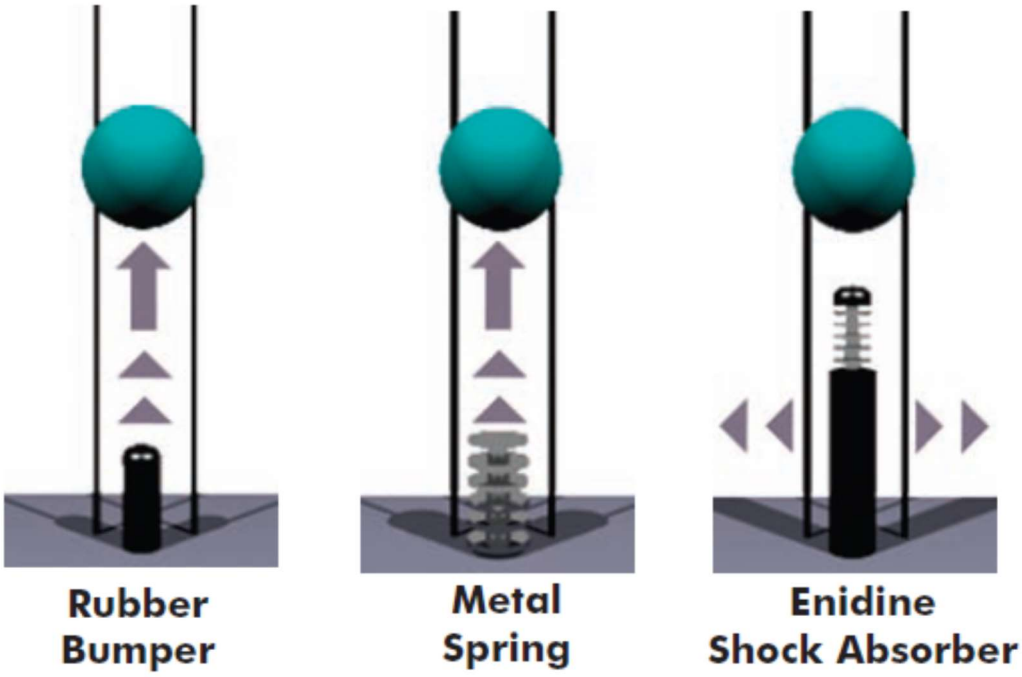

FIGURE 1.1 Energy absorber [1]

It is evident that kinetic energy can be availed from all moving mechanisms/bodies. This energy made available from such mechanism/body is largely governed by its mass and velocity. Any mechanism/device which generates diametric force in opposite direction of rotation is normally used to restrict the movement of mechanism/body. It can also be used to stop the movement of moving mechanism/body. Even though springs and rubber bumpers are cheaper, they have drawback of recoil effect. They also tend to absorb and

subsequently store the energy received by them during impact loading. Such stored energy is transferred back to load and results in rebound and this phenomena may be harmful to moving mechanism/body. Resisting force of springs and rubber bumpers is in proportion of stroke movement and this relation is sketched in Fig. 1.2a.

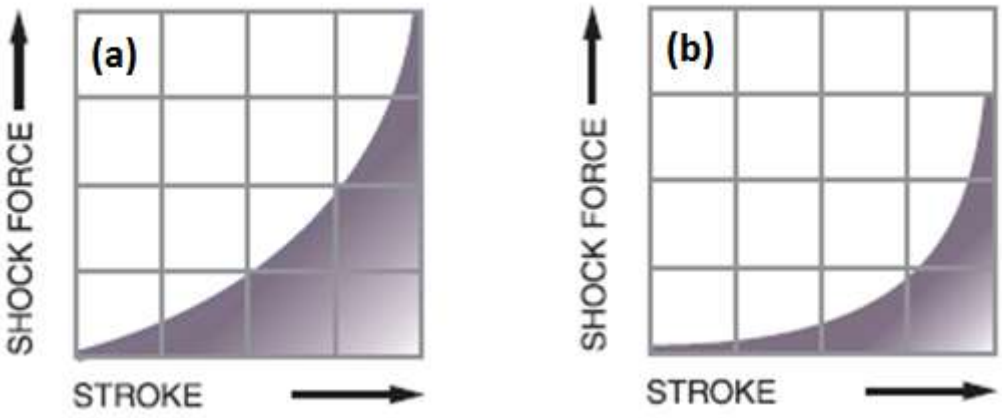

FIGURE 1.2 Force Stroke curve for (a) Rubber bumpers and spring (b) Cylinder cushion [1]

Operational range of cylindrical cushions has narrow band and due to this, they are not found proficient to absorb system energy. Since stroke length at lower pressure is shorter, cylindrical cushions do not offer capability to absorb total energy (Fig. 1.2b).The residual energy is then transmitted to the system which results in increased shocks and vibrations.
Loss of speed can be organised and calculated for dampers. The operational principle of dampers is transformation of kinetic energy to heat energy. Very precisely, it can be said that when reciprocating piston of hydraulic damper is forced to move, it exerts pressure on hydraulic fluid, which in turn moves the fluid through pre-defined size of orifice. Heat energy is then transmitted to environment through system body. Major benefits which are availed from use of dampers in the system are listed below.

(i) Prolonged system life: It helps to decrease the shocks and vibrations of the system in which it is applied. This also helps to prevent harmful actions to the system. Maintenance is reduced which in turn will enhance productive time and will cut the cost of maintenance. The resultant effect is improvement in process capability and useful life of system.

(ii) Improved operational parameters: Systems, for e.g., machines, can withstand higher speeds. This is feasible because of damper helps to resist

and minimize effect of vibrations and noise. This yields with improved productivity.

(iii) Enhanced quality level: Since disturbing causes like vibration, noise, impact, etc. are eradicated to great extent; geometrical accuracy and precision are improved.

(iv) Reliable and safe operational condition: As dampers safeguard the operational condition, it is easier to anticipate the values of disturbing causes like vibration, noise, impact, etc. which in turn helps to design and operate the system reliably and safely with required safety norms.

(v) Improved market share: On account of above benefits, it has edge to have better and improved market share.

1.2 Damper or Shock Absorber

Damper, also known as a shock absorber, shocks or spring energy dissipaters, is basic portion of shock resisting (normally termed as suspension) system. This is complicated portion of the system which is complex and hard to interpret. Such system have sprung and unsprung masses. The transient behaviour of these masses are governed by dampers and by this way, such governs become basic functional area of the dampers.

Fundamental know-how of whole suspension arrangement of automobile applications is required to be understood for further exploration and applications of dampers. Fig. 1.3 shows an automobile suspension system.

Automobile suspension system is mainly assembled with following parts/components:

(i) Sprung mass

(ii) Unsprung mass

(iii) Suspension spring

(iv) Tire spring

(v) Damper

The suspension supports the sprung mass and this consists almost half portion of suspension mass also. Remaining masses like masses of wheel, brakes, spindles and left half portion of suspension members are assigned for unsprung mass. The suspension spring and damper are aligned collinear (or parallel) and have their working flanked by sprung

and unsprung masses. In the same manner, tire spring working is flanked by ground and unsprung masses.

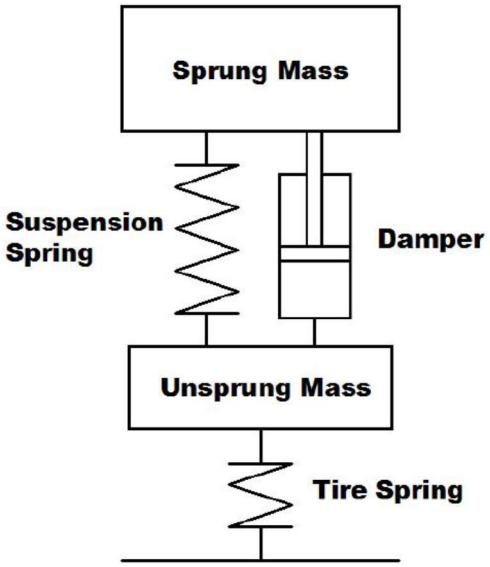

FIGURE 1.3: Suspension system of automobile application

Suspension system shown in Fig. 1.3 is basically 2 DOF system having effect of forces on top and bottom portion/surfaces. Independent movement of sprung and unsprung masses is experienced since the system is 2 DOF. The load transfer of automotive vehicle causes the load on sprung mass. This load transfer also causes the vehicle to undergo change of gradual increment in speed on road. This change in gradual increment in speed may be either longitudinal or lateral. Longitudinal change may be in the form of braking and then increment in speed. Lateral change may occur during cornering.

The magnitude of such load transfer is mainly dependent on following criteria:

(i) Centre of gravity of vehicle
(ii) Magnitude of rate of change of gradual increment in speed
(iii) Mass of the vehicle
(iv) Condition of tract and/or wheelbase
(v) Direction of vehicle

It is also important to note that condition or topology of road surface and velocity at which vehicle moves are also variables to determine the force affecting at bottom.

Amongst sprung and unsprung masses, relative displacement, velocity and gradual increase in speed takes place on account of forces which are induced from gradual increase in speed. The suspension spring and damper produces the forces which are behaving as

constraints to the forces between sprung and unsprung masses. The force produced by spring is outcome due to relative displacement whereas force produced by a damper is outcome due to relative velocity. The rate of spring is the base to determine magnitude of the spring force. However, to determine the magnitude of damper force, the phenomena is little bit complex. The relation of damper force is based on characteristic curve of the damper. Fig. 1.4 exhibits this characteristic curve which is shock dyno plots. Internal construction plays a vital role to determine trends of characteristic curve and in this context, it can have various trends.

This includes design of followings:

(i) Shock piston
(ii) Shim stakes
(iii) Internal orifices

Output force produced by the shock absorber or damper is function of developed internal pressure due to flow of oil through passages.

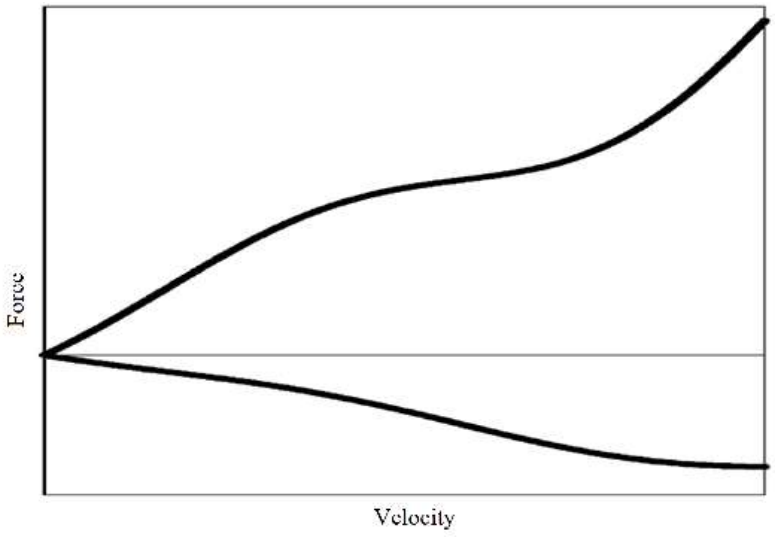

FIGURE 1.4: Damper characteristic curve (F-V Curve)

The upward trend in the graph denotes compression stroke whereas the downward trend in the graph denotes rebound stroke. On X axis, the plotted damper shaft velocity is in fact relative velocity only which is also the velocity in-between sprung and unsprung masses. Y-axis denotes forces which are bi-directional. The compressive force is lesser compared to rebound force and this leads to conclude that control of unsprung mass and sprung mass are executed by compression damping and rebound damping respectively. It may be noted

that force required to control motion of unsprung mass is less due to lower mass of it. Additional contributing parameter is the fact that during compression stroke, forces of spring and damper are in same direction while during rebound stroke, these forces are in opposite direction.

When there exist relative velocity amongst the sprung and unsprung masses, shock is produced which in turn produces force.

The transient maneuvers are in following conditions:

(i) During corner entry
(ii) During corner exit
(iii) Passing maneuvers
(iv) Braking
(v) Acceleration
(vi) Track unevenness due to bumps/uneven road surface

In reality there exist only transients. Transients are differentiated based on the speed and accordingly they are categorised as high and low speed transients. The speed range for low speed transients is 0-125mm/s whereas the speed range for high speed transients is greater than 125 mm/s. Low speed transients characterise the handling whereas high speed characterise the ride. These speed range varies from case to case and are approximated for the purpose of analysis.

Various kinds of parameters are required to determine the damping coefficient which in turn helps to find optimum shock for given set of conditions.

Damping coefficient is function of followings:

(i) Sprung mass
(ii) Unsprung mass
(iii) Tire spring rate
(iv) Wheel rate

Wheel rate is the modified suspension spring rate and for modification, installation ratio is applied. Installation ratio, also termed as motion ratio is the ratio of the wheel travel to the shock travel. During analysis of damping characteristics under roll, spring rate of the anti-roll bar is considered. This is also modified by applying installation ratio. The ultimate important variable is then damping ratio. The damping ratio is useful to determine the stiffness of the shock in context of rest of suspension system. If this ratio is 1, it is

interpreted that system is critically damped. The value of this ratio also helps to locate where shock will fall in terms of trade-off between ride and handling. The normal starting value of this ratio for track car is 0.65[2].

Coilovers is the right selection to upgrade spring and damper. For car, it performs at much higher spring rate and against a stiffer shock. Manufacturer always specify spring rate but seldom specify damping coefficient. However, this may not be an indicator for coilovers quality, but at the same time, it certainly creates ambiguity of the process. Damping coefficient is an important indication for the buyer to determine whether his/her car matches the shocks or not.

The ride and handle of an automobile vehicle are governed by shocks valving. An overlay stiff shock in compression normally produces bouncy ride but do not absorb the bumps in desired manner. An initial loss of traction is experienced when shock with very stiffly valve in rebound case. However in this position, it produces kind of jacking down effect. During jacking down effect, unsprung mass comes closer to sprung mass after experiencing series of bumps. This happens only in the case when there is excessive rebound during compression and spring rate. At this instance, shock bottoms out this will cause the loss in traction.

The performance of automobile vehicle is adversely affected by softly valve shocks. The rate of load transfer is decided when shock do not affect the load transfer or amount of load transfer. Subsequent to steering input, a soft shock will have lag feeling. It is better to wait to catch up the input for a desired attitude of automobile vehicle rather than to get the desired attitude through a turn. Such behaviour may be acceptable for a normal passenger vehicle having when damping ratio is about 0.30. However, this is never desirable for any kind of vehicle even if it is thought to drive on race track.

This phenomena leads to fact that ideal damping has very little chance to occur. Here the chance is based on extent to which trade-off is made between ride and handling. For better handling of race car, harsher ride is desirable and under this situation, adjustable damper offers easier life. Adjustable damper also provides the scope to the driver to monitor and control magnitude of damper's characteristics curve. At present, prevailing market offers adjustable dampers. However they are single adjustable and more often, they do not offer the facility to change both rebound and compression simultaneously. Even though the adjustability is yet good feature, it is one more trade-off for mix. For some specific cases, single adjustable damper affecting only the rebound may be better choice in place of dampers which offers adjustments for compression and rebound simultaneously. However

few expensive coilovers are able to make double adjustable setup permitting independent adjustments of rebound and compression. This provides easiness to driver to dial an automobile vehicle more accurately compared to single adjustable shock. Three and four dampers at even higher costs are also available which allows independent adjustments of low and high speed compression and rebound. In prevailing market, decent coilovers are also available and due to this reason, costly coilovers are put aside.

Irrespective of type of damper used for automobile vehicle, they must offer correct dialling for best performance. For this purpose, advisable way is to start with the dampers on the softest setting. Then driver is expected to drive with set course and pragmatically try and feel the way automobile vehicle enters the corner and performs on rougher roads. If feeling is too soft, progressively enhance the damping till little stiffer feeling is experienced. After experiencing this point, back off the adjuster a click or two and then set the damper. For same feeling, each corner may require little bit different change in setting. In the same way for the same feeling, little change in setting may require for rear and front. Body movement and the wheel movement must be analysed simultaneously for the single adjustable shock. For double adjustable setup, two motions should be decoupled. This may look unscientific but it is fact that driver is a very important part of the equation. The feeling of the driver driving an automobile vehicle will greatly affect behaviour of driver.

The perfect solution of this complexity is to use semi active damper, which gives required damping effect in any situation. Present research work is focused on the design of such type of dampers, which give required output, i.e. damping coefficient in any input parameters.

1.3 Controllable Fluid as an Energy Absorber

Controllable fluids are responsive mediums to an external excitation field. When this medium is subject to an electric or magnetic field, its rheological properties undergoes significant changes. This phenomena makes these fluids as smart fluids and normally such fluids are named as Magneto Rheological (MR) fluids, Electro Rheological (ER) fluids and Ferro fluids. From such smart fluids, MR fluids are getting more acceptance because of their ability to produce highest stress. This highest stress has many applications. An MR fluid is a suspension of micron-sized magnetically soft particles mixed in a carrier liquid. This suspension is able to undergo dramatic changes in rheological properties. For instance, when magnetic field is applied, MR fluid changes from free-flowing liquid state

to a solid-like state in reversible way. Iron powder has high saturation magnetization property and because of this, it is used as particle inclusion. When magnetic field is applied, these particles are arranged to form a very strong chain of flux with the pole of one particle being attracted to the opposite pole of another particle [4, 5]. Once particles are arranged in this pattern, these are restrained from moving away from their respective flux lines and behaves as barrier against the flow of the carrier fluid.
This work is solely based for automotive type damper with magnetoreholocal fluid as working medium.

1.4 Motivation

People are most sensitive for vertical vibrations between 5 & 16 Hz & to the lateral vibration between about 1 & 2 Hz. Women are more sensitive than men to vertical vibration above about 10 Hz. Most responses of seated subjects implicated the lower abdomen at 2 Hz moving up to body at 4 & 8 Hz, with most responses implicating head at 16 Hz. At 32 Hz the responses are divided between the head & lower abdomen [2].
It is seen that often trade-offs influences the design process of any item. The design process of automotive suspension system is also not the exception from this. The general trade-off between ride comfort and vehicle stability is the motive for advancements in design of automotive suspension systems. Measurement of ride comfort is subjective but it can be quantified by the amount of energy transmitted through the suspension into the passenger compartment (sprung mass). Ride quality is derived closely with respect to the acceleration of the sprung mass [2]. Passengers feel few road disturbances in a Cadillac vehicle and this is a good example of this kind. Opposite to this, passengers feel many of the road disturbances transmitted by a Corvette's suspension which has higher vehicle stability. Vehicle stability is also known as road holding ability. Compared to a Cadillac, a Corvette is a much more maneuverable vehicle and holds the way appreciably better. In an ideal world, a vehicle suspension would react just as to aggressive driving as it does to highway cruising. The objective of this discussion is to emphasis the approach towards this ideal concept. Fig. 1.5 illustrates the classic suspension compromise.

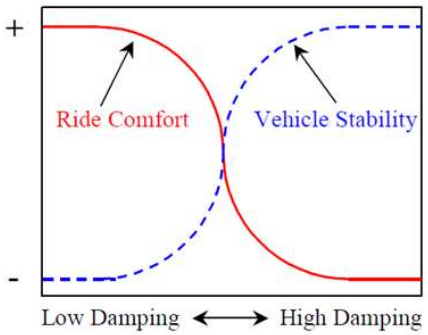

FIGURE 1.5 Suspension compromise [2]

Spring and damper are two critical components for a specific suspension vehicle. Weight of the vehicle is an exclusive important selection criterion for spring whereas suspension's placement on the compromise curve is mainly determined by damper. Damper selection is mainly governed by type of vehicle keeping the performance of vehicle at its optimum level. Theoretically, passengers should not be affected by low-frequency road disturbances when dampers are used. At the same time, dampers must absorb high-frequency road disturbances. When high damping effect is achieved, ideally passengers do not have any effect of low-frequency road disturbances. However this situation leads to absorb high-frequency at very poor rate. If damping effect is made low, this situation leads to absorb high-frequency at very good rate but this is achieved at the cost of low-frequency isolation. In the field of automotive suspensions, many innovative and improved concepts are emerged due to requirement to reduce the effect of this trade-off.

Following types of suspensions are reviewed here:

(i) Passive
(ii) Fully active
(iii) Semi-active

The conventional passive suspension system consists spring and damper. Spring is used to store the energy in suspension and at the same time, damper is used to dissipate the energy. Both components are finalised at design stage only. Due to this, this type of suspension is paralysed and known as classic suspension compromise.

Interchanging force actuator with damper, suspension is converted into fully active suspension. However, looking to the constraints like difficulty in operation and higher power utilisation, fully active suspensions are not yet came in regular use. The basic concept for fully active suspension is to apply the force either in the form of jounce or in the form of rebound to suspension using force actuator. Such force is dynamically

monitored and controlled by the control system integrated in the suspension itself. Various control systems will be narrated later in this thesis.

Semi-active suspension is last (third) type of suspension and same is discussed further. In this type, passive damper is interchanged with a semi-active damper which is having the potential to change the damping characteristics. This type of damper has also the ability to offer wider band of damping using mechanically controlled orifices or by monitoring and controlling fluid viscosity. It should be noted that damping value is changed in accordance with control algorithm used.

An exhaustive literature review (discussed in chapter-3) is carried out to understand the present practices and theories in damper design. It will also help to obtain a better understanding of how individual internal components and internal flows had been designed and modelled in the past.

Research Gap:

Design of semi active damper instead of passive damper with the application of smart fluid i.e. Magneto Rheological Fluid.

1.5 Definition of the Problem

- To understand basics of the force- displacement, force-velocity and force-time behavior of a new magneto-rheological (MR) fluid damper.
- To develop a theoretical study to predict behavior of new MRF dampers; and
- To conduct a comprehensive experimental study on the proposed MRF damper to validate all theoretical results.

This study aims design, fabrication and characterization of an MRF damper with design and fabrication of test rig for characterization of developed damper.

1.6 Research Objectives

The primary objectives of this research are:

1. To develop the MR fluid for application of damper
2. To conceptually design an MR damper
3. To develop the prototype of the MR damper
4. To evaluate the performance of the MR damper experimentally.

1.7 Research Methodology and scope of work

One of the most promising new device proposed for various system protections is magneto rheological (MR) fluid damper. Because of its mechanical simplicity, high dynamic range, low power requirements, large force capacity and robustness, this class of device has been shown to mesh well with application demands and constraints to offer an attractive means of protecting various engineering systems against interrupted force. MR dampers are being developed for a wide variety of applications where controllable damping is desired. These applications include dampers for automobiles, heavy trucks, bicycles, prosthetic limbs, gun recoil system and possibly others.

Rheological properties of MR fluids can be monitored and controlled. Changes on account of such monitoring and control are reversible and vary as there is change in intensity of excited magnetic field. Favourable applications can be availed from MR fluids when they are used with different loading modes (shear, valve and squeeze).When MR fluid is geometrically placed between two flat solid surfaces opposite to each other and such surfaces are at equidistance. Such arrangement is also defined as squeeze mode. Equidistance between such two solid surfaces is also defined as gap size.

This study focuses on the theoretical analysis, design, fabrication and characterization of a small Magneto-Rheological (MR) fluid damper. This study first introduces MR technology through a discussion of MR fluid and then by giving a broad overview of MR devices. After giving the broad overview of MR technology and devices, MR damper basics are presented.

With the necessary background information covered, a prototype MR damper for a case study is designed, developed, tested and then discussed, specifically for automobile suspension system. These test results are presented and compared with the traditional hydraulic dampers. In conclusion, recommendations are made for materials as well as for seal selection and other design aspects.

In summarized form, following are the scope for present research project:

- Understand basic theory of vibration
- Understand MR fluid basics, behavior, production and applications in various fields as a smart fluid
- Understand various designs which are commonly used for MR dampers
- Develop design alternatives from existing MR damper designs

- Design of the prototype damper
- Prototype fabrication of improved design MR damper
- Design and fabrication of test rig for testing damper
- Testing of the newly developed damper for optimization
- Comparison of MR damper with conventional damper

Data analysis is carried out with the help of statistical software like Design Expert, ANOVA and EXECL (MS OFFICE) with C programming whenever needed.

1.8 Original Contribution by the Thesis.

The entire work in this thesis is the original work with the research papers presented/published in international journals and conference as the back bone. The proposed model has been visualized as a collection of various modules, each of which with relevant publications. The details of the associated papers are listed in appendix A: List of Publications (page no: xxxii).

Furthermore, the MR fluid used in this project is designed and developed as our original product. Test rig is designed, fabricated and instrumented according to experimental requirement is as our original product.

1.9 Outline

Chapter 1 gives a brief description of the research work. It includes background and motivation for present work. The boundary conditions are represented along with the pre-defined constraints for present work. It also covers problem definition, research objectives, Research Methodology with scope of work and original contribution by the thesis.

Chapter 2 covers the basics of vibration. This study includes types of vibrating motion with parameters related to the vibrating motion. Different vibration control systems (passive control system, semi-active control system and active control system) are discussed in detail which is very important for damper characteristic requirement.

Chapter 3 presents the MR fluid properties and application. An exhaustive literature review is carried out to understand the theories and present practices in magnetorheological

(MR) fluid and damper design. It will help to obtain a better understanding of how MR fluid behaves under different mode of application. It will also help to obtain a better understanding of how the individual internal components and internal flows in damper had been designed and modelled in the past. This section presents background information on MR fluid and damper technology. The information here is a summary of important information found in a comprehensive literature review. Journal articles, thesis, and books were searched for topics relating to MR fluid, shock absorbers, dampers, active damper, magnetorheological dampers, MR damper models, probability models, and stochastic models. Each result of this search was examined for relevance to the subject.

Chapter 4 present two quasi-static models, an axisymmetric model and a parallel-plate model, based on the Navier-Stokes equation.
The Herschel-Bulkley visco-plasticity model is used to define the MR fluid field-dependent characteristics and shear thinning/thickening effects. At initial design phase, simple equations based on these damper models can be used. Geometry as governing parameter for controllable force, dynamic range and MR damper performance is also narrated.

Chapter 5 covers MR damper geometry and magnetic circuit design review. Damper piston centring and voltage surge suppression are added practical parameters which are also narrated in this chapter along with problems resolutions. The discussion is started with description of MR fluid used for present investigation.

Chapter 6 related with testing of developed MR damper. To investigate the fundamental behaviour of the designed small-scale MR damper, a series of quasi-static experiments were conducted at the Physics Department Laboratory, Bhavnagar University. In this chapter, detailed discussion of the experimental setup and experimental results for the different test carried out are presented. The experiment results are then used to compare with theoretical results. This chapter also included discussion on test rig requirement and development for carried out complete experiment. Some phenomena observed during the experiment are also discussed, and possible explanations are given.

Chapter 7 includes complete discussion on results available during experiment. For the validation of experiment procedure, first complete Design of experiment is carried out with

the help of Design Expert software on the data received during experiment. This chapter also includes key features of MR damper. Finally conclusion and future scope of the thesis are listed for future work on same field.

CHAPTER 2
BASICS OF VIBRATION

2.1 Introduction

Elastic elements like a spring, a beam and a shaft are displaced from its equilibrium situation using the use of external forces, and then released, they effect a vibratory motion. This is because of, once an element is displaced from its original situation, the internal forces in the form of elastic or strain energy are existent in the element. After releasing an element, these internal forces take the element to its initial situation. After the element reaches to its equilibrium situation, the total energy which is in the form of elastic energy or strain energy is changed in the form of kinetic energy. For that reason, the body remains to move in the reverse direction. The entire kinetic energy is further changed into strain energy. Again for that reason the element comes back to the equilibrium situation. By means of above discussion, the vibratory motion is repeated indefinitely.

2.2 Types of Vibratory Motion

The subsequent forms of vibratory motions are significant with respect to present study:

- **Free or natural vibrations**

  An element without affecting any external force, will be vibrate due to displacement from its equilibrium condition, then the element is known as under free or natural vibrations. The frequency of the free vibrations is called free or natural frequency.

- **Forced vibrations**

  An element which is under influence of any external force, will be vibrate due to displacement from its equilibrium condition, then the element is known as under forced vibrations. The influence force subjected to the element is a periodic disturbing force produced by unbalance. It is important to note that the applied force and vibration have a same frequency. When the frequency of the influence force is equal as that of the natural vibrations, resonance takes place.

- **Damped vibrations**

  The motion is said to be damped vibration if there is a decrease in amplitude for every completed cycle of vibration. This happens due to definite quantity of energy possessed by the vibrating system is continuously rejected in overcoming frictional resistances to the motion.

  If no energy is lost or dissipated in friction or other resistance during oscillation, the vibration is known as un-damped vibration. If any energy is lost in this way, however, it is called damped vibration. In many physical systems, the amount of damping is so small that it can be disregarded for most engineering purposes. However, consideration of damping becomes extremely important in analysing vibratory systems near resonance.

Vibrations or oscillations can be regarded as a subset of dynamics in which a system subjected to restoring forces swings back and forth about an equilibrium position, where a system is defined as an assemblage of parts acting together as a whole. Restoring forces are due to elasticity, or due to gravity.

In most of the engineering applications, vibration is signifying to and fro motion, which is undesirable. Galileo discovered the relationship between the length of a pendulum and its frequency and observed the resonance of two bodies that were connected by some energy transfer medium and tuned to the same natural frequency. Vibration may results in the failure of machines or their critical components. The effect of vibration depends on the magnitude in terms of displacement, velocity or accelerations, exciting frequency and the total duration of the vibration. The vibration of a single-degree-of-freedom (SDOF) system will be discussed in this section.

A vibratory system, in general, includes a means for storing potential energy (spring or elasticity), a means for storing kinetic energy (mass or inertia) and a means by which energy is gradually lost (damper).

The vibration of a system involves the transfer of its potential energy to kinetic energy and of kinetic energy to potential energy, alternately. If the system is damped, some energy is dissipated in each cycle of vibration and must be replaced by an external source if a state of steady vibration is to be maintained.

Following are important terminology related to vibration system analysis.

1. **Time Period (Period of Vibration)**

   Time period is the time interval of vibration system after which the motion is repeated itself. It is generally presented in seconds.

2. **Cycle**

   It is the motion accomplished for the duration of one period of vibration.

3. **Frequency**

   It is the number of cycles refer to in one second. In S.I. system of units, it is represented by hertz (briefly written as Hz) which is equal to one cycle per second.

2.3 One degree of freedom (1-dof) Free Un-damped Vibration

The simplest possible example that may help to understand the dynamics of vibrations is the oscillating point mass, which has one degree of freedom. Such a system is schematically illustrated in Fig. 2.1. Let us assume for now that damping is negligible and there is no external force acting on the system. In free vibration, a mechanical system is excited by an initial condition, such as a displacement, velocity or acceleration and then is allowed to vibrate freely without further force interaction. A mechanical system in free vibration will oscillate with its natural frequency and eventually settle down to zero due to damping effects. In forced vibration, an external force is supplied to the system.

Fig. 2.1 displays the most elementary probable structure, a mass, assumed accomplished of vertical translation only attached by a spring to the ground. Damping is ignored at this condition.

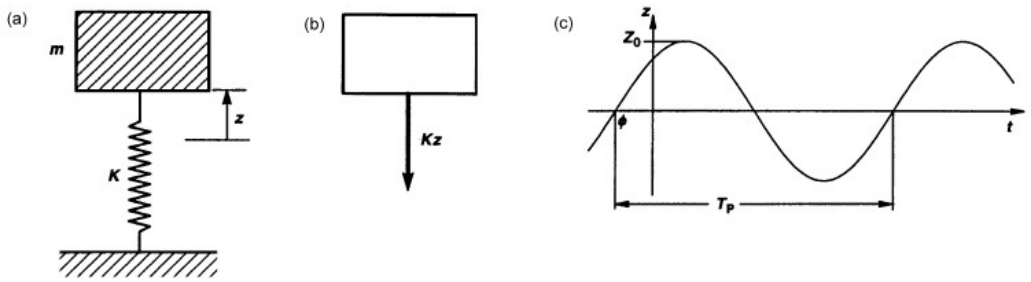

FIGURE 2.1 Simple un-damped 1- DOF vibrating system, position factor z from the equilibrium situation: (a) meaning sketch; (b) free body illustration of mass; (c) free vibration motion $z(t)$ [3].

Let

K = spring stiffness, defined as the force necessary to make unit displacement in the direction of vibration. It is generally presented by N/m.

m = Mass of the element hanged from the constraint in kg,

z = Displacement given to the element by the outside force, in metres.

One degree of freedom (1-dof) Free Un-damped Vibration

Once the mass is moved by a displacement z from its equilibrium situation, then, by meaning of *K*, there is a spring force, positive in the z direction, specified by:

$$F_z = -Kz$$

Hear negative sign point out that the force is reverse in path to the movement for positive spring stiffness *K*; for that reason it is known as a restoring force. This force gives an acceleration to the element, stated by Newton's second law as [6, 7]

$$m\ddot{z} = -F_z$$

The equation of motion used for the system of Fig. 2.1, by substituting for F_z, turn into:

$$\ddot{z} + \frac{K}{m}z = 0 \tag{2.1}$$

The fundamental equation of simple harmonic motion is

$$\ddot{z} + \omega_n^2 z = 0 \tag{2.2}$$

Comparing equations (2.1) and (2.2), ω_n is given by

$$\omega_n = \sqrt{\frac{K}{m}} \tag{2.3}$$

$$T_p = \frac{2\pi}{\omega_n} = 2\pi\sqrt{\frac{m}{K}} \tag{2.4}$$

$$f_n = \frac{1}{T_p} = \frac{1}{2\pi}\sqrt{\frac{K}{m}} \tag{2.5}$$

Where

ω_n = Angular velocity in rad/sec

T_p = Time period and

f_n = natural frequency

The natural frequency for that reason be influenced by the mass and the stiffness. With constant spring stiffness, if the mass increases, the natural frequency decreases. This is a important problem due to the variation of mass with luggage and passengers, mainly for light weight automobile vehicle where the comparative size of the difference tends to be larger. As a result 'rising rate' springs are frequently used. If the stiffness has an appropriate positional requirement so that it is proportional to the mass then the frequency of small amplitude vibrations will be self-governing of ride height.

Above section discussed free vibration of a mass without damping. This means that a mass connected to a spring and deflected to the initial position of z, would oscillate with the

same amplitude indefinitely. As we can see, this is a very unrealistic model - we have to add some sort of energy dissipation mechanism, or in other words, damping.

2.4 One degree of freedom (1-dof) Free Damped Vibration

Suspension system is provided to overcome the uneasiness rising from road roughness in automobile application. On the other hand, in actual practice, the automobile vehicle is very prone to vibrate at its natural frequency presented above, about 1–2 Hz. To govern this occurrence, some damping must be added. Damping is energy dissipation from the system when movement is present. In a mechanism for example an automobile suspension, damping is intentionally presented by the combination of the dampers. There is additional damping from material hysteresis in the rubber bushes, tyres and in certain circumstances as of Coulomb friction at sliding connections. Useful analysis of vibration may frequently be accomplished without reflection of the damping, for example to determine un-damped mode shapes and natural frequencies. On the other hand in certain cases it is required to include it. Frequently it is demonstrated as basically linear, proportionate to speed, for the reason that this can be studied more easily compare to other forms. The motion of a element is resisted by frictional forces. The influence of friction is mentioned to as damping in vibrating systems. The viscous damping is a damping providing by fluid resistance.

A complete damping system consist of mass, spring and damper. Systems with a single degree of freedom help to illustrate some fundamental relations. It is considered a concentrated mass on a damped spring element. The spring force is supposed as directly related to the spring´s deformation (compression or extension), with the spring factor *K*, which is the spring´s stiffness. The damping force is supposed as directly related to the velocity, with the damping constant c, defined as force per unit velocity.

The amplitude of the subsequent vibration progressively reduces in damped vibrations. It happens because of a definite quantity of energy is continuously rejected from vibrating system to overcome the friction effect. The resistance because of friction effect to the motion of the element is delivered partially by the medium where the vibration takes place and partially by the internal friction, and in certain cases partially by a dash pot or additional outside damping device.

Assume a vibrating system, as presented by Fig. 2.2, which includes a coiled spring with a mass suspended from one end and the other end of which is fixed. A damper is attached among the mass and the rigid support.

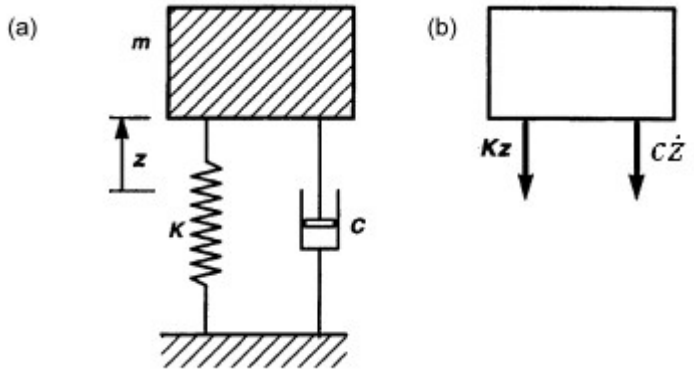

FIGURE 2.2. Simple linearly-damped 1–dof system: (a) description sketch; (b) free body diagram [3].

Let

m = Suspended mass from the spring,

K = Spring Stiffness,

z = Movement of the mass from the mean position on time t,

c = Damping coefficient defined as the ratio of damping force to piston velocity.

Damping is a complex phenomenon, not very well understood and modelled in science. Different damping models exist; however, these represent reality only under certain conditions and assumptions. Probably the most popular damping model is viscous damping, which expresses the damping force that is proportional to velocity by a damping coefficient c. This force can be expressed by [7]:

- Damping force or frictional force on the mass:

$$= c * \dot{z}$$

  The direction of damping force is in reverse to the motion of mass.

- Accelerating force on the mass:

$$= m * \ddot{z}$$

  The direction of accelerating force is along the motion of the mass.

- Spring force on the mass:

$$= K * z$$

  The direction of spring force is in reverse to the motion of mass.

Therefore the equation of motion can be represented as:

$$\ddot{z} + \frac{1}{m} * c * \dot{z} + \frac{1}{m} * K * z = 0 \quad (2.6)$$

This is a second order differential equation. By utilising the Heaviside operational symbolisation D for d/dt, or imagine a solution of the form e^{Dt} and replacing, this turn out to be:

$$D^2 z + \frac{c}{m} Dz + \frac{K}{m} z = 0 \quad (2.7)$$

Dividing by z to the above differential equation, it provides the algebraic characteristic equation. This algebraic characteristic equation is presented as:

$$D^2 + \frac{c}{m} D + \frac{K}{m} = 0 \quad (2.8)$$

The physical outcomes of the solution be determined by the value of D whether it is real (non-oscillatory) or complex (damped oscillatory). D is calculated by the normal typical form of quadratic equation solution:

$$D = \frac{-b \pm \sqrt{b^2 - 4ac}}{2a} \quad (2.9)$$

Giving

$$D = -\frac{c}{2m} \pm \sqrt{\left(\frac{c}{2m}\right)^2 - \frac{K}{m}} \quad (2.10)$$

$$D = \alpha \pm \sqrt{\alpha^2 - \omega_n^2} \quad (2.11)$$

Where α (units of s^{-1}) is the real part of the root, named the damping factor, negative in value, and ω_n is the undamped natural frequency (rad/s).

The most general solution of the differential equation (2.3) with its right hand side equal to zero has only complementary function and it is given by

$$z = Ae^{D_1 t} + Be^{D_2 t} \quad (2.12)$$

Where A and B are two arbitrary constants which are to be determined from the initial conditions of the motion of the mass.

The form of the solution of this equation depends upon whether the damping coefficient is equal to, greater than, or less than the critical damping coefficient c_c, mathematically given by

$$c_c = 2\sqrt{Km} = 2m\omega_n \quad (2.12)$$

The critical damping coefficient is the amount of damping required for a system to be critically damped.

The ratio of damping coefficient and critical damping coefficient is defined as the fraction of critical damping or damping ratio, denoted by ζ, mathematically damping ratio is given by

$$\zeta = \frac{c}{c_c}$$

It is important to be noted that the outcomes of D_1 and D_2 might be real, imaginary or equal. The possibilities for these three cases are as below:

1. **While the roots are real (Over-damping)**

   When $\left(\frac{c}{2m}\right)^2 > \frac{K}{m}$ (or $\zeta > 1$) then the roots D_1 and D_2 are real but negative. This condition express over damping or big damping. In over damping condition the mass moves slowly to the equilibrium situation. This type of motion is recognised as aperiodic. While the roots are real, the best general solution of the differential equation is:

$$z = Ae^{\left[-\frac{c}{2m}+\sqrt{\left(\frac{c}{2m}\right)^2-\frac{K}{m}}\right]t} + Be^{\left[-\frac{c}{2m}-\sqrt{\left(\frac{c}{2m}\right)^2-\frac{K}{m}}\right]t} \quad (2.13)$$

   Or

$$z = e^{-ct/2m}\left(Ae^{\omega_n\sqrt{\zeta^2-1}\ t} + Be^{-\omega_n\sqrt{\zeta^2-1}\ t}\right) \quad (2.14)$$

   In real practice, the over damped vibrations are avoided.

2. **While the roots are complex conjugate (underdamping)**

   If $\left(\frac{c}{2m}\right)^2 < \frac{K}{m}$ (or $\zeta < 1$), then the radical (i.e. the term under the square root) come to be negative. The roots D_1 and D_2 are at that time recognised as complex conjugate. This is the best practical situation of damping, known as underdamping or small damping. The damping of the system is less than critical damping. The most general solution of the differential equation is

$$z = e^{-\frac{ct}{2m}}(A\sin\omega_d t + B\cos\omega_d t)$$

   or

$$z = Ce^{-\frac{ct}{2m}}\sin(\omega_d t + \theta) \quad (2.15)$$

   Where

   $C = \sqrt{A^2 + B^2}$

$\theta = \tan^{-1}\left(\frac{B}{A}\right)$ known as a phase angle.

The damped natural frequency ω_d is related to the undamped natural frequency ω_n by the equation

$$\omega_d = \omega_n \left(\sqrt{1-\zeta^2}\right) \qquad (2.16)$$

From the above equation, it can be concluded that the motion of the mass is simple harmonic with circular damped frequency ω_d and amplitude $Ce^{-\frac{ct}{2m}}$. The frequency and amplitude were diminishes exponentially with respect to time as presented in Fig. 2.3. However the mass finally comes back to its equilibrium situation due to its inertia, however it overshoots and the oscillations may take certain significant time to die away.

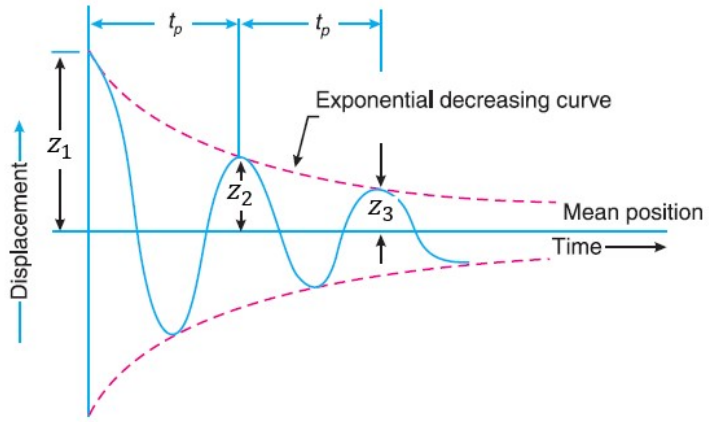

FIGURE 2.3 Underdamping or small damping.

When a system is without damper, the damper coefficient value c = 0. As a result the frequency of the un-damped vibration is the equal as discussed under free vibrations.

3. While the roots are equal (critical damping)

For the condition $\left(\frac{c}{2m}\right)^2 = \frac{K}{m}$ (or $\zeta = 1$), the radical turn out to be zero and both D_1 & D_2 roots are identical. This is a situation of critical damping. By means of other words, the critical damping is supposed to take place when frequency of damped vibration f_d stands zero (i.e. motion is aperiodic). This kind of damping is furthermore avoided for the reason that the mass moves back rapidly to its equilibrium situation, in the shortest probable time. For critical damping there is no

oscillation or a damping is called critical when the amplitude decays from the maximum displacement to the rest position without changing the sign without oscillation. The solution of the differential equation is

$$z = (A + B)e^{-\frac{c}{2m}t} = (A + B)e^{-\omega_n t} \qquad (2.17)$$

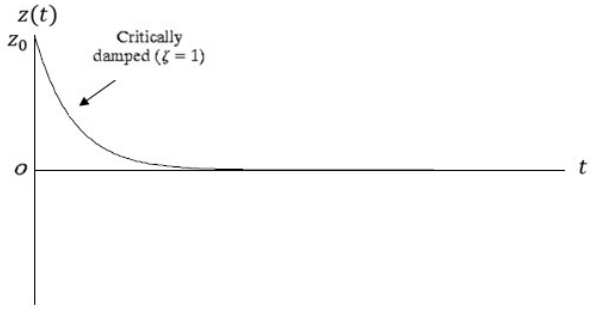

FIGURE 2.4 Critical damping [3].

Thus the motion is again aperiodic. The quantity of damping essential for a system to be critically damped is recognised as a critical damping coefficient. Fig. 2.4 shows the behaviour of critical damping.

Most of automobile vehicles are operated with under-damped situation, i.e. lower than critically damped. This is for the reason that subcritical damping or say under-damping make available the finest balance of operation (ride and handling), therefore the oscillatory solution is the important one of attention at this time:

$$z = z_0 e^{\alpha t} \sin(\omega_d t + \Phi) \qquad (damped) \qquad (2.18)$$

This may be compared with the one found for un-damped vibration motion

$$z = z_0 e^{\alpha t} \sin(\omega_n t + \Phi) \qquad (undamped) \qquad (2.19)$$

There are important differences that:

1. The damped natural frequency ω_d is reduced from the undamped natural frequency ω_n, the former falling to zero when the damping reaches critical.
2. There is an additional exponential term $e^{\alpha t}$ which causes the free oscillation to die away, which is, of course, the intended purpose of damping. Parameter α in the exponent is the damping factor, $\alpha = -\zeta\omega_n$ and is negative in value. Here α is used for the real part of the complex root.

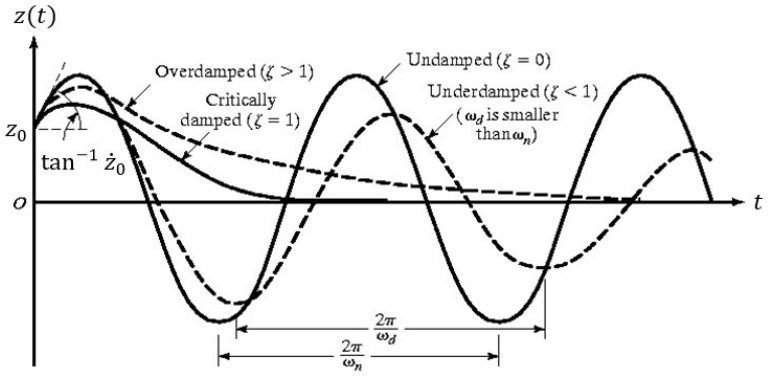

FIGURE 2.5 Comparison of vibrating motion [3].

Fig. 2.5 shows various types of vibrating motion.

The earlier detected outcome for un-damped vibrating motion remains correct: the initial amplitude z_0 as well as the phase angle Φ be subject to the initial position and initial velocity, at time *t=0*, rather than on the integral system parameters *m, K* and *c*.

It is important to differentiate obviously among three damping parameters:

(1) Damping coefficient c (N s/m)

(2) Damping factor α (1/s)

(3) Damping ratio ζ (dimensionless)

These parameters are related by:

$$-\alpha = \zeta\omega_n = \frac{c}{2m} \tag{2.20}$$

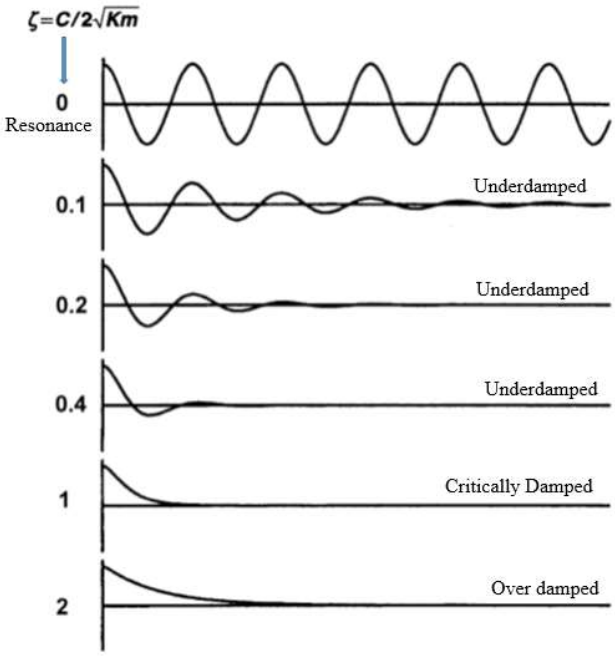

FIGURE 2.6 Free vibration of system with linear damping for various damping ratios ζ [3].

Fig. 2.6 shows the behaviour of damping ratio on the free vibration from an initial displacement. It is understood from an applied approach that the most rapid and controlled coming back is attained using damping nearby to critical (i.e. ζ=1) [2]. Curb side vehicles possibly will have an operative mean damping coefficient of about 0.3 [8]. In heave, for the reason that the control is poorer, the softer dampers contribute a lesser amount of discomfort. However a racing vehicle would be superior using a greater operative damping ratio, in an ideal world reaches to 1.0. It is also concluded that, subject to road situations, the best possible over-all drive can take place for a damping ratio about 0.2 but the best possible handling take place for a damping ratio of possibly 0.8; the real value selected inside this range be determined by the drive/handling compromise accepted for the specific automobile vehicle. For the value of damping ratio 0.2, the value of damped natural frequency is approximately 2% smaller than the un-damped value. On ζ=0.4 the percentage reduction is almost 8%, and at ζ=0.8 it is 40% lower than when un-damped [8].

The damping ratio possibly will fall down lower than 0.1 in the occasion of too much damper wear, which is source of severe piston and seal leak or loss of damper fluid [9]. From Fig. 2.6, it can be concluded that damping ratio lower than 0.1 will provide poor controller of oscillations. This result produces unfavourable 'wallowing' of the vehicle. This circumstances is dangerous on rough roads or at over speed on normal roads by means of loss of control.

Above mentioned examination can be directly assigned to a motor vehicle in the direction of find the estimated actual damping coefficients necessary. An automobile vehicle having mass of 1500 kg and a elementary un-damped natural frequency is 1.5 Hz, 9.4 rad/s, the total suspension stiffness is $K = m\omega^2$ = 133 kN/m, an average of 33 kN/m at each of four wheels. To obtain a damping ratio ζ of 0.4, the damping factor required is $\alpha = -\zeta\omega = -3.76\, s^{-1}$. The total damping coefficient is therefore $c = -2\alpha m = 11.28\, kNs/m$. At each of four wheels this is 2.82 kNs/m. This numerical analysis summarised that the dampers themselves must permit for the installation motion ratio.

Critical damping situation is the unique which just breaks overshoot. Damping outside this value reasons a slower coming back to the equilibrium situation. On the other hand Fig. 2.6 shows the results related only with free vibration and is not the complete analysis. Over-critical damping is in fact applied for regulate certain vibrations, even though it almost not rises in the example of automobile vehicles [9].

2.5 Vibration control system

In the recent years many techniques have been developed to reduce the vibration response in structure of machine and automobile vehicle. This part is focused on the difference among various types of vibration control techniques, say passive, semi active and active control system.

2.5.1 Passive Control System

To understand the necessity and opportunity for better selaction arrangment the passive, semi-active and active control system, a single degree of freedom system, in which a vibratory machine is supported on a rigid base through a spring and a damper is considered as shown in Fig. 2.7.

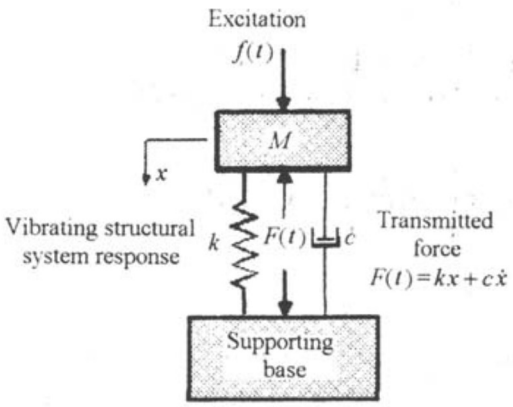

FIGURE 2.7: Passive viscous damper to control the vibrating system response [82].

Passive control system consist one or more elements which are jointed or set in to a vibrating system. This passive control system is intended to revise the stiffness value or the damping value of the vibrating structure in a suitable way without demanding an exterior power source to activate and develop the control forces reverse in the direction of the motion of controlled vibrating system.

As of literature review, passive control methods were implemented first having base isolation and passive control elements. Many researchers have analysed vibrating systems fitted out using these passive technique and numerous concrete recognitions have already been applied in various nations.

Isolation or reducing vibrations produced either by automobile vehicle or any other machines are accomplished in order to reduce the force transmitted by these to the chassis or foundations or other structures. This reason has been applied in the field of automobile

engineering for better comfort as well as in mechanical engineering for safety and life of machine and structure. Usually a damping system is introduced between the vibratory machine and its supporting base as shown in Fig. 2.7.

The implementation of passive dissipating device into the structure can lead to undesired situations, especially during the transient response, as the case of automobile vehicle. Damping for passive control system can be dependent on the time, frequency, mass and environment and well as to be non-linear. To avoid such constrain, semi-active or active vibration control system can be implemented.

2.5.2 Semi Active Control System

With a semi-active control system the damping characteristics of devices can be changed in a desired manner continually or chosen within a range with pre-established values with respect to the functioning conditions. Implementation of semi-active control law is very simple, as shown in Fig. 2.8 taking into account the model with a vibratory machine supported on a foundation. Example of such common semi-active devices known in literature and which could be implemented are: semi-active hydraulic devices, variable stiffness devices, controllable friction dampers, controllable fluid dampers or dampers with smart fluid. This is the case of present investigation.

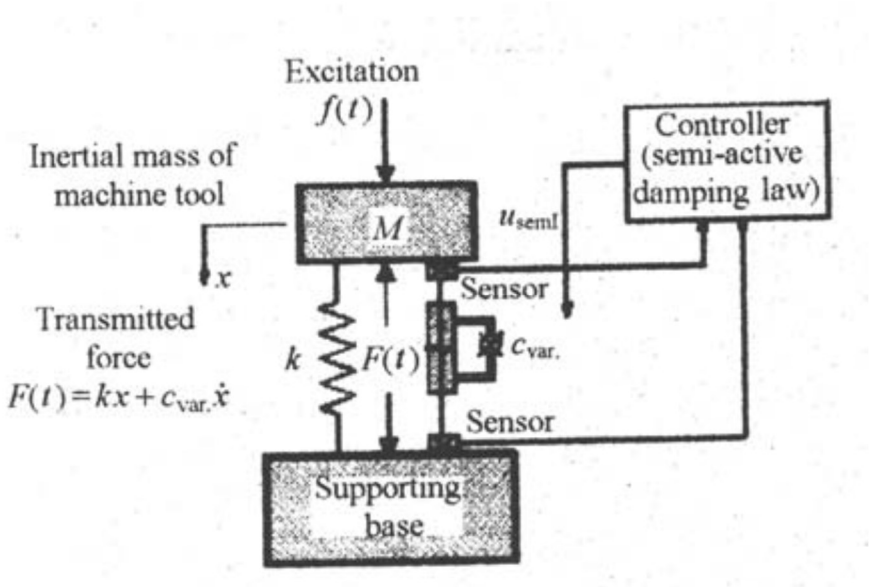

FIGURE 2.8 Semi-active viscous damper to control the vibrating system response [82].

Let us consider now a semi-active hydraulic damper with on and off behaviour. A high value of damping is used when a machine starts or stops having a low speed (during the acceleration or deceleration). For high speed the value of damping is low. This type of

control is very useful only if the dynamic characteristics and the excitation conditions are very well known.

Semi-active control systems are a class of active control system for which the external energy requirements are smaller amounts than those of typical active control. A battery power, for instance, is sufficient to activate semi-active control system in operation. It cannot add or remove energy to the vibrating structure but can control in real time parameters of the vibrating structure such as spring stiffness or coefficient of viscosity of damper. In present investigation, semi-active control technique is achieved by controlling damping co-efficient value. The stability is guaranteed, in the sense that no instability can occur due to semi-active device utilise the motion of the vibrating structure to develop the control forces.

2.5.3 Active Control System

An active control system is defined as one in which an enormous external power availability having 10 kW to several MW (depends on structure mass and operating conditions) required to control actuators that apply forces to the structure in a prescribed manner. These forces can be used to both addition and dissipation of energy in the structure. For these reasons, active control strategies are adopted in the field of automobile engineering, mechanical engineering, electrical engineering and safety of civil structures. The real problem of active system is the large energy requirement and complexity.

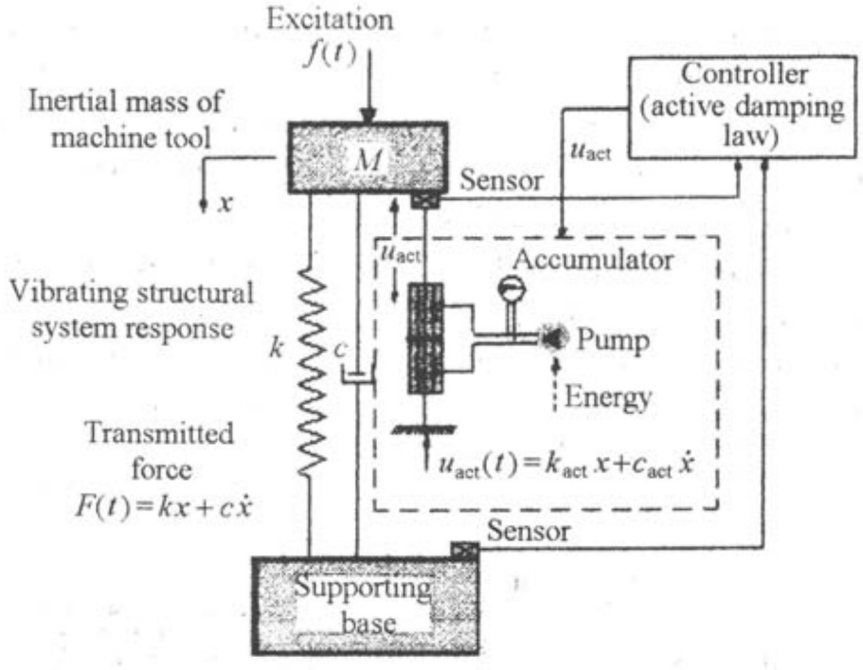

FIGURE 2.9 Semi-active viscous damper to control the vibrating system response [82].

A schematic diagram of active control system is shown in Fig. 2.9. The control forces inside the structure of an active control system are created using a comprehensive selection of actuators that be able to performance pneumatic, hydraulic, piezoelectric, electromagnetic or motor operated ball-screw actuation. The computer used as a controller, accepts signals after the reaction of the vibrating system measured by means of measuring device (inside active control using response) and that on basis of a pre-set control procedure matches the conventional signals with a preferred reaction and usages the inaccuracy to create a suitable control signal [11]. The actuator receives the control signals. In feed-forward control, the input signals and output signals are recorded and utilised to create the control signals. Both feedback and feed-forward principles are utilised together in the same active control system.

The difference among passive, semi-active and active control system is shown in a simple way in Fig. 2.10, taking into account that only the damping is inserted with active control law and also the figure represent the magnitude and phase angle curves of the receptacle transfer function of the considered single degree of freedom between the excitation and displacement response. The results are obtained using quadratic optimal control. The area between the active and passive response curves can offer theoretical possibilities for a semi-active vibration control system.

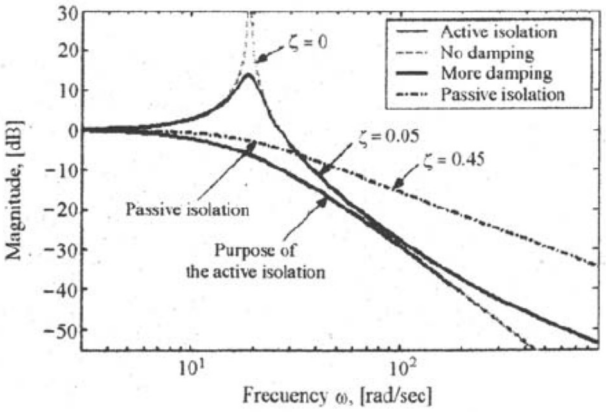

FIGURE 2.10 Passive, Semi-active and Active control system response [82].

In another way, it can be stated as semi-active control system make the reintegration of passive control systems, while they can occur similar performances of active control systems.

CHAPTER 3
LITERATURE REVIEW

3.1 Introduction

An exhaustive literature review is carried out to understand the theories and present practices in magnetorheological (MR) fluid and damper design. It will help to obtain a better understanding how MR fluid behaves under different mode of applications. It will also help to obtain a better understanding how the individual internal components and internal flows in damper had been designed and modelled in the past. This section presents background information on MR fluid and damper technology. The information here is a summary of important information found in a comprehensive literature review. Journal articles, thesis and books were searched for topics relating to MR fluid, shock absorbers, dampers, active damper, magnetorheological dampers, MR damper models, probability models and stochastic models. Each result of this search was examined for relevance to the subject. The following sections review the information which are searched and organized by subject.

3.2 Controllable Fluids

Solids deformation and flow of fluid under stress phenomena is normally termed as rheology science. Electric field governs the properties of ER (electro-rheological) liquids whereas magnetic field governs MR (magneto rheological) liquids. Indeed this kind of behaviour is outcome of response only. ER and MR fluids are also recognised as controllable fluid, smart fluids or intelligent fluids. Such fluids are nonsensical hype and they do not have any dynamic information processing or intelligence ability. Liquid properties are function of electric or magnetic field applied and these properties govern the damping force. From this, it is clear that damping force cannot exclusively be governed by the extension or compression speed. Hence it can be concluded that damping force is required to be monitored and controlled by changing the properties of ER and MR fluids on continual base. Newtonian liquid having simple viscosity is the temperature driven liquid and conventional damper oil is one of such Newtonian liquid. ER and MR fluids are

Bingham plastics and are characterised by the yield shear stress τ_y and marginal viscosity μ and these both are driven by applied electrical field for ER fluid and magnetic field for MR fluid. In practice, marginal viscosity μ is governed by yield stress which is major operational parameter.

Non-colloidal (i.e. non-homogeneous) suspensions of polarisable micron-sized particles forms chain like structures when external field is applied. Examples of such structures are ER and MR fluids. This concept is shown in Fig. 3.1.

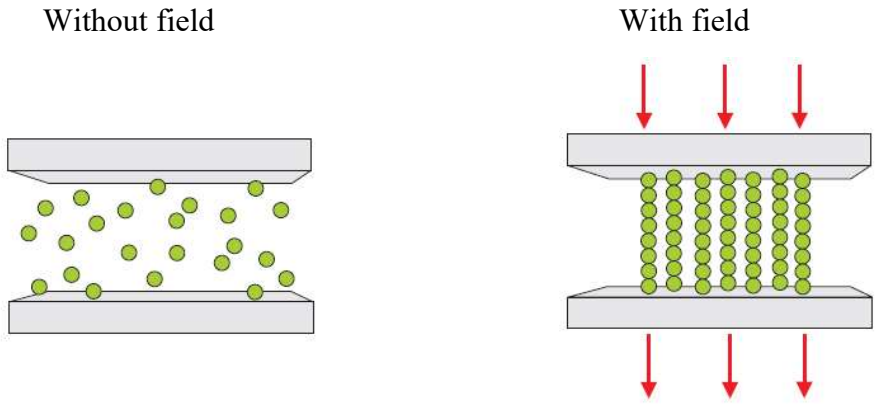

FIGURE 3.1: Chain-like arrangement in controllable fluids

The particles in the chain like structure is parallel to field direction and it limit the fluid flow. To initiate this fluid flow, minimum field dependent shear stress (also known as yield stress) is required.

It is also important to avoid confusion between ER and MR fluids with colloidal ferrofluids composed of nano-sized particles. Ferrofluids are also attracted by a magnetic field but do not exhibit any rheological change (and in particular, no yield stress). They are mainly used within oil seals characterized by very low friction.

3.3 MR fluid

The history of MR fluid goes back to AD 1940. These fluids were discovered and developed by Jacob Rainbow at US National Bureau of Standards (now the National Institute of Standards and Technology) and patent application was registered in AD 1947. MR fluids developed by Rabinow exhibited comparable yield strength and were applied for the purpose to use in clutches. They were almost similar to MR fluids being used today. In the era of 1950-1960, Rabinow led the developmental work and created interest for users.

Further in 1974 AD, William carried the work ahead on magneto rheological (MR) fluids. These MR fluids were suspensions of micron-size ferromagnetic particles made from iron and oil or water. The viscosity of such MR fluid is driven by change in applied magnetic field. As magnetic field is changed stronger, fluid changes to stiffer phase. Intensity of applied magnetic field governs the ability of either kind of fluid to transmit the force. Initially, smart MR fluids were used for civil and mechanical applications such as bark, clutch, vibrational damping and actuators [33]. The major challenge was to develop stable MR fluid suspensions in place of thick paste like mixture made up of solids and liquid characterised as state-of-art mixture. To measure mechanical properties of MR fluids in a magnetic field [4, 5, 13], J.D.Carlson and few researchers accompanying him developed first magneto rheometer with use of a stable MR fluid.

During the years 1991-1996, development and applications of MR fluid were initiated. In 1996, engineering system was recognised and in 1997, world's first ever commercial MR product was launched which was also named as MR rotary brake. Later in 1998 AD, Motion Master Seat Suspension system was launched. When commercial production began in 1999, industry experienced a new direction of technology applications. The Annual MRF volume grew by hundreds of tons. By the same year, it developed Integrated Cab Suspension which means air spring, MR damper and electronics. Currently, Lord Corporation is the leading producer of MR fluids and devices.

MR fluid is made up of non-colloidal suspensions of magnetically soft ferromagnetic ferrimagnetic or paramagnetic particles compounded in non-magnetic medium. MR fluids are made from appropriate magnetisable particles made from iron, iron alloys, iron oxides, iron nitride, iron carbide, carbonyl iron, nickel and cobalt materials [19, 30]. Mostly carbonyl iron is recommended to prepare MR fluids. Minimum value of coercivity and the maximum value of magnitude of saturation magnetization of the dispersed particles govern the probable highest value of yield stress produced by MR effect. Carbonyl iron powder is soft magnetic material with high purity and hence this is major magnetic phase for most of the MR fluids compounds [30]. In addition to carbonyl iron, alloys of Fe-Co and Fe-Ni are also used as MR materials. Here Fe provides to high saturation magnetisation. Ferrites of Mn-Zn, Ni-Zn and ceramic provide low saturation magnetisation and hence such ferrimagnetic materials are applied for low yield stress applications [18].

Mainly Hydrogen reduction of ferric oxide [32] and Chemical Vapour Deposition (CVD) methods are employed to prepare iron powder from the iron pentacarbonyl $Fe(CO)_5$[34]. After the particles are magnetized, the oriented domains can grow with the magnetization

persisted and enhanced permeability. Once all such domains are oriented in desired pattern, iron is magnetised at saturated level. The domain walls slides easily and this phenomenon makes magnetisation as ideal single valued function of magnetic field. This will prevent hysteresis loss during frequent reversals of field. It is important to note that selection of particle size should be optimum because these particles are subject to an external magnetic field. The selection of particles is also important from the view point of ensuring multi-domain characteristics. The size of MR particles are normally in the range of 0.1 to 10 μm [13, 15]. This size is almost 1000 times higher than those particles in the ferrofluids [5]. When particular size distribution of magnetic particles is selected for MR fluid, it gives maximum volume fraction. It should also be noted that change happens only within the acceptable limits of zero field viscosity. For example, electromechanically controllable torque-applying device had fluid composition of 50 % volume of carbonyl iron powder. This MR material was used as link to drive two independent rotating components [33].

The carrier liquid creates continuous phase of MR fluid. Following are the suitable examples of fluids [17, 30]:

i. Silicone oils
ii. Mineral oils
iii. Paraffin oils
iv. Silicone copolymers
v. White oils
vi. Hydraulic oils
vii. Transformer oils
viii. Halogenated organic liquids
ix. Diesters
x. Polyoxyalkylenes
xi. Fluorinated silicones
xii. Cyanoalkyl siloxanes
xiii. Glycols
xiv. Water
xv. Synthetic hydrocarbon oils

The carrier liquid can also be prepared with combination of two or more fluids from above. In past, it is found that older patents were with magnetisable particles dispersed in light weight hydrocarbon oil. This oil may be liquid, coolant, antioxidant gas or semi-solid

grease. It can also be silicone oil, chlorinated or fluorinated suspension fluid. However when field induced particles are settled, they form best chains structure incompletely. Under these circumstances, MR fluid response was critically degraded. To improve the stability of MR fluid to great extent, further sedimentation must be prevented. To prevent further sedimentation, considerations on viscoelastic and viscoplastic continuous phases are necessary to formulate new compositions of MR fluids [23]. A composite MR fluid was also prepared with combination of iron particles powder, gelatine and carrier fluids by Seval et. al. [37]. This composition gave the evidence of having superior MR effects under low magnetic field strength and better stability compared to pure iron carbonyl powder alone.

Following magnetisable particles in the liquid phase can be added to reduce the sedimentation of heavy particles [24, 31]:

i. Surfactants
ii. Nano particles
iii. Nano magnetisable or coating

The suspension experiences shear thinning actions due to sedimentation [41]. When sedimentation is continued for longer time in MR fluid under the effect of high stress and high shear rate, the fluid becomes thicken (in use thickening) [18, 38]. It is worthwhile to note that sedimentation process reduces the MR effect. In sedimentation process, particles in the MR fluid are settled down and form a hard “cake” which is made up of firmly bound primary particles due to incomplete chain formation [23]. Carbonyl iron as one of the MR particle has the particle erosion which has structure like onion and same can be easily peeled using jolt or frictions. Soft sedimentation is achieved through use of anti-settling agent like organoclay. Low viscosity MR fluids do not settle hard and at the same time they can be easily –re-dispersed [30]. Magnetic properties of the particles are also affected by coating of the polymer layer. This kind of coating makes particles to re-disperse very easily as soon the magnetic field is removed [39]. However addition of this kind of coating certainly degrades shear and yield stresses properties of MR fluid. This is because of shielding of the coating which affects the magnetic properties of the particles [39, 40]. Some specific additives are also helpful to improve properties like oxidation stability or abrasion resistance. Following sections we will summarize the main trends observed for MR-fluid composition.

3.3.1 Magnetisable Particles

Maximum inter-particle attraction (and thus maximum yield-stress) increases with the square of the saturation magnetization J_s of the particles [16].

Since carbonyl iron particle has the high saturation magnetization [27], it is most preferred for MR fluids. The process of thermal decomposition of iron penta carbonyl ($Fe(CO)_5$) is carried out to get the carbonyl iron powder in the form of highly spherical particles having size in the range of 1-10μm. The spherical particles have following advantages:

i. Less abrasive
ii. More robust
iii. Durable

Further, the spherical particles have onion skin structure and has the iron content up to 97.8% (Fig. 3.2). Water atomization is one of the process through which iron powder can be achieved. This is less expensive and can also be used for MR fluid formation. However it should also be noted that particles having range from 10 to 100μm are larger and irregular in shape. Such shapes affects their abrasiveness and durability. Highly irregular particles also tends to increase fluid viscosity compared to spherical particles [47]. Here volume fraction of both the particles is assumed to be same.

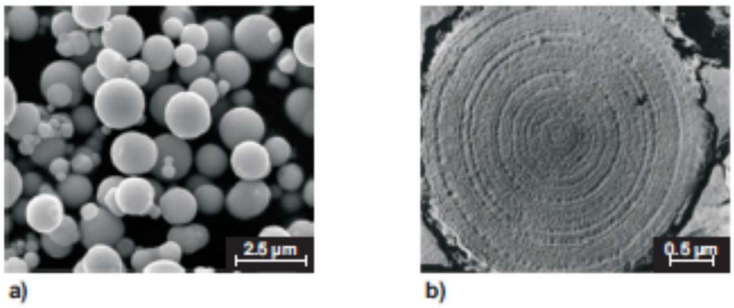

FIGURE 3.2: Scanning electron microscope images of carbonyl iron powder:
a) Spherical particles [adapted from 65] b) Onion skin structure [adapted from 65]

3.3.2 Carrier Fluid

Followings are the selection criteria for carrier fluids:

i. Intrinsic viscosity
ii. Temperature stability
iii. Compatibility with other materials of the device

The hydrocarbon oils (Mineral oils or Synthetic oils or a combination of both) is the most common carrier fluids. These fluids have property of good lubrication. In addition to this, durability is available in a large range of additives. Alternatively silicon oils can also be

used to achieve a broader operating temperature range and to dissolve compatibility issues with other materials of the device (e.g. rubber seals) to great extent. Jolly et.al. [5] has provided the recommendations for the temperature range of some MR-fluid formulations. Jolly et. al. [5] has also recommended their compatibility with typical seals materials.

3.3.3 Additives

Various kinds of additives, often proprietary, are used in MR-fluid preparations. They have a lot of purposes such as inhibit particle settling and agglomeration, reduction in friction and prevention of particle oxidation and wear. The major impact of these properties on the MR-fluid stability and durability, which are crucial in industrial applications, explains the fact that, in recent years, much of the MR-fluid research effort was focused on the development of new additive packages.

Particle settling may appear in MR-fluids due to the large difference between particles and carrier fluid densities. This phenomenon may be accompanied by particle agglomeration, which means that particles are sticking together in the absence of magnetic field (due, for example, to a small level of remnant magnetization in the particles). A small level of particle settling is not really an issue in devices when the fluid is naturally and efficiently remixed during operation (such as dampers and dampers in automotive applications [38]).In other applications such as seismic dampers, agglomeration has to be avoided since in that case, particle redispersion is much more difficult to achieve and may lead to alteration of the MR-fluid properties.

3.4 Magnetic properties of MR fluids

The static magnetic properties of MR fluids are important to design any MR fluid-based devices and can be characterized by *B*-*H* and *M*-*H* hysteresis. Through the magnetic properties, the dependence of the MR fluid response on the applied current in the device can be predicted. There are many methods to measure the hysteresis loops for the fluid under different fields such as vibrating sample magnetometer (VSM) [15, 41], alternating gradient magnetometer (AGM) and other induction techniques.

The standard model for the structure is considered to predict the behaviour of MR fluid particle under the impact of the magnetic field [27]. This model is dependent on a cubic network of infinite chains of the particles. These particles are arranged in a line with respect to the direction of the magnetic field. This pattern is shown in Fig. 3.3. The chains

are allowed to deform when distance between any pair of neighbours in the chains is same. If MR fluid is strained, the deformation also increases at the same strain rate. In reality, these chains are formed having compact pattern of aggregates of spheres. However same can also have the cylindrical formation. This phenomena makes the model quite simple. When these aggregates are subjected to shear stress, they might deform and ultimately may break also. The standard model has its utility [54] specifically to reliably predict yield stress in-spite of development of particles into different complicated structures under different conditions [29].

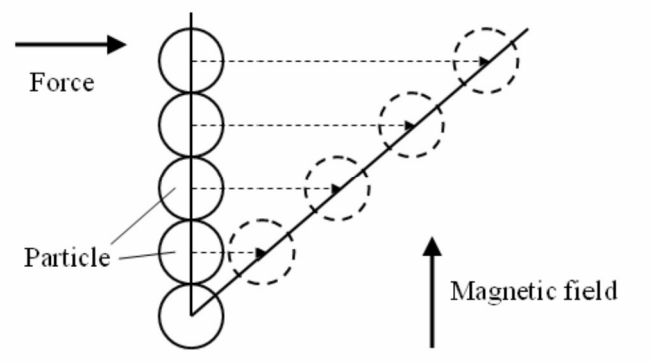

FIGURE 3.3: Schematic representation of the affine deformation of a chain of spheres [54].

Under magnetic field, the equation of motion of each particle should be in direction to estimate the bulk property of MR fluids. The magnetic force tensor F_{ij} is achieved as point-dipole similar to the pair interaction at a very low magnetic field. For an unmagnified and isolated sphere under a uniform magnetic field, the magnetic dipole moment is induced by other particles and surrounding walls. This phenomena can be expressed by equation as under [26]:

$$F_{ij} = \frac{3}{4\pi\mu_f\mu_0}\left[m^2\frac{r_{ij}}{r_{ij}^5} - 5\left(mr_{ij}\right)^2\frac{r_{ij}}{r_{ij}^7} + 2\left(mr_{ij}\right)m\frac{1}{r_{ij}^5}\right] \tag{3.1}$$

Where

F_{ij} is the magnetic force tensor acts on particle *i* from *j*,

μ_f is the specific permeability of particles,

μ_0 is the vacuum permeability,

m is magnetic dipole moment of particles and

r_{ij} is position from j to i.

The magnetic dipole moment which takes place in particles within MR fluid is expressed as under [42]:

$$m = 4\pi\mu_f\mu_0\beta a^3 H \tag{3.2}$$

Where

H is the uniform magnetic field,

a is the diameter of the particles and

β is given by,

$$\beta = \frac{\mu_p - \mu_f}{\mu_p - 2\mu_f} \tag{3.3}$$

Where

μ_p is the specific permeability of carrier liquid.

If magnetization of the particle reaches saturation and if there is higher magnetic field, the magnitude of the moment can be assumed to be independent point dipoles. Magnetic moment is given by [28].

$$m = \frac{4}{3}\pi a^3 \mu_s M_s \tag{3.4}$$

Where $\mu_s M_s$ is the saturation magnetization of the particle, which is around 1.7 x 10^6 A/m for majority iron and 0.48 x 10^6 A/m for the magnetite.

3.4.1 Off-state Viscosity

The most critical off-state property of MR-fluids is the field-independent viscosity (η). This is because of its direct impact on the velocity-dependent minimum output force. This may be also due to torque of a given device in the absence of magnetic field. In addition to this, this viscosity is also accountable for the temperature dependence of the device output force or device output torque.

The intrinsic viscosity of the carrier fluid and the particle volume fraction are two major parameters affecting the viscosity of the MR-fluid. If particle volume fraction is higher, the

MR-fluid viscosity is also higher. Most MR-fluid viscosities are in the range from 50 to 200mPas at room temperature [27].

3.4.2 Yield Stress

The field-dependent maximum yield stress (τ_y) is the utmost critical on-state property of MR fluids. This is because of its direct impact on the maximum output force or torque of a given device.

The value of maximum yield stress increases in proportion to the square of the saturation magnetization of the particles due to particles materials [16].

The particle volume fraction is another factor affecting the maximum yield stress. Rabinow, in 1954 [33], identified and showed that when there is increase in particle volume fraction, there is also increase in the output torque of MR-fluid clutch. Since then, number of researchers have studied this effect [33, 52] and have shown that the maximum yield stress increases non-linearly with growing particle volume fraction [53] (Fig. 3.4a). Unfortunately, the off-state plastic viscosity also increases when particle volume fraction increases. This phenomena occurs even at faster rate than the yield stress (Fig. 3.4b). This further leads to decrease in potential dynamic range (ratio between maximum and off-state force and torque) of a device using this kind of fluids.

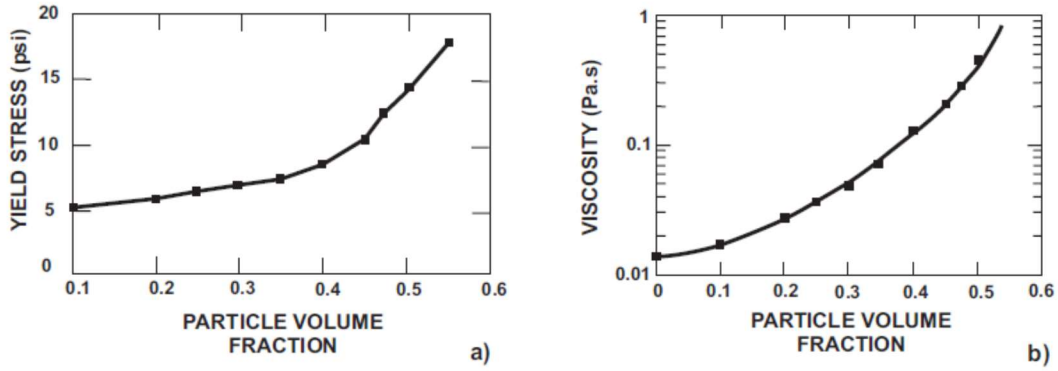

FIGURE 3.4:

(a) Maximum yield stress versus particle volume fraction (under magnetic flux density of 1Tesla)

(b) Viscosity versus particle volume fraction [adapted from 53]

Alternatively, one more method to increase the maximum yield stress is to increase the particle size distribution inside the MR-fluid. The advantage of this method is that it allows the viscosity reduction in upholding the same particle volume fraction [66]. A particular

case of this method is to use bimodal particle distributions. In bimodal particle distribution, two different size groups of particles are combined [20, 53, 67].As shown in Fig. 3.5, substantial increase in yield stress can be achieved by small increase in the proportion of small particles (25% in weight). This effect can be explained by an increased particle packing when chains are formed.

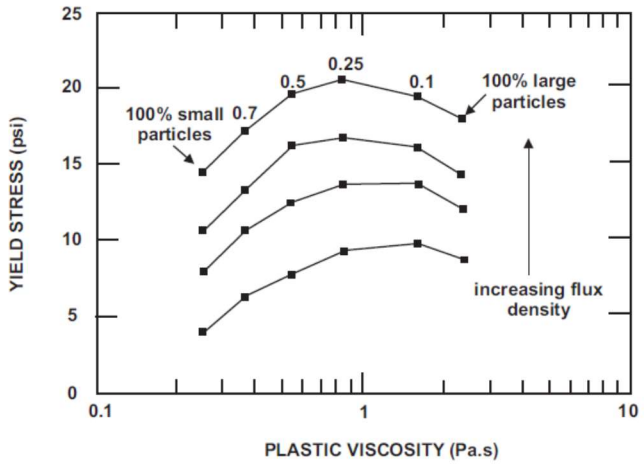

FIGURE 3.5: Maximum yield stress versus plastic viscosity for various bimodal formulations (unchanged total particle weight fraction of 55%) [Adapted from 53]

Fig. 3.6 show graphs of the yield stress (τ_y) versus magnetic field (H) for some typical MR-fluids from LORD Corporation and ISC FraunhoferInstitutSilicatforschung (data obtained from product datasheets).

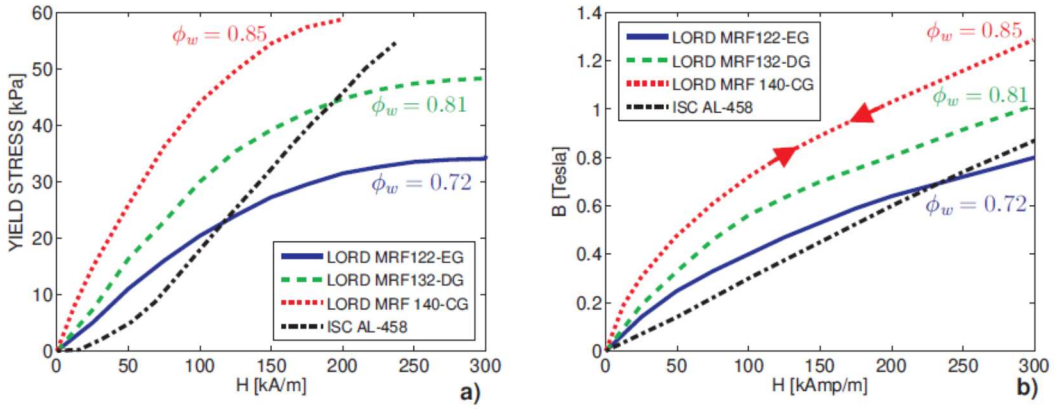

FIGURE 3.6:

(a) Maximum yield stress versus magnetic field (b) B-H characteristic, for various fluid formulations (ϕ_w is the particle weight fraction)

Very different behaviours can be observed due to different fluid formulations (in particular various particle weight fractions, ϕ_w). Furthermore, differences between the shape of the curves for LORD and ISC fluids may also be explained by different experimental protocols used to measure the yield stress. For the fluids provided by LORD Corporation, it can be seen that the yield stress begins to saturate for magnetic fields above 250kA/m.

3.4.3 B-H Relationship

The B-H curve characteristic of MR fluid provided by LORD within the advantageous span is mostly non-linear whereas it is linear if fluid is ISC (Fraunhofer Institut Silicatforschung). This is based on the data extracted from the respective product sheets. This kind of difference may be described based on different MR fluid properties, experimental protocols and formulation processes. For various fluid formations, fig3.6 (b) is plotted for induction field (B) on Y axis and magnetic field (H) on X axis.

From the B-H curve plotted in fig.3.6 (b), it can be interpreted that there is no or very little hysteresis. Such kind of behaviour is the result of magnetically soft properties which are made from the iron used for the particles. In addition to this, this is also result of the mobility of these particles [5].

3.4.4 Durability and In-Use-Thickening

By the end of 1990s, durability tests were executed on MR fluids. These test results concluded that when an ordinary MR fluid experiences high stress and high shear rate for longer time period, it is thickened [38]. This phenomena is also defined as “In-Use-Thickening (IUT)”. Initially an MR fluid shows low value of off-state viscosity. Afterwards as MR fluid progresses further, off-state viscosity is increased and it thickens until it ultimately changes to thick paste. However such phase is not advisable for normal applications.

When MR fluid is subjected to stress for continuous longer time, the friable surface layer of the iron particles peals away. Further it also breaks into small pieces and gets separated from the primary particles. This kind of phenomena occurs because of IUT. This is very true for specifically carbonyl iron particles having onion skin structure. Use of particles having higher hardness and/or with the use of anti-wear and anti-friction additives (at levels of 0.5 to 3% by volume) is one of the better solution to such phenomena [66].

3.5 Basics of Rheological Properties

Basically the study of the flow properties and the behaviour or the response of materials to applied stress is defined as Rheology [43]. Rheology is an interdisciplinary field and is used to define the properties of various types of materials such as oil, food, ink, polymers, clay, concrete, asphalt and others. A rheometer is an instrument used to measure the rheological properties of the material and it works on the principal of a viscometer. Variety of rheometers are available having useful controls. Some of the rheometers with controls are stress and/or strain rheometers and capillary rheometers. For variety of industrial applications, important interpretations are derived for product and process performance from the data of rheological properties measured for suspension, colloidal dispersion and emulsion. For proper performance and efficient process, materials must be stable [43].Stability is often affected by complex formulations of solvents (or fluids), suspended particles of varying sizes & shapes and various additives used.

Following factors are included which affects the stability:

i. Hydrodynamic forces
ii. Brownian motion
iii. Strength of the antiparticles interaction
iv. Volume fraction
v. Electrostatic forces
vi. Size & shape of particles
vii. Steric repulsion

Above factors are accountable for the unique rheological properties of MR fluids. For example, a quick formation of a network in response to an external field generates a rapid liquid-to-solid transition [44]. Rheology measurement of any particular MR fluid formulation is also signs of the colloidal state and the interactions taking place in it. To predict the flocculation, coagulation or coalescence of any formulation, rheology-based measurements are helpful. Such kinds of formulations gives undesired effects such as settling, creaming, separation and others.

Followings are brief behaviour of such kinds of formulations:

- Flocculation is referred as the process in which particles are initiated to stick together in flock (formation of loose or open aggregates)

- Coagulation is referred as the process in which dispersed colloidal particles agglomerate (formation of compact aggregates)
- Coalescence is referred as the process in which the boundary between two particles in contact disappears or is referred as the process in which particles merge and pull each other to make the slightest contact

Normally rheology measurements and derived parameters from such parameters are used to determine followings:

i. Processing behaviour of non-Newtonian materials
ii. Viscoelastic behaviour as a function of time
iii. The degree of stability of a formulation at rest condition
iv. The degree of stability of a formulation during transportation
v. Zero shear viscosity or the maximum viscosity of the fluid phase to prevent sedimentation

Einstein about 100 years ago developed the viscosity equation on the basis of a hydrodynamic theory for dilute dispersions of spherical particles [45]. This equation is expressed as under:

$$\eta_r = 1 + 2.5\phi \tag{3.5}$$

In above equation, η_r expresses the relative viscosity of the suspension and ϕ expresses the volume fraction of the suspended solutes or particles. In this equation, particles are assumed to be spherical. To increase the amount of particles and consequently to increase the volume fraction of the particles, addition of the solid particles to the liquid is required. It should also be noted that as there is increase in volume fraction of particles, there will be an increase in the fluid's viscosity also. Poloskiet at. al. [46] has suggested to incorporate the maximum concentration of the particles $\phi_{\max}$ in the relationship between viscosity and concentration. Such expression is given as under:

$$\eta_r = \frac{1-0.5\phi}{(1-\phi)^3} \tag{3.6}$$

and

$$\eta_r = \frac{1+0.5\kappa\phi-\phi}{(1-\kappa\phi)^2(1-\phi)} \tag{3.7}$$

In above expressions, κ is the correction factor which may be dependent on particles size and concentration. When κ =1, the size effect is neglected and equation (3.7) is transformed into equation (3.6).

Addition of solid particles increases the viscosity of the fluid. Off course at this instant, fluid behaviour changes and diverges from a Newtonian fluid. Newtonian fluid has the stress at any point is proportional to the applied strain rate at that point. Shear stress τ increases with the shear rate $\frac{du}{dy}$ which often can be expressed by the relationship as under:

$$\tau = \tau_y + \eta \left(\frac{du}{dy}\right)^m \tag{3.8}$$

Where τ_y, η and m are constants. τ_y is the yield stress and η is the dynamic viscosity.

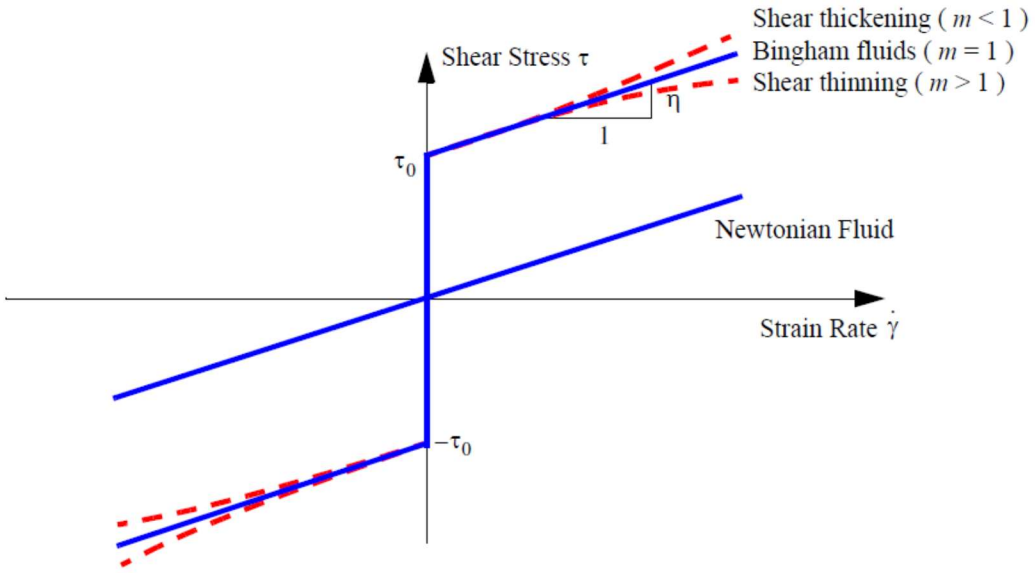

FIGURE 3.7: Visco-plasticity models of MR fluids.

When fluid indicate zero yield stress and m = 1, it is said to be Newtonian fluid. This is shown in Fig. 3.7. The viscosity of a Newtonian fluid is not dependent on time and shear rate. However when shear is applied, viscosity changes and this leads to change the behaviour of Newtonian fluid. Such kind of change in behaviour of Newtonian fluid converts it in to a non-Newtonian fluid.

The described behaviour of fluids leads to classify them in to Newtonian fluids and non-Newtonian fluids. Examples of non-Newtonian fluids includes plastic, Bingham plastic, pseudo-plastic and dilatant fluids [43]. When shear stress is applied, fluid begins to change

its phase. During this application, the fluid is said to be plastic when the value of minimum shear stress applied at the state just before fluid begins to flow is attained. Referring equation 3.8, if m=1, the fluid is said to be Bingham plastic. When applied shear stress is increased, dynamic viscosity reduces and under these circumstances, the fluids are said to be pseudo-plastic or shear-thinning fluid. In contrast to this kind of phenomena; that is when applied shear stress is increased, dynamic viscosity also increases; fluids are said to be shear-thickening or dilatant fluids. Such kinds of fluids are also known as pseudo-plastics. If τ_y, in equation 3-8, is equal to 0, the shear thickening fluid is characterised by $m > 1$ and shear thinning fluid by $m < 1$.

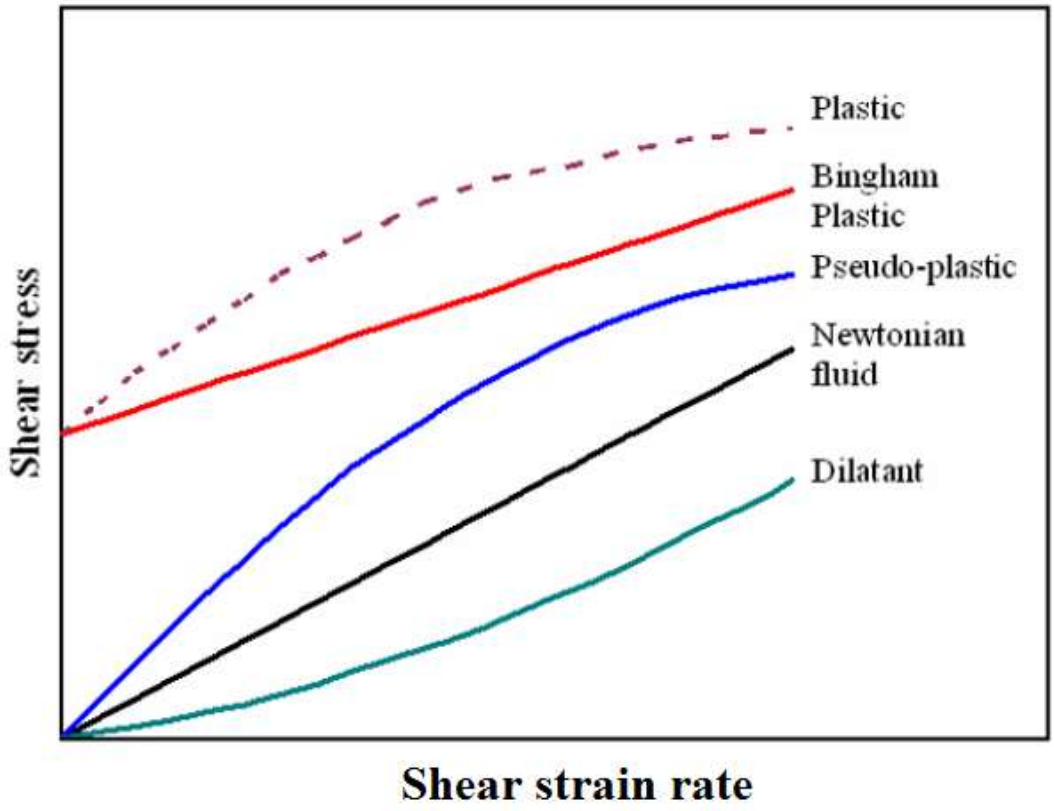

FIGURE 3.8: Classification types of the behaviour of the fluids [43].

Rheopecty and thixotropy are few more non-Newtonian behaviour or time dependent properties [43]. From principle point of view, shear thickening and shear thinning proceeds from rheopecty and rheopecty respectively. The fluid is said to be rheopectic if during the application of shear stress, apparent viscosity increases. In contrast to this, if the apparent viscosity decreases with the duration of stress, the fluid is then said to be thixotropic. In place of breakdown due to collision of the attractive particles, when temporary aggregation due to interaction between the particles takes place, there is occurrence of rheopectic. However when there is breakdown of the microstructure and it behaves like a liquid, it

decreases the viscosity of the thixotropic fluid. This time related behaviour is reversible. That is when stress is released, the structure which was disturbed by shearing builds up in the thixotropic material and breaks down in the rheopectic material. In this manner, the material is settled and regains its original consistency.

3.5.1 Basic Principles of MR Fluids

MR fluids are responsive to the applied external field and due to this, particles are arranged together and forms chains parallel to the applied field. The continuous interaction between the particles is delayed to a specific level of the shear stress and this causes the increases in the viscosity of the fluids [48]. In the majority of the cases, such kind of effect of MR fluid is described by Bingham Plastic model [25]. Few more models are also used to describe the behaviour of MR fluid [49, 50]. These includes the modified or extended Bingham model, combination of Bingham model with other models such as viscous and coulomb friction. When external field is removed, MR fluid behaves like normal fluid. This is also known as Newtonian fluid. Rheological studies have shown and led to the concept of dynamic yield stress. Rheology basically studies the interrelationship of shear stress and shear strain of solid and liquid materials. The conceptual behaviour of a fluid element under shear stress application is exhibited in Fig. 3.9.

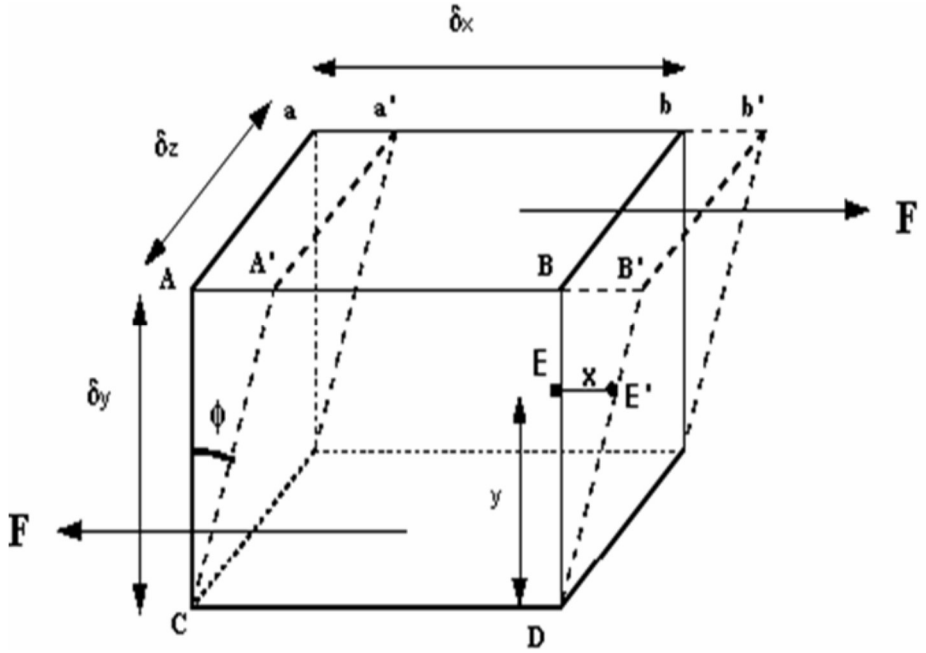

FIGURE 3.9: Fluid element under a shear force [51].

Referring Fig. 3.9, it can be seen that on application of shear force F on the top of the element area, shear stress is calculated by taking the ratio of force over effective area. This ratio is also termed as force per unit area. This ratio can be expressed as under.

$$ShearStress\tau = \frac{F(Force)}{A(Area)} \quad (3.9)$$

Where Area = $\delta_x\delta_z$ (as shown in Fig. 3.9)

Shear stress produces the shear strain which can be measured by the size of the angle ϕ. For a fixed value of shear stress in a solid state the value of ϕ is constant. However depending on the time duration, the value of ϕ is proportional to the applied shear stress for the fluid state.

Distance x is on account of shear stress and can be defined as the small particle movement from point E to point E'.

$$ShearSrain, \gamma = \frac{x}{y} \quad (3.10)$$

$$RateofShearSrain, \dot{\gamma} = \frac{\gamma}{t} = \frac{x}{ty} = \frac{x}{t}\frac{1}{y} = \frac{u}{y} \quad (3.11)$$

Where $\frac{x}{t} = u$ is the velocity of the particle at E.

Shear stress is proportional to the rate of shear strain, therefore:

$$\tau = Constant * tant * \frac{u}{y} \quad (3.12)$$

The term $\frac{u}{y}$ is the change in velocity with y, or the velocity gradient, and may be written in the differential form $\frac{du}{dy}$. The constant of proportionality is known as the dynamic viscosity η of the fluid, giving equation as under:

$$\tau = \eta\frac{du}{dy} = \eta\dot{\gamma} \quad (3.13)$$

Equation (3-13) can be recognized as a Newtonian fluid's equation.

For a non-Newtonian fluid with shear stress τ above the yield stress τ_y, the equation can be represented by Bingham plastic's equation as:

$$\tau = \tau_y + \eta\dot{\gamma} \text{ for } \tau > \tau_y \quad (3.14)$$

Below the yield stress, material behaves viscoelastically as denoted by:

$$\tau = G\gamma \text{ for } \tau < \tau_y \quad (3.15)$$

Where G is the complex material modulus. If the shear stress τ and shear strain rate $\dot{\gamma}$ are known, the kinematic viscosity ν can be calculated from,

$$\nu = \frac{\eta}{\rho} \tag{3.16}$$

Where ρ is the density of the fluid and η is the dynamic viscosity.

3.5.2 Rheology of MR Fluids

The suspension of magnetically soft micron-sized particles in a carrier liquid is known as MR fluid. When MR fluid is subjected to magnetic field, it exhibits an ability to change its viscosity within fraction of seconds by multi orders of magnitude.

Followings factors governs the rheological properties of controllable MR fluid:

i. Concentration
ii. Density of particles
iii. Particle size
iv. Particle shape distribution
v. Properties of the carrier fluid [31, 54]
vi. Additional additives
vii. Applied field, and
viii. Temperature.

Above all factors are complex and interrelated with each other. They are useful in setting procedure to improve the efficiency of MR fluids for appropriate applications.

An excellent MR fluid have following characteristics:

i. Low viscosity
ii. Low coercivity of particles without the influence of an external magnetic field, and
iii. Can achieve maximum yield stress when external magnetic field is applied

Gross [34] in his research on the valve used for magnetic fluids invented that the advantage of bigger particle sizes or heavy suspensions can raise the size of the gap. This helps to increase the flow of the fluid. On other hand, the bigger particles of the magnetically active phase of MR fluids lead to a strong tendency for particles to settle out of the liquid phase [39].

In order to have general use, few techniques are important to enhance the yield stress. This is done in two ways. One by increasing the volume fraction of MR particles and another by increasing the strength of the applied magnetic field. Off course both these ways yields with increase in the overall off-state viscosity of the material and increase volume fraction of the MR particles. In addition, increased volume fraction of the MR particles may

increase the weight of MR devices also. In this context, none of the ways is desirable. In this continuation only, if size and geometry of MR device are restricted, it significantly increases the power requirement of the device. Here it should be noted that MR devices are assumed to be capable of utilizing that material and a higher magnetic field. According to Carlson and Weiss [52] patents, such difficulties can be dissolved by introducing alloy-particles material as solid particles in place of common carbonyl iron. This MR fluid then enhances yield stress independently. Such enhancement then do not require increment of either the volume fraction of particles or magnetic field strength.

3.5.3 Off- and On-State Rheology

The uniqueness of MR fluids includes minimization of the off-state viscosity and maximization of the yield stress of the fluid [53]. To attain optimum MR effect, both off-state viscosity and the on-state yield stress are very significant. The ratio of differences between off-state viscosity and on-state yield stress is defined as turn-up ratio. The turn-up ratio is also defined as the ratio of the force output when MR fluid is magnetically activated with on-state phase to the force output in the off-state controlled by viscosity. As stated earlier, the increase in the volume fraction of the particle can increase the yield stress and viscosity of MR fluids. At any instance, both on- and off-states of MR fluids are linked. This is in context to maximize the on-state yield stress by increasing the solid volume fraction. This will lead to cause a great penalty in turn-up ratio since the viscosity in the off-state will also be increased at the same time [20]. When the material is in the turned off condition, relatively high viscosity has to be allowed to achieve suitably high yield stress. It can also be said that material containing particles of a single particle size mode may lead to have crucial turn-up ratio. Hence it may be advisable to maximize the turn-up ratio. Turn-up ratio may be significantly improved with mixture of two different particle sizes or bi-model [53].

When magnetic field is zero, the viscosity of controllable fluid ranges from 0.1 KPa-s to 1.0 KPa-s [39] and this depends on following factors:

i. Function of carrier liquid
ii. Additives
iii. Surfactants [31]
iv. Particle loading. and
v. Particle size distribution [54].

Chains are formed when field is applied under field responsive effect. This induce a dipole moment in each particle in the same direction of the magnetic field. When such chains formations are subjected to magnetic field, they increases yield stress at least by 100 times [39]. When high magnetic field is applied, magnetically soft particles are changed to solid within milliseconds. However as soon magnetic field is removed, they largely and uniformly re-disperses in the solvent. According to Foister [53], when fluid is at the off-state condition, the blend of large and small particles do not cause any change in the viscosity but it causes an increase in yield stress. It can also be stated that off-state viscosity and on-state yield stress are affected by the size distribution of particles since particles of different sizes may have different magnetic properties. It is also true to say that turn-up ratio can be increased by using volume fraction of a bimodal particle population with appropriate fraction of the small particles [54].

3.5.4 Volume Fraction and Particle Size Factors

Previous few studies on the field-induced structures have contributed to identify the fundamental properties of MR fluids. Researchers have identified that the cell thickness and the volume fraction of particles are the driving parameters for the structures of self-assembly MR fluids [28, 54]. An increase in the magnetic flux density is directly proportional to the increase in the volume fraction of particles of the fluid [5]. This leads to increase the yield stress also. In order to realise this phenomena, Simon et. al. developed a mathematical model based on the theory of homogenization [55]. However, this model excluded the consideration of particle shapes and the microstructure of the fluid. According to Lemaire et. al., when the fluid undergoes phase transition from liquid to solid, the structure of MR fluid with low volume fraction was found as uniformly spaced columns [28]. Lemaire et. al. had also observed that at a higher volume fraction and with 0.5 μm particles size, the shape experiences a change from an ellipsoid shape to a cylinder shape of particle size 100 - 400 μm. Another researcher Bossis et. al. observed the formation of a periodic planar structure in the plane of rotation of the field between parallel walls [54]. They also concluded that the shape of the domain is driven by the geometry of the cell. The structures become complex (either the pattern forms like individual chains, walls or a mixture of chains and walls) and in turn it is highly reliant on the cell thickness. Srikala et. al. [41] observed and stated that compared to microsphere shaped particles, aligned magnetic rods forms uniform structures having larger magnetic anisotropy of particulate magnetic materials. Davis et. al. [56] also observed the roll-slip behaviour. The

researcher also identified that there is effect of surface roughness on viscosity. For this case, it reduces the effective viscosity. This is also due to reduction in the viscous dissipation of flowing suspensions.

Hydrodynamic interactions with each other and with the walls of the container is experienced by colloidal particles at high volume fraction. The friction on account of this phenomenon at about half of the concentration results in significant increase in the viscosity. Other than that, following parameters also contribute strongly to determine the viscosity:

i. Particle size distribution [54]
ii. Particle shape [41, 59]
iii. Surface roughness [56]

Further, larger particle sizes give higher yield stress and they consume more magnetization compared to fine particles [15]. In present era, particles for MR fluids have spherical shapes. According to Starkovich and Shtarkman [22], particles with non-conventional shapes like cubic or cylindrical shapes are able to exert at least 10 times higher yield stress compared to the conventional shapes. This phenomenon is due to following reasons:

i. Increase in packing density
ii. Improved field homogeneity
iii. Larger interaction (contact area)

This generates the necessary forces between the particles even at the low intensity level of magnetic fields. In addition to this, such shapes add to a larger magnetic anisotropy compared to the spherical shapes [41].

Normally magnetic characteristics (such as permeability) of the MR fluids are driven by the volume fraction but are independent from the type of particle size distribution [20]. To achieve required yield stress which is based on the volume fraction of bimodal particle population, it is necessary to reduce the off-state viscosity. Off-state viscosity can be reduced by utilizing proper fraction of the small particle sizes. The off-state viscosity is largely dependent on combination of small and big particles. In order to control off-state viscosity, it is evident that sizes of the small and large particles in the bimodal size distribution families have to be controlled. For fixed size of larger particles, size ratio directly affects the off-state viscosity according to Bossiset et. al. [54]. For a fixed size of larger particles, minimum viscosity is achieved at a higher volume ratio of smaller particles in the system if size ratio is enhanced. When larger particles are used, they create voids. To

fill up such voids, small particles are used which in turn produces efficient packing structure and forms better distinct chains [25]. In addition to this, small particles also help to reduce to great extent the settling rate of MR fluid. For a fixed volume fraction of solid, if a ratio of particle sizes is at least five times larger, it will raise the on-state yield stress and it will not affect the off-state viscosity also [53].

3.6 Operating Modes of MR-Fluids

Following are different modes (Fig. 3.10) on which MR fluids are operated:

i. Valve mode
ii. Direct shear mode
iii. Squeeze mode
iv. Pinch mode

Two modes, namely valve and direct shear, are widely applied whereas amongst remaining modes, squeeze mode is rarely used and pinch mode has started recognisation in recent time only [69].

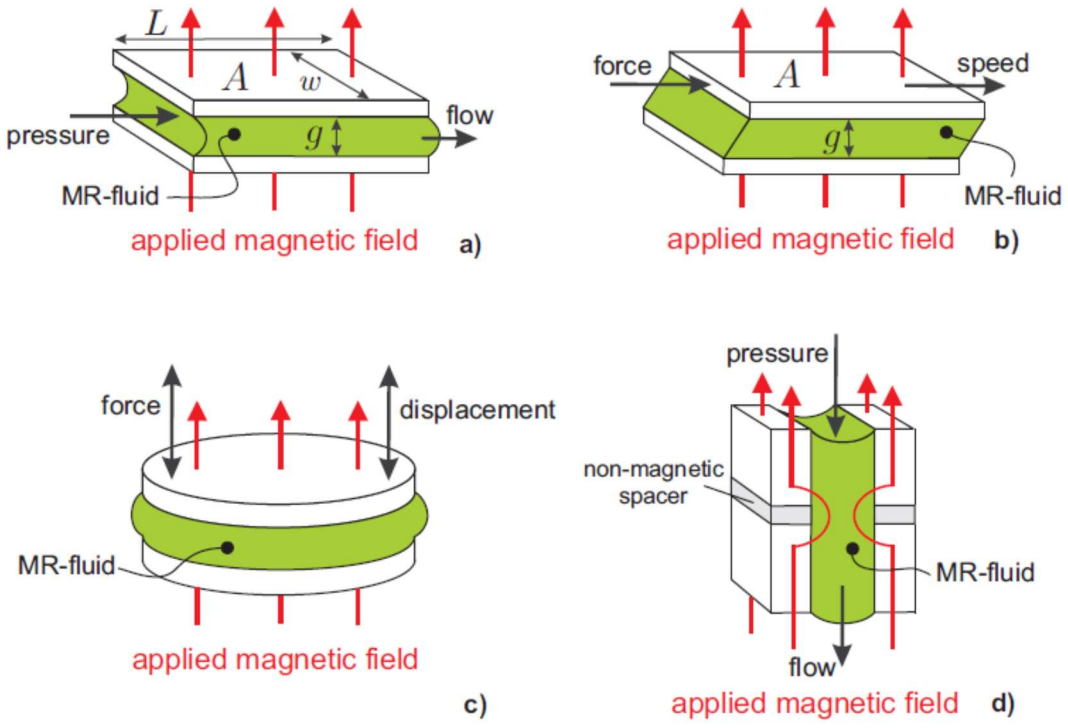

FIGURE 3.10: Operating modes of MR-fluids [73]:
(a) Valve mode (b) direct shear mode (c) squeeze mode (d) pinch mode

3.6.1 Valve Mode

In the valve mode (Fig. 3.10a), the external magnetic field is applied perpendicular to flow direction of MR fluid which is flows through channel. However such flow experiences resistance proportional to magnetic field intensity. In other words, it can be said that applied magnetic field can be used to monitor and control the resistance and such control is established without any mechanism. Such devices have broader applications and are valve mode devices consisting fundamentally dampers and shock absorbers.

3.6.2 Direct Shear Mode

In the direct shear mode (Fig. 3.10b), the MR fluid is kept in-between two poles. These poles are parallel to each other. In this position, external magnetic field perpendicular to poles is applied. One of the pole is moved relative to another pole by applying external force and due to this phenomena, MR fluid layer experiences direct shear. Here the amount of force required to shear the fluid layer is dependent on following two major factors:

i. Intensity of applied magnetic field
ii. Resulting shear stress developed in the MR fluid

Normally brakes and clutches are considered for broader range of applications working on this mode. This mode is used in the device described in this thesis.

3.6.3 Squeeze Mode

In the squeeze mode (Fig. 3.10c) [70], the MR fluid is kept in-between two poles. These poles are parallel to each other. In this position, external magnetic field perpendicular to poles is applied. One of the pole is moved towards another pole by applying external force perpendicular to one of the pole and due to this phenomena, MR fluid is compressed. It is evident that distance travelled by one of the pole towards another pole is dependent on intensity of applied magnetic field. This distance travelled, also termed as displacement, has very small amplitudes ranges up to few millimetres only but has very high resistive force. Even though the application range is too low, this mode has found the applications for small vibration and impact dampers [71, 72].

3.6.4 Pinch Mode

In the pinch mode (Fig. 3.10d), as for the valve mode, the MR-fluid flows through a channel. But, here the external magnetic field is applied more or less parallel to the flow direction by arranging the poles axially along the flow path and separating them by a non-

magnetic spacer. On the contrary to all previous operating modes, such configuration leads to a highly non-uniform magnetic field inside the MR-fluid. The main idea is rather than solidifying the fluid throughout the valve (as in the valve mode), the MR-fluid is solidified by the magnetic field only near the walls, changing in that way the effective orifice diameter through which the fluid flows [69].

3.7 Applications of MR Fluid

3.7.1 Dampers and shock absorbers

MR-fluid dampers and shock absorbers developments have mainly been driven by the requirements of the automotive industries and these industries are largely benefited from previous R&D work conducted on ER-fluid devices in the 1980s.

Early commercial products appeared in 1998 with MR-fluid dampers to be used in semi active seat suspensions for trucks and with adjustable MR-fluid based primary suspension for racing cars [73]. However, the first real commercial breakthrough was made in 2002 with the introduction by Delphi, of the MagneRide developed by Delphi. This was the first commercial suspension system having real-time controllable MR-fluid dampers that automatically adapt to changing road conditions with a faster response time, fewer moving parts and lower power requirements than previous hydraulic systems shown in Fig. 3.11.

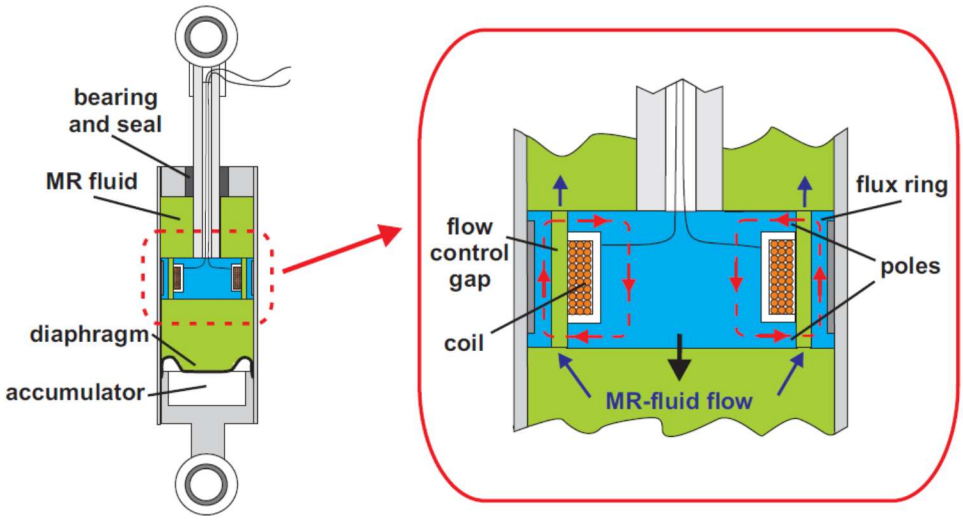

FIGURE 3.11: Schematic cross-section view of a magneto-rheological damper [adapted from 73]

Another application under development for the automotive industry is the MR-fluid engine vibration isolation. Using MR-fluids inside such engine mounts allows to modify their

stiffness in real-time and achieve the best possible isolation for each RPM of the engine shown in Fig. 3.12 [68, 73].

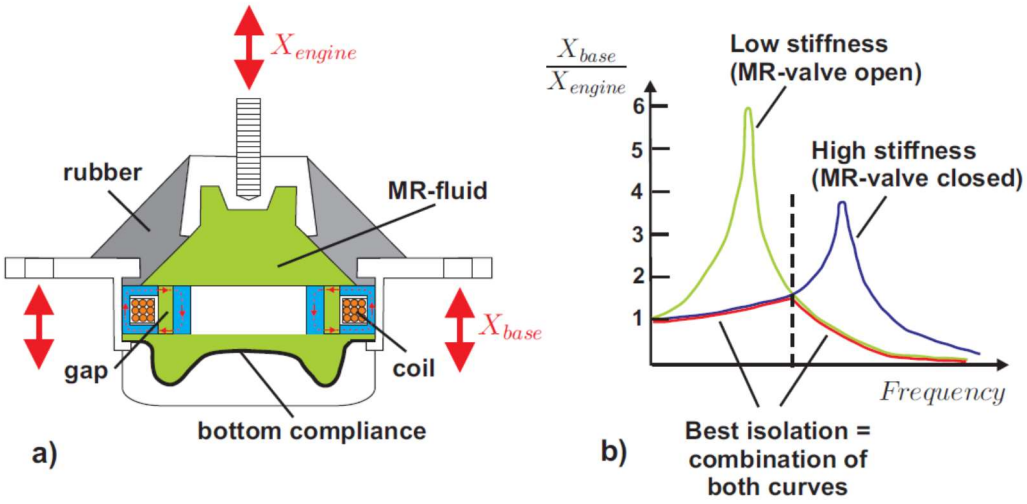

FIGURE 3.12: (a) MR-fluid engine mount (b) vibration isolation performances [adapted from 73]

The automotive industry is not the only one to benefit from developments in the field of MR-fluid devices. Large MR-fluid dampers (capacity up to 300kN) (Fig. 3.13a) have also been developed and implemented for semi-active vibration control in civil engineering structures. They have been used in bridges and buildings to limit the effects of seismic and wind excitation [73]. It is important to note that for seismic applications, sedimentation is a real issue since the damper may not be used for a very long period of time.

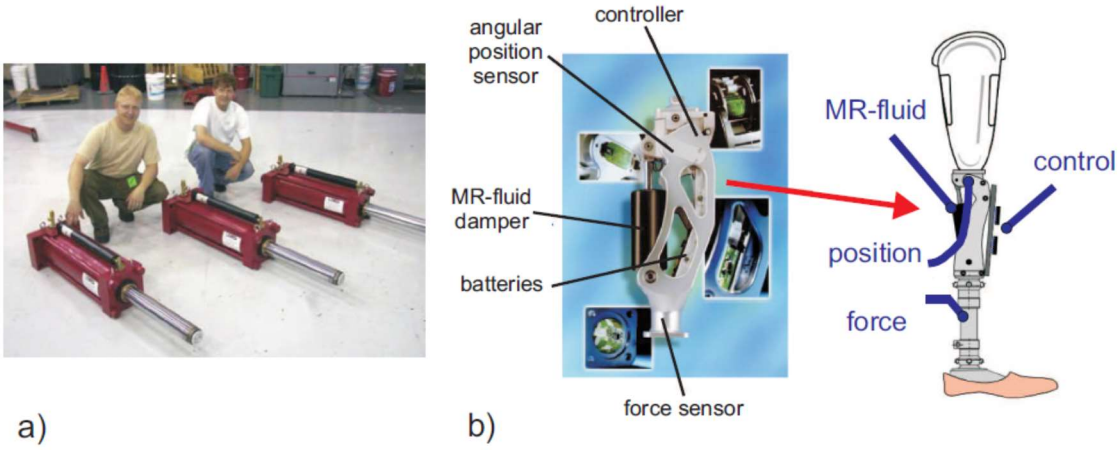

FIGURE 3.13: (a) MR-fluid high capacity dampers for vibration control in civil engineering structures
(b) Biedermann-Motech above-knee prosthesis based on MR-fluid damper
[Both (a) and (b) adapted from 73]

MR-fluid technology, thanks to its inherent compactness, has also been implemented in portable rehabilitation applications. In 2000, BiedermannMotech introduced an above-knee prosthesis based on a real-time controlled MR-fluid damper, increasing gait balance, stability (even when walking on stairs or ramps) and energy efficiency [74,75](Fig. 3.13b).

3.7.2 Brakes and Clutches

Despite the fact that, today, the major part of commercial MR-fluid devices is MR-dampers used in the automotive industry. This was first commercial application of a MR-fluid device introduced in 1995 as to exercise market as variable resistance brake for use in aerobic stair-climbers and cycling machines developed by Nautilus [73, 76](Fig. 3.14a). Indeed, such MR-brake was quieter, less expensive and more compact than previous eddy-current brakes. Furthermore, MR-brakes are running at much lower voltages which reduces the cost of power supply [73]. Unfortunately, due to the intense use to which some exercise equipment can be subjected, problems of fluid deterioration (IUT, see section 2.4.4) caused reliability issues. However in recent time, fluid formulation may solve this problem.

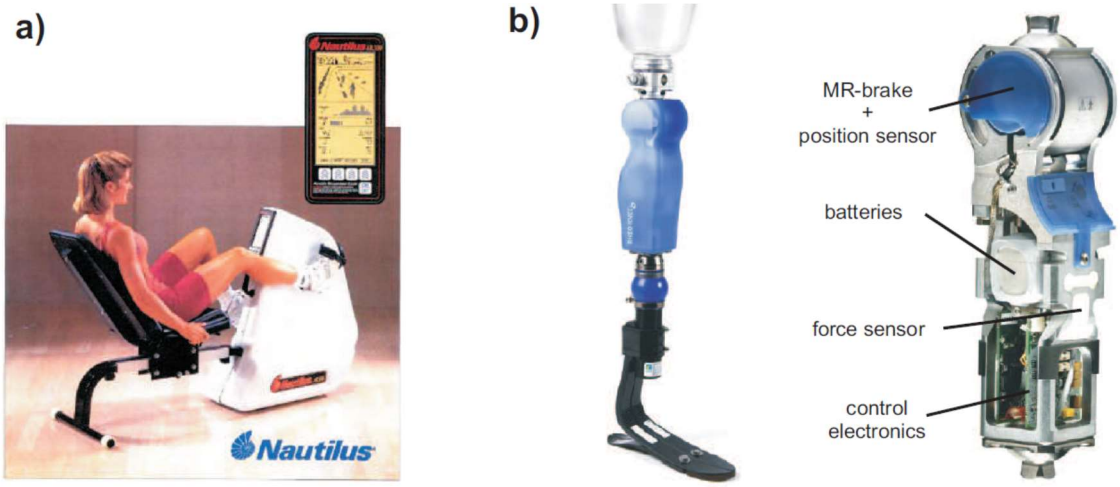

FIGURE 3.14: (a) Nautilus aerobic cycling machine (b) Rheoknee / knee prosthesis based on a rotary MR-brake commercialized by OSSUR [adapted from [77])

Real-time controlled “smart” prosthesis can also integrate rotary MR-brakes instead of linear MR-dampers. This is the case of the knee prosthesis developed by the MIT [78] and commercialized by OSSUR [77] (Fig. 3.14b). It seems indeed more logical to make use of a rotational device to implement the knee joint.

As can be seen on Fig. 3.14b, thanks to the high level of compactness of the MR-brake used (moment: 40Nm - diameter: 0.06m), all electronics, sensors and batteries can fit within the lower part of the prosthesis. Other applications in the same field and based on the same technology include “smart” orthoses for various human joints as described in the patent by [73]. Some developments in this area have already been conducted by Furusho et. al., 2007 [79], leading to a first prototype of ankle-orthosis.

Force-feedback (haptic) interfaces also benefit from the high compactness and high torques of MR-brakes and clutches. Furthermore in such applications, brakes offer a major advantage over motors since they can only apply resistive forces ensuring user safety. This property is also a drawback since they cannot simulate all types of forces (like a spring in its extension phase, for instance). An example of industrial application is the use of a rotary brake implemented as actuator within a steer-by-wire system for electric forklift trucks eliminating the mechanical connection between the steering wheel and the ground wheels [73]. Two degree-of-freedom pantograph type haptic displays have also been developed by Yamaguchi et. al., 2003 [80], respectively using MR brakes and MR-clutches. The compactness and absence of backlash of MR-brakes have also been exploited in the development of haptic knobs to be used as multipurpose user interface in automotive vehicles.

Other automotive applications include the use of MR-clutches. Since 2003, General Motors studied the feasibility of using them as radiator fan drive clutches instead of conventional silicon oil clutches in trucks and SUVs with the objective of reducing the fuel consumption by 2.5%. This was because of lower off-state viscosity and smoother torque transitions [73]. MAGNA Powertrain, in cooperation with BASF also developed and tested a 700Nm MR-fluid rotational clutch used as a coupling unit between front and rear axle on a 4-wheel drive vehicle [73]. The results showed superior driving performance compared to what can be achieved with the current technology. Finally in 2002, preliminary tests in weightlessness have also been conducted by the NASA to validate the feasibility of using MR-brakes as part of deployment mechanisms for space structures.

As can be seen from these few examples, MR-fluid devices, thanks to their numerous advantages (compactness, high forces or torques, low power consumption, smoothness and safety of operation), can be used in a wide variety of fields ranging from automotive to rehabilitation. Many of these characteristics will also be exploited in the rehabilitation device described in this thesis.

CHAPTER 4
QUASI-STATIC MODELING FOR MR DAMPERS

This chapter presents two quasi-static models namely axisymmetric & parallel-plate model, based on the Navier-Stokes equation are established for MR damper behaviour. The Herschel-Bulkley visco-plasticity model is used to define the MR fluid field-dependent features and shear thinning/thickening effects. Simple equations created on these damper models are given which can be used in the initial design phase. Effects of geometry on Controllable force, dynamic range and MR damper performance are also discussed.

4.1 Introduction

Magneto rheological fluids (or simply "MR" fluids) be a member of a class of controllable fluids which react to an applied magnetic field with a dramatic change in their rheological behaviour. Generally, this change is expressed by a very big change of the dampeing force in which MR fluid is used. A small-scale MR fluid damper has been designed and constructed to show the scalability of MR fluid technology to devices of applicable size for engineering uses. A schematic diagram of the small-scale MR fluid damper is shown in Fig. 4.1. The damper uses a particularly simple geometry in which the outer cylindrical housing is part of the magnetic circuit. The operative fluid orifice is the whole annular space between the piston outside diameter and the inside of the damper cylinder housing. A detail explanation of this damper and a summary of nominal design parameters are specified in chapter 5.

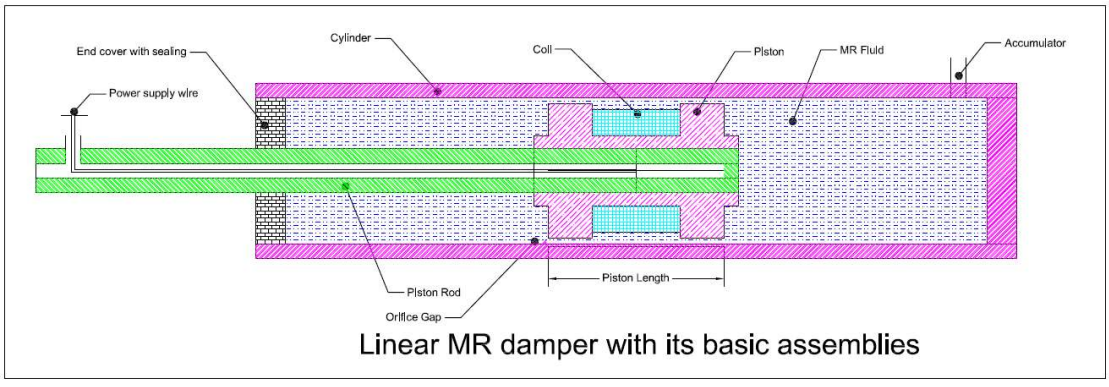

FIGURE 4.1 Schematic of small scale MR fluid damper

Fig. 4.1shows the fluids flow in the annular gap between the piston and the cylinder housing during motion of the MR damper piston.

Following assumptions are made for quasi-static analysis of MR fluid dampers:

1) MR fluid flow is fully developed
2) MR dampers move at a constant velocity; and
3) The Herschel-Bulkley visco-plasticity model is applied to describe MR fluid field-dependent characteristics and shear thinning/thickening properties.

The whole shear stress in the Herchel-Bulkley model is specified by:

$$\tau = (\tau_0(H) + K|\dot{\gamma}|^{\frac{1}{m}}) \operatorname{sgn}(\dot{\gamma}) \tag{4.1}$$

Where

τ_0= yield stress due to the applied magnetic field

H = magnitude of the applied magnetic field

$\dot{\gamma}$ = shear strain rate and

m, K = fluid parameters and $m, K > 0$.

Note that the Herschel-Bulkley model is reduce to the Bingham visco-plasticity model while the fluid parameter $m = 1$.

Many efforts have been made to develop quasi-static models for governable fluid damper investigation by the Bingham model of MR fluids. Phillips (1969) [59] established a set of non-dimensional variables and a corresponding quantic equation to describe the pressure gradient of flow through a parallel duct. This method was utilized by Gavin et. al. (2004) [26] in their studies. An axisymmetric model is necessary to exactly describe MR dampers quasi-static behaviour because of having cylindrical geometry. Gavin et. al. (2004) [26] developed such an axisymmetric model. From all these study, it is assumed that yield stress is constant in the annular gap. To account for the radial field distribution, Gavin et. al. (2004) [26] assumed that the yield stress satisfied an inverse power law.

To reflect MR fluid shear thinning/thickening properties, Wang and Gordaninejad (2001) [17] applied the Herschel-Bulkley model to predict fluid flow in a parallel duct with fixed boundaries. Wang and Gordaninejad also established an axisymmetric model for a circular pipe with constant yield stress. However, to precisely model the small-scale prototype damper given in Fig. 4.1, an annular duct model is necessary.

In the subsequent section, an axisymmetric model is established which is based on the Navier-Stokes equation for the MR flow through an annular duct. To accommodate MR fluid shear thinning/thickening properties, the Herschel-Bulkley visco-plasticity model is applied. The pressure gradient can be explained numerically from the resulting equations, and the damping force can then be calculated. The resulting equations of the Herschel-Bulkley model can be replaced by the Bingham model when the post-yield shear thinning or thickening effect is ignored by assigning the fluid parameter $m = 1$. Section 4.3 displays that a considerably simpler parallel-plate model is perfect for a wide range of device parameters and can be applied to examine the damper's behaviour. Simple equations based on the parallel-plate model are given which can be employed in the initial design phase. Controllable force, dynamic range and effects of geometry on MR damper performance are also discussed.

4.2 MR Fluid Flow in an Annular Duct

The pressure gradient along the flow is resisted by the fluid shear stress, which is governed by the Navier-Stokes equation (Constantinescu 1995):

$$\frac{\partial p}{\partial x} = \rho \frac{\partial}{\partial t} u_x(r) + \frac{\partial}{\partial r} \tau_{xr}(r) + \frac{\tau_{xr}(r)}{r} \tag{4.2}$$

Where

$u_x(r)$ = flow velocity

$\tau_{xr}(r)$= shear stress

r = radial co-ordinate

x= longitudinal co-ordinate

ρ = density of fluid and

$\frac{\partial p}{\partial x}$ = pressure gradient.

To analyse the quasi-static motion of the flow inside the damper, the fluid inertial can be ignored. Due to this effect, Eq. (4.2) can be expressed as:

$$\frac{dp}{dx} = \frac{d}{dr} \tau_{xr}(r) + \frac{\tau_{xr}(r)}{r} \tag{4.3}$$

It is important to note that for oscillatory or unsteady flow, the fluid inertia must be taken into account.

The solution of Eq. (4.3) is:

$$\tau_{rx}(r) = \frac{1}{2}\frac{dp(x)}{dx}r + \frac{D_1}{r} \tag{4.4}$$

Where D_1= a constant, can be estimated with boundary conditions.

A typical shear stress diagram along with variation of velocity for MR fluid flow through the annular gap is presented by Fig. 4.2 (Spencer et. al. 1998) [44]. In areas I and II, the shear stress has exceeded the yield stress and fluids flow. In area C, there is no shear flow. It is because of the shear stress is less than the yield stress. This is often referred to as the plug flow area.

4.2.1 Modelling based on the Herschel-Bulkley model

To interpretation for the fluid shear thinning or thickening influence, the Herschel-Bulkley visco-plasticity model is employed. In area I, the shear strain rate $\dot{\gamma} = \mathrm{d}u_x/\mathrm{dr} \geq 0$.

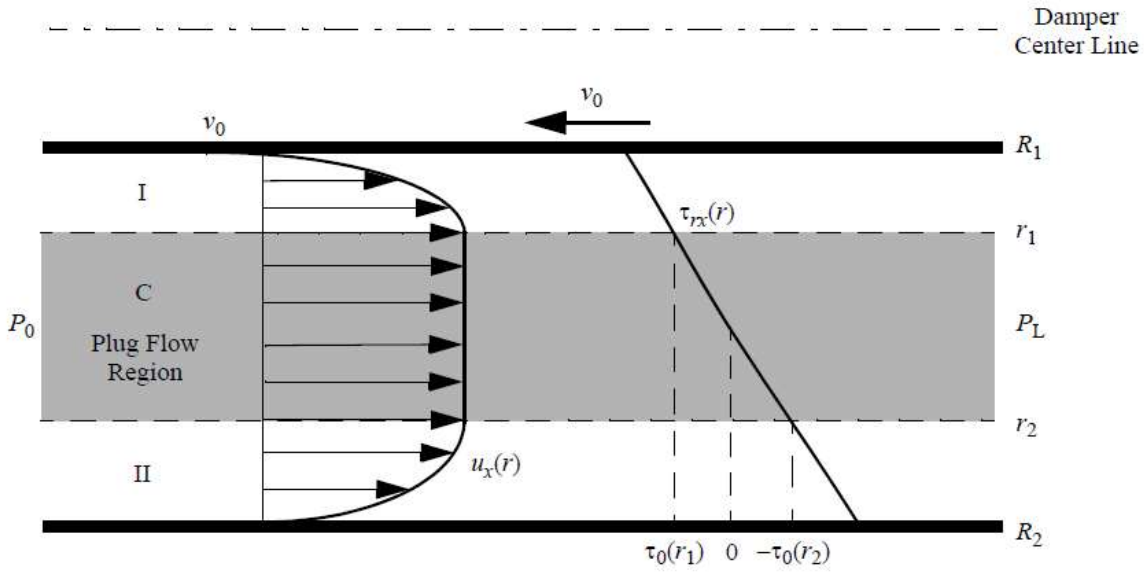

FIGURE 4.2: Velocity and stress profiles of MR fluids through an annular duct [63].

Hence, the shear stress $\tau_{rx}(r)$ given by Eq. (4.1) becomes:

$$\tau_{rx}(r) = \tau_0(r) + K\left(\frac{du_x(r)}{dr}\right)^{\frac{1}{m}} \tag{4.5}$$

This is replaced into Eq. (4.4) and integrated once with respect to *r*. One gets:

$$u_x(r) = \int_{R_1}^{r} \left[\frac{1}{K}\left(\frac{1}{2}\frac{dp(x)}{dx}r + \frac{D_1}{r} - \tau_0(r)\right)\right]^m dr - v_0 \qquad (R_1 \le r \le r_1) \tag{4.6}$$

By imposing the boundary condition that the flow velocity at $r = R_1$ is $u_x(R_1) = -v_0$

In area II, the shear strain rate $\dot{\gamma} = du_x/dr \le 0$. Therefore the shear stress is specified by:

$$\tau_{rx}(r) = -\tau_0(r) - K\left(-\frac{du_x(r)}{dr}\right)^{\frac{1}{m}} \tag{4.7}$$

Similarly, proceeding in area II with the boundary condition $u_x(R_2) = 0$ at $r = R_2$ gives:

$$u_x(r) = \int_{r}^{R_2} \left[-\frac{1}{K}\left(\frac{1}{2}\frac{dp(x)}{dx}r + \frac{D_1}{r} + \tau_0(r)\right)\right]^m dr \qquad (r_2 \le r \le R_2) \tag{4.8}$$

Note that the flow velocity is a constant in the plug flow area because the shear stress is less than the yield stress. Thus, the flow velocity at boundaries of the plug flow area satisfies $u_x(r_1) = u_x(r_2)$. Combining Eqs. (4.6) and (4.8) yields:

$$\int_{R_1}^{r_1} \left[\frac{1}{K}\left(\frac{1}{2}\frac{dp(x)}{dx}r + \frac{D_1}{r} - \tau_0(r)\right)\right]^m dr - \int_{r_2}^{R_2} \left[-\frac{1}{K}\left(\frac{1}{2}\frac{dp(x)}{dx}r + \frac{D_1}{r} + \tau_0(r)\right)\right]^m dr = v_0 \tag{4.9}$$

Also the shear stresses τ_{rx} satisfy $\tau_{rx}(r_1) = \tau_0(r_1)$ and $\tau_{rx}(r_2) = -\tau_0(r_2)$, therefore, D_1 can be determined by using Eq. (4.4) as:

$$D_1 = \frac{r_1 r_2(\tau_0(r_2)r_1 + \tau_0(r_1)r_2)}{r_2^2 - r_1^2} \tag{4.10}$$

The expression for the volume flow rate Q is given by:

$$Q = 2\pi \int_{R_1}^{R_2} r u_x(r) dr \tag{4.11}$$

Because the shear strain rate $du_x(r)/dr$ is zero in the plug flow region $r_1 < r < r_2$, Eq. (4.11) can also be written as:

$$Q = v_0 A_p = \pi R_1^2 v_0 - \pi \int_{R_1}^{r_1} r^2 \frac{du_x(r)}{dr} dr - \pi \int_{r_2}^{R_2} r^2 \frac{du_x(r)}{dr} dr \tag{4.12}$$

Where

A_p= cross section area of the piston head; and

v_0 = piston head velocity.

Substitution of Eqs. (4.6) and (4.8) into Eq. (4.12) gives:

$$Q = v_0 A_p = \pi R_1^2 v_0 - \pi \int_{R_1}^{r_1} r^2 \left[\frac{1}{K}\left(\frac{1}{2}\frac{dp(x)}{dx} r + \frac{D_1}{r} - \tau_0(r)\right)\right]^m dr + \pi \int_{r_2}^{R_2} r^2 \left[-\frac{1}{K}\left(\frac{1}{2}\frac{dp(x)}{dx} r + \frac{D_1}{r} + \tau_0(r)\right)\right]^m dr \quad (4.13)$$

Fig. 4.3 shows the free body diagram of MR fluids through an annular duct.

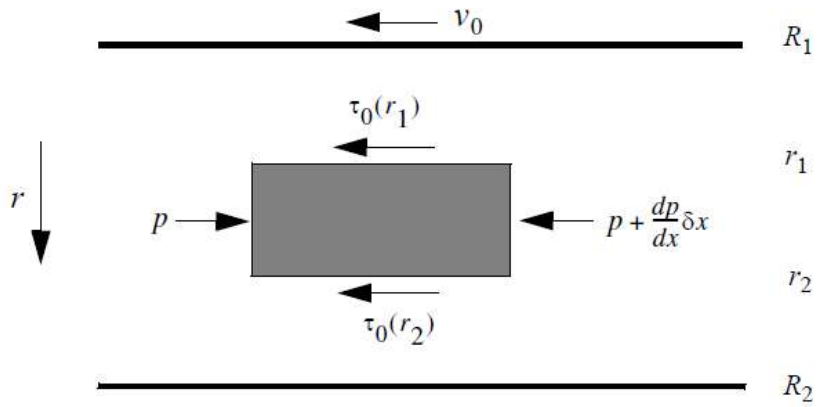

FIGURE 4.3: Free body diagram of MR fluids through an annular duct [63].

The equation of motion of fluid materials bounded by $r = r_1$ and $r = r_2$ is:

$$\frac{dp}{dx}\pi(r_2^2 - r_1^2)dx + 2\pi r_2 \tau_0(r_2)dx + 2\pi r_1 \tau_0(r_1)dx = 0 \quad (4.14)$$

These yields:

$$\frac{dp(x)}{dx}(r_2^2 - r_1^2) + 2[\tau_0(r_2)r_2 + \tau_0(r_1)r_1\,] = 0 \quad (4.15)$$

In summary, the resulting equations which can be solved numerically to determine r_1, r_2, and the pressure gradient dp/dx between the two ends of the cylinder using the Herschel-Bulkley model are given by:

$$v_0 = \int_{R_1}^{r_1} \left[\frac{1}{K}\left(\frac{1}{2}\frac{dp(x)}{dx}r + \frac{D_1}{r} - \tau_0(r)\right)\right]^m dr - \int_{r_2}^{R_2} \left[-\frac{1}{K}\left(\frac{1}{2}\frac{dp(x)}{dx}r + \frac{D_1}{r} + \tau_0(r)\right)\right]^m dr \tag{4.16}$$

$$\begin{aligned} Q = v_0 A_p = \pi R_1^2 v_0 & \\ - \pi \int_{R_1}^{r_1} r^2 & \left[\frac{1}{K}\left(\frac{1}{2}\frac{dp(x)}{dx}r + \frac{D_1}{r} - \tau_0(r)\right)\right]^m dr \\ + \pi \int_{r_2}^{R_2} r^2 & \left[-\frac{1}{K}\left(\frac{1}{2}\frac{dp(x)}{dx}r + \frac{D_1}{r} + \tau_0(r)\right)\right]^m dr \end{aligned} \tag{4.17}$$

$$\frac{dp(x)}{dx}(r_2^2 - r_1^2) + 2[\tau_0(r_2)r_2 + \tau_0(r_1)r_1\,] = 0 \tag{4.18}$$

Where

$$D_1 = \frac{r_1 r_2[\tau_0(r_2)r_1 + \tau_0(r_1)r_2\,]}{r_2^2 - r_1^2} \tag{4.19}$$

To solve the resulting algebraic equations numerically, a method based on the constrained nonlinear least-squares algorithm [87] is applied in combination with the cubic polynomial interpolation and extrapolation method. The integrals in Eqs. (4.16) and (4.17) are evaluated by the adaptive recursive Newton–Cotes approach [86].

From Eq. (4.18), the thickness of the plug flow region can be achieved by:

$$r_2 - r_1 = -\frac{2[\tau_0(r_1)r_1 + \tau_0(r_2)r_2\,]}{\frac{dp(x)}{dx}(r_2 + r_1)} \tag{4.20}$$

Which varies with the fluid yield stress τ_0. Note that the flow can only be established when $r_2 - r_1 < R_2 - R_1$, which implies that the plug flow needs to be within the gap. Otherwise, there is no flow.

The damper force is then computed as:

$$F = \Delta p A_p \tag{4.21}$$

Where $\Delta p = P_L - P_0 = -L(dp(x)/dx)$; and L = effective axial pole length. The velocity profile can be determined from Eqs. (4.6) and (4.8) as follows:

$$u_x(r) = \begin{cases} \int_{R_1}^{r} \left[\frac{1}{K}\left(\frac{1}{2}\frac{dp(x)}{dx}r + \frac{D_1}{r} - \tau_0(r)\right)\right]^m dr - v_0 & R_1 \le r \le r_1 \\ \int_{r_2}^{R_2} \left[-\frac{1}{K}\left(\frac{1}{2}\frac{dp(x)}{dx}r + \frac{D_1}{r} + \tau_0(r)\right)\right]^m dr & r_1 < r < r_2 \\ \int_{r}^{R_2} \left[-\frac{1}{K}\left(\frac{1}{2}\frac{dp(x)}{dx}r + \frac{D_1}{r} + \tau_0(r)\right)\right]^m dr & r_2 \le r \le R_2 \end{cases} \tag{4.22}$$

Further, the shear stress illustration can be achieved from Eq. (4.4).

Note that when the yield stress $\tau_0 = 0$, there is no plug flow area which indicates that $r_2 = r_1$. Hence, Eqs. (4.18) and (4.19) are no longer effective due to the singularity. On the other hand, in this case, the velocity reaches its maximum at $r = r_1$ wherever the shear stress is zero. By using Eq. (4.4), the subsequent equations can be employed to find pressure gradient when yield stress $\tau_0 = 0$:

$$v_0 = \int_{R_1}^{r_1} \left[\frac{1}{K}\left\{\frac{1}{2}\frac{dp(x)}{dx}r + \frac{D_1}{r}\right\}\right]^m dr - \int_{r_1}^{R_2} \left[-\frac{1}{K}\left\{\frac{1}{2}\frac{dp(x)}{dx}r + \frac{D_1}{r}\right\}\right]^m dr \tag{4.23}$$

$$Q = v_0 A_p = \pi R_1^2 v_0 - \pi \int_{R_1}^{r_1} r^2 \left[\frac{1}{K}\left\{\frac{1}{2}\frac{dp(x)}{dx}r + \frac{D_1}{r}\right\}\right]^m dr + \pi \int_{r_1}^{R_2} r^2 \left[-\frac{1}{K}\left\{\frac{1}{2}\frac{dp(x)}{dx}r + \frac{D_1}{r}\right\}\right]^m dr \tag{4.24}$$

$$D_1 = \frac{1}{2}\frac{dp}{dx}r_1^2 \tag{4.25}$$

Note that the solution of the MR flow in an annular duct does not reduce to that of the pipe flow as $r_1 \to 0$. This is for the reason that the annular duct model has a boundary condition at r_1; but, there is no boundary condition at $r = 0$ for the pipe flow.

4.2.2 Modelling based on the Bingham model

The Herschel-Bulkley model reduces to the Bingham model once the MR fluid parameter $m = 1$. Using Eq. (4.16) – (4.18), the resultant equations for the Bingham model are (Spencer et. al. 1998) [44]:

$$\frac{\frac{dp(x)}{dx}\left(R_2^2 - r_2^2 - R_1^2 + r_1^2\right)}{4} + D_1 \ln\left({R_2 r_1}/{r_2 R_1}\right) + D_2 - \eta v_0 = 0 \tag{4.26}$$

$$Q = v_0 A_p = \pi R_1^2 v_0 = \frac{\pi}{8\eta}\left[\frac{dp(x)}{dp}\left(R_2^4 - r_2^4 - R_1^4 + r_1^4\right) + 4D_1\left(R_2^2 - r_2^2 - R_1^2 + r_1^2\right) + 8D_3\right] \tag{4.27}$$

$$\frac{dp(x)}{dx}\left(r_2^2 - r_1^2\right) + 2[\tau_0(r_2) r_2 + \tau_0(r_1) r_1] = 0 \tag{4.28}$$

Where

$$D_1 = \frac{r_1 r_2 [\tau_0(r_2) r_1 + \tau_0(r_1) r_2]}{r_2^2 - r_1^2} \tag{4.29}$$

$$D_2 = \int_{r_2}^{R_2} \tau_0(r) dr + \int_{r_1}^{R_1} \tau_0(r) dr \tag{4.30}$$

$$D_3 = \int_{r_2}^{R_2} \tau_0(r) r^2 dr + \int_{r_1}^{R_1} \tau_0(r) r^2 dr \tag{4.31}$$

And the velocity profile is given by:

$$u_x(r) = \begin{cases} -\frac{1}{4\eta}\frac{dp}{dx}\left(R_1^2 - r^2\right) + \frac{D_1}{\eta}\ln\frac{r}{R_1} - \frac{1}{\eta}\int_{R_1}^{r} \tau_0(r) dr - v_0 & R_1 \le r \le r_1 \\ -\frac{1}{4\eta}\frac{dp}{dx}\left(R_2^2 - r_2^2\right) - \frac{D_1}{\eta}\ln\frac{R_2}{r_2} - \frac{1}{\eta}\int_{r_2}^{R_2} \tau_0(r) dr & r_1 < r < r_2 \\ -\frac{1}{4\eta}\frac{dp}{dx}\left(R_2^2 - r^2\right) - \frac{D_1}{\eta}\ln\frac{R_2}{r} - \frac{1}{\eta}\int_{r}^{R_2} \tau_0(r) dr & r_2 \le r \le R_2 \end{cases} \tag{4.32}$$

In the absence of the magnetic field, the yield stress $\tau_0 = 0$. The pressure gradient can be achieved directly from:

$$\frac{dp}{dx} = \frac{8\eta v_0}{\pi} \frac{\frac{\pi}{2}\left\{2R_1^2 - \frac{R_2^2 - R_1^2}{\ln(R_2/R_1)}\right\} - A_p}{R_2^4 - R_1^4 - \frac{(R_2^2 - R_1^2)^2}{\ln(R_2/R_1)}} \tag{4.33}$$

Generally, the yield stress τ_0 in the axisymmetric model will be a function of *r*. But while $R_2 - R_1 \ll R_1$, variation of the yield stress in the gap can be ignored, and Eqs. (4.29) – (4.31) can be further simplified significantly as follows:

$$D_1 = \frac{\tau_0 r_1 r_2}{r_2 - r_1} \tag{4.34}$$

$$D_2 = \tau_0 (R_2 + R_1 - r_1 - r_2) \tag{4.35}$$

$$D_3 = \frac{1}{3}\tau_0 (R_2^3 + R_1^3 - r_1^3 - r_2^3) \tag{4.36}$$

Note that in this case, the thickness of the plug flow area can be calculated by using Eq. (4.20):

$$r_2 - r_1 = -\frac{2\tau_0}{\frac{dp(x)}{dx}} \tag{4.37}$$

Which is a constant, and only depends on the yield stress and pressure gradient of the flow.

4.3 MR Fluid Flow in a Parallel Duct

Due to the small ratio among the flow gap (between the cylinder housing and the piston) and the diameter of the piston, one might conjecture that the axisymmetric flow create in the damper can be approximated as the flow through a parallel duct as presented in Fig. 4.4. Connecting the parallel- plate model to the axisymmetric model, the parameter *w* is taken to be the mean circumference of the damper's annular flow path which equals to $\pi(R_1 + R_2)$, and *h* is taken to be the gap width, equal to $(R_2 - R_1)$, (Spencer et al 1998) [44].

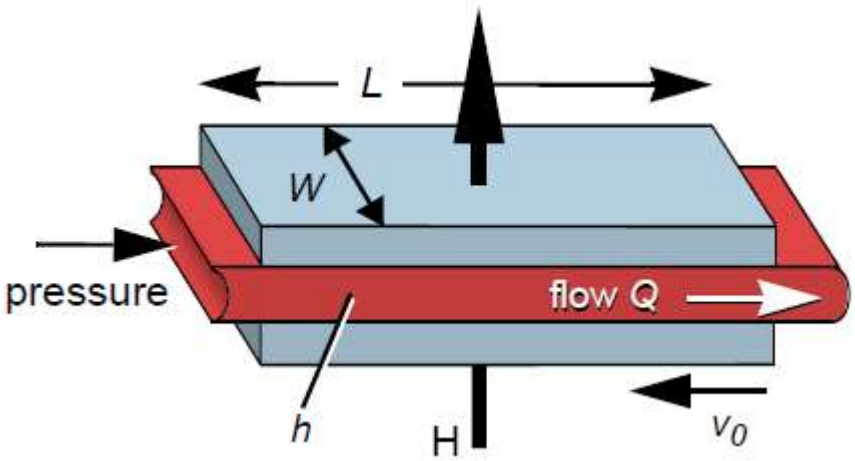

FIGURE 4.4: MR fluid flow through a parallel duct.

Fig. 4.5 provides the free body diagram and stress and velocity profiles of MR fluids through a parallel duct.

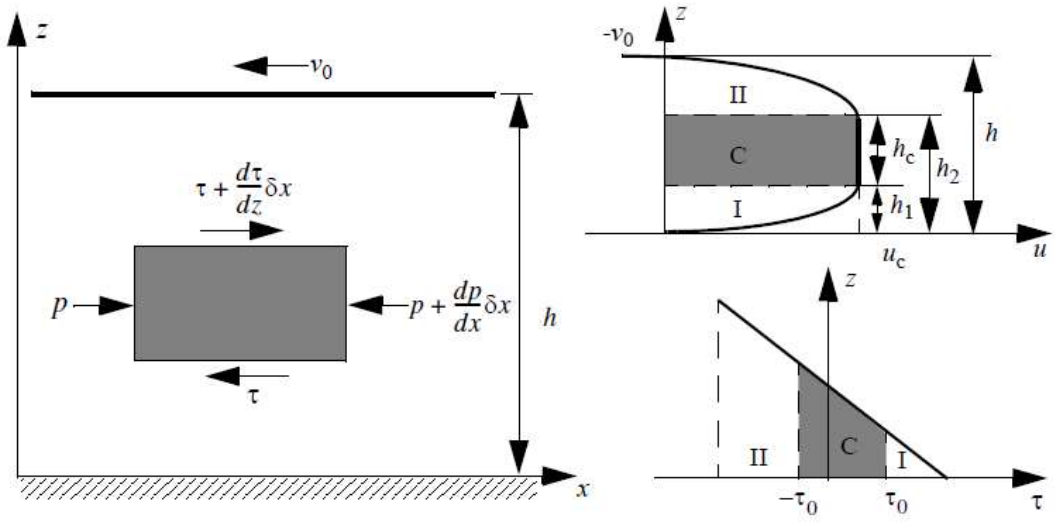

FIGURE 4.5: Free body diagram and stress and velocity profiles of MR fluids through a parallel duct [63]

The governing equation for the flow of the parallel-plate model is:

$$\frac{d\tau}{dz} = \frac{dp}{dx} \tag{4.38}$$

Therefore,

$$\tau(z) = \frac{dp}{dx} z + D \tag{4.39}$$

In which D is a constant which can be evaluated with boundary conditions.

4.3.1 Modelling based on the Herschel-Bulkley model

Like to the axisymmetric model, the shear stress τ in area I (Fig. 4.5) is given by:

$$\tau(z) = \tau_0 + K\left(\frac{du_x}{dz}\right)^{\frac{1}{m}} \tag{4.40}$$

Replacement of Eq. (4.40) into Eq. (4.39) and applying the boundary condition $u_x(0) = 0$ gives:

$$u_x(z) = \frac{1}{m+1}\left(-\frac{1}{K}\frac{dp}{dx}\right)^m \{h_1^{m+1} - (h_1 - z)^{m+1}\} \qquad (0 \le z \le h_1) \tag{4.41}$$

In area II, the shear stress is specified by:

$$\tau = -\tau_0 - K\left(-\frac{du_x}{dz}\right)^{\frac{1}{m}} \tag{4.42}$$

By the same procedure as in area I, with boundary condition $u_x(h) = -v_0$, gives:

$$u_x(z) = \frac{1}{m+1}\left(-\frac{1}{K}\frac{dp}{dx}\right)^m \{(h - h_2)^{m+1} - (z - h_2)^{m+1}\} - v_0 \qquad (h_2 \le z \le h) \tag{4.43}$$

The flow velocity at the boundary of the plug flow area satisfies $u_x(h_1) = u_x(h_2)$.

Joining Eq. (4.41) and (4.43) yields:

$$\frac{1}{m+1}\left(-\frac{1}{K}\frac{dp}{dx}\right)^m h_1^{m+1} = \frac{1}{m+1}\left(-\frac{1}{K}\frac{dp}{dx}\right)^m (h - h_2)^{m+1} - v_0 \tag{4.44}$$

The volume flow rate Q is specified by:

$$Q = A_p v_0 = w\int_0^h u_x(z)dz$$

i.e.

$$Q = \frac{w}{m+1}\left(-\frac{1}{K}\frac{dp}{dx}\right)^m h_1^{m+1}\left[h - \frac{1}{m+2}(h + h_1 - h_2\right] - \frac{w}{m+2}v_0(h - h_2) \tag{4.45}$$

Where A_p= piston head cross section area

v_0= velocity of piston head.

With reference to Fig. 4.5, the equation of motion for fluid materials bounded by $h = h_1$ and $h = h_2$ is:

$$\frac{dp}{dx}(h_2 - h_1)\delta x + 2\tau_0 \delta x = 0 \tag{4.46}$$

Which yields

$$h_2 - h_1 = -\frac{2\tau_0}{dp/dx} \tag{4.47}$$

Hence, the resulting equations for the parallel-plate model using the Herschel- Bulkley model consist of Eq. (4.44), (4.45) and (4.47). The pressure gradient dp/dx can be resolved numerically, and the damper resisting force is then calculated with Eq. (4.21). Note that $h_2 = h_1$ when the yield stress $\tau_0 = 0$.

The velocity profile, which satisfies the boundary conditions $u_x(0) = 0$ and $u_x(h) = -v_0$, is then specified by:

$$u_x(z) = \begin{cases} \frac{1}{m+1}\left(-\frac{1}{K}\frac{dp}{dx}\right)^m [h_1^{m+1} - (h_1 - z)^{m+1}] & 0 \le z \le h_1 \\ \frac{1}{m+1}\left(-\frac{1}{K}\frac{dp}{dx}\right)^m h_1^{m+1} & h_1 < z < h_2 \\ \frac{1}{m+1}\left(-\frac{1}{K}\frac{dp}{dx}\right)^m [(h - h_2)^{m+1} - (z - h_2)^{m+1}] - v_0 & h_2 \le z \le h \end{cases} \tag{4.48}$$

Note that when $v_0 = 0$, the resulting equations are the same as those provided by Lee and Wereley (2000).

4.3.2 Modelling based on the Bingham model (Γ P V)

Once more for the Bingham model, the fluid parameter is $m = 1$. Replacement of Eq. (4.44) and (4.47) into Eq. (4.45), and describing non-dimensional variables:

$$\mathrm{V} = -\frac{wh v_0}{2Q} = -\frac{wh}{2A_p} \tag{4.49}$$

$$\mathrm{P} = -\frac{wh^3}{12\eta Q}\frac{dp}{dx} = -\frac{wh^3}{12\eta A_p v_0}\frac{dp}{dx} \tag{4.50}$$

$$\Gamma = \frac{wh^2\tau_0}{12\eta Q} = \frac{wh^2\tau_0}{12\eta A_p v_0} \tag{4.51}$$

Results in the non-dimensional quantic equation (Phillips 1969) [59]:

$$3(\mathrm{P}-2\Gamma)^2(\mathrm{P}^3 - (1+3\Gamma-\mathrm{V})\mathrm{P}^2 + 4\Gamma^3) + \Gamma\mathrm{V}^2\mathrm{P}^2 = 0, \qquad |\,\mathrm{V}\,| < 3(\mathrm{P}-2\Gamma)^2/\mathrm{P} \tag{4.52}$$

Note that $\mathrm{V} < 0$, if the piston motion is in the reverse direction of the fluid flow. The force created by the damper is then specified by:

$$F = -\frac{dy}{dx}A_p L = \frac{12\eta A_p^2 L v_0}{wh^3}\,\mathrm{P} \tag{4.53}$$

When $|\,\mathrm{V}\,| > 3(\mathrm{P}-2\Gamma)^2/\mathrm{P}$, the flow is directed by the subsequent dimensionless equations which are independent of the dimensionless yield stress Γ (Phillips 1969) [59]:

$$\mathrm{P} = \frac{4\mathrm{V}^3}{27(2\mathrm{V}-1)^2} \qquad 3(\mathrm{P}-2\Gamma)^2/\mathrm{P} \le \mathrm{V} \le 3\mathrm{P} \tag{4.54}$$

$$\mathrm{P} = -\frac{4\mathrm{V}^3}{27} \qquad -3\mathrm{P} \le \mathrm{V} \le -3(\mathrm{P}-2\Gamma)^2/\mathrm{P} \tag{4.55}$$

$$\mathrm{P} + \mathrm{V} = 1 \qquad |\,\mathrm{V}\,| > 3\mathrm{P} \tag{4.56}$$

Eq. (4.54) – (4.56) specify that the pressure gradient be governed by the geometry of the device, and that a controllable yield stress has no effect on the force of the damper.
If the piston head velocity $v_0 = 0$, then $\mathrm{V} = 0$, and Eq. (3.52) turn into a cubic equation for P. This cubic equation has the achievable root at (Gavin et. al. (2004) [26]):

$$\mathrm{P}(\Gamma) = \frac{2}{3}(1+3\Gamma)\left[cos\left(\frac{1}{3}acos\left(1-54\left(\frac{\Gamma}{1+3\Gamma}\right)^3\right)\right)+\frac{1}{2}\right] \tag{4.57}$$

Normally, there is no analytical solution for Eq. (4.52), but it can be easily solved numerically. An approximate solution can be used to estimate the desired root for the condition $0 < \Gamma < 1000$ and $-0.5 < \mathrm{V} < 0$, which encompasses most practical designs in which the flow is in the opposite direction of the piston velocity (Spencer et. al. 1998) [44]:

$$\mathrm{P}(\Gamma, \mathrm{V}) = 1 + 2.07\Gamma - \mathrm{V} + \frac{\Gamma}{1+0.4\Gamma} \tag{4.58}$$

4.4 Simple Geometry Design Considerations

With reference to the parallel-plate Bingham model which was established in prior sections, simple equations that make available the understanding on the influence of various damper parameters are given; these equations can be used in the preliminary design stage. Special effects of geometry on controlled force, dynamic range and MR damper performance are also discussed in this segment.

4.4.1 Controlled force and dynamic range

The "controlled force" and the "dynamic range" are two most significant parameters in estimating the complete performance of the MR damper. As shown in Fig. 4.6, the over-all damping force can be divided into a controlled force F_τ due to governable yield stress τ_o and an uncontrolled force F_{uc} . The uncontrolled force comprises a plastic viscous force F_η and a friction force F_f . The "dynamic range" (D) is defined as the ratio of the damper controlled force F_τ and the uncontrolled force F_{uc} as follows:

$$D = \frac{F_\tau}{F_{uc}} = \frac{F_\tau}{F_\eta + F_f} \tag{4.59}$$

With reference to the parallel-plate Bingham model, F_τ and F_η are defined as:

$$F_\tau = \frac{c\tau_0 L A_p}{h}\, sgn(v_0) \tag{4.60}$$

$$F_\eta = \left(1+\frac{whv_0}{2Q}\right)\frac{12\eta Q L_p}{wh^3} \tag{4.61}$$

and

$c \approx 2.07 + 1/(1 + 0.4\,\Gamma)$ restricted in between the value of 2.07-3.07. (Spencer et. al. 1998).

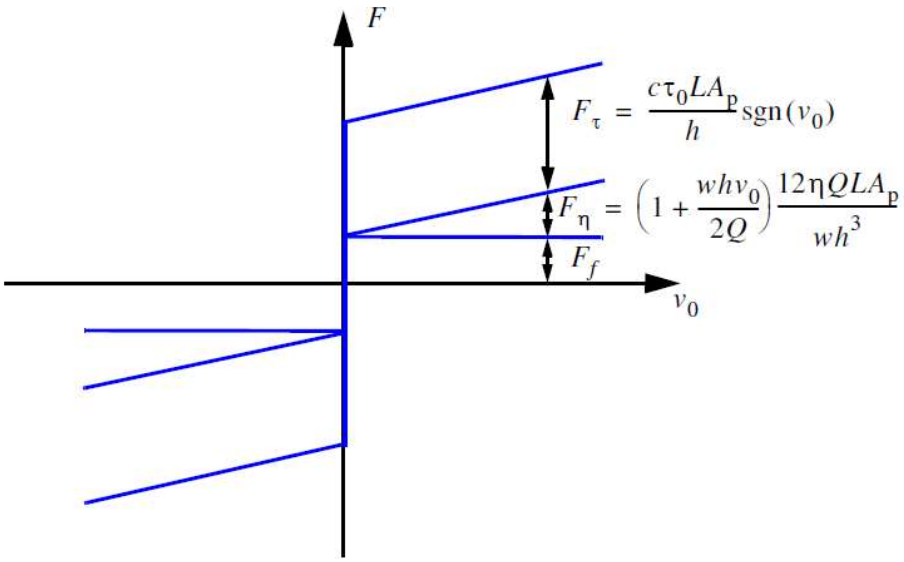

FIGURE 4.6: Decomposition of force developed in MR dampers.

The controlled force in Eq. (4.61) can furthermore be written by using Eq. (4.51) as:

$$F_\tau = \left(2.07 + \frac{12Q\eta}{12Q\eta + 0.4wh^2\tau_0}\right)\frac{\tau_0 LA_p}{h}\, sgn(v_0) \tag{4.62}$$

The above equation (4.62) specifies that the controlled force is inversely related to the gap dimension. The controlled force should be as large as possible to optimize the effectiveness of the MR damper; for that reason, a small gap size is compulsory.

However, a small gap size reduce the dynamic range. As presented in Eq. (4.60) and (4.61), the uncontrolled force (viscous force) rises two orders of magnitude faster than the controlled force with a small gap dimension if one assumes that the magnetic field is saturated; therefore, the dynamic range is reduced which tends to zero. As the gap dimension becomes large, the controlled force and the uncontrolled force are decreased. It is important to note that the friction force is a constant, so once more the dynamic range reduced which tends to zero. It is obvious that an optimum dynamic range must exist.

4.4.2 Geometry constraints

Eq. (4.60) and (4.61) are definitely suitable in the design of MR dampers; but, they frequently do not provide the finest understanding into the importance of various parameters. Hence, the "minimum active fluid volume" V is presented. Minimum active fluid volume V is the volume of MR fluids exposed to the magnetic field and thus

accountable for providing the desired MR effect. With the help of Eq. (4.60) and (4.61), we obtain the conclusion as:

$$wh^2 = \frac{12k}{c}\left(\frac{\eta}{\tau_0}\right)\left(\frac{F_\tau}{F_\eta}\right)Q \tag{4.63}$$

Where $k = 1 + (whv_0)/(2Q)$. Because eq. (4.60) can also be written as:

$$\Delta p_\tau = \frac{F_\tau}{A_p} = \frac{c\tau_0 L}{h} \tag{4.64}$$

Eq. (4.63) can be further manipulated to give

$$V = \frac{12k}{c^2}\left(\frac{\eta}{\tau_0^2}\right)\left(\frac{F_\tau}{F_\eta}\right)Q\Delta p_\tau \tag{4.65}$$

Where $V = Lwh$ which is the "minimum active fluid volume"; and Δp_τ is a pressure reduced due to the yield stress. Note that for most design cases, $whv_0 \ll Q$ and as a result $k \approx 1$.

For preliminary geometric design of MR dampers, it can be assume that the friction force (F_f) has the same value as the uncontrolled force (plastic viscous force) (F_η). Therefore, $\frac{F_\tau}{F_\eta} \approx 2D$, Where D is the necessary dynamic range. From the known value of the damper flow rate Q, necessary dynamic range D, yield stress τ_0, housing dimension w, plastic viscosity η, and pressure drop Δp_τ, the gap dimension h and active pole length L can be achieved from Eqs. (4.63) and (4.65). However, this preliminary design needs to be confirmed by a more precise axisymmetric model. Typically, a complete design also includes iterations with the magnetic circuit design.

CHAPTER 5
MR DAMPER DESIGN AND FABRICATION

This chapter presents details of MR damper geometry and magnetic circuit design. Supplementary practical considerations for MR damper design, such as damper piston centring and voltage surge suppression are also discussed. Problem solution are also discuss. The discussion is started with description of MR fluid used for present investigation.

5.1 MR Fluid for present investigation

The MR fluid has been prepared using mechanical stirrer as shown in Fig. 5.1. The electronic weighing machine is used to measure the amount of additives required in the composition. Initially the mixture of carrier fluid and additive is prepared and stirred for 4 hrs. The amount of carbonyl iron particles as mentioned in Table 5.1 are then added into the prepared mixture and stirred for 72 hrs.

FIGURE 5.1: Mechanical stirrer for preparation of MR Fluid

The magnetorheological fluid, developed in house, is used in the prototype damper. The fluid is a suspension of a 4 to10 micron diameter sized magnetically susceptible particles mixed in Castor oil carrier fluid. According to the data available by testing this MR fluid on rheometer at this laboratory, the density of the liquid is around 3 gm/cm^3 and off state viscosity of a 3.5 Pa-s. The maximum yield stress value is 15 kPa and it is achieved with

the magnetic induction of 0.7 T. As soon as exposed to a magnetic field, the rheology of the fluid reversibly and instantly alterations from a free-flowing liquid to a semi-solid state with the controlled yield strength as a consequence of the sudden change in the particles arrangement. Fig. 5.2 shows the detail relations of magnetic flux density, viscosity and shear stress available from rheometer. Table 5.1 summarise the properties of MR fluid for present investigation.

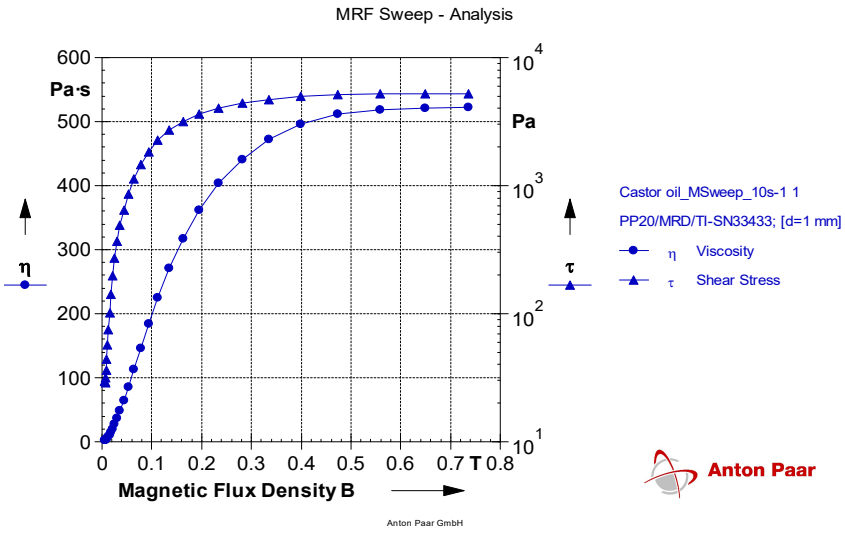

FIGURE 5.2: Relation between Magnetic flux density, Viscosity and Shear stress

TABLE 5.1 Properties of MR fluid used for present investigation.

Property	**Value**
Appearance	Dark Gray Liquid
Off State Viscosity (at 33 ^{0}C)	3.5 Ps (Pascal-second)
Density	3 gm./cm^3
Solid Contains by Weight	40%
Flash Point	> 140 ^{0}C
Operating Temperature	-30 to 120 ^{0}C
Carrier fluid	Castor Oil
Solid particles	Iron particles having 4-10 micron size
Maximum Yield Stress	@ 5000 N/m^2 at 0.75 T
Response time	Some millisecond
Stability	Good for most impurities
Relative permeability of MR Fluid	6 H/m
Saturation Magnetic Induction for MR Fluid.	0.75 T

5.2 MR Damper Design

It is a need to develop a comprehensive algorithm for designing devices utilizing the unique properties of the magnetorheological fluids. Following sections are representing the same.

Simplifications concerning the magnetorheological fluid behaviour were assumed prior to the experiments. Fluid features include the fast response time, high yield strength in the presence of the magnetic flux and very low yield strength in the absence of magnetic flux. These features allows wide range of controllability. The fluid also provides hard settling resistance and it does not abrade the device.

For further analysis it is assumed that the liquid properties would be described by the phenomenological and viscoplastic Bingham model. The properties of this model are illustrated in Fig. 5.3(a).

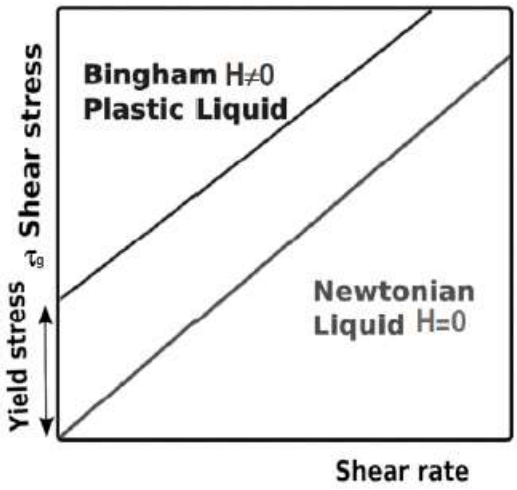

FIGURE 5.3 (a): Bingham model for different liquid states, activated by the magnetic field [64]

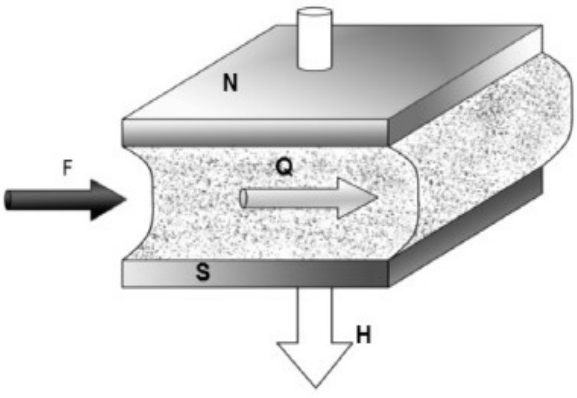

FIGURE 5.3(b): The valve mode of the flow - the throttled flow through the gap [64]

The work regime of the MR fluid inside the damper is called the valve mode. In the valve mode, the fluid flows through an orifice as presented in Fig. 5.3(b). In this model the annular flow is treated as a flow between two parallel still plates. The principle of operation resembles throttling (Kim et al, 2001). The resistance to flow of a liquid through the narrow gap is controlled by the change in the magnetic field H, whose vector is normal to the path of the flow. The adjustment of the magnetic field is performed by the change of the current in the coil winding mounted on the piston.

Further simplifications which are crucial for the computation of the damper's performance are made asunder:

- the damping force acts linear
- the flow gap is formed by the stationary walls
- the height of the gap is much smaller than its length and the width, therefore the flow is considered as a flow between parallel plates, and thus the valve mode simplification is reasonable
- Stress value is constant along the gap, and it depends only on the value of the magnetic flux in the gap (Mukhlis et al, 2006).

5.2.1 MR Damper Geometry Design

The cross-section view of the annular flow gap for linear damper prototype is presented in Fig. 5.4.

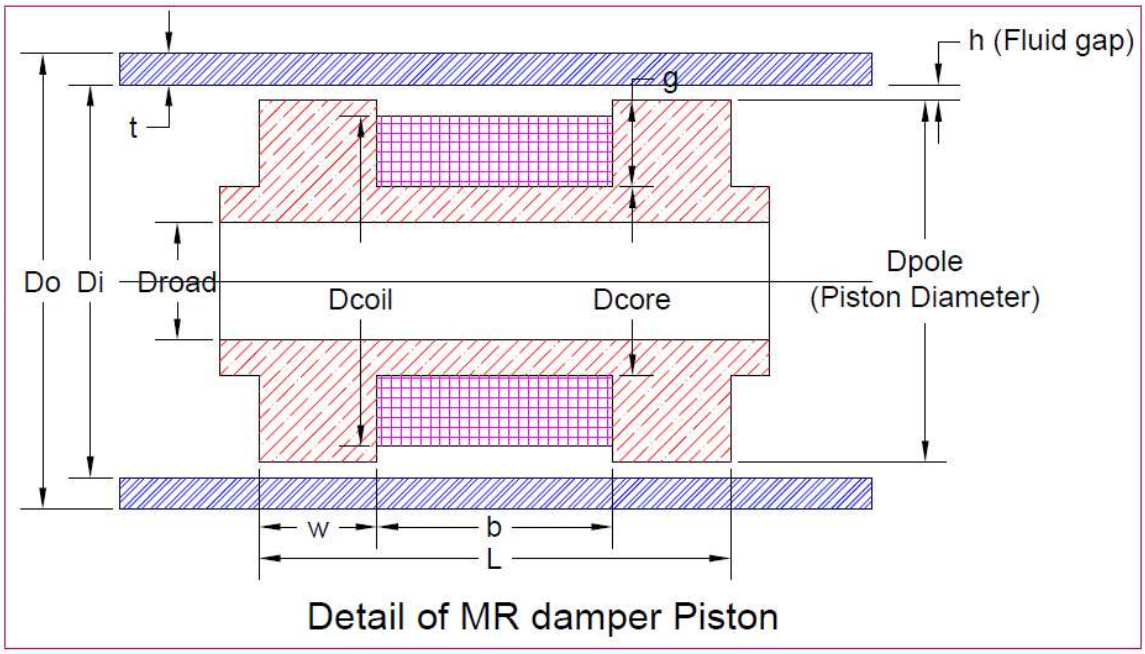

FIGURE 5.4: Detail of MR Damper Piston

The MR damper geometry design is started by assuming following parameters:

(1) MR fluid yield stress τ_0 , and fluid factors K and m

(2) MR damper dimension D_{i} (i.e. Inner Diameter of Housing)

(3) Maximum permissible velocity of the MR damper

Table 5.2 shows the terminology used during discussion for MR fluid base damper geometric design.

TABLE 5.2 Nomenclature of parameters used in design

Diameter of piston	D_p
Length of Piston	L
Width of Piston pole	w
Diameter of Road	D_r
Core Diameter	D_{core}
Cylinder Inside Diameter	D_i
Core Width (Length of Coil)	b
Thickness of cylinder	T
Cylinder Outside diameter	D_o
Fluid gap	h
Radius of Fluid Annulus	R_{fa}
Core Depth	g
Area of Piston Annulus	A_{pa}
Area of Fluid Annulus	A_{fa}
Core Area	A_{core}
Path Area	A_{path}
Pole Area	A_{pole}
Number of Turns of Piston Coil	N
Vacuum Permeability	μ_0
Relative permeability of Piston	μ_{rp}
Relative permeability of Cylinder	μ_{rc}
Relative permeability of MR Fluid	μ_{MR}
Saturation Magnetic Induction for Piston.	BS_p
Saturation Magnetic Induction for Cylinder.	BS_c
Saturation Magnetic Induction for MR Fluid.	BS_{MR}
Ratio of shear stress and magnetic induction	$C_{\tau B}$

The geometry design of MR damper is to select a suitable gap dimension h and active pole length L such that the design requirements of "dynamic range" D and controlled force F_τ , are attained.

The controllable force and the dynamic range are two of the most important parameters in evaluating the overall performance of the MR damper.

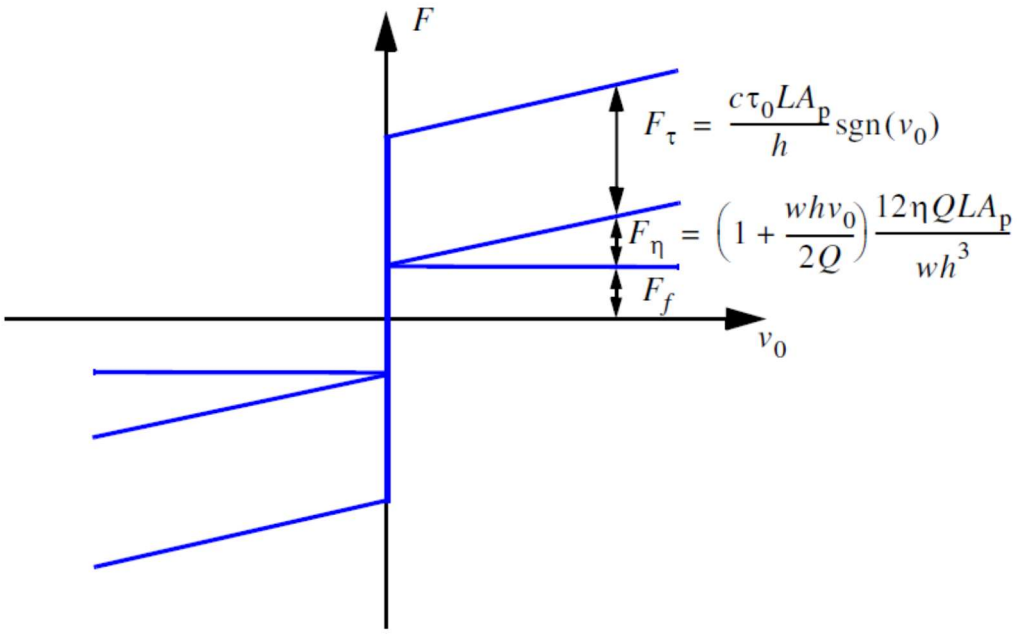

FIGURE 5.5: Illustration of force decomposition of MR dampers.

As illustrated in Fig. 5.5,

F_τ = A controlled force due to controllable yield stress τ_0

F_{UC} = An uncontrolled force which is sum of plastic viscous force F_η due to viscosity of fluid and friction force F_f

F = Total damping force which is sum of controllable force and uncontrollable force.

The dynamic range is given by the ratio of damper controlled force F_τ and the uncontrolled force F_{UC} as:

$$D = \frac{F_\tau}{F_{UC}} = \frac{F_\tau}{F_\eta + F_f} \tag{5.1}$$

It is not possible to find out the precise value of the friction force in advance the damper is fabricated and tried. On the other hand one can practically assume that $F_\eta = F_f$ (Engineering Note 1999a) [60].

Furthermore, since $F_\eta + F_f \gg F_f$, Eq. (1) can be written as

$$D = \frac{F_\tau}{F_{UC}} = \frac{F_\tau}{2F_\eta} \tag{5.2}$$

Let

$$F_\tau = \left(d_p/d_x\right)_{\tau_0} A_p L \text{ and } F_\eta = \left(d_p/d_x\right)_{\tau_{0=0}} A_p L$$

Where

$A_p =$ Piston cross sectional area

L = Active pole length

$\left(d_p/d_x\right)_{\tau_0}$ = Pressure gradient with fluid yield stress

$\left(d_p/d_x\right)_{\tau_{0=0}}$ = Pressure gradient without fluid yield stress

The Eq. 5.2 can be further manipulated as

$$D = \frac{1}{2}\frac{\left(d_p/d_x\right)_{\tau_0}}{\left(d_p/d_x\right)_{\tau_{0=0}}} \tag{5.3}$$

Using Eq. (4.16) – (4.19) and (4.23) – (4.25), a gap dimension h can be find out such that

$$D \leq \frac{1}{2}\frac{\left(d_p/d_x\right)_{\tau_0}}{\left(d_p/d_x\right)_{\tau_{0=0}}} \tag{5.4}$$

It is important that the gap must be selected having a practical dimension so that it will not have any manufacturing problems. The active pole length L can then be achieved by the equation:

$$L = \frac{F_\tau}{A_p\left[\left(d_p/d_x\right)_{\tau_0} - \left(d_p/d_x\right)_{\tau_{0=0}}\right]} \tag{5.5}$$

And the damping force or damper resisting force F can be calculated by

$$F = \left[\left(d_p/d_x\right)_{\tau_0} + \left(d_p/d_x\right)_{\tau_{0=0}}\right] A_p L \tag{5.6}$$

Proposing the approximate diameters of the piston and the rod, the effective circumference of the flow gap may be expressed as:

$$A_{gap} = \pi(R_1 + R_2)h$$

Where: $h = R_1 - R_2$ is the gap height.

The surface area of the piston denoted as Ap is expressed as:

$$A_p = \pi(R_3^2 - R_{rod}^2) - A_{gap}$$

The volumetric flow rate of the MR fluid through the gap can be expressed as:

$$Q = v_0 * A_p$$

Where v_0 = velocity of piston

Finally the total damping force can be evaluated by summation of all three components, i.e. Viscous force, Friction force (both are uncontrolled force) and shear force known as controlled force which is controlled by changing magnetic field. Following are important equations for various forces derived from above discussion.

Viscous Force (F_η):

Let the pressure drop caused by the Newtonian fluid viscotic flow, can be expressed as [64]:

$$\Delta P_\eta = \frac{12 A_p L v_0 \eta}{w h^3}\left(1 - \frac{w h v_0}{2Q}\right) \tag{5.7}$$

The damping force related only to the viscosity of the fluid is equal to [64]:

$$F_\eta = \Delta P_\eta A_p = \frac{12 A_p L Q \eta}{w h^3}\left(1 - \frac{w h v_0}{2Q}\right) \tag{5.8}$$

Including the previous equations and utilizing the simplifying formula ($A_p >> w$), the above equation can be transformed into:

$$F_\eta = \frac{12A_p^2 L v_0 \eta}{\pi(R_1 + R_2)h^3} \quad (5.9)$$

Shear Force (F_τ):

The decrease of the pressure along the gap caused by the non-zero yield stress value is given by the equation [64]:

$$\Delta P_\tau = \frac{c\tau_0 L}{h}$$

The constant value c, which is related to the geometrical dimensions of the damper and the damping force can be approximated with the accuracy of 3% by the relation given below (Poynor, 2010):

$$c = 2.07 + \frac{wh^2\tau_0}{1 + 0.4\sigma}$$

Where σ the stress gradient is described by the formula (Milecki, 2010) and is given by:

$$\sigma = \frac{wh^2\tau_0}{12Q\eta}$$

Taking into consideration the simplifying assumptions, we can determine the value of the damping force due to shearing of fluid controlled with the magnetic field [64]:

$$F_\tau = \frac{c\tau_0 L A_p}{h} sgn(v_0) \quad (5.10)$$

Total Damping Force:

The final form of the sum of the forces is then as follows [64]:

$$\boldsymbol{F_{damp} = \frac{12A_pLQ\eta}{wh^3}\left(1 - \frac{wh_0}{2Q}\right) + \frac{c\tau_0 LA_p}{h} sgn(v_0) + F_f} \quad (5.11)$$

The value of the friction force F_f depends on the types of the used construction materials, types of sealing & methods of their machining, piston velocity and duration of the piston

rest time. In the discussed example of the calculations for the prototype device, the friction force value is preliminarily estimated on the basis of the experimental data. From the equation 5.8 and 5.10, it can be concluded that by reducing the height of the flow gap, the maximum damping force of the device can be increased. The increase of the non-controlled visco-elastic force is in proportion to the third power of the gap height. The value of the shear force (controlled force) increases slower than the value of the viscous force (uncontrolled force). It is caused by the fact that the height of the gap in equation 5.10 is in the first power.

The order of calculation allows determination of most of the parameters which are crucial for the proper design of the small scale linear damper with MR fluid.

5.2.2 MR Damper Magnetic Circuit Design

A typical MR damper consists of housing, piston, excitation coil and MR fluid enclosed in housing. Just a device turn on magnetic influence, the MR damper should be designed optimally to achieve the magnetic performance and ultimately to attain acceptable semi active control effect. The important requirement of MR fluid should have low viscosity in absence of magnetic field, high yielding stress, small reactive time and good stability of sediment & agglomeration. Principally important, MR fluid must have higher saturation magnetic induction to make sure MR damper adequate force alteration range. Likewise the piston and cylinder should be magnetically soft material with higher saturation magnetic induction and smaller hysteresis loop region.

For optimal design, the description of the magnetic circuit design described in the Lord Corporation Engineering Note-1999b [61] is summarized in this section. The MR damper magnetic circuit typically uses low carbon steel as a piston and cylinder material which has higher magnetic permeability and saturation as magnetic flux channel to guide and focus magnetic flux into the fluid cavity. A magnetic circuit design is carried out to find out required amp-turns (NI) for the magnetic circuit. An optimum design of the magnetic circuit necessitates to minimize the energy loss in steel flux conduit and regions of non-working areas while maximize magnetic field energy in the fluid cavity. The whole quantity of steel in the magnetic circuit correspondingly needs to be minimized. But, adequate cross-section of steel must be preserved such that the magnetic field intensity in the steel should be low.

The design procedure for a magnetic circuit is carried out in following step:

(1) To find out the magnetic induction B_f in the MR fluid to make available required yield stress τ_0 (Fig. 5.6a)
(2) To find out the magnetic field strength H_f in the MR fluid (Fig. 5.6b)
(3) The total magnetic induction flux is given by:

$$\phi = B_f A_f \tag{5.12}$$

Where

A_f is the effective pole area including the fringe of magnetic flux.

Because of the continuity of magnetic induction flux, the magnetic induction B_s in the steel is given by:

$$B_s = \frac{\phi}{A_s} = \frac{B_f A_f}{A_s} \tag{5.13}$$

(4) To find out the magnetic field intensity H_s in the steel using Fig. 5.6c
(5) With the help of Kirchhoff's Law of magnetic circuit, the required number of amp-turns (NI) is:

$$NI = \sum H_i L_i = H_f * (2h) + H_s L \tag{5.14}$$

Where

$2h$ = total length of gaps (refer to Fig. 5.7) and

L = steel path length which is equal to $L_s + L_c$.

Additional things should also be keep in mind throughout the circuit design process such as nonlinear magnetic properties of piston & cylinder material and MR fluid; probable losses at boundaries & junctions; limits on voltage, current and inductance; probable inclusion of permanent magnets for reliable action and eddy currents.

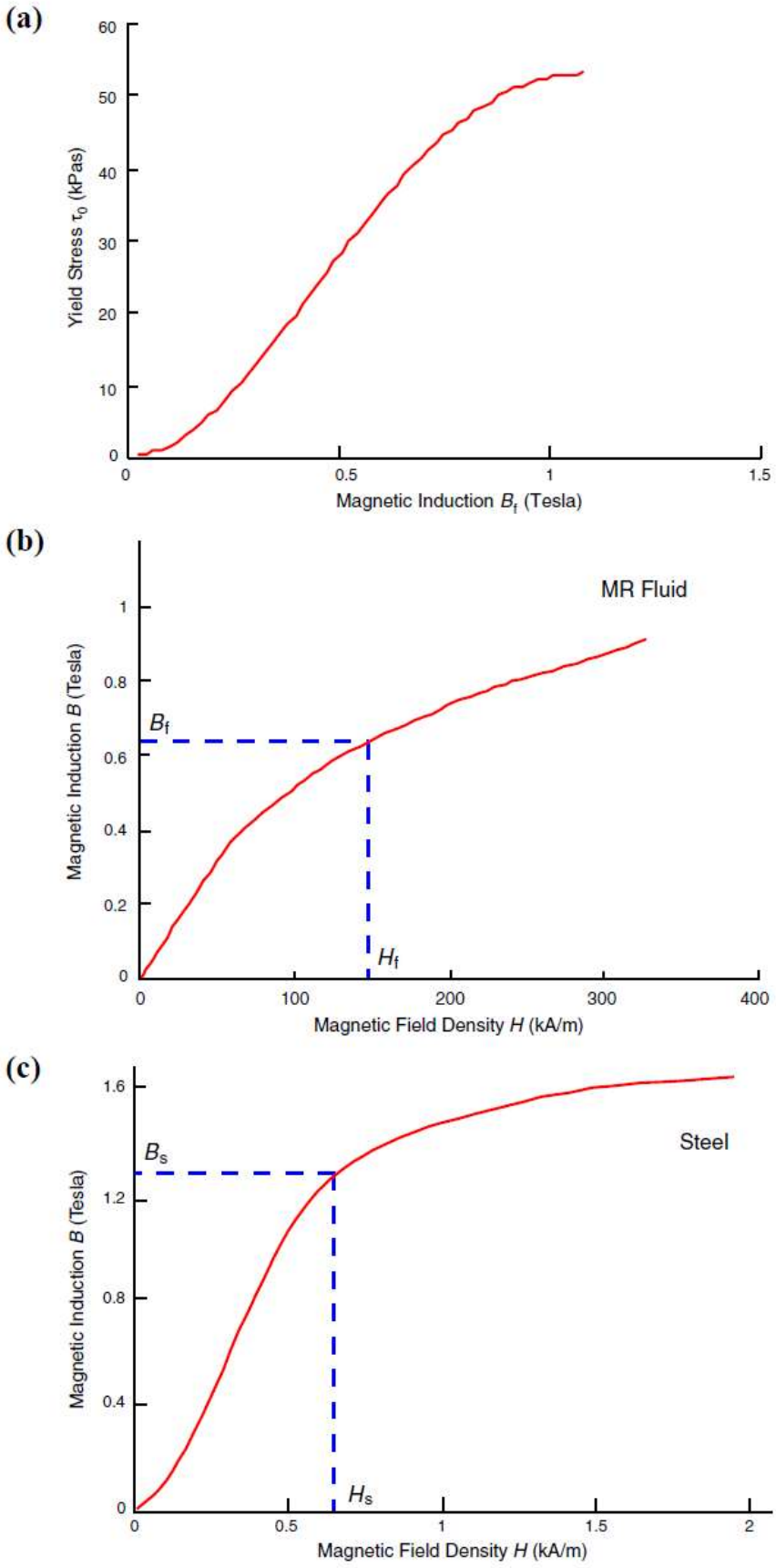

FIGURE 5.6: Basic magnetic circuit design procedure (Engineering Note 1999b) [61].

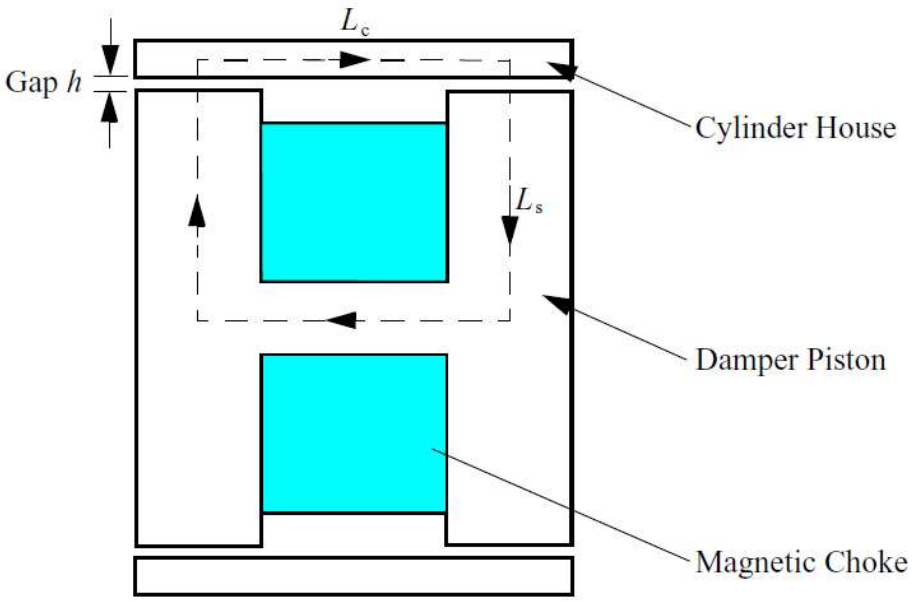

FIGURE 5.7: Magnetic circuit of MR dampers.

To finalise outstanding magnetic material and MR fluid is the main step of magnetic circuit design to the fulfilment of design intent. Better magnetic design is also carried out by magnetic structure design. The magnetic field forms a loop in the magnetic material. If the magnetic loop gets saturate anyplace, it will stop the continuous rise of the entire loop. However at the same time, the magnetic structure must confirm the execution of structure function.

Parameters of magnetic field:

The concept of magnetic circuit is established on the phenomenon that magnetic conductor permeability is considerably higher than the insulated material. The magnetic leakage is ignored since the magnetic loop is formed only in magnetic material.

Based on ohm's law, the magnetic circuit factors are magnetic reluctance R_m, magnetic flux ϕ, magnetic potential F, no of coil turns N and current passing through the coil is I. The relation between this parameters are given by:

$$F = R_m\phi = NI \tag{5.15}$$

For complete magnetic design, the structure of MR fluid damper magnetic loop is divided into three parts as shown in Fig. 5.8.

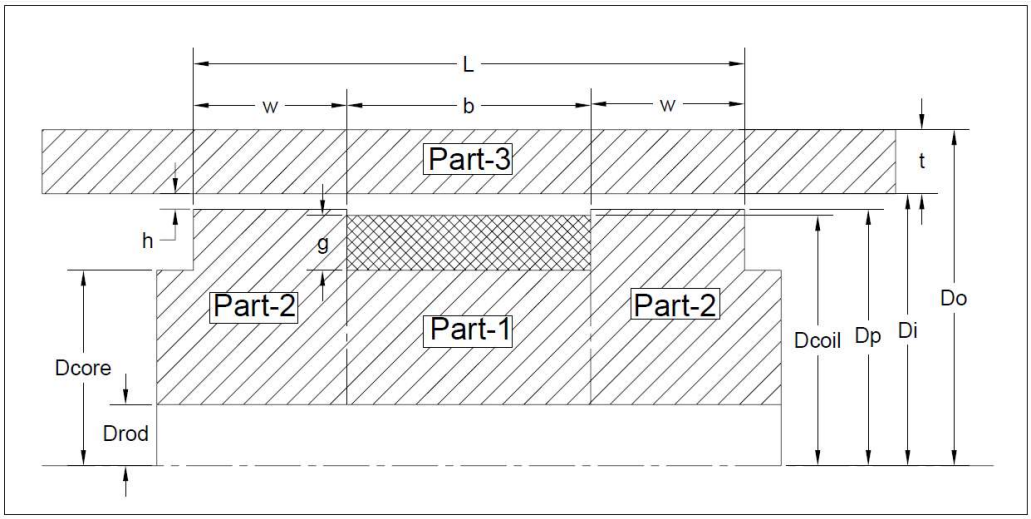

FIGURE: 5.8: Conductor magnetic reluctance calculator

The complete magnetic circuit design is carried out in following steps.

Step 1: Calculation of magnetic reluctance for damper circuit.

Portion 1, portion 2, portion 3 and MR fluid cavity consist of the magnetic loop as shown in Fig. 5.8.

For part 1, the magnetic reluctance for piston core section is:

$$R_{m1} = \frac{L-2w}{\left[\mu_0\mu_{rp}(\pi/4)\left\{(D_p-2g)^2-{D_r}^2\right\}\right]} \tag{5.16}$$

In a similar way

The magnetic reluctance for piston legs (part 2) is:

$$R_{m2} = \frac{D_p-D_r}{2\mu_0\mu_{rp}\pi D_p w} \tag{5.17}$$

The magnetic reluctance for cylinder wall (part 3) is:

$$R_{m3} = \frac{L-w}{\mu_0\mu_{rp}\pi(D_p+h+t/2)t} \tag{5.18}$$

The magnetic reluctance of MR fluid in flow gap is:

$$R_{mr} = \frac{\ln\left\{1+\left(2h/D_p\right)\right\}}{2\mu_0\mu_{rp}\pi w} \tag{5.19}$$

So the total magnetic reluctance of magnetic circuit is [62]

$$\boldsymbol{R = R_{m1} + 2R_{m2} + R_{m3} + R_{mr}} \tag{5.20}$$

Step 2: To find out optimum magnetic flux for MR damper circuit (ϕ):

Receiving the magnetic induction range of MR fluid from the experiment curve and assuming the shear stress as τ, saturated magnetic induction as BS_{MR} and the magnetic field as constant in the MR fluid cavity (which is much smaller than the piston diameter D_p), the magnetic flux can be stated as:

$$\phi = \int BdS \tag{5.21}$$

In the magnetic loop, the magnetic flux is uniform when the magnetic leak is ignored. Therefore, assuming the material property "saturation magnetic induction" of piston, cylinder and MR fluid is BS_{piston}, $BS_{cylinder}$ and BS_{MR}. The magnetic flux area is S_{MR}, S_1, S_2 and S_3 respectively (1, 2, and 3 designated the tree part shown in Fig. 5.8). Now by multiplying the saturation magnetic induction with the flux area, the lowermost value will get saturate first and will be the optimum magnetic flux value for the circuit. Mathematically it found as:

Magnetic flux developed in MR fluid flow annulus:

$$\phi_{MR} = \pi D_p w * BS_{MR} \tag{5.22}$$

Magnetic flux developed in core area of piston (Part – 1 as shown in Fig. 5.8):

$$\phi_{piston-1} = \left(\frac{\pi}{4}\right)\left[\left(D_p - 2g\right)^2 - D_r^2\right] * BS_{piston} \tag{5.23}$$

Magnetic flux developed in pole area of piston (Part – 2 as shown in Fig. 5.8):

$$\phi_{piston-2} = \pi D_p w * BS_{piston} \tag{5.24}$$

Magnetic flux developed in cylinder wall (Part – 2 as shown in Fig. 5.8):

$$\phi_{cylinder} = \pi\left(D_p + h + {}^{t}/_{2}\right)t * BS_{cylinder} \tag{5.25}$$

The optimum value of magnetic flux for the circuit is given by [62]:

$$\boldsymbol{\phi_{opt} = min(\phi_{MR}, \phi_{piston-1}, \phi_{piston-2}, \phi_{cylinder})} \quad (5.26)$$

The magnetic circuit design should be such that the value of ϕ_{opt} should be maximum possible [62].

Step 3: To find out Optimum (Maximum) current value which can produce magnetic induction in circuit (I_{max})

Based on the entire magnetic potential F, power and heat dispersion, it can be find out the upper limit of the effective current value I_{max} and the required coil turn from following equation:

$$\boldsymbol{I_{max} = \frac{F}{N} = \frac{R_m \phi}{N}} \quad (5.27)$$

Beyond this limit, current cannot improve magnetic induction in circuit.

5.2.3 Considerations with Applied Design

In the course of the design of the MR damper with recommended performance, real difficulties such as voltage surge suppression and damper piston centring must be overcome. In the subsequent segments, reasons of these difficulties are deliberated and determinations are given.

5.2.3.1 MR damper piston centring

Commonly, without any special arrangement, the MR damper piston does not remain centred during operation. This may be due to either side loads due to inappropriate installation or manufacturing errors, which may result in:

(1) Non-uniform temperature increases and local overheating
(2) Bearing malfunction and leakage
(3) Scratching of the insulation and causing a short in the magnetic coil.

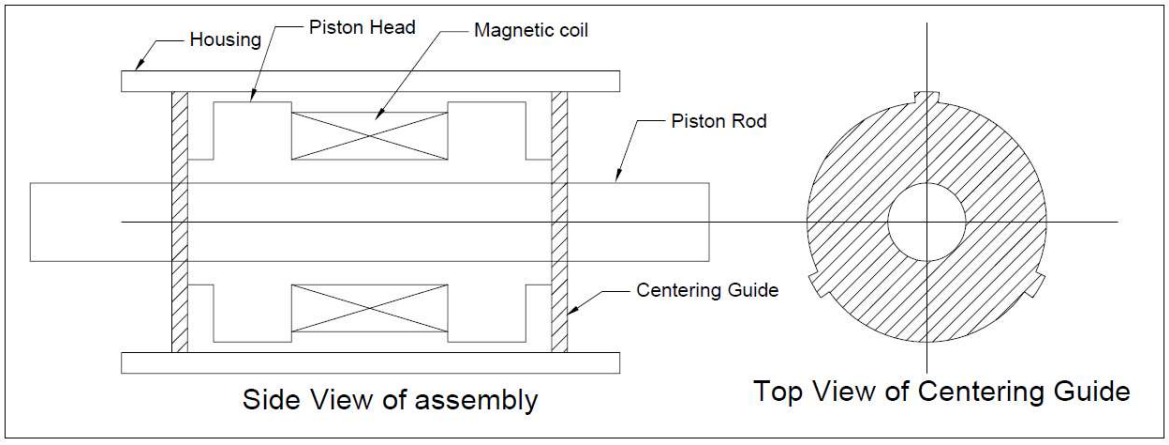

FIGURE 5.9: Schematic of piston head installed with guide rails.

To overcome this problem, a total of 2 guide rails made from bronze material are installed on the MR fluid damper reflected in this research work. The representation of the piston head using the guide rail mounted is shown in Fig. 5.9. The guide rails have a precise close fit with the housing and hold onto the piston centred within gap "h". Moreover, bronze is softer than housing material, in present case carbon steel, will not damage the housing surface.

5.2.3.2 Voltage surge suppression

To create a magnetic field and consequently a yield stress in the MR fluid, MR dampers utilize the current flowing through the damper coil. The current can be supplied by either a current driver or a voltage source. If the power source or the MR damper quickly has a connection breakdown, affecting an open circuit, current flow from the coil will immediately stop.

With reference to Faraday's law of induction, a voltage settled through the coil is specified using equation:

$$V(t) = -L\frac{di}{dt} \tag{5.28}$$

It is to be seen from above equation that the voltage is proportionate to the time rate of variation in current flow. As soon as the connection breaks, the current variation rate is very high; this can reason a voltage surge through the coil, particularly in the MR damper coil due to its large inductance. This voltage surge will breakdown the coil insulation and effect an electric short. Due to this reason, the coil cannot produce adequate magnetic field in the MR fluid flow cavity and the damper force decreases considerably.

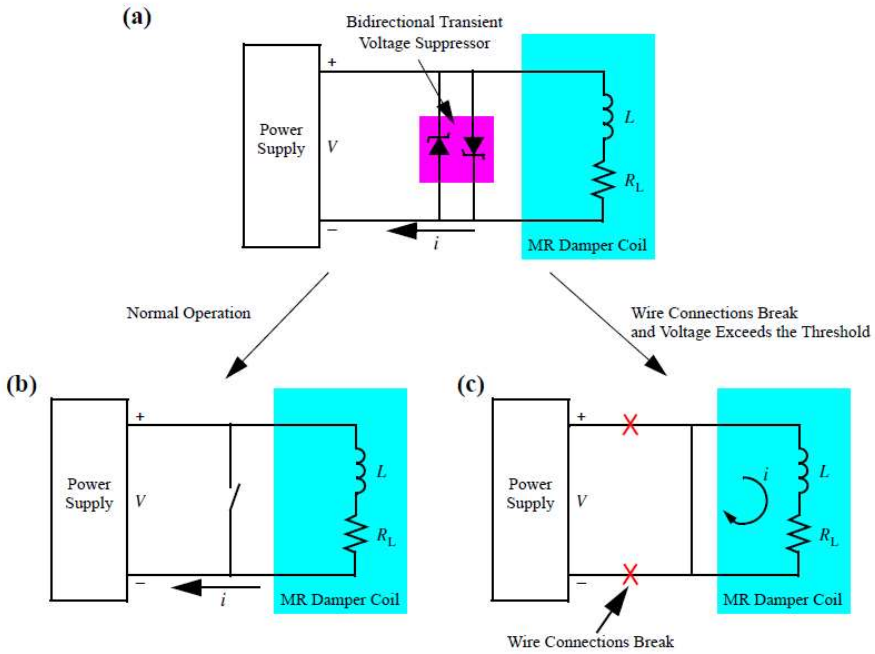

FIGURE 5.10: Electric circuit with bidirectional transient voltage suppressor [63].

To care for the coil from such voltage surges, a “transient voltage suppressor” (TVS) attached with damper coil in parallel can be used to bounds voltage to tolerable level. Generally, TVS has a high value of resistance when the voltage is under its threshold. On the other hand, as soon as its threshold voltage is cross the limited value, the TVS begins conducting due to the avalanche failure of the PN junction and it wheel clamp the voltage to a harmless level. TVS bring back to the non-conducting mode when voltage drops under its threshold level. Fig. 5.10(a) indicates a schematic of the electric circuit of the damper coil connected with a bidirectional transient voltage suppressor. During normal action, the current passes through the TVS is very small, below 5 mA, performing like an open switch (Fig. 5.10(b)). As soon as a wire joining breaks, the voltage through the coil will go beyond the threshold and the TVS starts to conduct (Fig. 5.10(c)). As a result, the voltage through the coil is blocked to a safe working level and the energy earlier kept in the coil is dissipated by the damper coil resistance. It is important to note that for a multi-stage coil, a TVS is connected with every coil to avoid the connection breaks among coils.

5.3 Fabrication of designed MR Damper

The aim of present section is to summarise the improvement of the MR fluid base damper used in present investigation. It will make known to the real physical component along with its manufacture.

5.3.1 Complete Construction of the Designed MR Dampers

The damper used in present investigation is similar to a conventional single tube damper. As précised in Table 5.3, the compressed length of the MR damper is 300 mm. After it is stretched, it extents 620 mm. The extreme stroke length of the present damper is 320 mm and the mid-stroke length of the damper is 460 mm. The damper cylinder is 44.55 mm in diameter.

TABLE 5.3. Magnetorheological Damper Working Dimensions

Damper Parameter	Dimension (in mm)
Total length (extended)	620
Total length (compressed)	300
Maximum stroke length	320
Mid stroke length	460
Inside shock tube diameter	44.55
inner/outer eyelet diameter	24/55

In relations of inside makeup, the MR damper, also known as a shock tube is similar to a conventional damper. The MR damper used in present investigation is presented in Fig. 5.11.

FIGURE 5.11: Magneto rheological Damper
(Designed and fabricated for the research experiment)

Magnetorheolocal damper and conventional mono-tube damper have few parts in common which include the lover and upper shock eyes, the housing, the centring guide which keeps the piston in centre of housing during operation, the piston rod and dynamic seals. These parts are shown in the damper schematic diagram in Fig. 5.12.

The developed MR damper include cylinder for inclosing required MR fluid volume, a piston adjusted for movement inside the cylinder, magnetic coil wounded inside the slot which is created in piston surface area with N number of winding of a conducive wire incorporate in that to express a coil that develop magnetic flux in and around the piston. The cylinder may be fabricate with an outer cover of ferrous metal to increase cross sectional area of the return flow path for the magnetic flux.

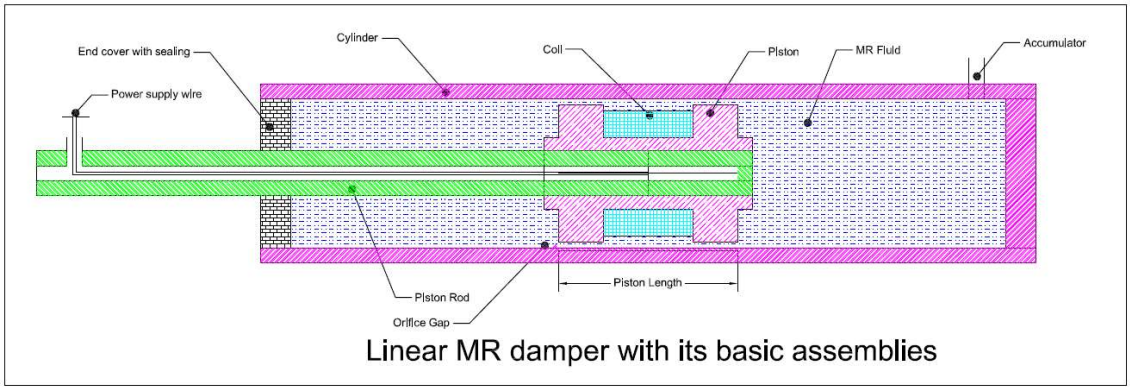

FIGURE 5.12: Structure of MR Damper Used

5.3.2 Fluid Paths in Conventional Mono-tube Damper and MR Damper

The fluid path in the MR damper used in present investigation is somewhat dissimilar as of a conventional monotube damper. As a conventional mono-tube damper compresses, the fluid runs through the gap provided in piston (fluid flow control valves) from one part to another separated by piston in cylinder, as shown in Fig. 5.13.

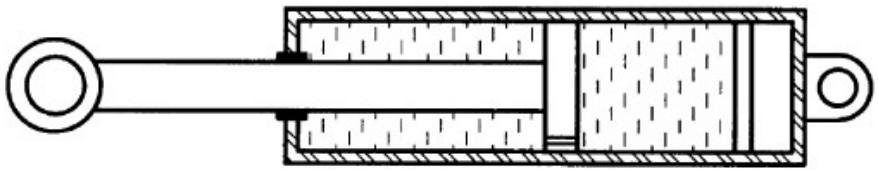

FIGURE 5.13: Conventional Mono-Tube Damper Flow Direction (adopted from 3)

As soon as the piston rod enters in the housing, the volume of MR fluid displaced by piston rod is filled by the air column of an accumulator. The flow directions in the housing are reversed, when the damper is in extension mode.

The monotube MR damper is composed of a piston, a main damper housing, and piston rod assembly and an accumulator as illustrated in Fig. 5.14.

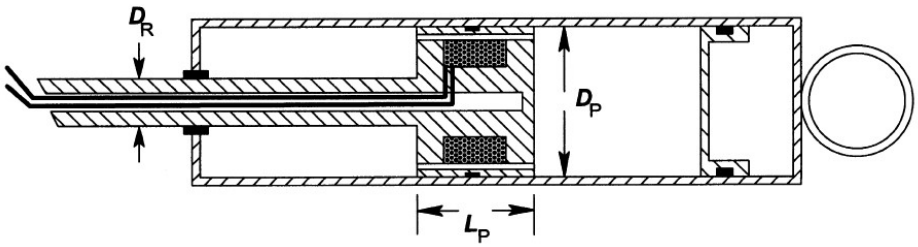

FIGURE 5.14: MR Damper Flow Direction (adopted from 3)

The main reservoir contains the piston and piston rod assembly submersed in the MR fluid while the accumulator reservoir contains a compressed and non-oxidizing gas (usually nitrogen). As the piston rod moves into the damper housing, volume of fluid equivalent to the volume of the intruding piston rod is displaced. The accumulator piston moves toward the bottom of the damper compressing the nitrogen charge to account for the change in volume. As the piston rod retracts, the accumulator piston moves up the damper tube to counteract for the loss of volume. The monotube damper design is the most versatile damper design since it can be mounted in any orientation without affecting the damper's performance.

5.3.3 Components of the Designed MR Dampers

Present segment gives details of the several components which are part of the developed MR dampers.

5.3.3.1 Damper Cylinder (Housing or Shock Tube)

The cylinder (shown in Fig.5.15) has several purposes including support and protection of the damper's inner parts, casing the liquid and removing heat from the damper liquid to the outsides. These purposes are similar in both conventional and MR dampers. The dissimilarity among the MR damper cylinder and the conventional damper cylinder is that the MR damper cylinder has more cross sectional surface area for higher value of magnetic saturation. One end of the cylinder is fitted with accumulator with an attachment eye associated therewith by lower end cap. Another or open end of the housing is closed by end member.

For best results (according to magnetic circuit design), the material of cylinder should have high permeability, high flux saturation level, small hysteresis loop area and should be magnetically soft. Particularly for this research project, low-carbon steel is selected as a cylinder material.

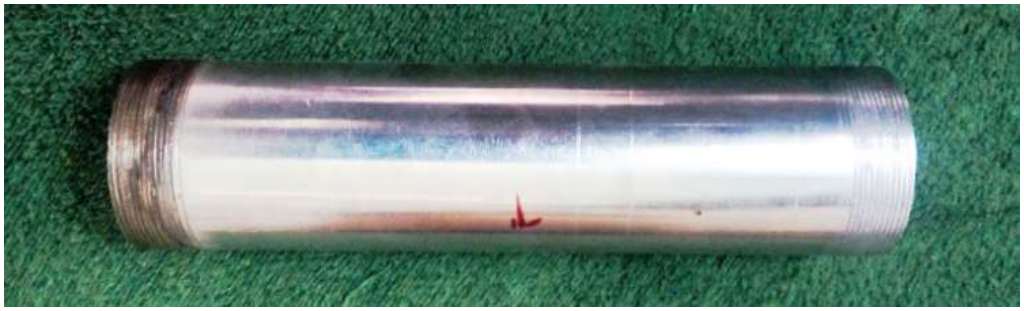

FIGURE 5.15: Damper Cylinder (Housing or Shock Tube)

Both ends of cylinder are open with external thread. At one end, accumulator is fitted. At other end, cap is fitted in which hole is drilled for passing piston road with oil seal. For MR damper and the conventional mono-tube damper, the cylinder is the tube that provide to reciprocate the piston of the damper. The liquid flows among the high pressure region and low pressure region is to some extent dissimilar in the MR damper than in a conventional mono-tube damper, however the purpose of the cylinder is unchanged. In the MR damper, as the piston reciprocates in the cylinder, liquid is forced in and out of alternating low pressure region and high pressure region of the cylinder. In order for the movement of the liquid to be mechanically advantageous, the flow has to pass through the damper valve i.e. through gap provided between cylinder and piston for MR damper.

5.3.3.2 Piston and Piston Rod

Fig. 5.16(a) shows the piston with piston road and other MR damper elements like magnetic coil and guide for cantering the piston in cylinder during operation. Both these part have more or less the similar purpose in the MR fluid base damper and conventional dampers. Single dissimilarity among these two is that a conventional mono-tube damper includes the valve into the piston whereas the MR damper incorporates the valve as a gap between inside wall of cylinder and piston. In both of MR and conventional dampers, movement of the piston has to force liquid through the damper's valving. The piston size of MR damper is higher than a conventional damper.

Magnetic field strength produced in the MR fluid be governed by the whole magnetic circuit and this should have a small reluctance. Soft iron or steel can be used to achieve

better result. For best result, low-carbon steel with high permeability and high flux saturation level is appropriate.

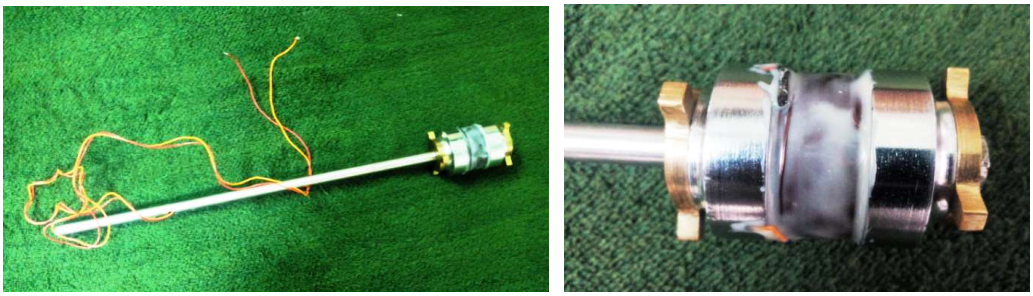

(a) (b)

FIGURE 5.16: Piston and Piston Rod Shown with magnetic coil and guide rail

Fig. 5.16(b) presents piston assembly in more detail. Head of piston is spool formed having an upper and lower externally extending projection. Magnetic coil is looped upon spool-shaped piston head among upper and lower externally extending projection.

The piston rod has two purposes. The first purpose is to comprise the channel of the inner cabling which is essential for controlling the damper. Connecting the assembly at outside of the damper body for achieving particular application with eye connected at other end of piston rod is second important purpose of piston rod.

5.3.3.3 Accumulator

The accumulator has the purpose of compensating for both variations in the volume of MR liquid. One is due to temperature change and other is due to change in the volume available to the liquid as the piston rod come in and out from the damper body.

FIGURE 5.17: Accumulator with lower end cap

Meanwhile MR liquid cannot work with a free air and liquid interface, it is essential to attach an accumulator to the design. The accumulator has to account for the variation in volume existing to the liquid as additional of the piston rod come into the housing and furthermore permit for thermal expansion of the MR liquid. The MR liquid used in present experiment has a coefficient of thermal expansion of approximately ten percent. The high pressure tubes increases and decreases as required and comprises one portion of a two portion accumulator system.

The lower shock eye of MR damper is constructed into the accumulator. Accumulator is connected with housing by lower end cap.

5.3.3.4 Lower and Upper End Caps

The lower and upper end caps are screwed on the lower and upper ends of the cylinder respectively. One end cap hold and guide piston rod with seal to prevent leakages of MR fluid from cylinder to outside. Fig. 5.18 shows upper end cap with seal. It also helps to keep the piston in centre of housing during operation. Other end cap holds the accumulator as shown in Fig. 5.17. The lower shock eye of MR damper is constructed into the lower end cap.

FIGURE 5.18: Upper end cap with seal

Two small adjustable screw fitted holes are provided in upper end cap for filling whole damper body with the MR fluid.

5.3.4 Assembly of Damper

The MR damper is bring together in stages. The main subassemblies and full assembly are shown in Fig. 5.19.

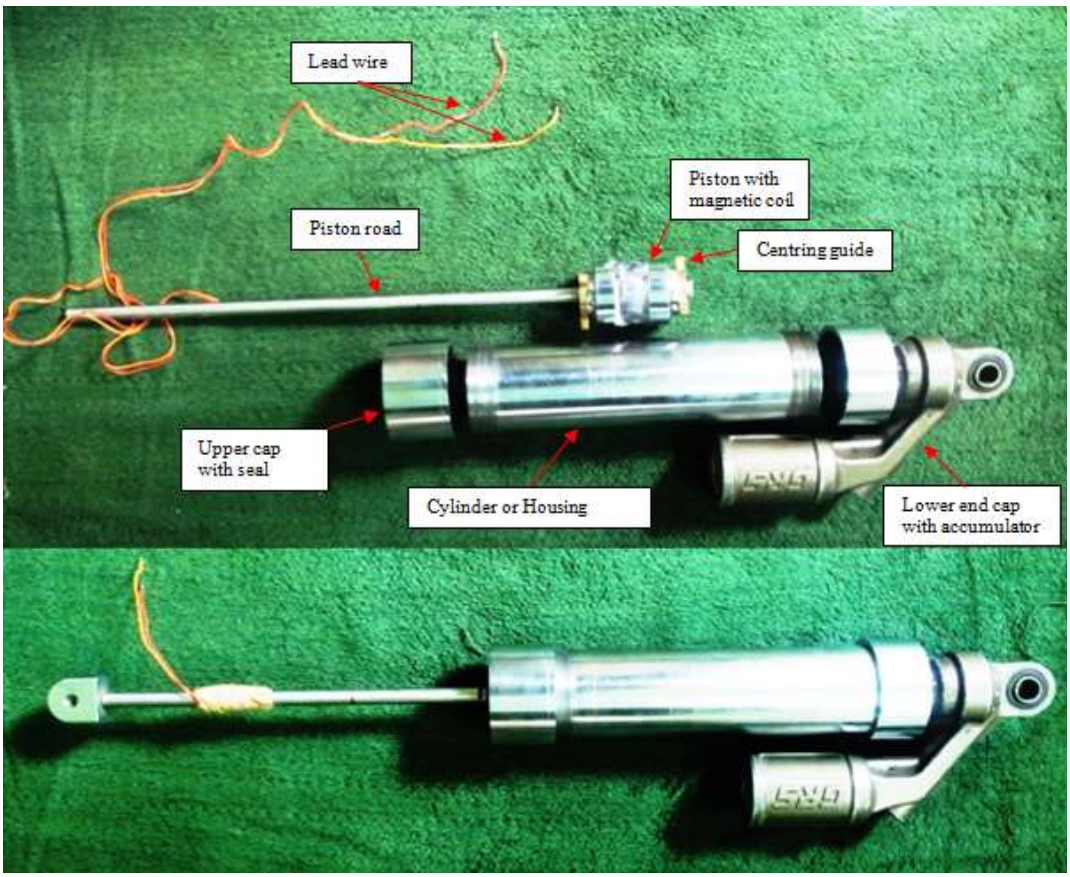

FIGURE 5.19: MR Damper Main Subassemblies

FIGURE 5.20: Filling of MR Damper by MR Fluid

The first step of the assemblies, presented in Fig. 5.19, comprises the piston rod and piston linked together, using the wire takes out from piston to piston road and it passes through inside of piston road. The second step of assembly consists of the housing with the accumulator via lower end cap. The third step of assembly comprises upper end cap with seal and piston road. Eye is fitted at other end of piston road for holding damper in test rig. After the subassemblies presented in Fig. 5.19 are piece together, the damper is assembled as presented in Fig. 5.11. The final step of assembly comprises to fill by addition MR liquid in the cylinder as presented in Fig. 5.20. This finalises the assembly of the damper. The completely assembled damper, presented in Fig. 5.11, is complete for force-velocity analysis.

MR damper for present investigation:

The damper of the current experiment is represented in Fig. 5.11. The damper is fabricated with two major components: cylinder and piston. Cylinder holds a volume of magnetorheological (MR) liquid. One liquid which contains of carbonyl iron elements suspended in castor oil. This liquid has shown itself to be predominantly well-suited for this application. Housing is a cylindrical pipe having one closed end with an accumulator and attachment eye connected therewith. Second or open end of the housing is closed by upper end cap. A seal is provided to prevent fluid leakage from housing. The accumulator has to account for the variation in volume existing to the liquid as additional of the piston rod come into the housing and furthermore permit for thermal expansion of the MR liquid. It also prevents cavitation effect. Piston head is spool formed having an upper and a lower outwardly extending flanges. Coil is wound upon spool-shaped piston head between upper flange and lower flange. Piston head is made of a magnetically permeable material, in this case, low carbon steel. Guide rails are attached above and below side of piston to keep the piston in centring position to housing during operation. Piston head is shaped with a smaller maximum diameter (in this case, D_{pole}) than the inside diameter, D_i of cylinder. The outside surfaces of guides are shaped to engage the inside diameter D_i of cylinder. Guides are made of non-magnetic material, in this case, bronze, and it maintains piston centred within cavity 'h'. In this model, cavity h (in combination with coil) works as a valve to govern the flow of MR liquid past piston. Electrical connection is provided to coil through piston rod by two lead wires. One wire is joined to a first end of an electrically conductive rod which extends through piston rod to outside of damper. The other end of the winding of coil is attached to a "ground" connection on the outside of damper. As

shown in figure, the upper end of piston rod has threads to allow attachment of damper. A current in the range of 0-4 amps at a voltage of 12-24 volts is provided by connecting the leads with an external power supply. The outside surface of coil is layered with epoxy paint as a protecting measure. The damper of present experiment works as a Bingham type damper, i.e., this structure come close to an ideal damper in which the force produced is not depends on piston velocity and big forces can be produced with small or zero velocity. This independence increases controllability of the damper making the force a function of the magnetic field strength, which is a function of current flow in the circuit

CHAPTER 6
TESTING OF DEVLOPED MR FLUID BASE DAMPER

6.1 Introduction

To investigate the fundamental behaviour of the designed small-scale MR damper, a series of quasi-static experiments were conducted at the Physics Department Laboratory, Bhavnagar University. In this chapter, subsequent segments describe the experimental setup and experimental results. Results are presented for the different test carried out like variable input current tests, amplitude-dependent tests and frequency-dependent tests. The experimental results are then used to compare with theoretical results obtained using a mathematical model described in the previous chapter. The experimental results are also used to validate experiment procedure by design of experiment methodology using design expert software. Very good comparisons in force-displacement behaviour are observed between theoretical and experimental results.

The damper, also known as a shock absorber, is characterized by its instantaneous value of position velocity, acceleration, force, pressure, temperature, etc. and various plots among these parameters. For the measurement of listed parameters of the damper, a test rig is designed and developed. An experiment on the test rig is carried out at different speeds and loads which led to the output in terms of sinusoidal waveform on attached oscilloscope. The waveform is used to find out the characteristics at different load-speed combination. The results obtained are used to find out the behaviour of damper at different speeds and loads.

Some phenomena observed during the experiment are also discussed and possible explanations are given.

6.2 Experimental Setup

This section presents a model test setup to calculate the characteristics of designed MR damper at various loading conditions. The principle mechanism for the basis of this experimental setup designed to measure the characteristics is single slider crank mechanism. This mechanism converts rotary motion of the circulating disc into the linear

motion of the damper. At various loads and speeds combinations, the readings on the test setup is taken with the help of various sensors mounted on test rig and by using these data, characteristics of damper are evaluated.

Analysis of damper could be categorized in two important headers [3]:

(1) Rig analysis of component or complete of the damper

(2) Road analysis of the damper on the motor vehicle.

Rig analysis of whole damper or their individual component may be placed in three supplementary headings:

(1) Performance measure

(2) Durability check

(3) Testing of theoretical models.

Analysis of theory is necessary to authorise techniques of examination and to give assurance in model for design work. This is to be expected to include testing of separate component or testing of whole damper to relate damping characteristics, to examine piston or rod seal friction effects, etc.

Durability check is executed by test rig and this can be suitable for preliminary testing of innovative materials or production techniques, but the primary durability testing is by road testing.

Following are typical plots of interest for damper to characterize it:

- Position with respect to Time
- Velocity with respect to Time
- Acceleration with respect to Time
- Force with respect to Time
- Force with respect to Position
- Force with respect to Velocity

For obtaining such parameters, experimental setup should be carried out properly.

There are three main types of testing methodology adopted according to technology applied and value of damping force [3]:

- Transient Testing
- Electromechanical Testers
- Hydraulic Tester

For present investigation, the experimental setup is designed based on electromechanical tester methodology.

6.2.1 Electromechanical Tester

Fig. 6.1 explain reciprocating type electromechanical testing fundamentals. In electro mechanical tester, cyclic tests are accomplished by reciprocating the piston in cylinder in an approximately sinusoidal fashion by means of a slider crank mechanisms. The force is measured by load cell attached at other end of the damper.

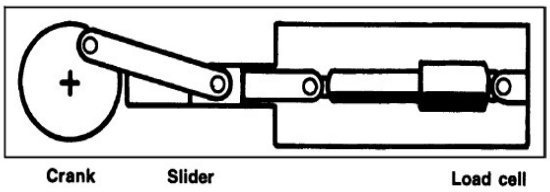

FIGURE 6.1: Reciprocating type electromechanical tester [3]

6.2.2 Design of Test Rig

The basic factors to be measured are instantaneous values of:

(a) X: Position
(b) V: Velocity
(c) A: Acceleration
(d) F: Force
(e) P: Pressure
(f) T: Temperature.

These requirement measuring device like sensors, pulse data processing and appropriate display. Moreover, the data stream will be handled to provide values for example cyclic extremes of position and force.

The basic damper analyser or shock analyser kit connections are shown in Fig. 6.2.

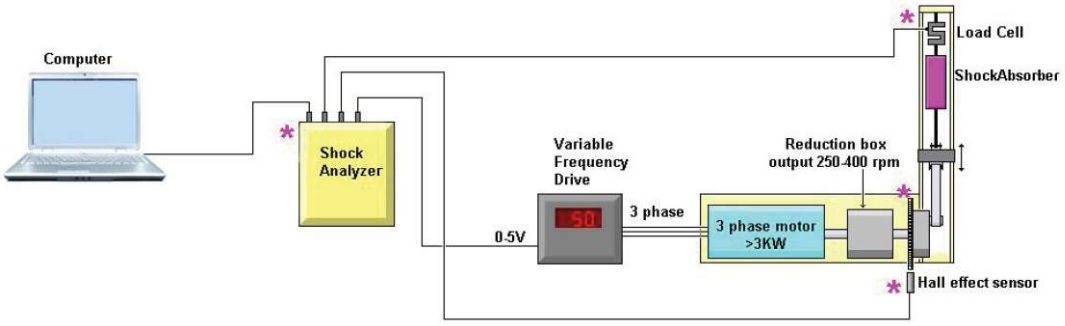

FIGURE 6.2: Lay out of damper analyser kit connections.

Following are various instruments required to achieve listed variables.

(1) Oscilloscope

The raw data which changes through the cycle are usually presented on an oscilloscope. The storing kind of oscilloscope attached with test rig is considerably superior in presenting the cyclic profile, for example force against position; F-X.

(2) Linear Variable Differential Transformer (LVDT).

LVDT is a position sensor and is put together into the ram. It will provide voltage output directly to computer by oscilloscope and it is linearly related to the location with a positional signal.

(3) Velocity Sensor

Velocity of piston is derived from velocity sensor. Velocity is also achieved by electronic differentiation of the positional signal gained by LVDT. In present case, velocity is achieved by differentiation of the positional signal gained by LVDT.

(4) Load cell

The shock force is measured by load cell. It is simply a slight elastic beam supporting the stationary end of the shock. It gives a slight deflection which can be measured to give a rapid load signal. The load signals in the form of voltage output are transferred directly to computer through oscilloscope.

(5) Accelerometer sensor

It gives instantaneous value of acceleration. Acceleration can also be achieved by differentiation of the velocity signal, but double stage of differentiation will significantly amplify any noise in the original position signal. Accelerometer measuring device is principally just a load cell with a known mass, with acceleration derived from $A = F/m$. Velocity could also be integrated from the acceleration.

(6) Pressure sensor

Damper liquid pressure is measured by pressure sensor. It is installed into damper body by means of welding or brazing of a tapped boss to accept a standard measuring device. It is if possible placed at the extreme ends of the shock so that the piston seals are not damaged

by passing over the hole and so that welding distortion of the working cylinder does not reason the leak.

(7) Thermocouple sensor

This one is used to measure temperature of damper body and damper fluid. The temperature value is affecting the performance. This tends to decrease the damping forces at a specified speed which are required to be measured. The most appropriate measuring device are thin flexible insulated wires and should be rated for the temperature up to 2000^0C or higher. These are without difficulty taped to the body of the shock.

Damper or Shock Absorber Test Rig

A damper or a Shock Absorber Test Rig, designed and developed at physics department, M. K. Bhavnagar University is shown in Fig. 6.3.

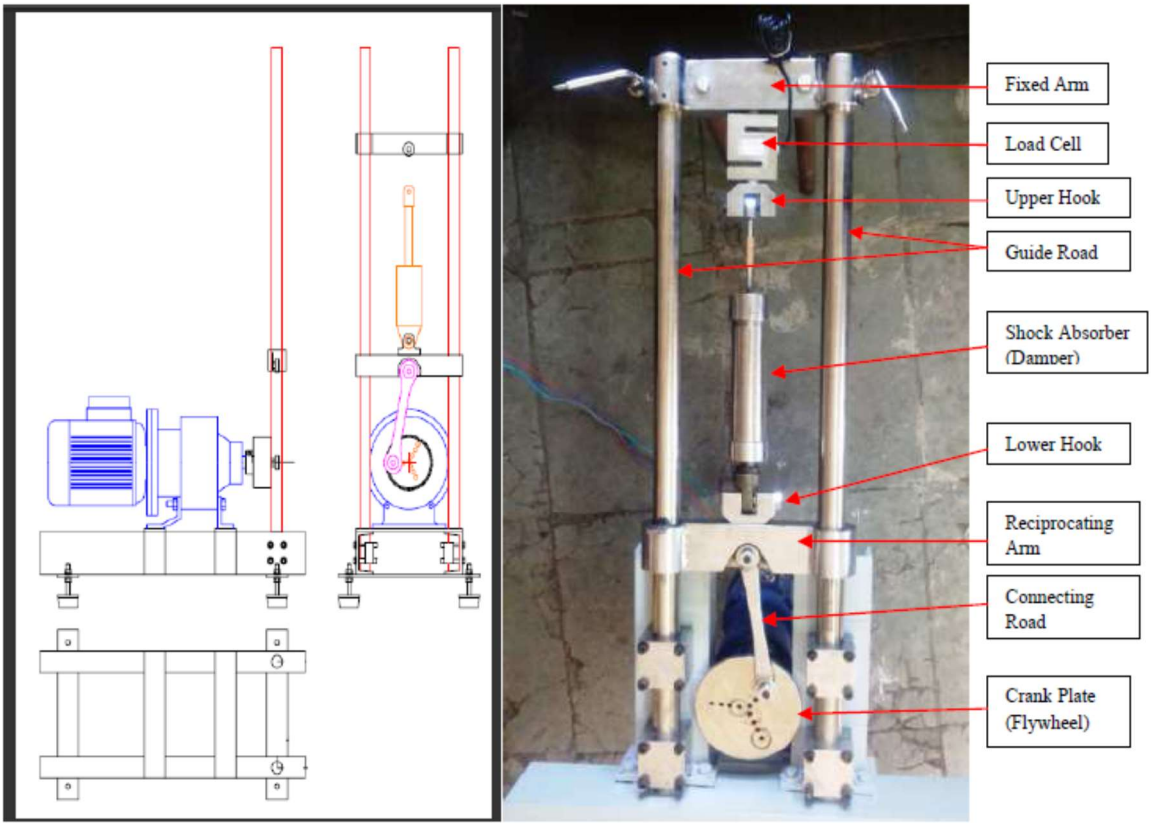

FIGURE 6.3: Damper Test Rig

The purpose of Damper Test Rig is to construct a damper dynamometer. Damper dynamometer is an instrument to examination dampers and produce charts for the damper characteristics. These charts are made for the dampers or stored so user could develop

database of in what way every damper works under the experiment conditions. This instrument switches the trial and error methodology into a reliable and effective process to decide the damper used during an operation.

Structure of developed test rig:

The Damper or Shock Absorber Test Rig be made up of a metallic main assembly, an electric motor with variable speed output gear box to decrease output speed, a piston-crank slider mechanism to cycle the damper and a computer connected with damper test rig by oscilloscope. The oscilloscope acquires data as well as displays the test graphs. Furthermore, it saves different test results and allows overlying several tests to match the performance. It is simple to construct using industrial devices and it is easy to use. The assembly consists of a robust steel frame using two vertical cylinder-shaped beams. Both cylinder-shaped beams tied together using a robust upper beam, have bolted load cell. The load cell has a connector for fastening the damper to it. The base frame act as a stand for the electric motor, gear box and the two cylinder-shaped shafts. A LVDT is mounted on any vertical beam which measures displacement with respect to time and gives velocity of the shock.

Basic characteristics of presented damper or Shock absorber test rig are:

- Range of Stroke 5-100 mm
- Range of Speed 0-500 mm/s
- Range of Force (Load Cell range) 0-1500 Kg (Output in terms of volt-0 to 10 V)
- Cycle frequency 0 to 400 rpm
- LVDT range 0 to 150 mm (Output is in terms of volt - 0 to 5 V)

Components:

Electric Motor and Gear Box:

Damper Test Rig is generally driven by 3-phase AC electric motor. The size of motor and power is limited to its voltage supply. For applications up to 2 HP, the motor can be driven by the normal single-phase power source. Bigger motor in the range of 2 HP to 10 HP can be driven by 3-phase power source. The motor is connected to an adjustable speed gear box to permit the user to cycle the damper at flexible cycles/minute to test various speed choice.

This setup of Damper Test Rig is powered by 3-phase, 2 HP, AC electric motor with variable speed gear box. The motor output is geared down by means of variable speed gear box. The maximum output shaft speed is in the range of 300 to 400 RPM.

Piston - Crank Mechanism

This mechanism be made up of a crank plate, connecting rod and piston like to the piston-crank mechanism in an I.C. engine. The crank has holes drilled to attain variable stroke lengths as shown in Fig. 6.4. The disadvantage of using this mechanism is that it does not produce perfect sinusoidal motion in the piston, but having a longer connecting rod can compensate for this. Although it is not necessary to have sinusoidal motion, it does help to reduce vibrations. The advantage to this mechanism is its cost effectiveness because there is less high tolerance machining.

Stroke length selector

There are twelve screwed holes positioned over spiral profile in crank plate as shown in Fig. 6.4. Connecting rod can be secure in any hole to choice stroke length. The longer the stroke, the greater the power needed on motor to move the damper. At higher stroke, it may be possible that the motor couldn't run the damper, thus it is recommend to start at position from minimum value and increasing it step by step. Table 6.1 represents the value of stroke length for hole position.

FIGURE 6.4: Disk type crank plate with stroke adjuster hole.
(Designed and manufactured for the research experiment)

TABLE 6.1: Hole position – Stroke length data

Position of Hole	Stroke Length in mm
1	10
2	20
3	30
4	40
5	50
6	60
7	70
8	80
9	90
10	100
11	110
12	120

Load Cell:

A load cell is a device which alters load acting on it into analog electrical signals. A load cell fitted with the crossbeam measures the force to be found on the damper.

Damper temperature sensor:

Damper temperature is recorded by means of a thermocouple fitted with the housing of the damper by a Velcro strap. Damper performance can vary dramatically at different temperatures. With the help of temperature monitoring arrangement, shock performance can be determined under various temperatures. In present case, performance is carried out at temperature maintained at 30 ^{0}C ± 3

Working of Damper Test Rig

Fig. 6.5 indicates fully instrumented damper test rig developed for present investigation with setup. The setup consist of piston and crank (Single Slider Crank Mechanism). This mechanism be made up of a crank, connecting rod and piston (reciprocating arm). The crank plate has holes drilled to achieve different stroke lengths shown in Fig. 6.4. The advantage of this mechanism is its cost effectiveness because there is less high tolerance machining. The frequency is adjusted by using variable gear drive system powered by

electric motor. The speed available from the motor is geared down by means of gearbox. The maximum output shaft speed is in the range of 350 to 400 RPM at full speed of motor having 1440 RPM. Variation of stroke is possible by fixing the connecting road in appropriate hole made in crank plate, as a result the stroke is fixed to provide the preferred maximum speed inside the limits of the damper and experiment apparatus. There are twelve screwed holes positioned over spiral form; connecting rod can be secure in appropriate hole to choice stroke length. The higher the stroke, the greater the power required on motor to move the damper.

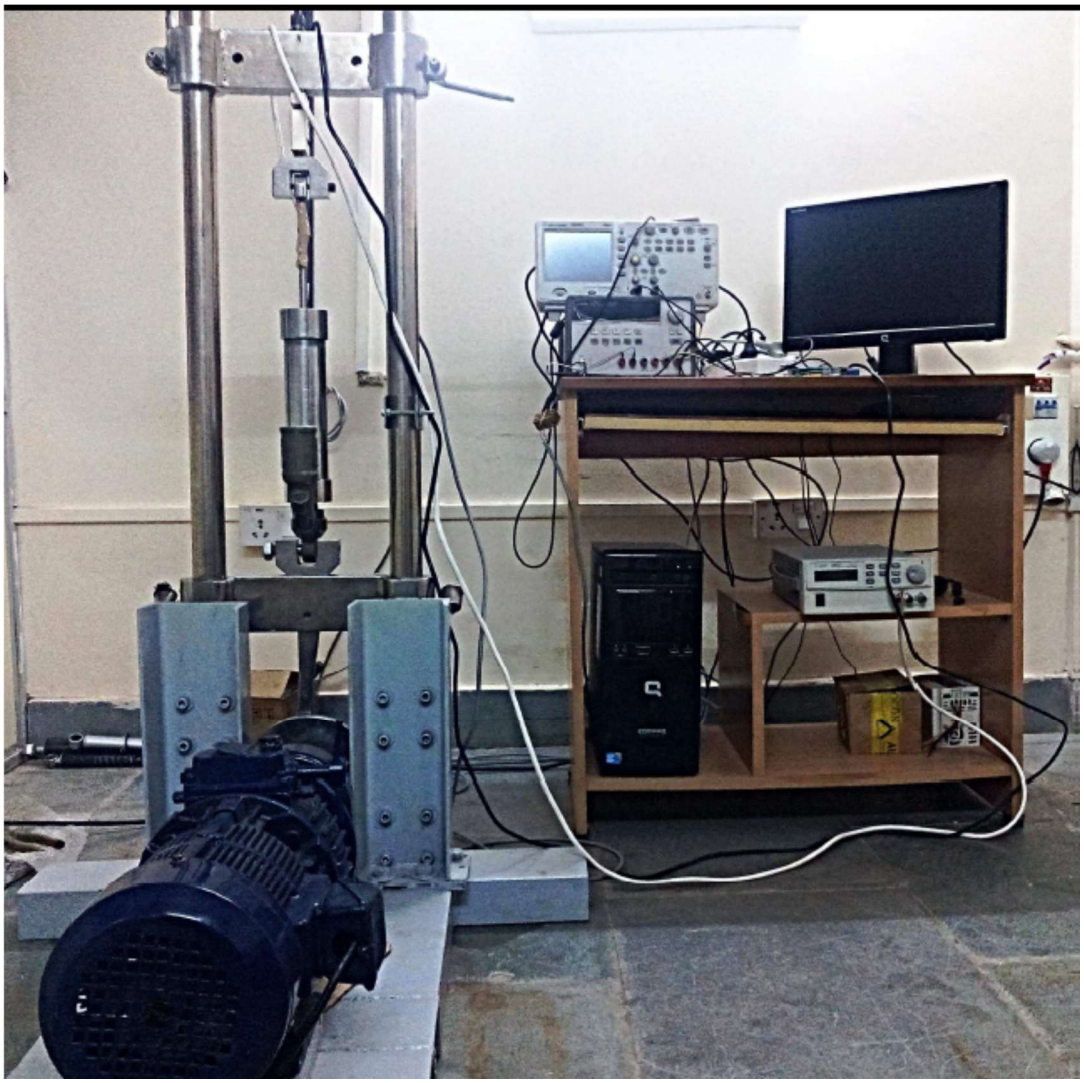

FIGURE 6.5: Fully instrumented damper test rig developed at physics department laboratory

Dampers are fastened into the test rig on the given mounting positions. The stroke and motor speed is fixed to a selected speed choice. The computer is set to obtain the data from oscilloscope. Initial damper body temperature is taken and system is provided which keep the damper body temperature constant during experiment. The test rig is then started and

the damper is operated within the selected velocity range. The data are directed to the computer via oscilloscope. The computer can then show the data in a numerical and graphical form that will permit the operator to regulate the damper accordingly

6.3 Testing of developed MR Fluid Damper under Sinusoidal Displacement Excitations

To obtain the data used to characterize the designed MR fluid damper behaviour, a series of experiments on the test rig were conducted under various sinusoidal displacement excitations while simultaneously altering the magnetic coil in a varying current range. The output of each test was the force generated by the damper. During all the experiments, the damping force response was measured together with the variation of piston displacement and supplied current for the damper.

The setting parameters for experiments are listed in Table 2. Instantaneous values of time, displacement and force for complete cycle are stored in computer via oscilloscope in voltage form. Finally, the data are converted in the form of physical unit by C program developed for this special application (listed in appendix-B). Instantaneous value of velocity is calculated by differentiation of displacement with respect to time. Observations are taken according to this plane and represented in graphical form.

TABLE 6.2: Setting parameters for experiment

Amplitude	Frequency In Hz	Current Value in Amp.				
0.5 cm	0.75	0	0.25	0.5	0.75	1
	1.0	0	0.25	0.5	0.75	1
	1.5	0	0.25	0.5	0.75	1
	2.0	0	0.25	0.5	0.75	1
1.0 cm	0.75	0	0.25	0.5	0.75	1
	1.0	0	0.25	0.5	0.75	1
	1.5	0	0.25	0.5	0.75	1
	2.0	0	0.25	0.5	0.75	1
1.5 cm	0.75	0	0.25	0.5	0.75	1
	1.0	0	0.25	0.5	0.75	1
	1.5	0	0.25	0.5	0.75	1
	2.0	0	0.25	0.5	0.75	1
2.0 cm	0.75	0	0.25	0.5	0.75	1
	1.0	0	0.25	0.5	0.75	1
	1.5	0	0.25	0.5	0.75	1
	2.0	0	0.25	0.5	0.75	1

The minimum shaft rotation connected with motor via gearbox is about 40 RPM. Due to that reason, the minimum frequency value is selected as 0.75 Hz and then increased it in terms of 1.0, 1.5 and 2.0 Hz. The intermediate value is sufficient for understanding the behaviour of damper with respect to frequency variation.

The current value is selected from 0 Amp to 1.0 Amp. Beyond maximum limit of 1.0 Amp current value, the magnetic circuit get saturated and there will be no effect of higher current value. It is also important to study the behaviour of damper at off state condition, i.e. at 0 Amp current value. Thus the range of current is selected form 0 Amp to 1.0 Amp with increment of 0.25 Amp for better understand of change in current behaviour.

Results of various experimental tests under sinusoidal displacement excitations are presented. These tests include: variable input current tests, frequency dependent test and amplitude-dependent tests.

Force-displacement, force-velocity and force-time experiments under sinusoidal displacement excitation at different frequencies with different constant current levels of 0, 0.25, 0.5, and 1 A were conducted. At each current level, excitations with altered amplitudes and frequencies were applied to the MR damper. The tests conducted for presented damper configuration are summarized in Table 6.3 to Table 6.6, and complete experimental results were presented in graphical form. Again, to reduce temperature effects, the tests were conducted at a temperature of 30 ^{0}C ± 3. It is also to be noted that experimental and theoretical data are presented and compared at each level.

The whole experiment procedure was carried out in four steps. During each step, the value of amplitude was keep constant and for each frequency level, instantaneous values of damping force, displacement and velocity were measured for complete cycle at different values of current as shown in Table 6.2.

6.3.1 Test with constant amplitude value of 0.5 cm (Stroke length 1.0 cm)

During first experiment, the amplitude value was set as 0.5 cm, by selecting appropriate hole in stroke selection plate. Frequency values were selected as 0.75, 1.0, 1.5 and 2.0 Hz with the help of variable gear drive system. Instantaneous values of damping force, displacement and velocity were measured and stored in a computer via oscilloscope for a complete cycle. The data for a cycle are analysed and presented in graphical form with theoretical values also as shown in Fig. 6.6 to Fig. 6.9. The data further analysed as maximum damping force, maximum controllable force and dynamic range for experimental values and theoretical values. The analysis is presented by Table 6.3 showing % of error between theoretical and experimental values.

Fig. 6.6 shows the experimental and analytical results variation during one complete cycle with following parameter value.

Amplitude A= 0.5 cm. (Stroke Z = 1.0 cm.)

Frequency f = 0.75 Hz. (Angular speed of crank plate = 45 RPM)

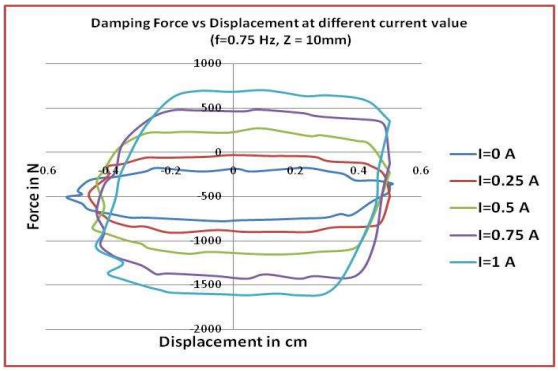

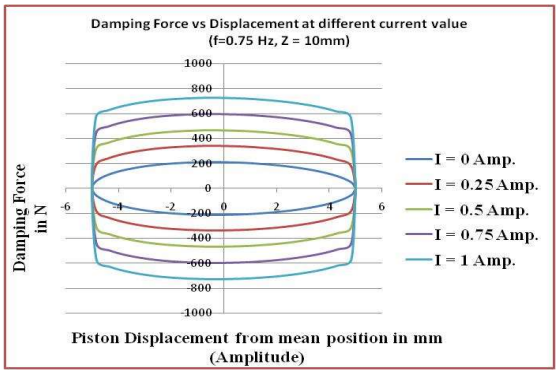

Measured value Analytical value

FIGURE 6.6 (a): Force-disp. relationships under 0.5 cm amplitude for different current values at f = 0.75 Hz

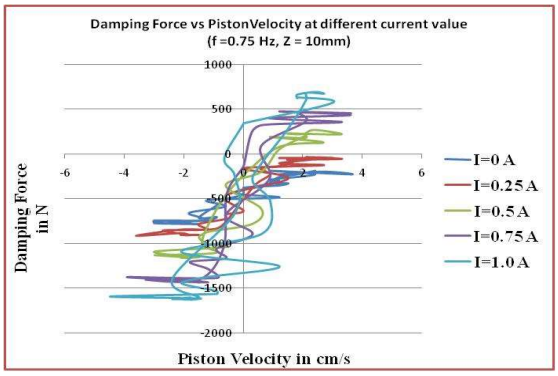

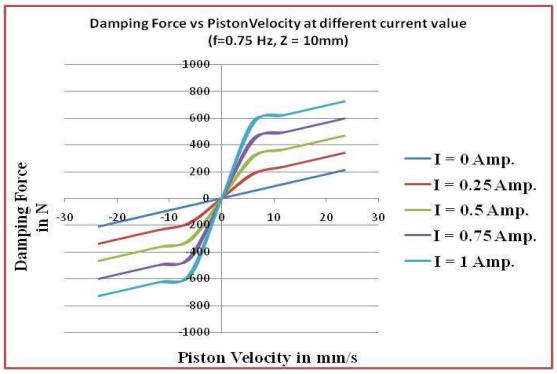

Measured value Analytical value

FIGURE 6.6 (b): Force-velo. relationships under 0.5 cm amplitude for different current values at f = 0.75 Hz

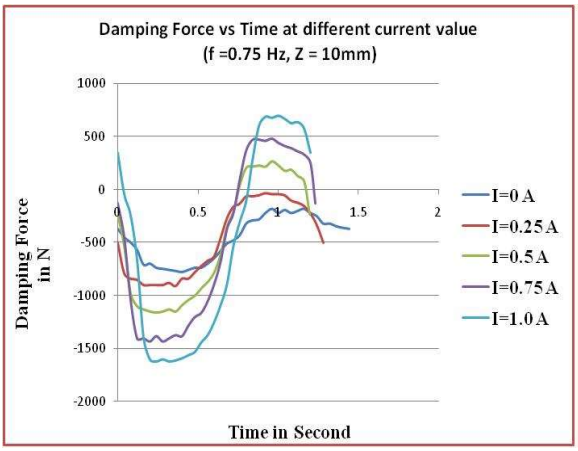

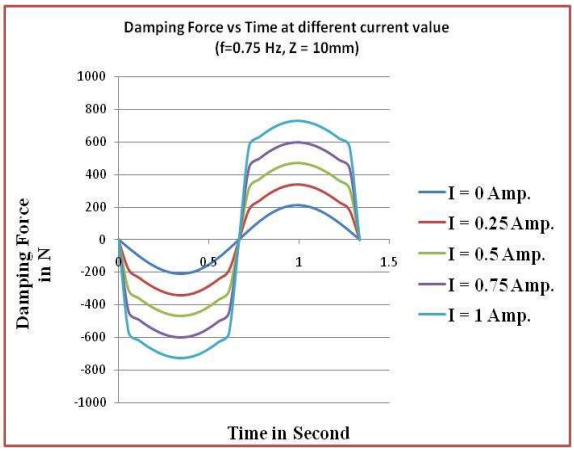

Measured value Analytical value

FIGURE 6.6 (c): Force-time relationships under 0.5 cm amplitude for different current values at f = 0.75 Hz

Fig. 6.7 shows the experimental and analytical results variation during one complete cycle with following parameter value.

Amplitude A= 0.5 cm. (Stroke Z = 1.0 cm.)

Frequency f = 1.0 Hz. (Angular speed of crank plate = 60 RPM)

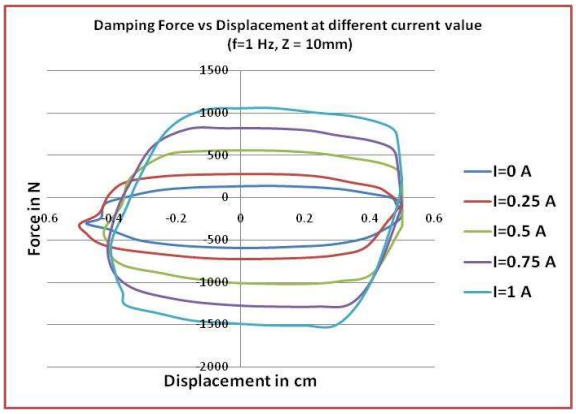

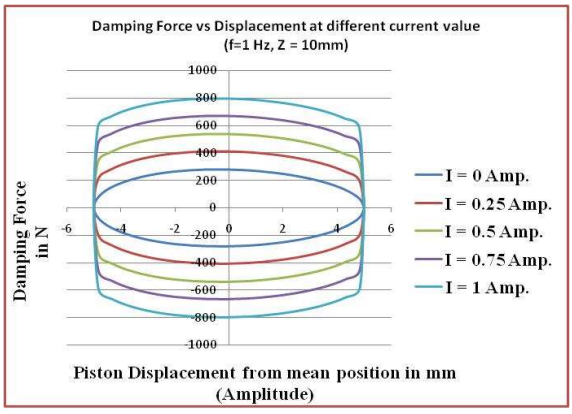

Measured value Analytical value

FIGURE 6.7 (a): Force-disp. relationships under 0.5 cm amplitude for different current values at f = 1.0 Hz

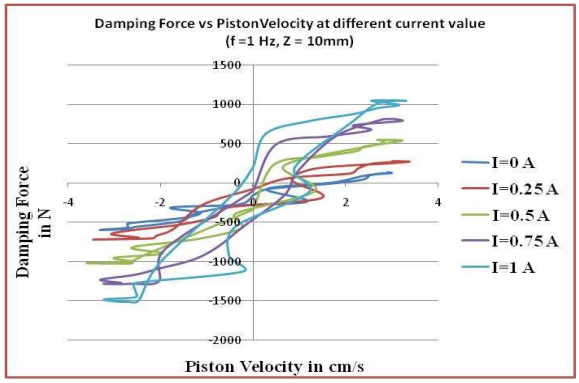

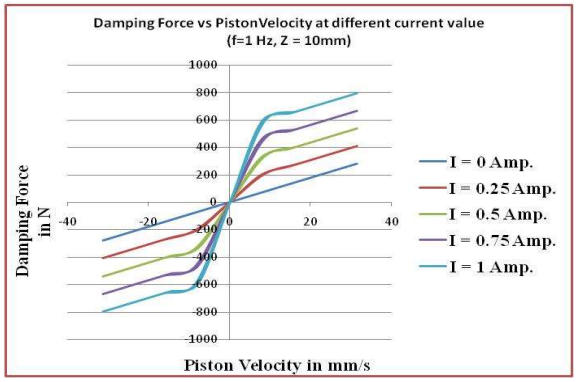

Measured value Analytical value

FIGURE 6.7 (b): Force-velo. relationships under 0.5 cm amplitude for different current values at f = 1.0 Hz

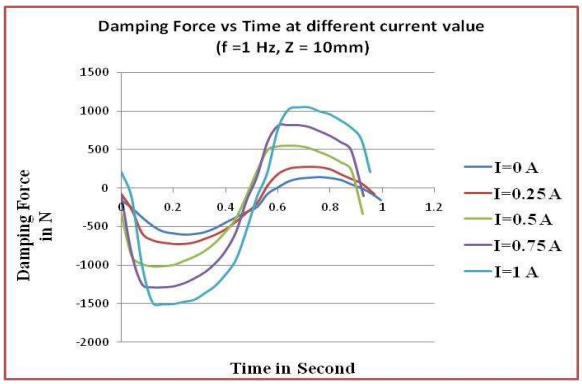

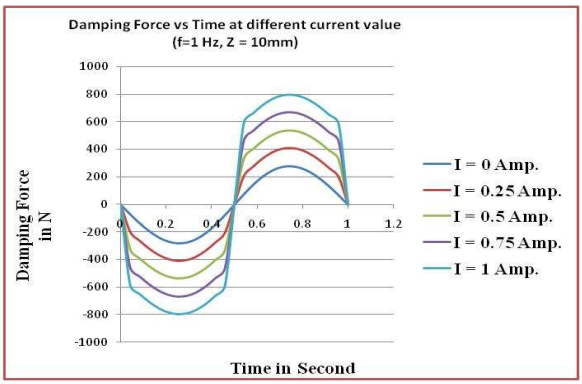

Measured value Analytical value

FIGURE 6.7 (c): Force-time relationships under 0.5 cm amplitude for different current values at f = 1.0 Hz

Fig. 6.8 shows the experimental and analytical results variation during one complete cycle with following parameter value.

Amplitude A= 0.5 cm. (Stroke Z = 1.0 cm.)

Frequency f = 1.5 Hz. (Angular speed of crank plate = 90 RPM)

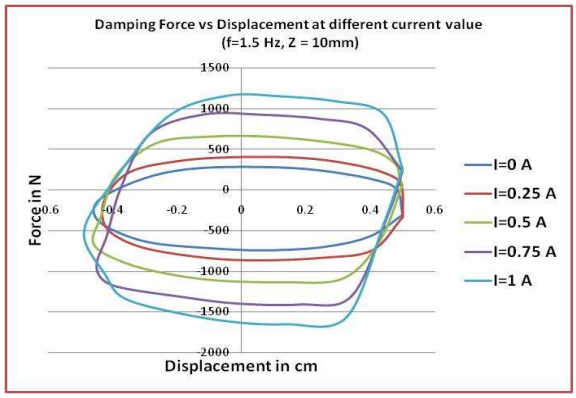

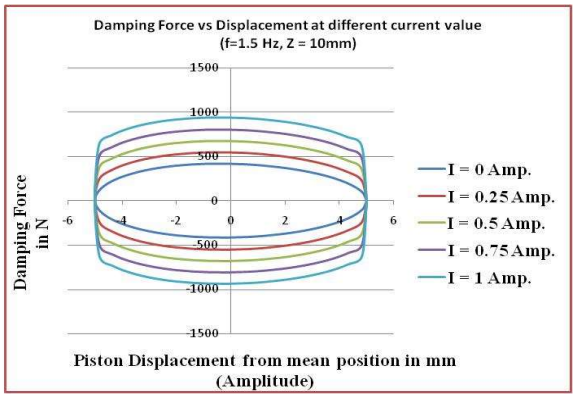

Measured value Analytical value

FIGURE 6.8 (a): Force-disp. relationships under 0.5 cm amplitude for different current values at f = 1.5 Hz

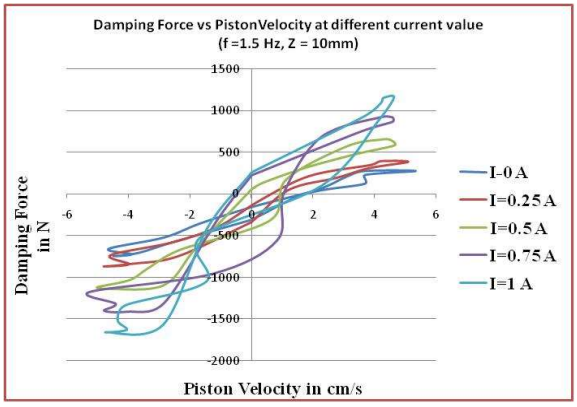

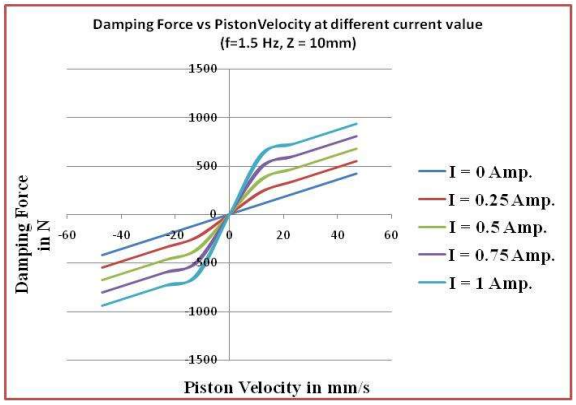

Measured value Analytical value

FIGURE 6.8 (b): Force-velo. relationships under 0.5 cm amplitude for different current values at f = 1.5 Hz

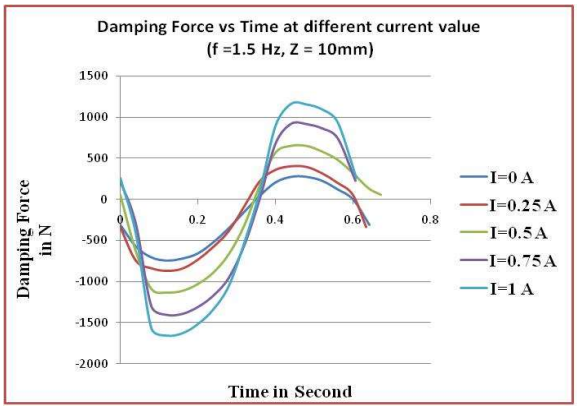

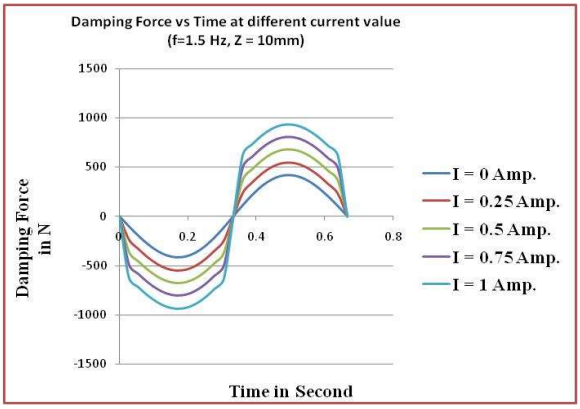

Measured value Analytical value

FIGURE 6.8 (c): Force-time relationships under 0.5 cm amplitude for different current values at f = 1.5 Hz

Fig. 6.9 shows the experimental and analytical results variation during one complete cycle with following parameter value.

Amplitude A= 0.5 cm. (Stroke Z = 1.0 cm.)

Frequency f = 2.0 Hz. (Angular speed of crank plate = 120 RPM)

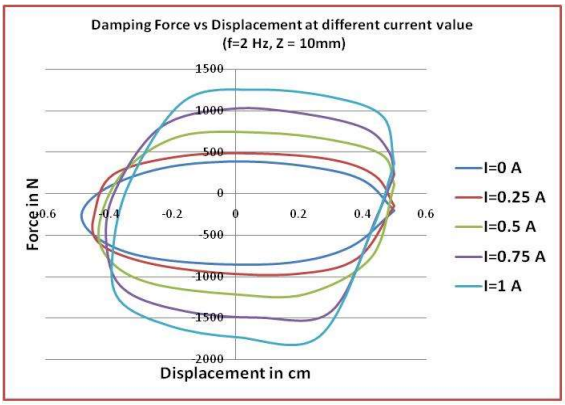

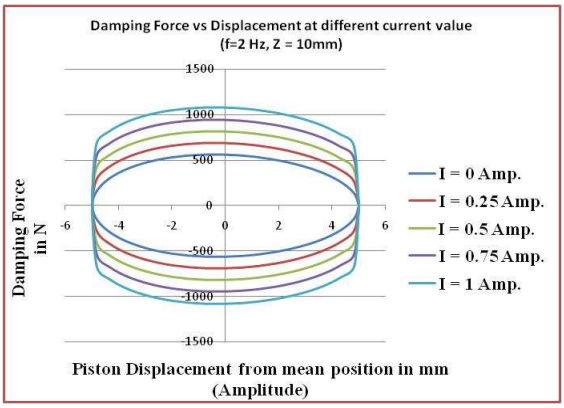

Measured value Analytical value

FIGURE 6.9 (a): Force-disp. relationships under 0.5 cm amplitude for different current values at f = 2.0 Hz

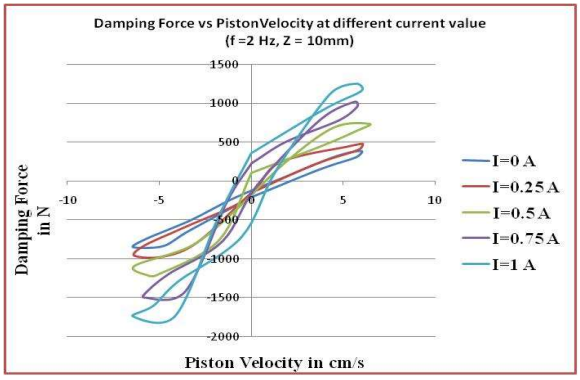

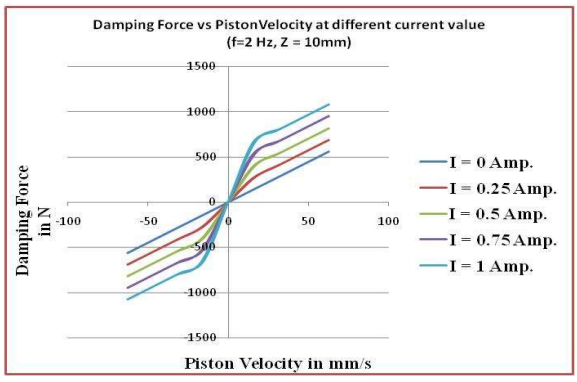

Measured value Analytical value

FIGURE 6.9 (b): Force-velo. relationships under 0.5 cm amplitude for different current values at f = 2.0 Hz

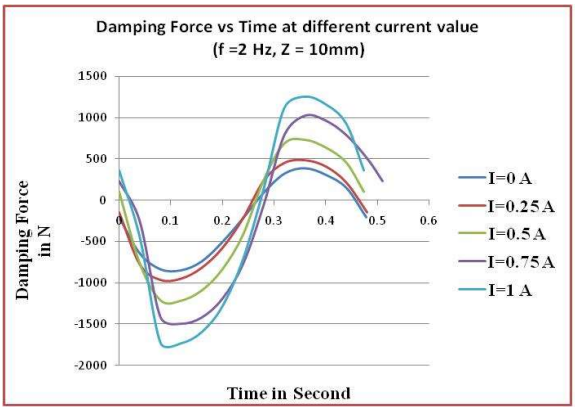

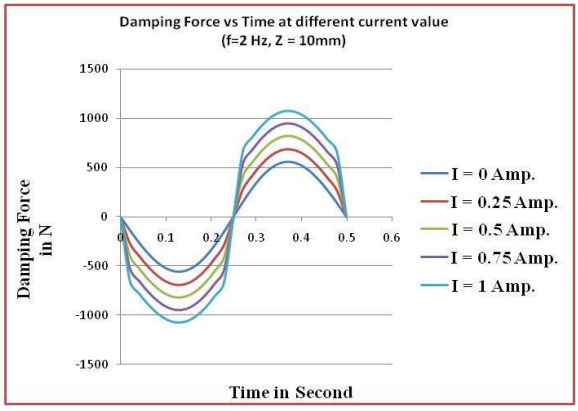

Measured value Analytical value

FIGURE 6.9 (c): Force-time relationships under 0.5 cm amplitude for different current values at f = 2.0 Hz

TABLE 6.3: Measured maximum force, controllable force and dynamic range and their comparison with analytical results for the value of **Amplitude = 0.5 cm.**

			For I = 0A	For I = 0.25A	For I = 0.5A	For I = 0.75A	For I = 1A
N=45 RPM, f=0.75 Hz	Max. Force in N At 0.5 cm amp. (Span/2)	Measured	249.00	404.00	562.00	703.00	868.00
		Predicted	209.83	339.26	468.70	598.13	727.57
		Error in %	18.67	19.08	19.91	17.53	19.30
	Controllable Force in N	Measured	0.00	155.00	313.00	454.00	619.00
		Predicted	0.00	129.43	258.87	388.30	517.74
		Error in %	0.00	19.75	20.91	16.92	19.56
	Dynamic Range	Measured	0.00	0.62	1.26	1.82	2.49
		Predicted	0.00	0.62	1.23	1.85	2.47
		Error in %	0.00	0.91	1.89	1.48	0.75
			For I = 0A	For I = 0.25A	For I = 0.5A	For I = 0.75A	For I = 1A
N=60 RPM, f=1 Hz	Max. Force in N At 0.5 cm amp. (Span/2)	Measured	342.00	500.00	638.00	803.00	958.00
		Predicted	279.83	409.26	538.70	668.13	797.57
		Error in %	22.22	22.17	18.43	20.19	20.12
	Controllable Force in N	Measured	0.00	158.00	318.00	461.00	616.00
		Predicted	0.00	129.43	258.87	388.30	517.74
		Error in %	0.00	22.07	22.84	18.72	18.98
	Dynamic Range	Measured	0.00	0.46	0.99	1.35	1.80
		Predicted	0.00	0.46	0.93	1.39	1.85
		Error in %	0.00	0.12	7.42	2.86	2.65
			For I = 0A	For I = 0.25A	For I = 0.5A	For I = 0.75A	For I = 1A
N=90 RPM, f=1.5 Hz	Max. Force in N At 0.5 cm amp. (Span/2)	Measured	510.00	634.00	794.00	996.00	1151.00
		Predicted	419.65	549.09	678.52	807.96	937.39
		Error in %	21.53	15.46	17.02	23.27	22.79
	Controllable Force in N	Measured	0.00	124.00	284.00	486.00	641.00
		Predicted	0.00	129.43	258.87	388.30	517.74
		Error in %	0.00	4.20	9.71	25.16	23.81
	Dynamic Range	Measured	0.00	0.24	0.56	0.95	1.26
		Predicted	0.00	0.31	0.62	0.93	1.23
		Error in %	0.00	21.17	9.73	2.99	1.87
			For I = 0A	For I = 0.25A	For I = 0.5A	For I = 0.75A	For I = 1A
N=120 RPM, f=2 Hz	Max. Force in N At 0.5 cm amp. (Span/2)	Measured	616.00	726.00	907.00	1104.00	1263.00
		Predicted	559.57	689.00	818.44	947.87	1077.31
		Error in %	10.09	5.37	10.82	16.47	17.24
	Controllable Force in N	Measured	0.00	110.00	291.00	488.00	647.00
		Predicted	0.00	129.43	258.87	388.30	517.74
		Error in %	0.00	15.02	12.41	25.67	24.97
	Dynamic Range	Measured	0.00	0.18	0.47	0.79	1.05
		Predicted	0.00	0.23	0.46	0.69	0.93
		Error in %	0.00	22.80	2.11	14.16	13.52

6.3.2 Test with constant amplitude value of 1.0 cm (Stroke length 2.0 cm)

During second experiment, the amplitude value was set as 1.0 cm, by selecting appropriate hole in stroke selection plate. Frequency values were selected as 0.75, 1.0, 1.5 and 2.0 Hz with the help of variable gear drive system. Instantaneous values of damping force, displacement and velocity was measured and stored in a computer via oscilloscope for a complete cycle. The data for a cycle are analysed and presented in graphical form with theoretical values also as shown in Fig. 6.10 to Fig. 6.13. The data further analysed as maximum damping force, maximum controllable force and dynamic range for experimental values and theoretical values. The analysis is presented by Table 6.4 showing % of error between theoretical and experimental values.

Fig. 6.10 shows the experimental and analytical results variation during one complete cycle with following parameter value.

Amplitude A= 1.0 cm. (Stroke Z = 2.0 cm.)

Frequency f = 0.75 Hz. (Angular speed of crank plate = 45 RPM)

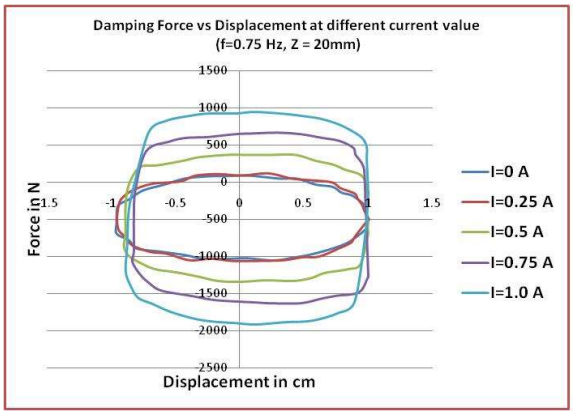

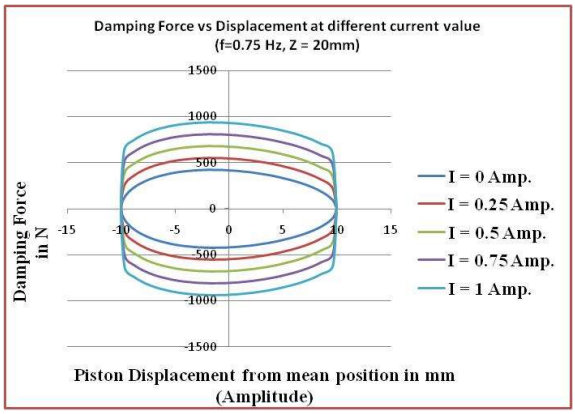

Measured value Analytical value

FIGURE 6.10 (a): Force-disp. relationships under 1.0 cm amplitude for different current values at f = 0.75 Hz

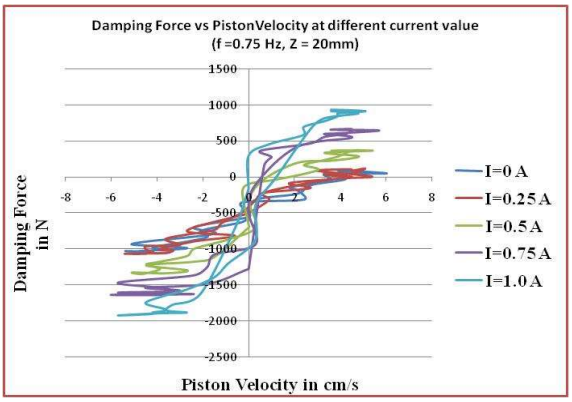

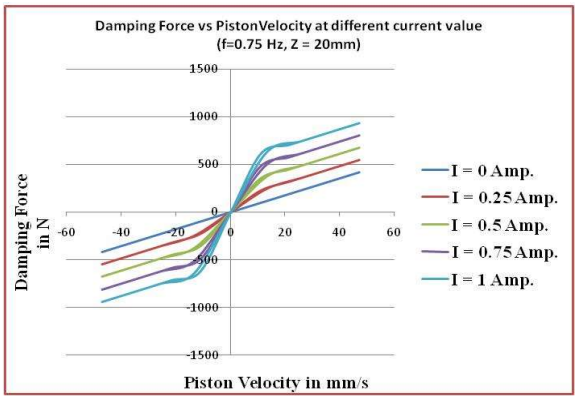

Measured value Analytical value

FIGURE 6.10(b): Force-velo. relationships under 1.0 cm amplitude for different current values at f = 0.75 Hz

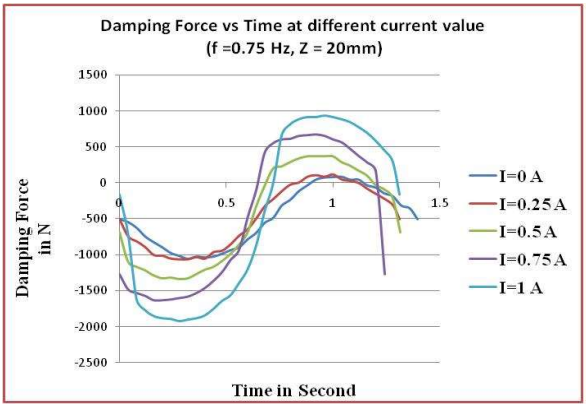

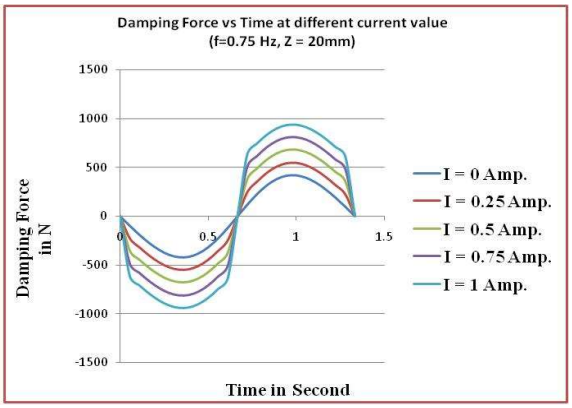

Measured value Analytical value

FIGURE 6.10 (c): Force-time relationships under 1.0 cm amplitude for different current values at f = 0.75 Hz

Fig. 6.11 shows the experimental and analytical results variation during one complete cycle with following parameter value.

Amplitude A= 1.0 cm. (Stroke Z = 2.0 cm.)

Frequency f = 1.0 Hz. (Angular speed of crank plate = 60 RPM)

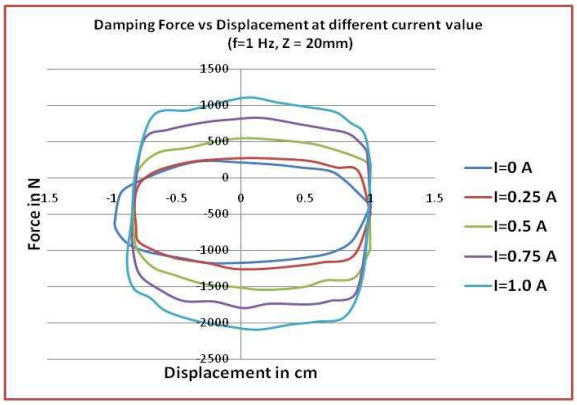

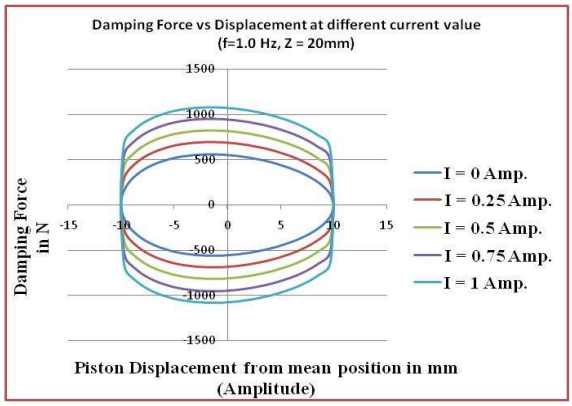

Measured value Analytical value

FIGURE 6.11 (a): Force-disp. relationships under 1.0 cm amplitude for different current values at f = 1.0 Hz

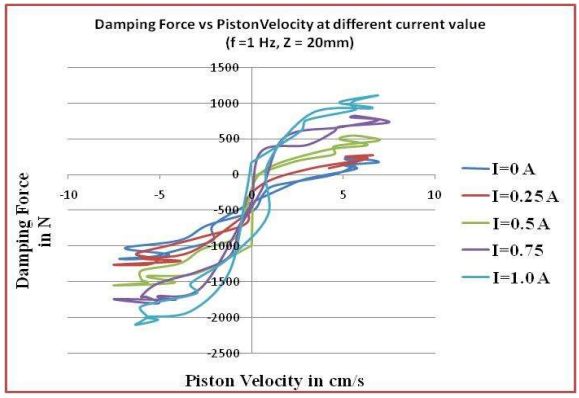

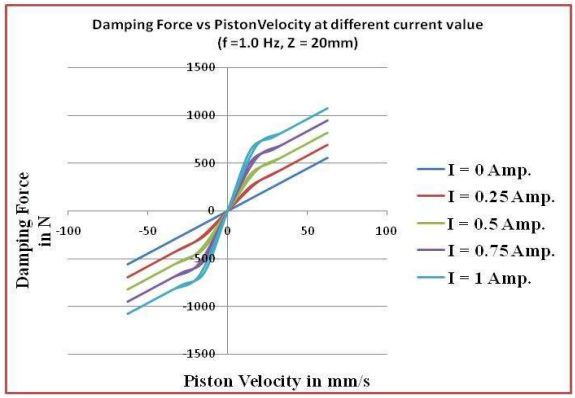

Measured value Analytical value

FIGURE 6.11(b): Force-velo. relationships under 1.0 cm amplitude for different current values at f = 1.0 Hz

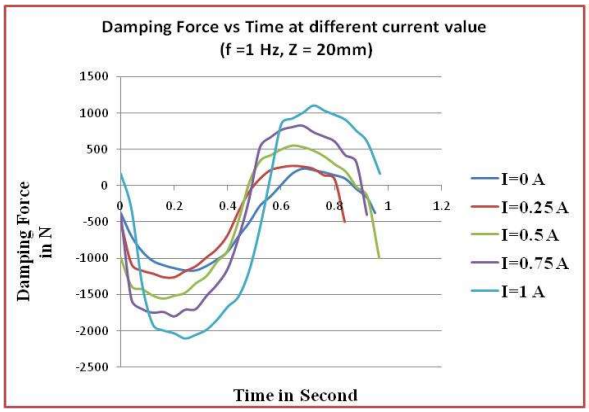

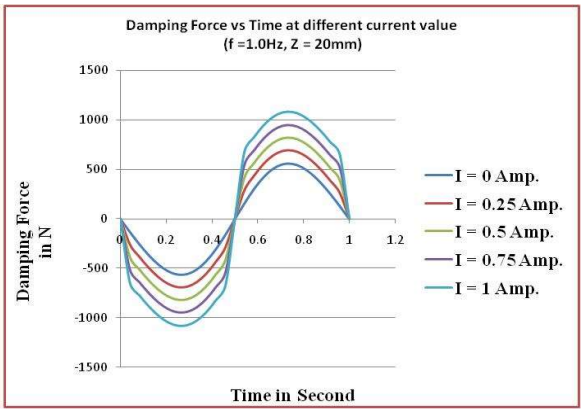

Measured value Analytical value

FIGURE 6.11 (c): Force-time relationships under 1.0 cm amplitude for different current values at f = 1.0 Hz

Fig. 6.12 shows the experimental and analytical results variation during one complete cycle with following parameter value.

Amplitude A= 1.0 cm. (Stroke Z = 2.0 cm.)

Frequency f = 1.5 Hz. (Angular speed of crank plate = 90 RPM)

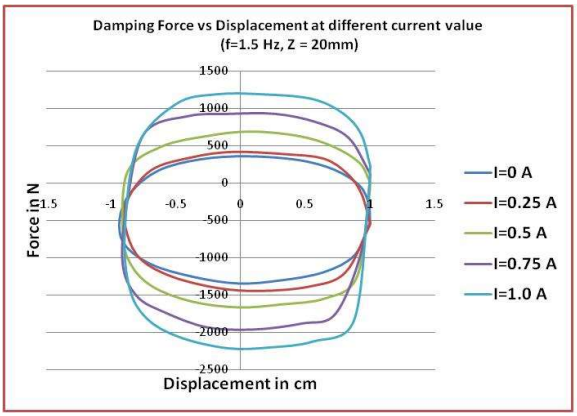

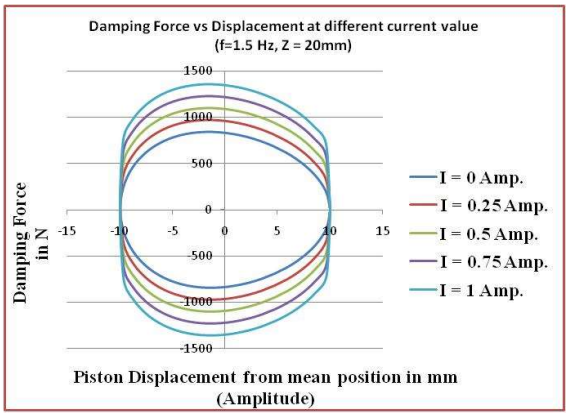

Measured value Analytical value

FIGURE 6.12 (a): Force-disp. relationships under 1.0 cm amplitude for different current values at f = 1.5 Hz

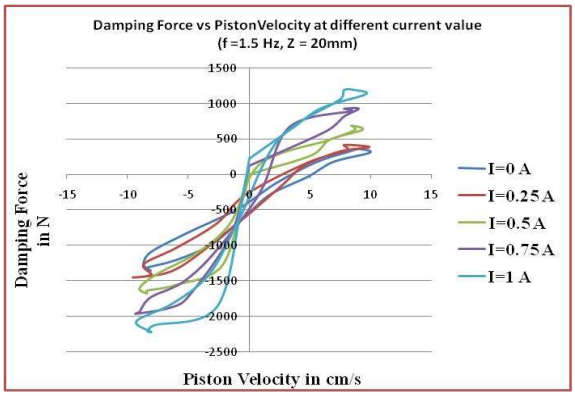

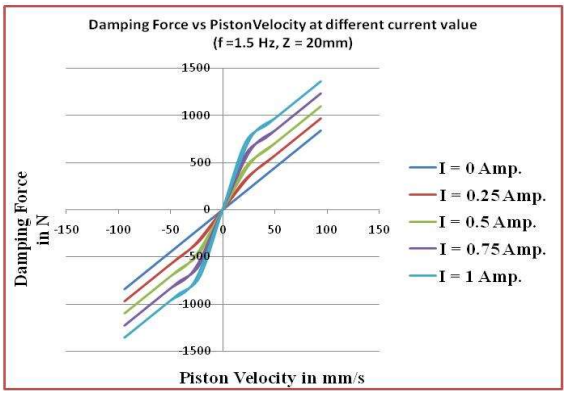

Measured value Analytical value

FIGURE 6.12(b): Force-velo. relationships under 1.0 cm amplitude for different current values at f = 1.5 Hz

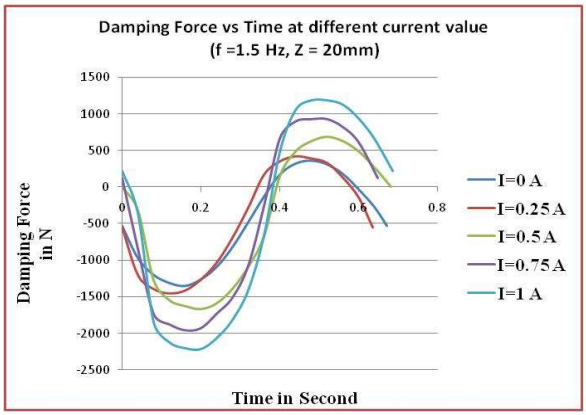

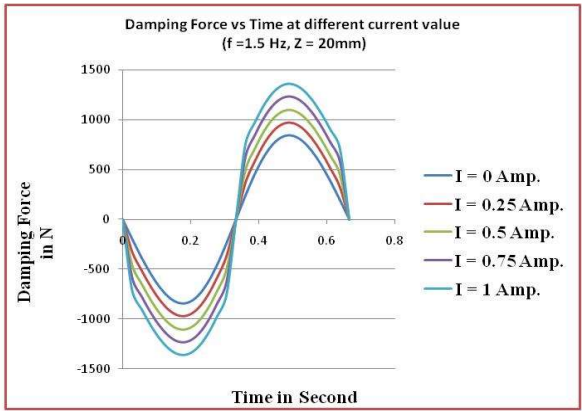

Measured value Analytical value

FIGURE 6.12 (c): Force-time relationships under 1.0 cm amplitude for different current values at f = 1.5 Hz

Fig. 6.13 shows the experimental and analytical results variation during one complete cycle with following parameter value.

Amplitude A= 1.0 cm. (Stroke Z = 2.0 cm.)

Frequency f = 2.0 Hz. (Angular speed of crank plate = 120 RPM)

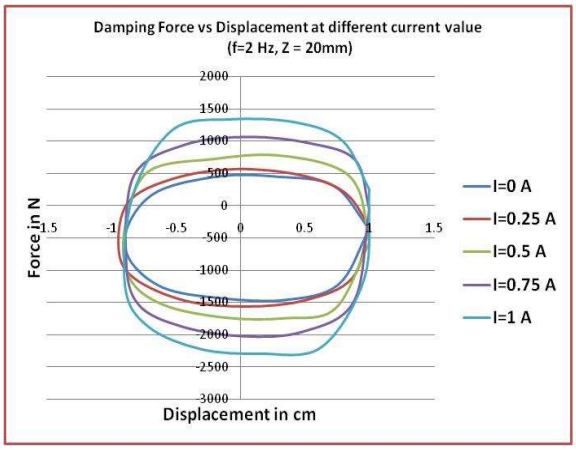

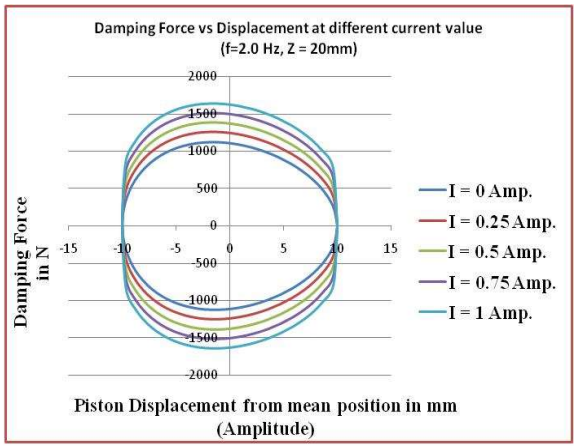

Measured value Analytical value

FIGURE 6.13 (a): Force-disp. relationships under 1.0 cm amplitude for different current values at f = 2.0 Hz

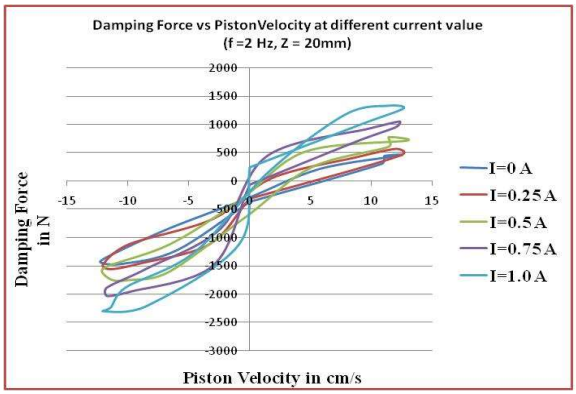

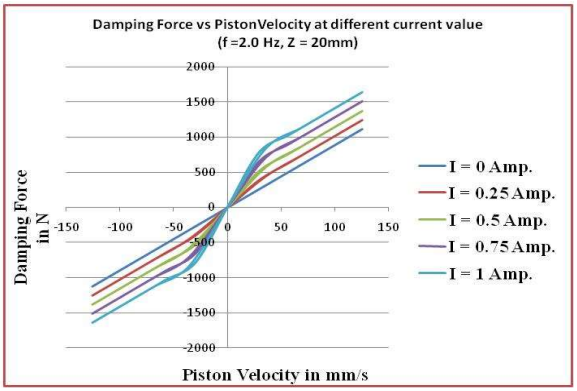

Measured value Analytical value

FIGURE 6.13(b): Force-velo. relationships under 1.0 cm amplitude for different current values at f = 2.0 Hz

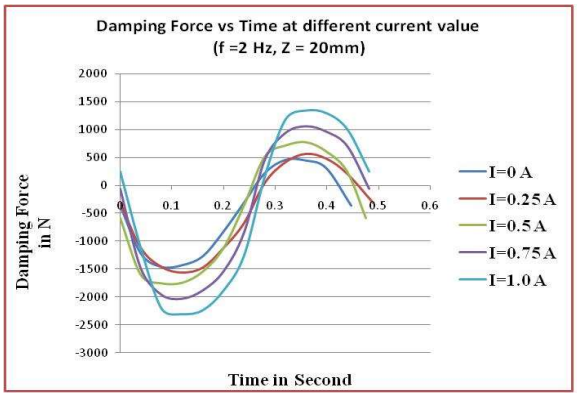

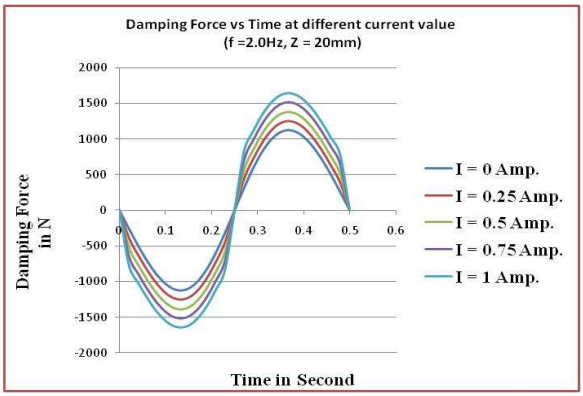

Measured value Analytical value

FIGURE 6.13 (c): Force-time relationships under 1.0 cm amplitude for different current values at f = 2.0 Hz

TABLE 6.4: Measured maximum force, controllable force and dynamic range and their comparison with analytical results for the value of **Amplitude = 1.0 cm.**

			For I = 0A	For I = 0.25A	For I = 0.5A	For I = 0.75A	For I = 1A
N=45 RPM, f=0.75 Hz	Max. Force in N At 1.0 cm amp. (Span/2)	Measured	476.00	598.00	755.00	933.00	1092.00
		predicted	419.65	549.09	678.52	807.96	937.39
		Error in %	13.43	8.91	11.27	15.48	16.49
	Controllable Force in N	Measured	0.00	122.00	279.00	457.00	616.00
		predicted	0.00	129.43	258.87	388.30	517.74
		Error in %	0.00	5.74	7.78	17.69	18.98
	Dynamic Range	Measured	0.00	0.26	0.59	0.96	1.29
		predicted	0.00	0.31	0.62	0.93	1.23
		Error in %	0.00	16.90	4.98	3.76	4.89
			For I = 0A	For I = 0.25A	For I = 0.5A	For I = 0.75A	For I = 1A
N=60 RPM, f=1 Hz	Max. Force in N At 1.0 cm amp. (Span/2)	Measured	599.00	747.00	903.00	1058.00	1215.00
		predicted	559.57	689.00	818.44	947.87	1077.31
		Error in %	7.05	8.42	10.33	11.62	12.78
	Controllable Force in N	Measured	0.00	148.00	304.00	459.00	616.00
		predicted	0.00	129.43	258.87	388.30	517.74
		Error in %	0.00	14.34	17.43	18.21	18.98
	Dynamic Range	Measured	0.00	0.25	0.51	0.77	1.03
		predicted	0.00	0.23	0.46	0.69	0.93
		Error in %	0.00	6.82	9.70	10.42	11.15
			For I = 0A	For I = 0.25A	For I = 0.5A	For I = 0.75A	For I = 1A
N=90 RPM, f=1.5 Hz	Max. Force in N At 1.0 cm amp. (Span/2)	Measured	805.00	935.00	1080.00	1201.00	1360.00
		predicted	839.39	968.83	1098.26	1227.70	1357.13
		Error in %	4.10	3.49	1.66	2.17	0.21
	Controllable Force in N	Measured	0.00	130.00	275.00	396.00	555.00
		predicted	0.00	129.43	258.87	388.30	517.74
		Error in %	0.00	0.44	6.23	1.98	7.20
	Dynamic Range	Measured	0.00	0.16	0.34	0.49	0.69
		predicted	0.00	0.15	0.31	0.46	0.62
		Error in %	0.00	4.73	10.77	6.34	11.78
			For I = 0A	For I = 0.25A	For I = 0.5A	For I = 0.75A	For I = 1A
N=120 RPM, f=2 Hz	Max. Force in N At 1.0 cm amp. (Span/2)	Measured	960.00	1065.00	1205.00	1359.00	1492.00
		predicted	1119.13	1248.57	1378.00	1507.44	1636.87
		Error in %	14.22	14.70	12.55	9.85	8.85
	Controllable Force in N	Measured	0.00	105.00	245.00	399.00	532.00
		predicted	0.00	129.43	258.87	388.30	517.74
		Error in %	0.00	18.88	5.36	2.75	2.75
	Dynamic Range	Measured	0.00	0.11	0.26	0.42	0.55
		predicted	0.00	0.12	0.23	0.35	0.46
		Error in %	0.00	5.43	10.33	19.79	19.79

6.3.3 Test with constant amplitude value of 1.5 cm (Stroke length 3.0 cm)

During third experiment, the amplitude value was set as 1.5 cm, by selecting appropriate hole in stroke selection plate. Frequency values were selected as 0.75, 1.0, 1.5 and 2.0 Hz with the help of variable gear drive system. Instantaneous values of damping force, displacement and velocity were measured and stored in a computer via oscilloscope for a complete cycle. The data for a cycle are analysed and presented in graphical form with theoretical values also as shown in Fig. 6.14 to Fig. 6.17. The data further analysed as maximum damping force, maximum controllable force and dynamic range for experimental values and theoretical values. The analysis is presented by Table 6.5 showing % of error between theoretical and experimental values.

Fig. 6.14 shows the experimental and analytical results variation during one complete cycle with following parameter value.

Amplitude A= 1.5 cm. (Stroke Z = 3.0 cm.)

Frequency f = 0.75 Hz. (Angular speed of crank plate = 45 RPM)

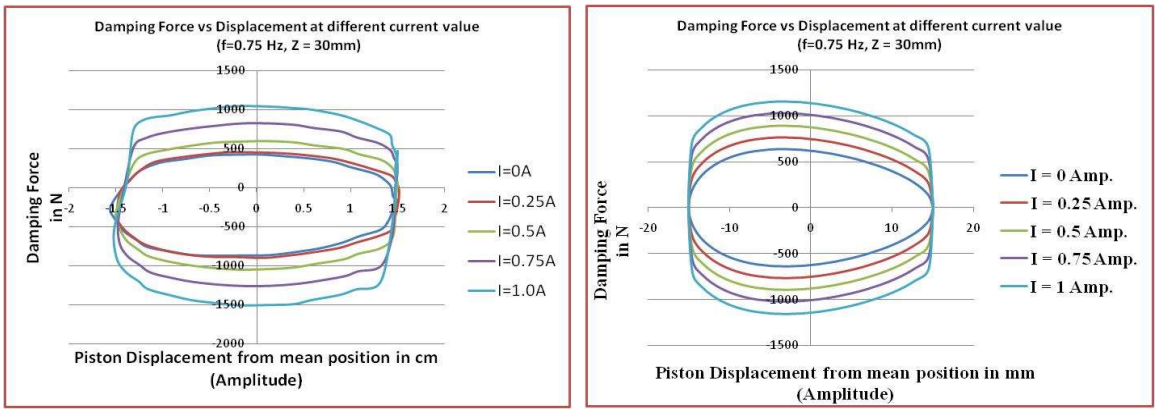

Measured value Analytical value

FIGURE 6.14 (a): Force-disp. relationships under 1.5 cm amplitude for different current values at f = 0.75 Hz

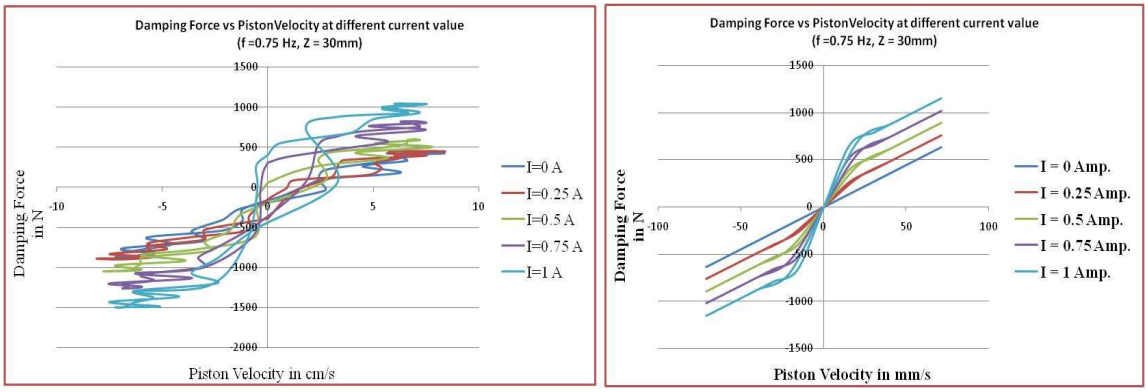

Measured value Analytical value

FIGURE 6.14(b): Force-velo. relationships under 1.5 cm amplitude for different current values at f = 0.75 Hz

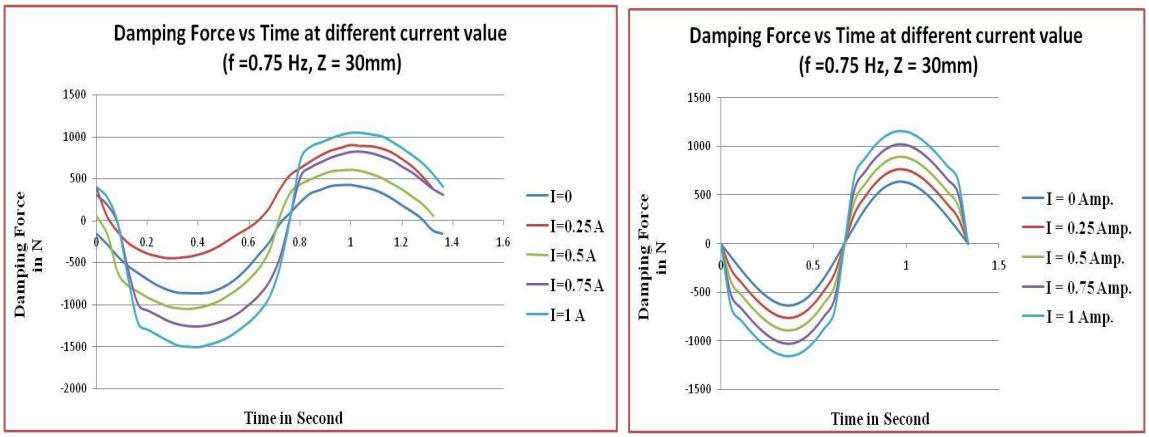

Measured value Analytical value

FIGURE 6.14 (c): Force-time relationships under 1.5 cm amplitude for different current values at f = 0.75 Hz

Fig. 6.15 shows the experimental and analytical results variation during one complete cycle with following parameter value.

Amplitude A= 1.5 cm. (Stroke Z = 3.0 cm.)

Frequency f = 1.0 Hz. (Angular speed of crank plate = 60 RPM)

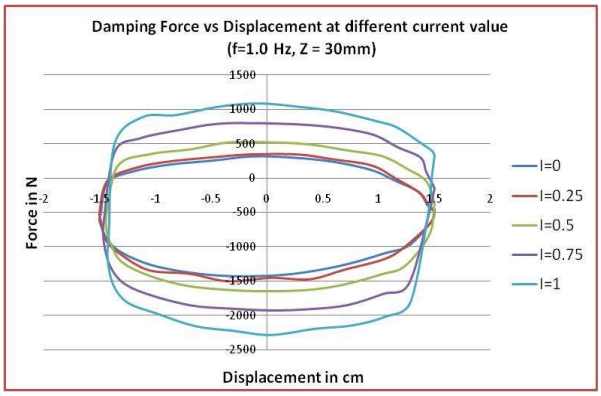

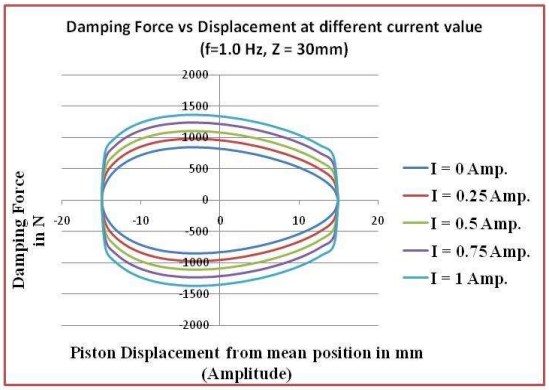

Measured value Analytical value

FIGURE 6.15 (a): Force-disp. relationships under 1.5 cm amplitude for different current values at f = 1.0 Hz

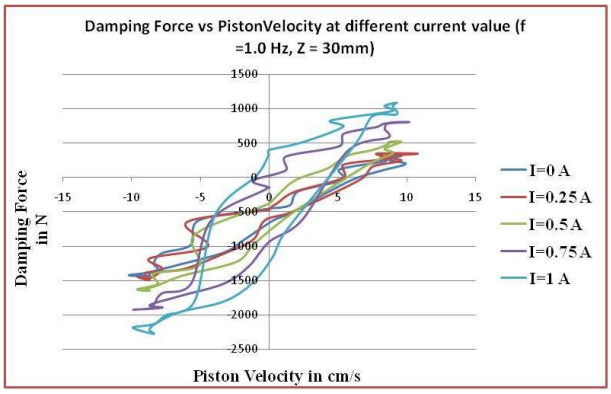

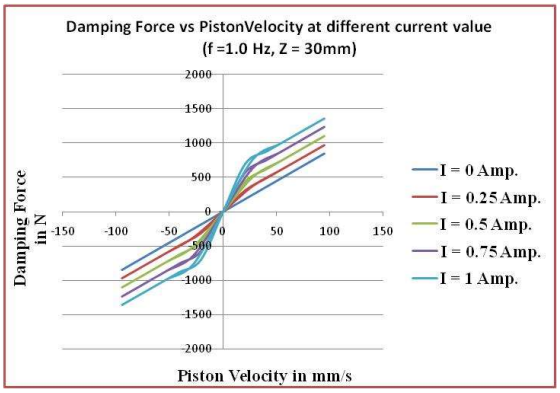

Measured value Analytical value

FIGURE 6.15(b): Force-velo. relationships under 1.5 cm amplitude for different current values at f = 1.0 Hz

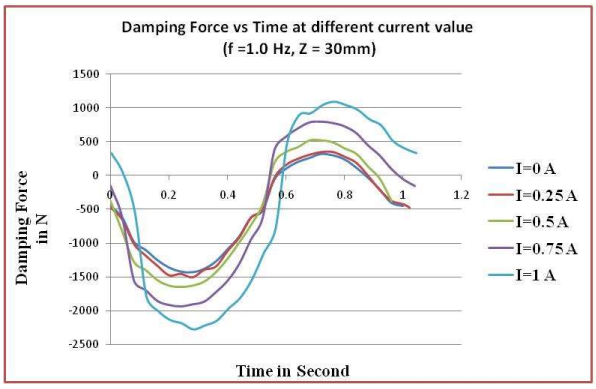

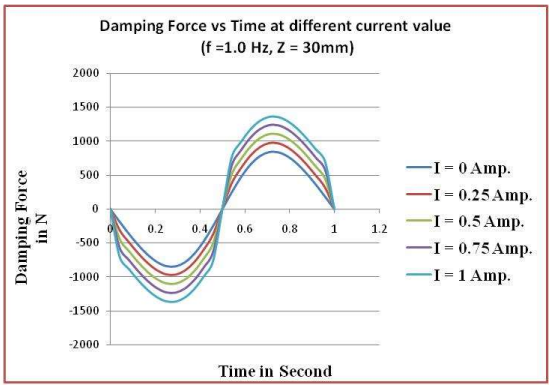

Measured value Analytical value

FIGURE 6.15 (c): Force-time relationships under 1.5 cm amplitude for different current values at f = 1.0 Hz

Fig. 6.16 shows the experimental and analytical results variation during one complete cycle with following parameter value.

Amplitude A= 1.5 cm. (Stroke Z = 3.0 cm.)

Frequency f = 1.5 Hz. (Angular speed of crank plate = 90 RPM)

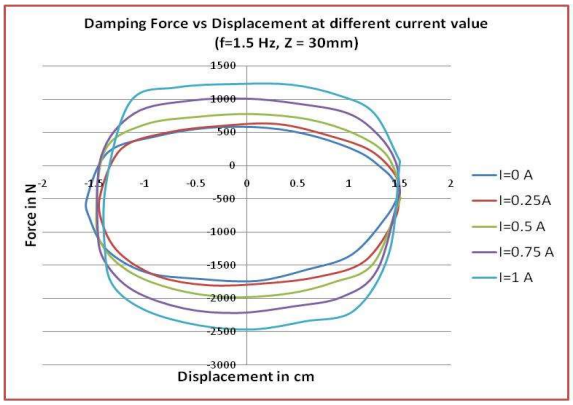

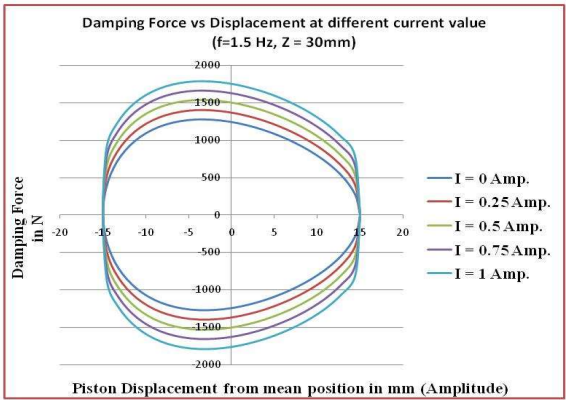

Measured value Analytical value

FIGURE 6.16 (a): Force-disp. relationships under 1.5 cm amplitude for different current values at f = 1.5 Hz

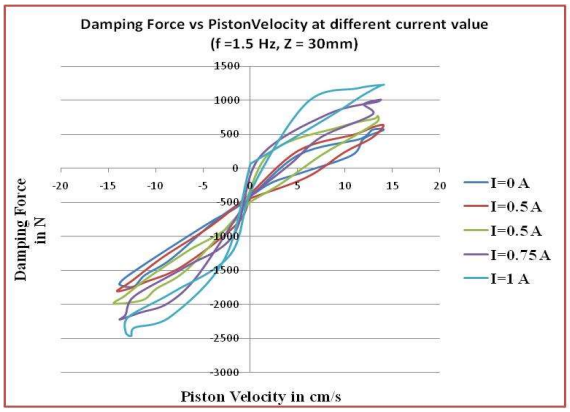

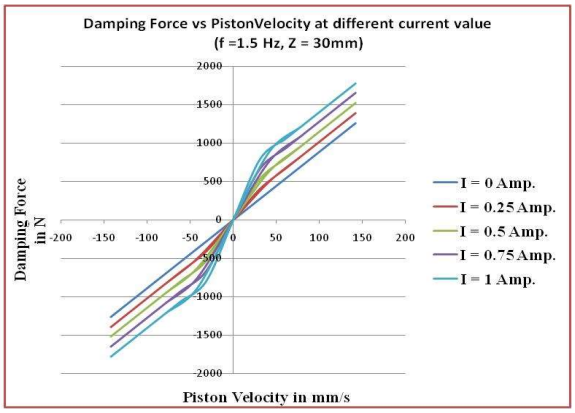

Measured value Analytical value

FIGURE 6.16(b): Force-velo. relationships under 1.5 cm amplitude for different current values at f = 1.5 Hz

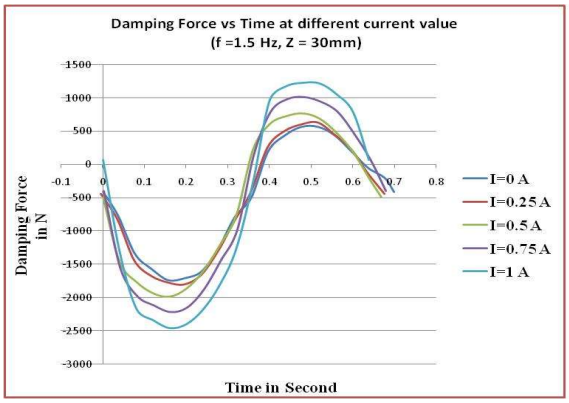

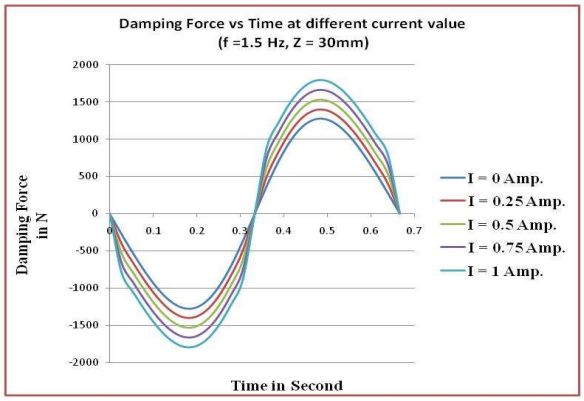

Measured value Analytical value

FIGURE 6.16 (c): Force-time relationships under 1.5 cm amplitude for different current values at f = 1.5 Hz

Fig. 6.17 shows the experimental and analytical results variation during one complete cycle with following parameter value.

Amplitude A= 1.5 cm. (Stroke Z = 3.0 cm.)

Frequency f = 2.0 Hz. (Angular speed of crank plate = 120 RPM)

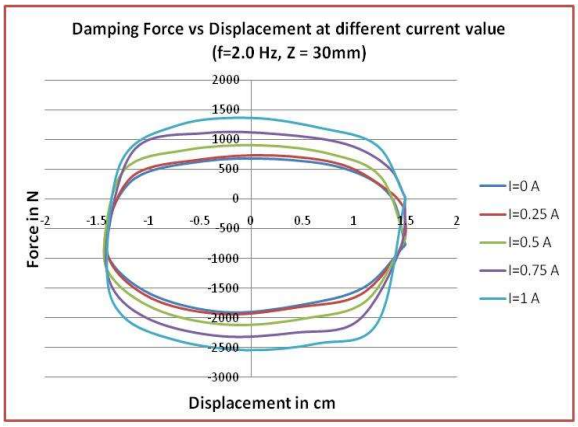

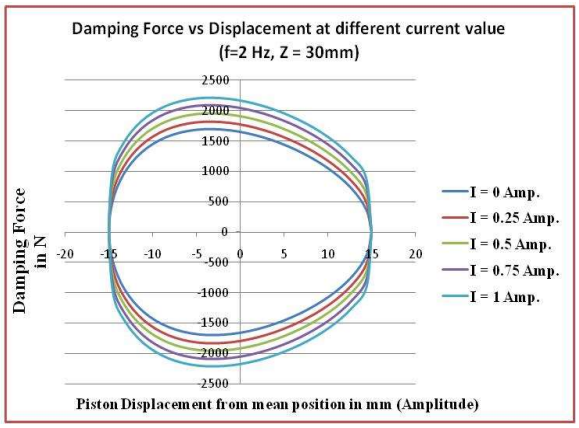

Measured value Analytical value

FIGURE 6.17 (a): Force-disp. relationships under 1.5 cm amplitude for different current values at f = 2.0 Hz

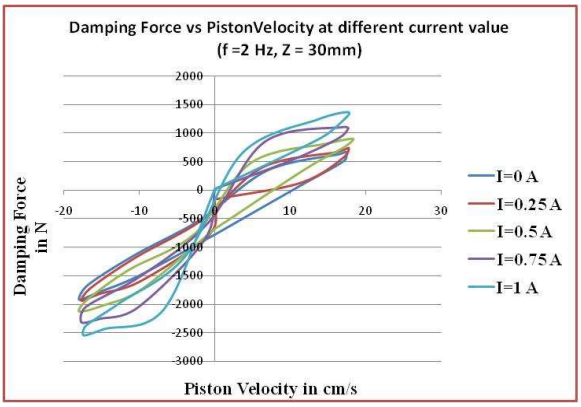

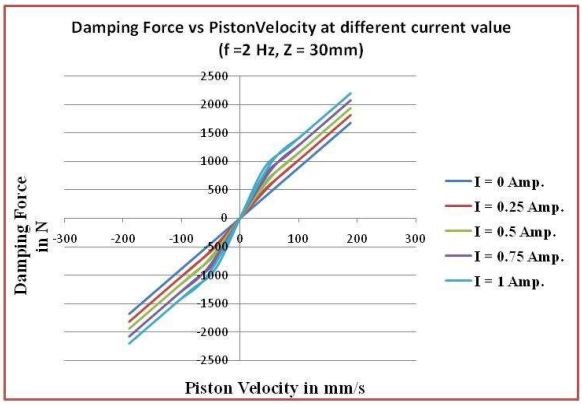

Measured value Analytical value

FIGURE 6.17(b): Force-velo. relationships under 1.5 cm amplitude for different current values at f = 2.0 Hz

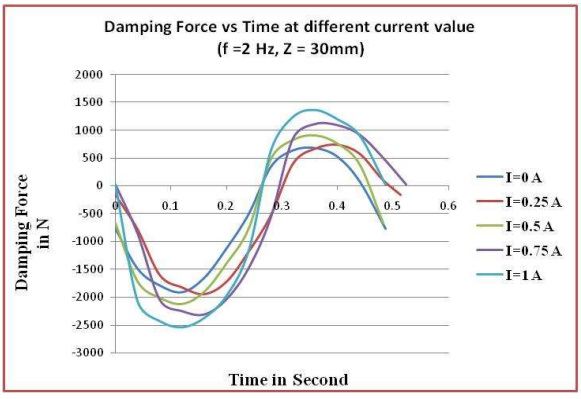

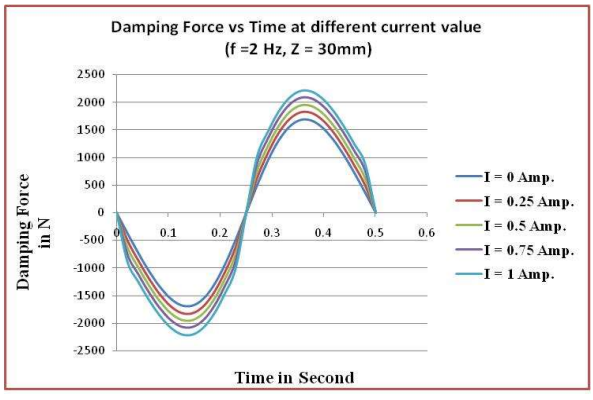

Measured value Analytical value

FIGURE 6.17 (c): Force-time relationships under 1.5 cm amplitude for different current values at f = 2.0 Hz

TABLE 6.5: Measured maximum force, controllable force and dynamic range and their comparison with analytical results for the value of **Amplitude = 1.5 cm.**

			For I = 0A	For I = 0.25A	For I = 0.5A	For I = 0.75A	For I = 1A
N=45 RPM, f=0.75 Hz	Max. Force in N At 1.5 cm amp. (Span/2)	Measured	566.65	694.00	823.50	925.00	1075.00
		predicted	631.97	761.41	890.84	1020.28	1149.71
		Error in %	10.34	8.85	7.56	9.34	6.50
	Controllable Force in N	Measured	0.00	127.35	256.85	358.35	508.35
		predicted	0.00	129.43	258.87	388.30	517.74
		Error in %	0.00	1.61	0.78	7.71	1.81
	Dynamic Range	Measured	0.00	0.22	0.45	0.63	0.90
		predicted	0.00	0.20	0.41	0.61	0.82
		Error in %	0.00	9.73	10.66	2.92	9.51
			For I = 0A	For I = 0.25A	For I = 0.5A	For I = 0.75A	For I = 1A
N=60 RPM, f=1 Hz	Max. Force in N At 1.5 cm amp. (Span/2)	Measured	875.00	1000.00	1124.50	1272.00	1434.50
		predicted	842.60	972.04	1101.47	1230.91	1360.34
		Error in %	3.85	2.88	2.09	3.34	5.45
	Controllable Force in N	Measured	0.00	125.00	249.50	397.00	559.50
		predicted	0.00	129.43	258.87	388.30	517.74
		Error in %	0.00	3.43	3.62	2.24	8.07
	Dynamic Range	Measured	0.00	0.14	0.29	0.45	0.64
		predicted	0.00	0.15	0.31	0.46	0.61
		Error in %	0.00	7.00	7.19	1.55	4.06
			For I = 0A	For I = 0.25A	For I = 0.5A	For I = 0.75A	For I = 1A
N=90 RPM, f=1.5 Hz	Max. Force in N At 1.5 cm amp. (Span/2)	Measured	1155.00	1285.00	1397.50	1542.00	1669.50
		predicted	1263.86	1393.29	1522.73	1652.16	1781.60
		Error in %	8.61	7.77	8.22	6.67	6.29
	Controllable Force in N	Measured	0.00	130.00	242.50	387.00	514.50
		predicted	0.00	129.43	258.87	388.30	517.74
		Error in %	0.00	0.44	6.32	0.34	0.63
	Dynamic Range	Measured	0.00	0.11	0.21	0.34	0.45
		predicted	0.00	0.10	0.20	0.31	0.41
		Error in %	0.00	9.90	2.51	9.06	8.74
			For I = 0A	For I = 0.25A	For I = 0.5A	For I = 0.75A	For I = 1A
N=120 RPM, f=2 Hz	Max. Force in N At 1.5 cm amp. (Span/2)	Measured	1545.00	1673.00	1803.00	1900.00	2070.00
		predicted	1685.20	1814.64	1944.07	2073.51	2202.94
		Error in %	8.32	7.81	7.26	8.37	6.03
	Controllable Force in N	Measured	0.00	128.00	258.00	355.00	525.00
		predicted	0.00	129.43	258.87	388.30	517.74
		Error in %	0.00	1.11	0.34	8.58	1.40
	Dynamic Range	Measured	0.00	0.08	0.17	0.23	0.34
		predicted	0.00	0.08	0.15	0.23	0.31
		Error in %	0.00	7.87	8.71	0.28	10.60

6.3.4 Test with constant amplitude value of 2.0 cm (Stroke length 4.0 cm)

During forth experiment, the amplitude value was set as 2.0 cm, by selecting appropriate hole in stroke selection plate. Frequency values were selected as 0.75, 1.0, 1.5 and 2.0 Hz with the help of variable gear drive system. Instantaneous values of damping force, displacement and velocity were measured and stored in a computer via oscilloscope for a complete cycle. The data for a cycle are analysed and presented in graphical form with theoretical values also as shown in Fig. 6.18 to Fig. 6.21. The data further analysed as maximum damping force, maximum controllable force and dynamic range for experimental values and theoretical values. The analysis is presented by Table 6.6 showing % of error between theoretical and experimental values.

Fig. 6.18 shows the experimental and analytical results variation during one complete cycle with following parameter value.

Amplitude A= 2.0 cm. (Stroke Z = 4.0 cm.)

Frequency f = 0.75 Hz. (Angular speed of crank plate = 45 RPM)

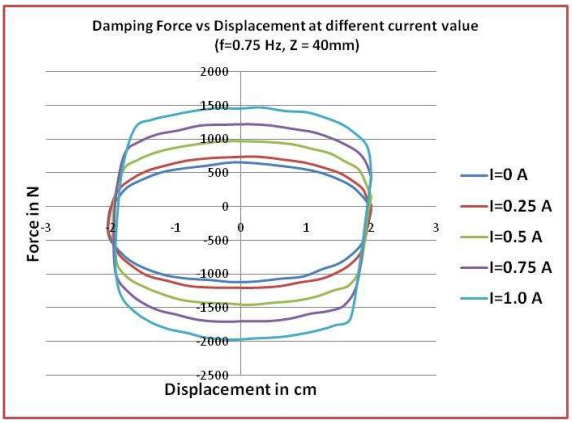

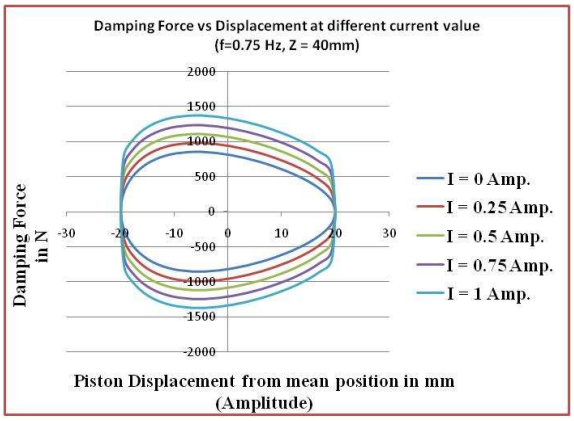

Measured value Analytical value

FIGURE 6.18 (a): Force-disp. relationships under 2.0 cm amplitude for different current values at f = 0.75 Hz

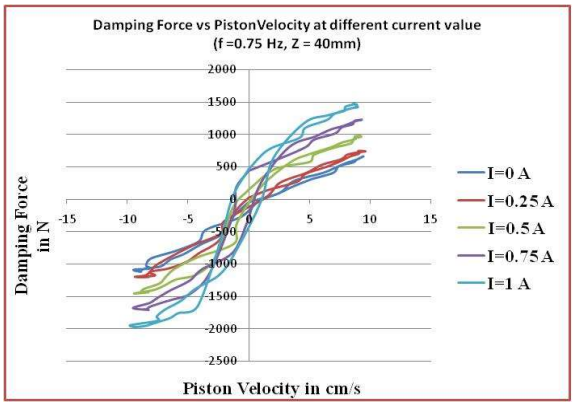

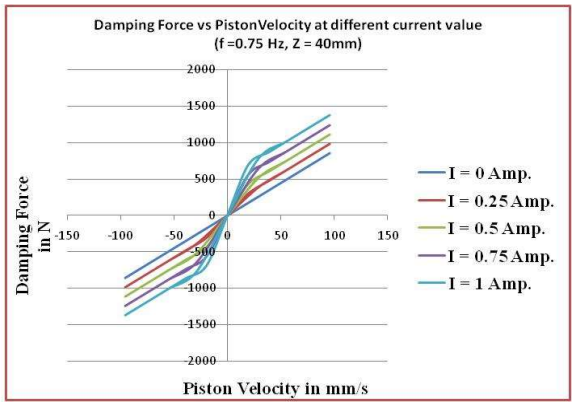

Measured value Analytical value

FIGURE 6.18(b): Force-velo. relationships under 2.0 cm amplitude for different current values at f = 0.75 Hz

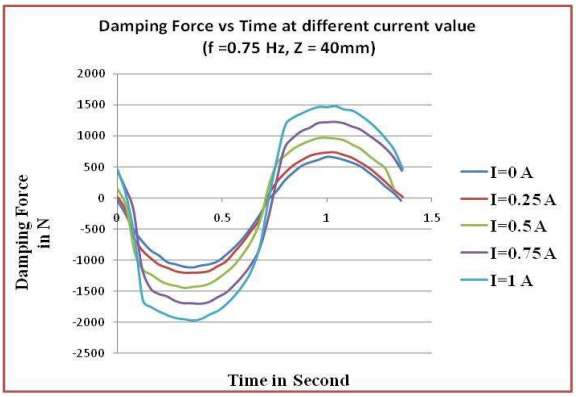

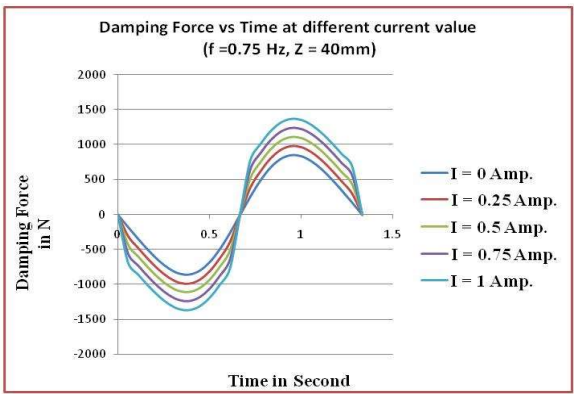

Measured value Analytical value

FIGURE 6.18 (c): Force-time relationships under 2.0 cm amplitude for different current values at f = 0.75 Hz

Fig. 6.19 shows the experimental and analytical results variation during one complete cycle with following parameter value.

Amplitude A= 2.0 cm. (Stroke Z = 4.0 cm.)

Frequency f = 1.0 Hz. (Angular speed of crank plate = 60 RPM)

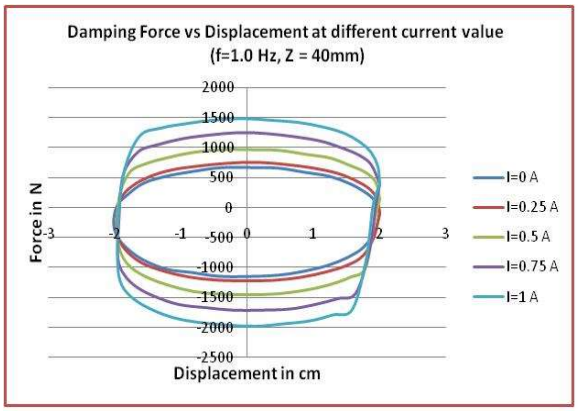

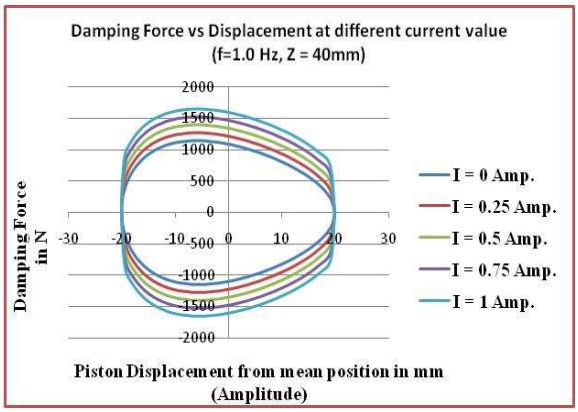

Measured value Analytical value

FIGURE 6.19 (a): Force-disp. relationships under 2.0 cm amplitude for different current values at f = 1.0 Hz

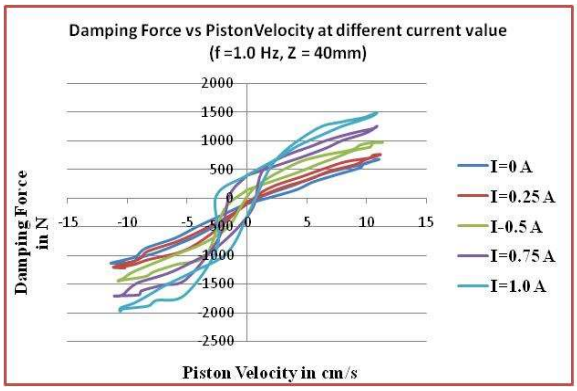

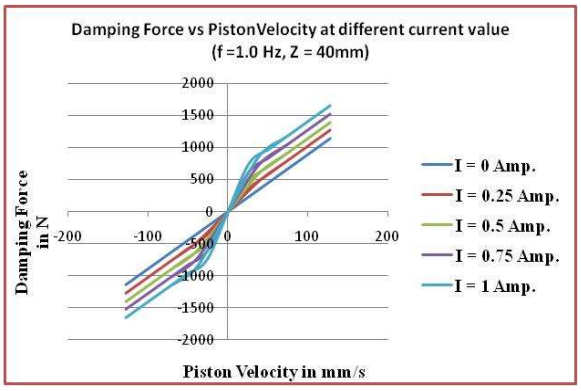

Measured value Analytical value

FIGURE 6.19(b): Force-velo. relationships under 2.0 cm amplitude for different current values at f = 1.0 Hz

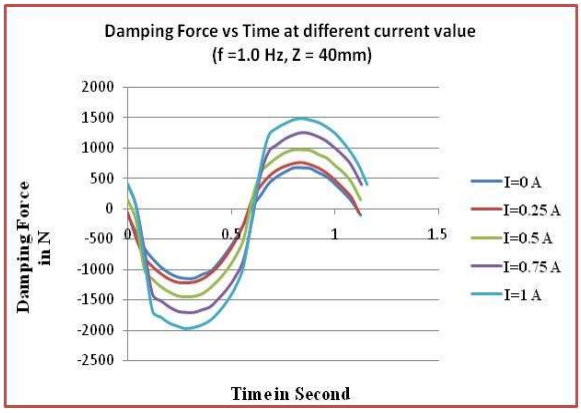

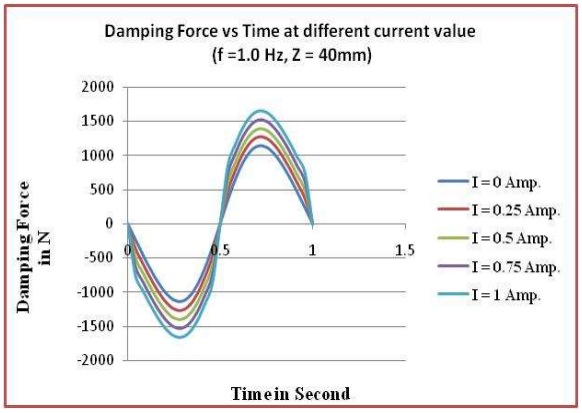

Measured value Analytical value

FIGURE 6.19 (c): Force-time relationships under 2.0 cm amplitude for different current values at f = 1.0 Hz

Fig. 6.20 shows the experimental and analytical results variation during one complete cycle with following parameter value.

Amplitude A= 2.0 cm. (Stroke Z = 4.0 cm.)

Frequency f = 1.5 Hz. (Angular speed of crank plate = 90 RPM)

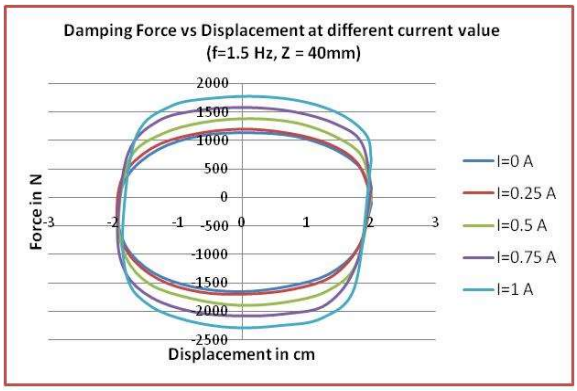

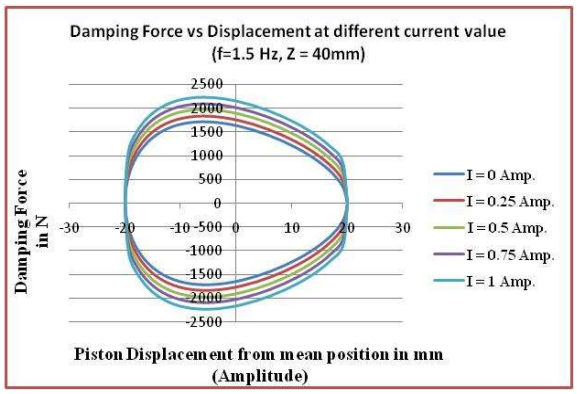

Measured value Analytical value

FIGURE 6.20 (a): Force-disp. relationships under 2.0 cm amplitude for different current values at f = 1.5 Hz

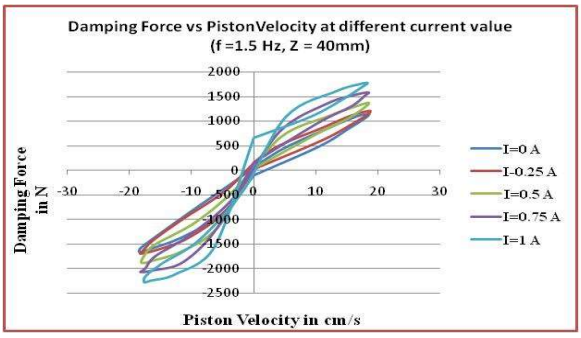

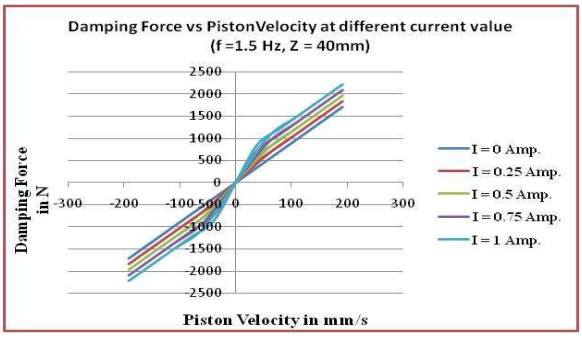

Measured value Analytical value

FIGURE 6.20(b): Force-velo. relationships under 2.0 cm amplitude for different current values at f = 1.5 Hz

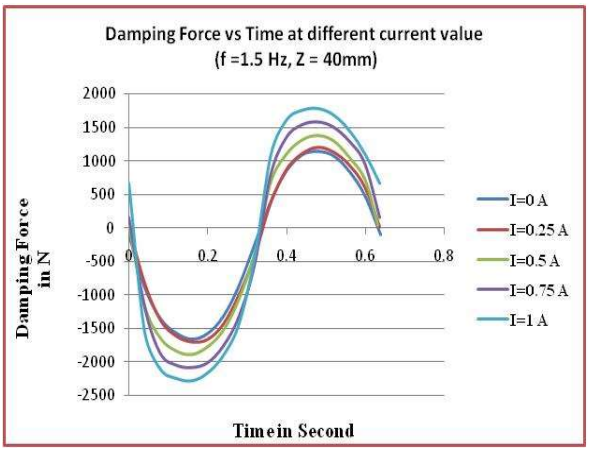

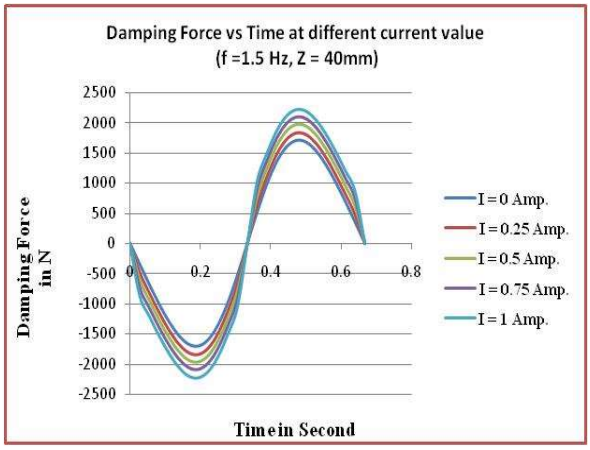

Measured value Analytical value

FIGURE 6.20 (c): Force-time relationships under 2.0 cm amplitude for different current values at f = 1.5 Hz

Fig. 6.21 shows the experimental and analytical results variation during one complete cycle with following parameter value.

Amplitude A= 2.0 cm. (Stroke Z = 4.0 cm.)

Frequency f = 2.0 Hz. (Angular speed of crank plate = 120 RPM)

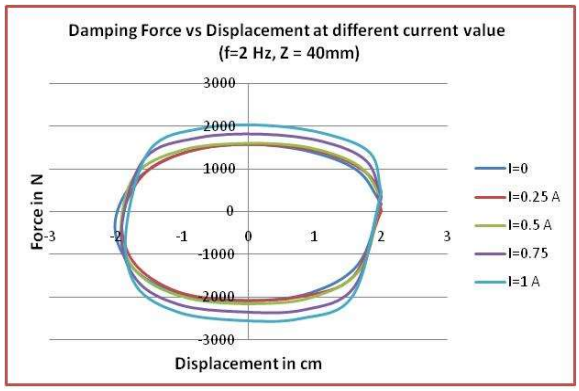

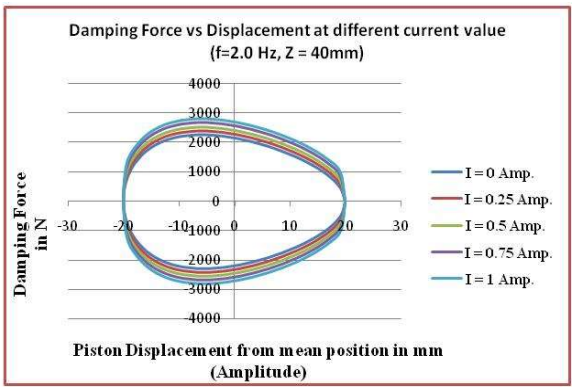

Measured value Analytical value

FIGURE 6.21 (a): Force-disp. relationships under 2.0 cm amplitude for different current values at f = 2.0 Hz

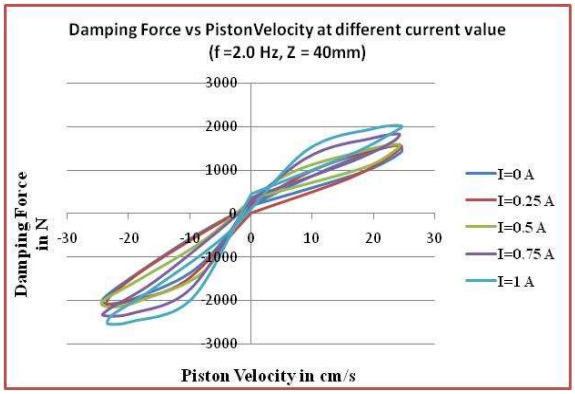

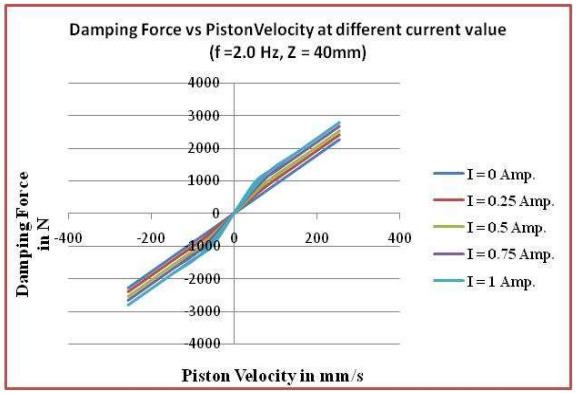

Measured value Analytical value

FIGURE 6.21(b): Force-velo. relationships under 2.0 cm amplitude for different current values at f = 2.0 Hz

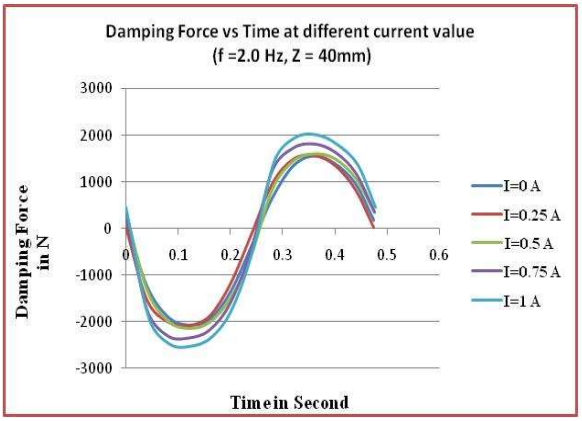

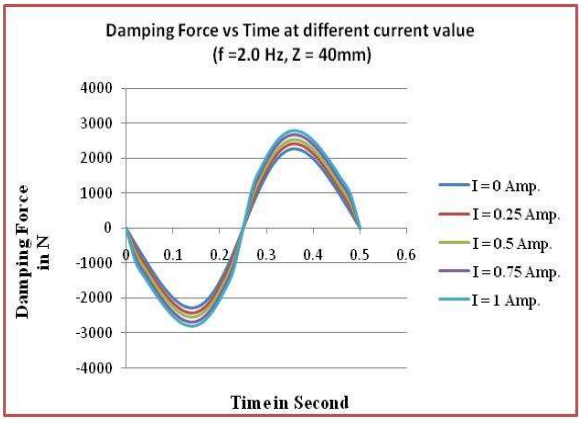

Measured value Analytical value

FIGURE 6.21 (c): Force-time relationships under 2.0 cm amplitude for different current values at f = 2.0 Hz

TABLE 6.6: Measured maximum force, controllable force and dynamic range and their comparison with analytical results for the value of **Amplitude = 2.0 cm.**

			For I = 0A	For I = 0.25A	For I = 0.5A	For I = 0.75A	For I = 1A
N=45 RPM, f=0.75 Hz	Max. Force in N At 2.0 cm amp. (Span/2)	Measured	888.00	998.00	1180.00	1220.00	1320.00
		predicted	853.56	982.99	1112.43	1241.86	1371.30
		Error in %	4.04	1.53	6.07	1.76	3.74
	Controllable Force in N	Measured	0.00	110.00	292.00	332.00	432.00
		predicted	0.00	129.43	258.87	388.30	517.74
		Error in %	0.00	15.02	12.80	14.50	16.56
	Dynamic Range	Measured	0.00	0.12	0.33	0.37	0.49
		predicted	0.00	0.15	0.30	0.45	0.61
		Error in %	0.00	18.31	8.42	17.82	19.80
			For I = 0A	For I = 0.25A	For I = 0.5A	For I = 0.75A	For I = 1A
N=60 RPM, f=1 Hz	Max. Force in N At 2.0 cm amp. (Span/2)	Measured	1040.00	1150.00	1310.00	1450.00	1602.00
		predicted	1138.10	1267.54	1396.97	1526.41	1655.84
		Error in %	8.62	9.27	6.23	5.01	3.25
	Controllable Force in N	Measured	0.00	110.00	270.00	410.00	562.00
		predicted	0.00	129.43	258.87	388.30	517.74
		Error in %	0.00	15.02	4.30	5.59	8.55
	Dynamic Range	Measured	0.00	0.11	0.26	0.39	0.54
		predicted	0.00	0.11	0.23	0.34	0.45
		Error in %	0.00	7.00	14.14	15.55	18.79
			For I = 0A	For I = 0.25A	For I = 0.5A	For I = 0.75A	For I = 1A
N=90 RPM, f=1.5 Hz	Max. Force in N At 2.0 cm amp. (Span/2)	Measured	1602.00	1713.00	1815.00	1928.00	2032.00
		predicted	1707.11	1836.55	1965.98	2095.42	2224.85
		Error in %	6.16	6.73	7.68	7.99	8.67
	Controllable Force in N	Measured	0.00	111.00	213.00	326.00	430.00
		predicted	0.00	129.43	258.87	388.30	517.74
		Error in %	0.00	14.24	17.72	16.05	16.95
	Dynamic Range	Measured	0.00	0.07	0.13	0.20	0.27
		predicted	0.00	0.08	0.15	0.23	0.30
		Error in %	0.00	8.62	12.32	10.54	11.50
			For I = 0A	For I = 0.25A	For I = 0.5A	For I = 0.75A	For I = 1A
N=120 RPM, f=2 Hz	Max. Force in N At 2.0 cm amp. (Span/2)	Measured	2024.00	2150.00	2236.00	2378.00	2470.00
		predicted	2276.12	2405.55	2534.99	2664.42	2793.86
		Error in %	11.08	10.62	11.79	10.75	11.59
	Controllable Force in N	Measured	0.00	126.00	212.00	354.00	446.00
		predicted	0.00	129.43	258.87	388.30	517.74
		Error in %	0.00	2.65	18.11	8.83	13.86
	Dynamic Range	Measured	0.00	0.06	0.10	0.17	0.22
		predicted	0.00	0.06	0.11	0.17	0.23
		Error in %	0.00	9.47	7.90	2.52	3.13

6.4 Summery on experiment

Tests were conducted to investigate the effect of various parameters like amplitude, frequency and input current on MR damper performance. In these tests, various sinusoidal displacement excitations with frequencies of 0.75, 1.0, 1.5 and 2.0 Hz were selected. For each frequency, excitations with different amplitudes were applied to the MR damper at current levels of 0, 0.25, 0.5, and 1 A. The tests conducted for each amplitude value are summarized in Table 6.3 to Table 6.6. Figs. 6.6–6.21 show the damper force-displacement, damper force-velocity and damper force-time relationships under different values of frequency and current. Each figure and table provides a comparison between the measured damper responses and analytical results using the axisymmetric Herschel-Bulkley model. When the displacement excitation is lesser, such as the displacement amplitude of 0.5 cm, the MR damper functions mainly in the pre-yield area. The velocity increases as the value of amplitude increases. Thus more MR fluids begin to yield, and a greater post-yield shear flow is developed. Consequently, the plastic viscous force becomes substantial, especially at large displacement amplitudes

Figs. 6.6–6.21 show the MR damper force-displacement, force-velocity and force-time actions under a different combination values of sinusoidal displacement excitations and frequencies at various input current levels. It is concluded that resisting force increases at larger amplitudes due to higher velocity. Note that the force-displacement loops develops along a clockwise path over time, whereas the force-velocity loops develops along a counter-clockwise path over time. As shown in the figures, the force-displacement, force-velocity and force-time actions for different displacement and frequency are quite consistent.

The special effects of changing input current are readily detected. At an input current of 0 A, the MR damper primarily displays the characteristics of only viscous device (i.e., the force-displacement relationship is approximately elliptical and the force-velocity relationship is approximately linear). As the input current increases, the force required to yield the MR fluid in the damper also increases and plastic-like actions are seen in the hysteresis loops. Figs. 6.6–6.21 compares the analytical values and measured values of experiments using the axisymmetric Herschel-Bulkley model. The force-displacement actions are seen to be reasonably modelled. Two extra clockwise loops are also observed at velocity extremes in the force-velocity plot. The stiction phenomenon of MR fluids (Weiss

et al 1995) [52] and probably the fluid inertial force contribute to these loops as well as to force overshoots at displacement maximums.

From Fig. 6.6 to 6.21 and summary Table from 6.3 to 6.6, one can also see that the maximum damping force increases when the frequency increases due to the larger plastic viscous force at higher velocity. It should also to be noted that the damper may be subjected to a small input current and a displacement excitation with a big amplitude. In these circumstances, the yield force level is low and damper functions mainly in post-yield area. Hence, as the frequency increases, the plastic viscous force starts to govern the damper reaction, especially at higher frequencies.

Moreover, the effect of accumulator pressure on MR damper reaction is discussed. A pressurized accumulator is shown to be effective in decreasing the force lag due to the residual air trapped in the damper. In addition, an approach for minimizing the air in the damper during the filling method is provided.

CHAPTER 7
RESULTS AND DISCUSSION WITH DESIGN OF EXPERIMENT

7.1 Introduction

This chapter includes complete discussion on results observed during experiment. For the validation of experiment procedure, Design Of Experiment (DOE) was carried out first with the help of Design Expert software using results observed during experiment.

7.2 Design Of Experiment (DOE)

Any scientific investigation involves formulation of certain assertions (or hypotheses) whose validity is examined through data generated from an experiment conducted for the purpose. Thus experimentation becomes an indispensable part of every scientific endeavour and designing an experiment is an integrated component of every research programme. Three basic techniques for fundamental designing of an experiment are replication, local control (blocking) and randomization. Whereas the first two helps to increase precision in the experiment, the last one is used to decrease bias.

In the existing study, an effort has been made to examine the influence of velocity, amplitude and current on total damping force in MR fluid base damper developed at Physics Department, Shri M.K. Bhavnagar University. Experimentations were conducted based on “Response Surface Methodology” (RSM) and “Sequential approach” by means of face cantered central composite design. Experimental outcomes indication that all the factors (piston velocity, Amplitude and Current) have significant effect on Total Damping Force. A linear model best fits the variation of total damping force by means of velocity, amplitude as well as current. Current is the leading contributor to the total damping force. A non-linear quadratic model is ideal to describe the variation of total damping force with major involvement of all parameters. The suggested model of total damping force satisfactorily map within the boundaries of the factors considered.

Present experimental research on damping force has been conducted with “three-level factorial design” (3^k) for studying effect of factors on total damping force. In “two-level factorial design”, one can study and model linear relationships only. For identifying the

nonlinearity existing in the output characteristics, minimum three levels of each elements are essential (i.e. three-level factorial design, 3^k). A central composite design, which needs less trials than alternative 3^k design, is usually better [81]. Again, sequential experimental approach in central composite design can be used to decrease the number of trials necessary. Keeping the preceding in mind, the current effort is concentrated on examinations of total damping force as a function of amplitude, velocity and current value using sequential approach in central composite design. The study was conducted on MR damper developed and tested for the same project work.

The information of experimental settings, instrumentations, measurements and the technique established for the investigation are described in previous chapter. Complete Design of Experiment is carried out with Design-Expert® software Version 6.0. Following section describe complete DOE procedure carried out for total damping force recorded during experimental procedure.

7.2.1 Experimental plan procedure

Three parameters namely amplitude, angular speed and current were selected to find out its effect on total damping force. Table 7.1 shows the parameters and their levels. Thirty two trial runs included of 23 factorial points, four centre points and five axial points were carried out in block 1. Table 7.2 shows whole design matrix with responses to total damping force. In design matrix, the coded variables are prescribed as: A: amplitude (A), B: angular speed (N) and C: current (I). F is the response representing total damping force. Experiments were conducted randomly as shown in design matrix (‘runs’ column in Table 7.2). The design matrix also show the factorial points, centre points and axial points with coded and actual values.

TABLE 7.1: Parameters and their levels

Factor	Unit	Low level (-1)	Centre level (0)	High level (1)
Amplitude	mm	5	10	15
Angular speed	RPM	60	90	120
Current	Amp	0	0.5	1.0

TABLE 7.2: Design matrix with responses (Total Damping Force)

Std	Run	Block	Type	A:A(mm)	B:N(rpm)	C:I(Amp)	A:A(mm)	B:N(rpm)	C:I(Amp)	F(N)
1	5	1	Axial	0	0	-1	10	90	0	805
2	16	1	Fact	-1	1	0	5	120	0.5	907
3	29	1	Centre	0	0	0	10	90	0.5	1080
4	14	1	Centre	0	0	0	10	90	0.5	1080
5	20	1	Fact	0	-1	1	10	60	1	1215
6	8	1	Fact	0	1	-1	10	120	0	960
7	12	1	Fact	1	-1	0	15	60	0.5	1124.5
8	13	1	Axial	-1	0	0	5	90	0.5	794
9	4	1	Fact	-1	0	-1	5	90	0	510
10	19	1	Fact	-1	-1	1	5	60	1	958
11	17	1	Axial	0	1	0	10	120	0.5	1205
12	27	1	Fact	1	1	1	15	120	1	2070
13	10	1	Fact	-1	-1	0	5	60	0.5	638
14	32	1	Centre	0	0	0	10	90	0.5	1080
15	7	1	Fact	-1	1	-1	5	120	0	616
16	30	1	Centre	0	0	0	10	90	0.5	1080
17	26	1	Fact	0	1	1	10	120	1	1492
18	18	1	Fact	1	1	0	15	120	0.5	1803
19	25	1	Fact	-1	1	1	5	120	1	1263
20	23	1	Fact	1	-1	1	10	90	1	1360
21	22	1	Fact	-1	0	1	5	90	1	1151
22	24	1	Fact	1	0	1	15	90	1	1669.5
23	11	1	Axial	0	-1	0	10	60	0.5	903
24	21	1	Fact	1	-1	1	15	60	1	1434.5
25	9	1	Fact	1	1	-1	15	120	0	1545
26	2	1	Fact	0	-1	-1	10	60	0	599
27	28	1	Fact	0	0	0	10	90	0.5	1080
28	6	1	Fact	1	0	-1	15	90	0	1155
29	1	1	Fact	-1	-1	-1	5	60	0	342
30	3	1	Fact	1	-1	-1	15	60	0	875
31	15	1	Axial	1	0	0	15	90	0.5	1397.5
32	31	1	Fact	0	0	0	10	90	0.5	1080

TABLE 7.3: ANOVA (partial sum of square) for total damping force (F)

Source	Sum of squares	d.f.	Mean square	F-value	Prob>F	Remark
Model	4365178	9	485019.7354	255.865	< 0.0001	Significant
A-A-Amplitude	1930613	1	1930612.5	1018.466	< 0.0001	Significant
B-B-RPM	790443.6	1	790443.5556	416.9868	< 0.0001	Significant
C-C-Current	1505691	1	1505690.889	794.3049	< 0.0001	Significant
AB	107541.3	1	107541.3333	56.73183	< 0.0001	Significant
AC	7752.083	1	7752.083333	4.089497	0.0555	
BC	638.0208	1	638.0208333	0.336578	0.5677	
A^2	17807.78	1	17807.77502	9.394227	0.0057	
B^2	2.640405	1	2.640405294	0.001393	0.9706	
C^2	874.9481	1	874.9480976	0.461566	0.5040	
Residual	41703.38	22	1895.60825			
Lack of Fit	41703.38	17	2453.140088			
Pure Error	0	5	0			
Cor Total	4406881	31				
Std. Dev.	43.53858		R-Squared	0.990537		
Mean	1102.25		Adj R-Squared	0.986665		
C.V. %	3.949974		Pred R-Squared	0.976504		
PRESS	103545.1		Adeq Precision	67.89797		

The Model F-value of 255.862 implies that the model is significant. There is only 0.01% chance that large value of "Model F-Value" could occur due to noise. Values of "Prob > F" less than 0.05 indicate that model terms are significant. In this case A, B, C and AB are significant model terms. Values greater than 0.05 indicate that model terms are not significant. The "Pred R-Squared" of 0.976504 is in practical agreement with the "Adj R-Squared" of 0.986665. "Adeq Precision" indicates the signal to noise ratio. A ratio greater than 4 is required. The ratio of 67.89797 point out an acceptable signal. This model can be used to navigate the design space.

7.2.2 Results and discussion based on DOE

Table 7.2 shows all values of total damping force. The total damping force was obtained in the range of 342 N to 2070 N.

The increase in total damping force is due to:

1. Increase in applied current value increases the shear stress of MR fluid
2. Increase in angular speed increases the velocity of piston
3. Increase in amplitude. This is also due to large displacement of fluid inside the piston cylinder assembly.

Fig. 7.1-7.3 shows relation between total damping force (measured force in N) with applied current values, angular speed and amplitude for different combinations. The rate of increase in total damping force is higher for increasing the value of current compared to amplitude and velocity. Fig. 7.1 also show that the total damping force is increased linearly with respect to increase in value of applied current. This comment come to an agreement well with results described by former investigators. [13, 14, 15, 17, 20]

Additionally, the results were analysed in "Design Expert V6" software. The results of the block 1 experiments in the method of analysis of variance (ANOVA) are shown. An ANOVA summary table is normally used to summarize the test of the regression model, test of the significance factors and their interaction and lack-of-fit test. If the value of 'Prob > *F*' in ANOVA table is less than 0.05 then the model, the factors, interaction of factors and curvature are said to be significant.

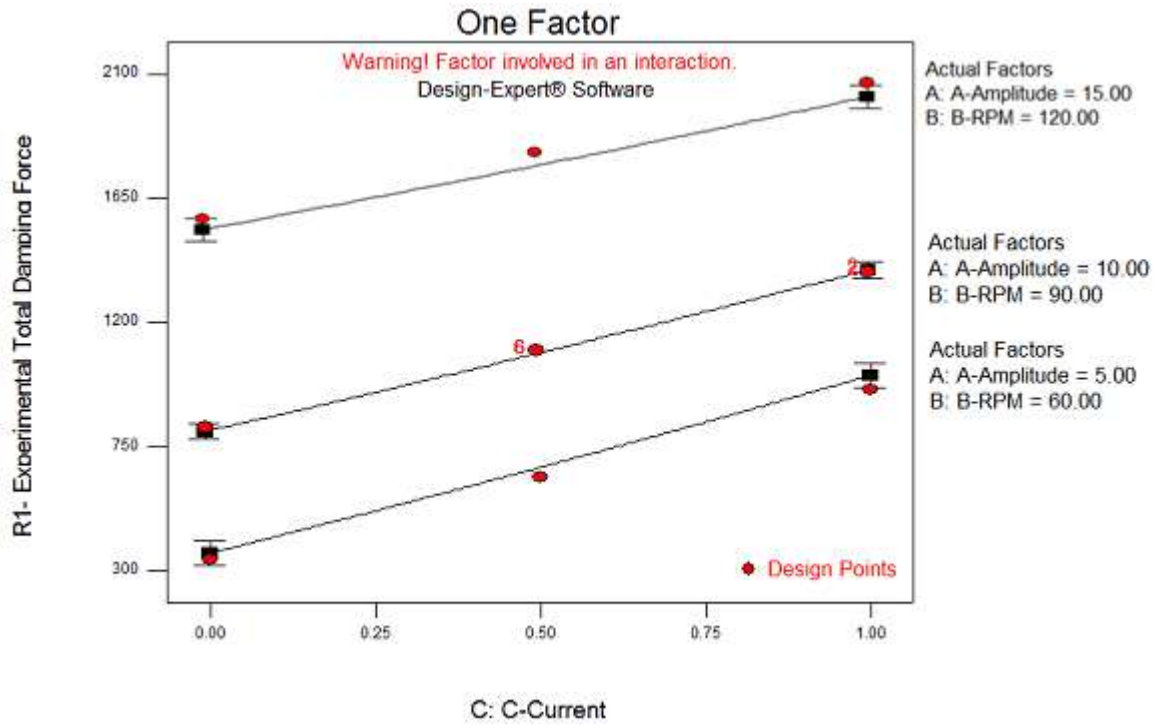

FIGURE 7.1: Total measured damping force vs. applied current at different values of amplitude and angular speed.

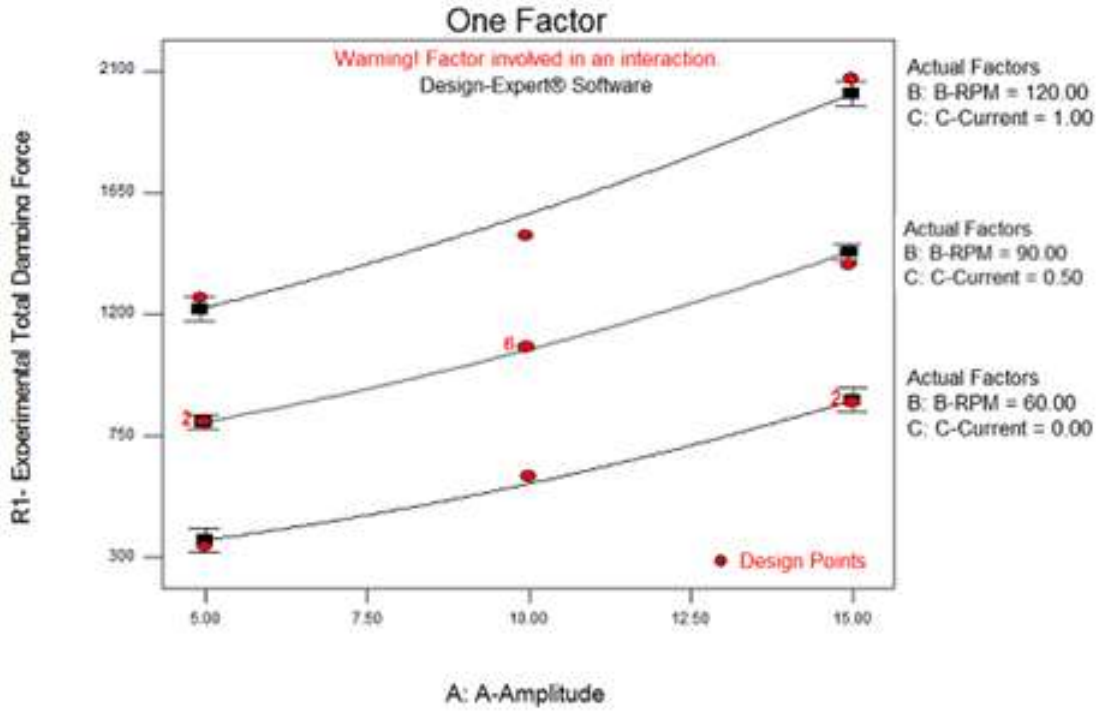

FIGURE 7.2: Total measured damping force vs. Amplitude at various angular speed and applied current.

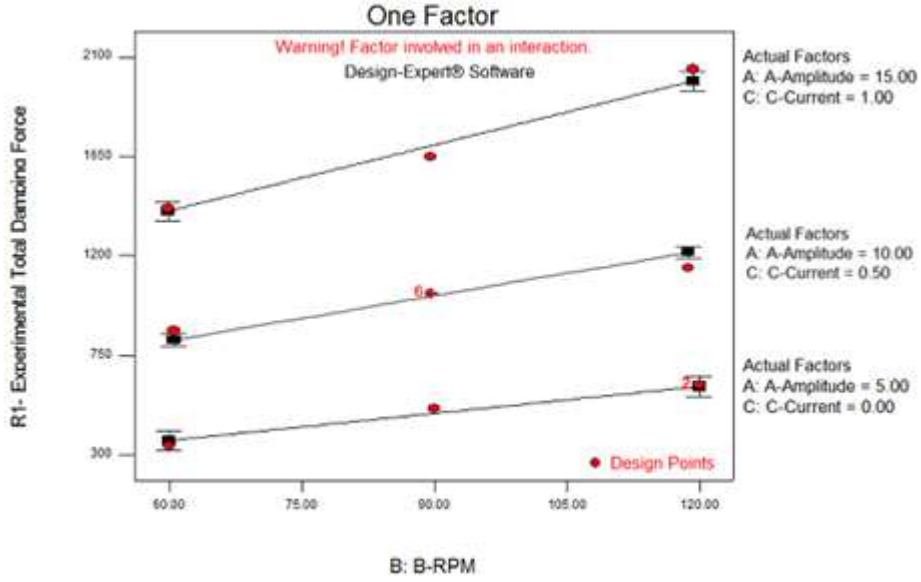

FIGURE 7.3: Total measured damping force vs. Angular velocity at various amplitude and applied current.

Table 7.3 shows that the model is significant and amplitude (A), angular speed (B), applied current (C) and (A, B) are only the important elements (terms) in the model. All remaining elements are insignificant. The influence of elements, their interaction and curvature are also presented in Table 7.3.

The various R^2 statistics (i.e. R^2, adjusted R^2 (R^2 Adj) and predicted R^2 (R^2 Pred)) of the total damping force are shown in Table 7.3. The value of R^2 = 0.990537 for total damping force indicates that 99.05% of the total variations are explained by the model. The adjusted R^2 is a statistic that is adjusted for the "size" of the model; that is, the number of factors (terms). The value of the R^2 Adj = 0.986665 indicates that 98.66% of the total variability is explained by the model after considering the significant factors. R^2 Pred = 0.976504 is in good agreement with the R^2 Adj and shows that the model would be expected to explain 97.65% of the variability in new data (Montgomery, 2001). 'C.V.' stands for the coefficient of variation of the model and it is the error expressed as a percentage of the mean ((S.D./Mean)×100). Lower value of the coefficient of variation (C.V. = 3.9%) indicates improved precision and reliability of the conducted experiments. As nonlinearity is not existing in the model, extra tests are not necessary to be performed. This is the main benefit of sequential approach in face cantered central composite design.

The normal probability plot of the residuals (i.e. error = predicted value from model−actual value) for Total damping Force shown in Fig. 7.4 reveal that the residuals lie reasonably close to a straight line, giving support that terms mentioned in the model are the only significant (Montgomery, 2001).

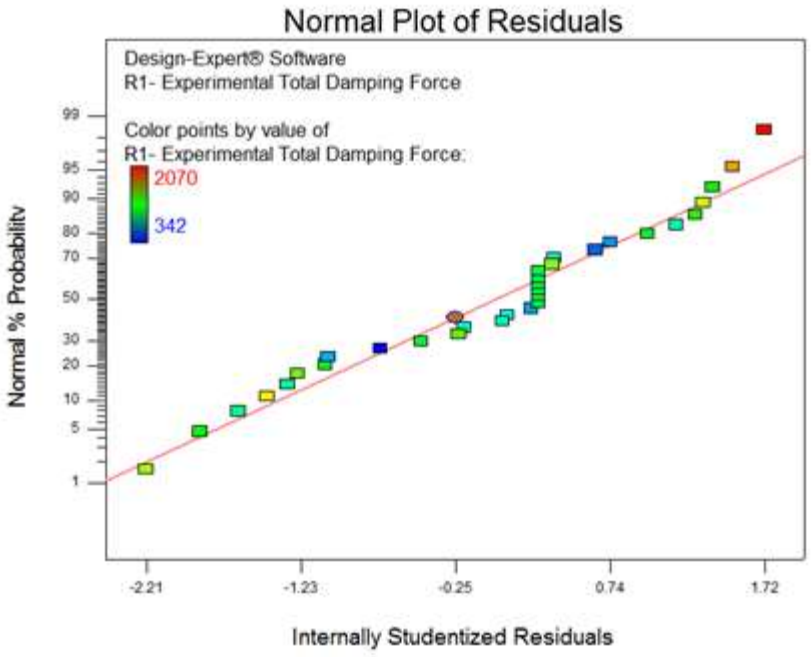

FIGURE 7.4: Normal probability plot of residuals for Total Damping Force.

After eliminating the insignificant elements, the response surface equations for Total Damping Force is achieved in the real values as:

Total Measured damping Force

$$F = -26.1306 * A + 1.038635 * B + 679.6246 * C + 0.631111 * A * B - 10.1667 * A * C - 0.48611 * B * C + 1.995699 * A^2 - 0.00068 * B^2 + 44.23656 * C^2 + 195.8705$$

Where F = Total damping force in N

A = Amplitude value in mm

B = Angular Speed value in RPM

C = Applied Current value in Amp.

The predicted results from the model (equation value) and the real (experimental) results are presented in Fig. 7.5.

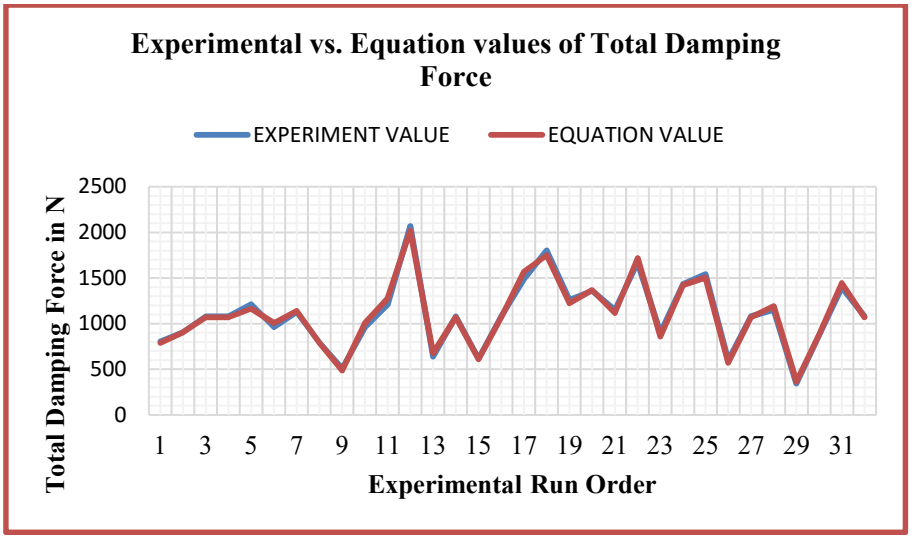

FIGURE 7.5: Actual vs. predicted values of total damping forces.

Variable damping force is required for replacing the passive vibration control system to a semi-active vibration control system. The main attention of this investigation is to find out total damping force for required damping coefficient. Therefore, the contour plots of the total damping force with relations of amplitude of vibration, angular velocity of vibrating device and applied current to MR damper are essential. The contour plot of the total damping force in angular velocity-amplitude at current value of 0.5 amp, current-amplitude at angular velocity value of 90 RPM and current-angular velocity at amplitude value of 10

mm are shown in Figs. 7.6-7.8 respectively. Figs. 7.6-7.8 clearly indication that an adequate total damping force can be attained for every level of amplitude and angular velocity when current value is changed from low to high. In present research work, the MR fluid based semi-active damper is designed to achieve variable damping force by changing the current value.

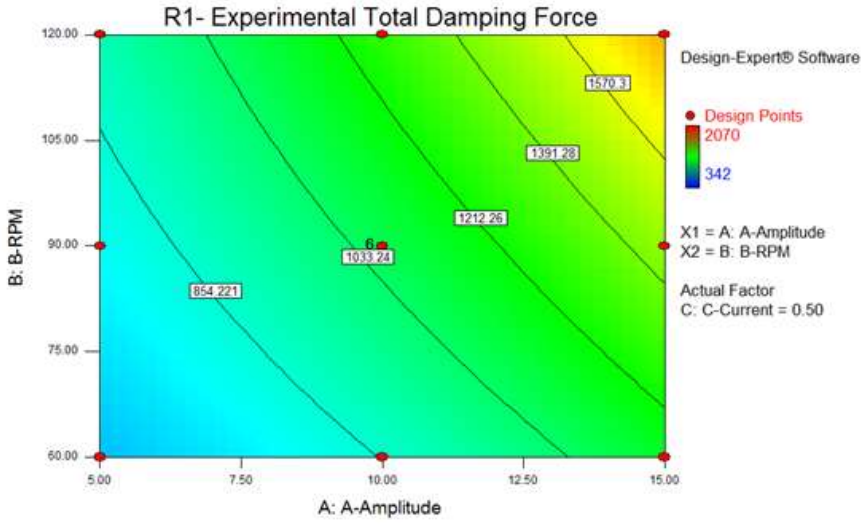

FIGURE 7.6: Measured Damping Force (N) contour in Angular speed (RPM) and Amplitude (mm) plane at current value of 0.5 Amp.

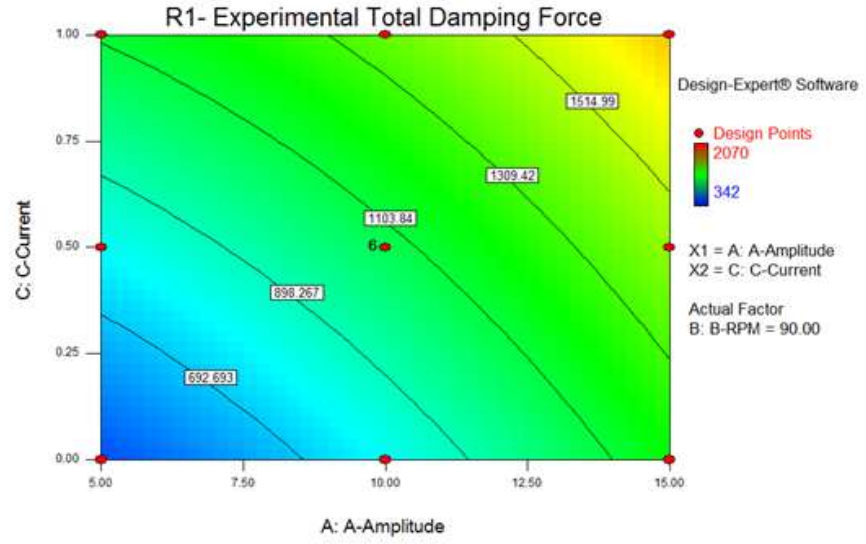

FIGURE 7.7: Measured Damping Force (N) contour in current (Amp) and Amplitude (mm) plane at Angular speed of 90 RPM.

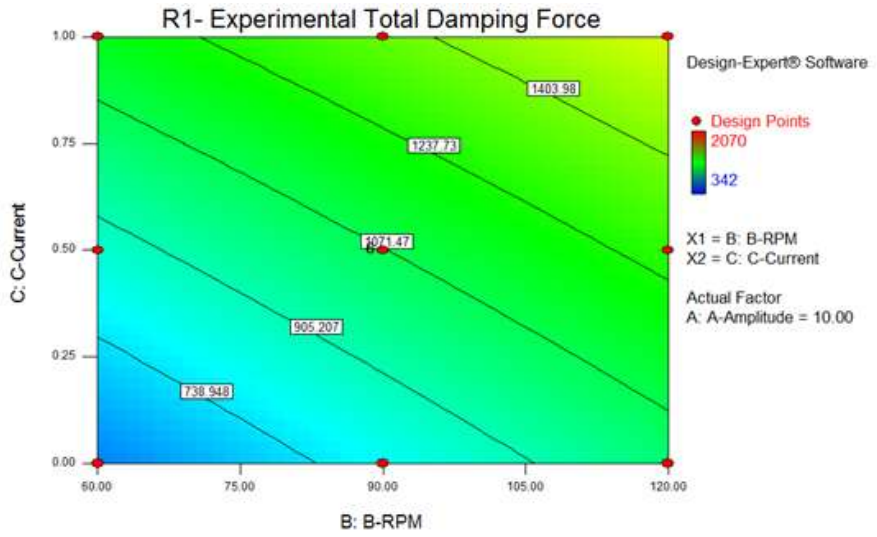

FIGURE 7.8: Measured Damping Force (N) contour in current (Amp) and Angular speed (RPM) plane at Amplitude of 10 mm.

7.3 Results and discussion based on Experimental and mathematical modelling data.

Tests were conducted to investigate the effect of various parameters like amplitude, frequency and input current on MR damper performance. In this test, various sinusoidal displacement excitations with frequencies of 0.75, 1.0, 1.5 and 2.0 Hz were selected. For each frequency, excitations with different amplitudes were applied to the MR damper at current levels of 0, 0.25, 0.5, and 1 A. The tests conducted for each amplitude value are summarized in previous chapter by Table 6.3 to Table 6.6. Figs. 6.6–6.21 show the damper force-displacement, damper force-velocity and damper force-time relationships under different values of frequency and current. Each figure and table provides a comparison between the measured damper responses and analytical results using the axisymmetric Herschel-Bulkley model. When the displacement excitation is lesser, such as the displacement amplitude of 0.5 cm, the MR damper functions mainly in the pre-yield area. The velocity increases according to the value of amplitude increases. Thus, more MR fluid begin to yield and a greater post-yield shear flow is developed. Consequently, the plastic viscous force becomes substantial, especially at large displacement amplitudes.

Figs. 6.6–6.21 show the MR damper force-displacement, force-velocity and force-time actions under different combination values of sinusoidal displacement excitation and frequencies at various input current levels. It is concluded that resisting force increases at

larger amplitudes due to higher velocity. Note that the force-displacement loops development takes place along with clockwise path over time, whereas the force-velocity loops development takes place along with counter-clockwise path over time. As shown in the figures, the force-displacement, force-velocity and force-time actions for different displacements and frequencies are quite consistent.

The special effects of changing input current are readily detected. At an input current of 0 A, the MR damper primarily displays the characteristics of viscous device only. (i.e., the force-displacement relationship is approximately elliptical and the force-velocity relationship is approximately linear). As the input current increases, the force required to yield the MR fluid in the damper also increases and plastic-like actions are seen in the hysteresis loops. Figs. 6.6–6.21 compares the analytical values and measured values of experiment using the axisymmetric Herschel-Bulkley model. The force-displacement actions are reasonably observed for the purpose of modelling. Two extra clockwise loops are also observed at velocity extremes in the force-velocity plot. The stiction phenomenon of MR fluid (Weiss et al 1995) [52] and probably the fluid inertial force contribute to these loops as well as to force overshoots at displacement maximums.

From Fig. 6.6 to 6.21 and summary Table from 6.3 to 6.6, one can also see that the maximum damping force increases when the frequency increases due to the larger plastic viscous force at higher velocity. It should also to be noted that the damper may be subjected to a small input current and a displacement excitation with big amplitude. In this circumstances, the yield force level is low and damper functions mainly in post-yield area. Hence, as the frequency increases, the plastic viscous force starts to govern the damper reaction especially at higher frequencies.

Moreover, the effect of accumulator pressure on MR damper reaction is discussed. A pressurized accumulator is seen effective to decreasing the force lag due to the residual air trapped in the damper. In addition, an approach for minimizing the air in the damper during the filling method is provided.

As can be seen, the MR damper resisting force increases as the applied current increases. Moreover, the area enclosed by the force-displacement loop also enlarges and more energy is dissipated. Fig. 6.6(b)-6.21(b) provide the measured MR damper force-velocity behaviours and comparisons with theoretical results. Due to the plastic viscous force, a larger damping force is seen at high velocity. Fig. 6.6(c)-6.21(c) provide the measured MR damper force-time behaviours and comparisons with theoretical results. Table 6.3-6.6 provides the measured maximum damping force, controllable force and dynamic range

with their comparison to analytical results. Again, close agreement is observed with maximum errors of about 10%.

7.3.1 MR fluid damper characteristic analysis

To design appropriate MR fluid damper model, examination of elements which affect the dynamic responses of the damping system has been done. The first affecting element is the applied displacement/velocity on the piston rod of the damper. Fig. 6.6-6.21 shows a comparison amongst damping results under various sine excitations with 0.5, 1.0, 1.5 and 2.0 cm amplitude and frequency 0f 0.75, 1.0, 1.5 and 2.0 Hz under the provided current level in range commencing 0 to 1A. Outcomes display that at fixed current level applied to the damper, the damping force fluctuates because of the change in piston rod velocity affected by the simultaneous variation of frequency and/or amplitude of the applied excitation. The second element affecting the damper behaviour is the change in current applied to the damper coil.

From Fig. 6.6-6.21, it is readily apparent that:

(1). The force produced by the damper is not centered at zero. This effect is due to the effect of an accumulator containing high pressure nitrogen gas in the damper. The accumulator helps to prevent cavitation in the fluid during normal operation and accounts for the volume of fluid displaced by the piston rod as well as thermal expansion of the fluid.

(2). Greater the current level, greater is the damping force. Increasing the current in the device's coil enlarges the magnetic field flux and thus, increases the yield stress denoted as $\tau_0(B)$ as shown in Fig. 7.9, increases the controllable force and the dynamic range.

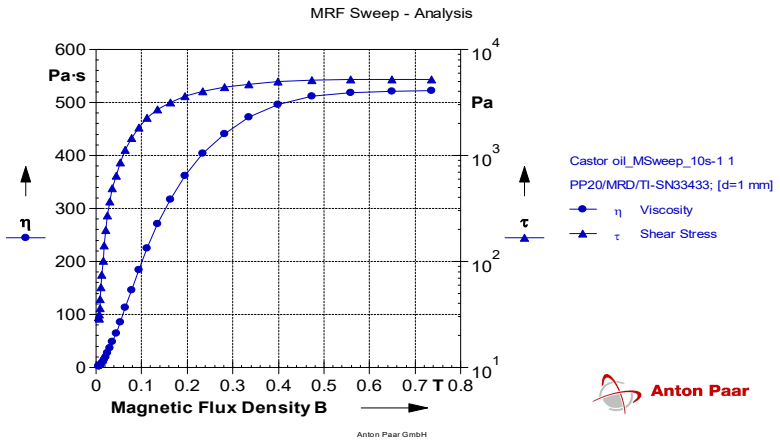

FIGURE 7.9: Relation between Magnetic flux density, Viscosity and Shear stress

(3). The alteration amount of force is more rapidly at lesser current levels due to the effect of magnetic field saturation. With respect to the above examines, it is clear that the damping force of the MR fluid damper be influenced by the displacement/velocity of the damper piston and the current supplied for the coil inside the damper.

(4). Referring to Table 6.3-6.6, MR damper with low frequency and high current value have higher dynamic ranges. Dynamic range is increased by increasing current value which increased controlled force up to saturation state. By increasing value of frequency, instantaneous value of velocity is increased which increased viscous force or uncontrolled force and reduction in dynamic range.

(5). As shown in Fig. 7.9, the magnetic field is almost saturated at the input current level of 1 A for MR fluid used for this investigation of MR damper; only very small increase in yield stress is observed when the input current increases from 0.9A to 1A. However, the yield stress increase is more noticeable in the current range of 0.2A to 0.8A, which is also effect of the material of cylinder housing; in this case it is low carbon steel.

(6). With the help of mathematical model (Fig. 7.10), if gap size for damper is increased, large gap size reduces the magnetic field due to its larger magnetic resistance. Consequently, it reduces the yield stress of the MR fluid; it assumes that the materials used in the magnetic loop are the same. This also implies that the use of proper material. In this investigation, it is low carbon steel having high conductive permeability increases the magnetic field in the gap at a high current level. This results in an increased yield stress. Moreover, these configurations also exhibit reduced damping forces due to their geometry.

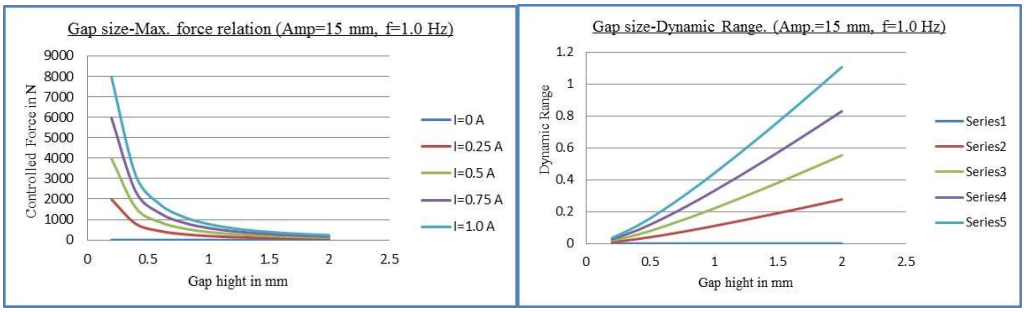

FIGURE 7.10: Effect of Gap height on controlled force and dynamic range

(7). From Fig. 6.6(a)-6.21(a) (measured), force overshoots are clearly seen at the displacement extremes, where the velocity changes its direction. These overshoots appear to be primarily due to the stiction phenomenon found in MR fluids. Because large acceleration occurs at these points due to the velocity discontinuity of the sinusoidal displacement excitation, other effects such as fluid inertial force may also be contributed to these overshoot.

(8). The predicted and measured values of damping forces controllable force and dynamic range are differing about $\pm 10\%$. This is due to the assumed simplifications of the phenomena connected with the operation of the device, revealed a major influence on the computational inaccuracies. This effect may also be related to the simplifications in calculation of the pressure drop.

(9). Precise computations of the magnetic induction are complicated, while the accurate experimental research is time and effort consuming. The $\tau_0(B)$ function provided by the manufacturer of the MR fluid is usually approximate and imprecise which negatively influence the accuracy of the computations. It is experimentally concluded that the maximum damping force varies linearly as the value of the yield stress varies. Difficulties in determining the magnetic induction value explain the high variation of the error. The most accurate calculations can be obtained for the smallest gap height due to the possibilities of the precise determination of the magnetic field and the small error of the simplified model of the flow between parallel plates.

7.4 Achievements with respect to objectives

All factors related to objectives of present research project are defined in section 1.6 of this report are achieved positively. MR fluid is prepared and tested with rheometer available in the laboratory of physics department, M. K. Bhavnagar University and the output is shown in Fig. 5.2. All the parameters are studied carefully related with MR damper design and finally a prototype of MR damper is designed and fabricated. Investigation is carried out by mathematical modelling and experiments on proto type MR damper test rig which has been designed and developed at this laboratory. Design of Experiment also carried out for validation of experiment procedure and the results of DOE is quite satisfactory.

7.5 Conclusions

In present research work, physical occurrences of a MR fluid base damper has been carefully examined through both experimental data and modelling methodologies. The test rig with the MR fluid damper has been fabricated appropriate to design the model in addition to assess the projected damper.

The assumed simplifications of the phenomena connected with the operation of the device, revealed a major influence on the computational inaccuracies. It can be concluded that the most accurate calculations can be obtained for the smallest gap height, due to the possibility of the precise determination of the magnetic field and the small error of the simplified model of the flow between parallel plates. The analysis suggests the need to develop more precise tools supporting the design process of the devices with MR fluids.

It seems reasonable to create a reverse algorithm that will allow estimation of the geometry of the device based on the desired value of the dissipated energy. In addition it is necessary to determine more accurately the value of the magnetic induction in the flow gap of the MR device. It would be also interesting to define the influence of the temperature on the viscosity and the yield stress, as well as to take this influence into account for the theoretical calculations.

Various tests have been carried out using a test rig to verify the damping characteristics of developed MRF dampers. The following test results are obtained:

(1) The damper functioned by using a unit of the electromagnet under an appropriate electrical current control

(2) The magnitude of the damping force depends on the input magnetic field but it has an upper limit

(3) In the absence of an applied magnetic field, an MRF damper exhibits viscous like behaviour, while it shows friction-like behaviour in a magnetic field.

Through a series of experiments, it is confirmed that the behaviour of the MRF damper is fairly predicted by the velocity-displacement and velocity-force relationship over a wide range of applied current, amplitude and frequency. It is clarified that the MRF dampers provide a technology that enables effective semi-active control in real development of various structures.

7.6 Future Scope

During the course of present study, a number of additional considerations and concepts be present. These possibly will be established into opportunities for forthcoming study, are point out as:

- The present investigation was directed assuming steady-state situations. In exercise, on the other hand, fluid flow inside a specific passage is rarely steady-state. Quite the reverse, the flow is mostly transient by means of a lot of variations in flow direction and flow velocity. For example, the study of current helps to recognize behavior under adverse steady-state circumstances. An addition would be toward consist of adverse, non-steady circumstances.
- The MR fluid utilized for present investigation was developed in house at Physics Department, Shri M K Bhavnagar University, Bhavnagar. This specific fluid consumed an iron particles of 40% by volume in castor oil. Forthcoming studies might reflect the influence of iron content on the behavior of the fluid when it operates with damper.
- Forthcoming effort may also consist of to recognize the dependency of normalized yield stress on magnetic field strength. It comprise several supplementary tests done at different magnetic field strengths. With adequate records to characterize the magnetic field dependency, it may be probable to redevelop the suggested model designed for the normalized yield stress such that this one be able to express clearly as a function of dwell time and magnetic field strength.
- Recognize a model for the response time of MR fluid as a function of magnetic field strength
- Examine the dependency of particle dimensions and form on behavior of MR fluid
- Examine the influence of the off-state behavior with respect to on-state behavior.
- Examine the temperature effect on overall performance of MR fluid base damper.

Reference

[1]. "Solutions in Energy absorption and vibration isolation", Enidine Incorporated, NY-14127, USA.

[2]. Jie Gao and Ke Chen (2011), "Frequency-Domain Simulation and Analysis of Vehicle Ride Comfort based on Virtual Proving Ground", International Journal of Intelligent Engineering and Systems, Vol.4, No.3, 2011.

[3]. John C. Dixon (2007), The Shock Absorber Handbook, John Wiley & Sons Ltd.

[4]. J. David Carlson, "Magnetorheological fluids – ready for real-time motion control", Lord Corporation, Materials Division, Cary, North Carolina, USA

[5]. M. R. Jolly, J. W. Bender and J. D. Carlson (1999), "Properties and Applications of Commercial Magnetorheological Fluids", Journal of Intelligent Material Systems and Structures, Vol. 10, No. 1, 1999, 5-13.

[6]. Inman D J (2006), Vibration with control, Wiley, Chichester.

[7]. De Silva CW (2006), Vibration: fundamentals and practice, 2nd edition. CRC Press, Boca Raton.

[8]. Katu U.S., Desavale R.G. and Kanai R.A., "Effect Of Vehicle Vibration on Human Body – RIT Experience", Department of Mechanical Eng., Rajarambapu Institute of Technology, Sakharale-415414.

[9]. Hiromichi Nozaki (2004), "Technology for Measuring the Damping Force of Shock Absorbers and the Constant of Coil Springs Mounted on a Motorcycle by the Un-sprung Mass Vibration Method", SAE Automotive Dynamics, Stability & Controls Conference and Exhibition, May 4-6, 2004.

[10]. Dr. Faramarz Gordaninejad (2011), "A novel magnetorheological shock absorber for vibration control", Department of the army, Army research office, February 2001.

[11]. E. Switonski, A. Mezyk, S. Duda, S. Kciuk (2007), "Prototype magnetorheological fluid damper for active vibration control system", Journal of Achievements in Materials and Manufacturing Engineering, Volume 21, Issue 1, March 2007.

[12]. Tjahjo Pranoto, Kosuke Nagaya and Atsushi Hosoda (2004), "Vibration suppression of plate using linear MR fluid passive damper", Journal of Sound and Vibration 276 (2004) 919–932.

[13]. M. R. Jolly, J. D. Carlson and B. C. Munoz (1996), “A Model of the Behaviour of Magnetorheological Materials”, Smart Materials and Structures, Vol. 5, 1996, 607-614.

[14]. Miao Yu, X.M.Dong, S.B.Choi and C.R.Liao (2009), “Human simulated intelligent control of vehicle suspension system with MR dampers”, Journal of Sound and Vibration 319 (2009) 753–767

[15]. R V Upadhyay, Zarana Laherisheth and Kruti Shah (2004), “Rheological properties of soft magnetic flake shaped iron particle based magnetorheological fluid in dynamic mode”, Smart Mater. Struct. 23 (2014) 015002 (8pp)

[16]. J. D. Carlson and M. R. Jolly (2000), “MR Fluid, Foam and Elastomer Devices”, Mechatronics, Vol. 10, Nos. 4-5, 2000, 555-569.

[17]. J Wang and G Meng (2001), “Magnetorheological fuid devices: principles, characteristics and applications in mechanical engineering”, Proc Instn Mech Engrs Volume 215 Part L.

[18]. Juan de Vicente (2013): Magnetorheology: a review, Vicente, e-rheo-iba, 1 (2013) 1-18

[19]. “MRF-132DG Magneto-Rheological Fluid”, Lord technical data, Lord Corporation, 2011, www.lord.com.

[20]. M. A. Golden, J. C. Ulicny, K. S. Snavely and A. L. Smith (2005), “Magnetorheological, Fluids”, US Patent 6932917.

[21]. Priyank Prakash and Ashok Kumar Pandey (2015), “Performance of MR damper based on experimental and analytical modelling”, The 22nd International Congress of Sound and Vibration, ICSV22, Florence, Italy, 12-16 July 2015.

[22]. J. A. Starkovich and E. M. Shtarkman (2003), “High Yield Stress Magnetorheological Material for Spacecraft Applications”, US Patent 6610404.

[23]. J. Claracq, J. Sarrazin and J. Monfort (2004), “Viscoelastic properties of magnetorheological fluids”, Rheol Acta 43: 38–49.

[24]. H. J. Choi, I. B. Jang, J. Y. Lee, A. Pich, S. Bhattacharya, and H.-J. Adler (2005), “Magnetorheology of Synthesized Core–Shell Structured Nanoparticle”, IEEE Transactions on magnetics, Vol. 41, NO. 10, OCTOBER 2005.

[25]. N. M. Wereley, A. Chaudhuri, S. Jhon, S. Kotha, A. Suggs, R. Radhakrishnn, B. J. Love and T. S. Sudarshan (2006), “Bidisperse Magnetorheological Fluids using Fe Particles at Nanometer and Micron Scale”, Journal of Intelligent Material and Structures, Vol. 17, 2006, 393-401.

[26]. T. Shiraishi, S. Morishita and H. P. Gavin (2004), “Estimation of Equivalent Permeability in Magnetorheological Fluid Considering Cluster Formation of Particles”, Journal of Applied Mechanics, Transactions of the ASME, Vol. 71, No. 2, 2004, 201-207.

[27]. Seung-Bok Choi and Young-Min Han (2013), Magnetorheological Fluid Technology, CRC Press.

[28]. E. Lemaire, Y. Grasselli and G. Bossis (1992), “Field Induced Structure in Magneto and Electro-Rheological Fluids”, Journal De Physique II, Vol. 2, 1992, 359-369.

[29]. Weijia Wen, Xianxiang Huang and Ping Sheng (2008), “Electrorheological fluids: structures and mechanisms”, Soft matter, 2008, 4, 200–210/201.

[30]. B. C. Munoz, G. W. Adams, V. T. Ngo and J. R. Kitchin (2001), “Stable Magnetorheological Fluids”, US Patent 6203717.

[31]. C. Fang, B. Y. Zhao, L. S. Chen, Q. Wu, N. Liu and K. A. Hu (2005), “The Effect of the Green Additive Guar Gum on the Properties of Magnetorheological Fluid”, Smart Materials and Structures, Vol. 14, No. 1, 2005, N1-N5.-not matched

[32]. S. Elizabeth Premalatha, R. Chokkalingam and M. Mahendran (2012), “Magneto Mechanical Properties of Iron Based MR Fluids”, American Journal of Polymer Science 2012, 2(4): 50-55

[33]. J. Rabinow (1951), “Magnetic Fluid Torque and Force Transmitting Device”, US Patent 2575360.

[34]. W. A. Gross (1961), “Valve for Magnetic Fluids”, US Patent 3010471.

[35]. J. Rabinow (1954), “Magnetic Fluid Shock Absorber”, US Patent 2667237.

[36]. E. Germer (1954), “Magnetic Valve”, US Patent 2670749.

[37]. Seval Genc¸ and Pradeep P Phule, Rheological properties of magnetorheological fluids, Smart Mater. Struct. 11 (2002)140–146.

[38]. J. D. Carlson (2002), “What Makes a Good MR Fluid?”, Journal of Intelligent Material Systems and Structures, Vol. 13, Nos. 7-8, 2002, 431-435.

[39]. P. P. Phule (1999), “Magnetorheological Fluid”, US Patent 5985168, Nov-1999.

[40]. J.D.Carlson, D.M.Catanzarite and K.A.St. Clair (1995), “Commercial magnetorheological fluid devices”, 5th Int. Conf. on Electro-Rheological, Magneto-Rheological Suspensions and Associated Technology Sheffield, 10-14 July 1995

[41]. D. Srikala, V. N. Singh, A. Banerjee and B. R. Mehta, “Effect of induced shape anisotropy on magnetic properties of ferromagnetic cobalt nanocubes”, School of Physical Sciences, Jawaharlal Nehru University, New Delhi 110067, India

[42]. C.C. Ekwebelam and H.See (2008), “Determining the flow curves for an Inverse Ferrofluid”, Korea-Australia rheological journal, Vol. 20, no.1, March 2008, pp. 209-224.

[43]. Egon Krause (2005), Fluid Mechanics with Problems and Solutions, ISBN 3-540-22981-7 Springer Berlin Heidelberg New York.

[44]. S. J. Dyke, B. F. Spencer Jr., M. K. Sain and J. D. Carlson (1996), “Modelling and Control of Magnetorheological Dampers for Seismic Response Reduction”, August 1, 1996.

[45]. P Sunthar, “Polymer Rheology”, Department of Chemical Engineering, Indian Institute of Technology (IIT) Bombay, Mumbai 400076 India.

[46]. AP Poloski, JJ Toth and JM Tingey (2009), “Deposition Velocities of Non-Newtonian Slurries in Pipelines: Complex Simulant Testing”, U.S. Department of energy, PNNL-18316, WTP-RPT-189 Rev. 0, 2009.

[47]. K. Toda and H. Furuse (2006), “Extension of Einstein's Viscosity Equation to That for Concentrated Dispersions of Solutes and Particles”, Journal of Bioscience and Bioengineering, Vol. 102, No. 6, 2006, 524-528.

[48]. Xiaocong Zhu, Xingjian Jing and Li Cheng (2012), “Magnetorheological fluid dampers: A review on structure design and analysis”, Journal of Intelligent Material Systems and Structures, 0(0) 1-35.

[49]. C. Wu, Y. C. Lin and D. S. Hsu (2008), “Performance test and mathematical model simulation of MR damper”, The 14th World Conference on Earthquake Engineering October 12-17, 2008, Beijing, China.

[50]. T. Butz and O. von Stryk (2002), “Modelling and Simulation of Electro- and Magnetorheological Fluid Dampers”, Zeitschrift Fur Angewandte Mathematik Und Mechanik, Vol. 82, 2002, 3-20.

[51]. Bong Jun Park, Fei Fei Fang and Hyoung Jin Chi (2010), “Magnetorheology: Materials and application”, Soft Matter, 2010, 6, 5246–5253, The Royal Society of Chemistry.

[52]. J. D. Carlson and K. D. Weiss (1995), “Magnetorheological Materials Based on Alloy Particles”, US Patent 5382373.

[53]. R. T. Foister (1997), “Magnetorheological Fluids”, US Patent 5667715.

[54]. G. Bossis, O. Volkova, S. Lacis and A. Meunier (2002), "Magnetorheology: Fluids, Structures and Rheology", Stefan Odenbach (Ed.): LNP 594, pp. 202–230.

[55]. T. M. Simon, F. Reitich, M. R. Jolly, K. Ito and H. T. Banks (2001), "The Effective Magnetic Properties of Magnetorheological Fluids", Mathematical and Computer Modelling, Vol. 33, Nos. 1-3, 2001, 273-284.

[56]. R. H. Davis, Y. Zhao, K. P. Galvin and H. J. Wilson (2003), "Solid-Solid Contacts Due to Surface Roughness and Their Effects on Suspension Behaviour", Philosophical Transactions. Series A, Mathematical, Physical, and Engineering Sciences, Vol. 361, No. 1806, 2003, 871-894.

[57]. N. P. Sherje and Dr. S. V. Deshmukh (2016), "Preparation and Characterization of Magnetorheological Fluid for Damper in Automobile Suspension", International Journal of Mechanical Engineering and Technology, 7(4), 2016, pp. 75–84.

[58]. B. F. Spencer Jr., S. J. Dyke, M. K. Sain and J. D. Carlson (1997)," Phenomenological Model of a Magnetorheological Damper", Journal of Engineering Mechanics, ASCE, 123:230–238.

[59]. Phillips, R.W. (1969), Engineering applications of fluids with a variable yield stress, Ph.D. thesis, University of California, Berkeley, California.

[60]. "Designing with MR Fluids", ENGINEERING NOTE, Lord Corporation, December-1999

[61]. M. Raju, N. Seetharamaiah, A.M.K. Prasad and M.A. Rahman (2016), "Experimental Analysis of Magneto-Rheological Fluid (MRF) Dampers under Triangular Excitation", International Journal of Mechanical Engineering and Technology, 7(6), 2016, pp. 284–295.

[62]. Honghui Zhang, Changrong Liao, Weimin Chen and Shanglian Huang, "A Magnetic Design method of MR fluid dampers and FEM analysis on magnetic saturation", http://www.paper.edu.cn

[63]. Guangqiang Yang, B.S., "Large-scale Magnetorheological Fluid Damper for Vibration Mitigation: Modeling, testing and Control", Ph.D. thesis, University of Notre Dame, Notre Dame, Indiana, December-2001.

[64]. Jacek Mateusz Bajkowski (2012), “Design, analysis and performance evaluation of the linear magnetorheological damper”, acta mechanica et automatica, vol.6 no.1.

[65]. “Carbonyl Iron Powder”, BASF-The chemical company.

[66]. Jason P. Rich, Patrick S. Doyle and Gareth H. McKinley, “Magnetorheology in an aging, yield stress matrix fluid”, Massachusetts Institute of Technology, Department of Chemical Engineering, Cambridge, MA USA.

[67]. Weiss et al. (1999), “Method and Magnetorheological Fluid formulation for increasing the output of a Magnetorheological Fluid device”, US Patent 5900184.

[68]. Daniel E. Barber and J. David Carlson, “Performance Characteristics of MR Fluid Engine Mounts”, LORD Corporation, Cary, NC USA.

[69]. F D Goncalves and J D Carlson (2009), “An alternate operation mode for MR fluids—Magnetic Gradient Pinch”, Journal of Physics: Conference Series 149 (2009) 012050.

[70]. Saiful Amri Bin Mazlan (2008), The behaviour of Magnetorheological Fluid in squeeze mode, Ph.D. thesis, Dublin City University, August-2008.

[71]. Changsheng Zhu, David A. Robb and David J. Ewins, “A Magneto-rheological Fluid Squeeze Film Damper for Rotor Vibration Control”, Department of Mechanical Engineering, Imperial College, London, SW7 2BX, UK.

[72]. Carlson (1996), “Multi-degree of freedom Magnetorheological device and system for using same”, US Patent 5492312.

[73]. More Thomas AVRAAM (2009), MR-fluid brake design and its application to a portable muscular rehabilitation device, Ph.D. thesis, Active Structures Laboratory Department of Mechanical Engineering and Robotics, November-2009.

[74]. Biedermann (2002), “Leg prosthesis with an artificial knee joint provided with an adjustment device”, US Patent 6423098, July-2002.

[75]. Biedermann et al. (2004), “Leg prosthesis with an artificial knee joint and method for controlling a leg prosthesis”, US Patent 6755870, Jun-2004.

[76]. Webb (1998), “Exercise apparatus and associated method including rheological fluid brake”, US Patent 5810696, Sep-1998.

[77]. RHEO KNEE-3, Technical Manual, OSSUR life without limitation, www.ossur.com, 2015.

[78]. Deffenbaugh et al. (2001), “Electronically prosthetic control”, US Patent US 2001/0029400 A1, Oct-2001.

[79]. Junji Furusho, Takehito Kikuchi and Miwa Tokuda (2007), “Development of Shear Type Compact MR Brake for the Intelligent Ankle-Foot Orthosis and Its Control”, 10th international conference on rehabilitation robotics, Noordvijk, Netherlands.

[80]. Yuhei Yamaguchi, Junji Furusho, Kenichi Koyanagi and Shinya Kimura (2003), “Development of 2-D Force Display System Using MR Actuators”, ICAT, Tokyo, Japan.

[81]. D. I. Lalwani, N. K. Mehta and P. K. Jain (2008), “Experimental investigations on cutting parameters influence on cutting forces and surface roughness in finish hard turning of MDN250 steel”, Journal of materials processing technology, 206 (2008), I67-I79.

[82]. Septimiu George Luca, Florentina Chira and Victor Octavian Rosca (2005), “Passive, active and semi active control systems in civil engineering”, Bul. Inst. Polit. Iasi.

[83]. A. G. Olabi and A. Grunwald, “Design and Application of Magneto-Rheological Fluid – MRF”, Dublin City University, School of Mechanical and Manufacturing Engineering, Glasnevin, Dublin 9, Ireland.

[84]. H. F. Lam, C. Y. Lai, and W. H. Liao, “Automobile suspension systems with MR fluid dampers”, smart materials and structures laboratory, Department of mechanical and automobile engineering, The Chinese University of Hong Kong.

[85]. Bhau K. Kumbhar and Satyajit R. Patil (2014), “A Study on Properties and Selection Criteria for MagnetoRheological (MR) Fluid Components”, International Journal of ChemTech Research, Vol.6, No.6, pp3303-3306, Aug-Sep 2014.

[86]. Terje O. Espelid (2003), “Doubly Adaptive Quadrature Routines based on Newton-Cotes rules”, BIT Numerical Mathematics, 43:319-337, 2003.

[87]. Nizam Mahdavi-Amiri and Richard Bartels (1987), “Constrained Nonlinier Least Squares: An Exact Penalty Approach with Projected Structured Quasi-Newton Updates”, Research Report, CS-87-44, July-1987.

Appendix A:
List of Publications

1) Hamir Sapramer, Dr. S. P. Bhatnagar and Dr. G. D. Acharya (2015), "Magneto rheological fluid (MRF) – Model, Operation mode and Application" (Proceedings of International Conference on Advances in materials and Product Design, AMPD-2015, ISBN: 978-93-5196-956-3, p: 398-405).
2) Hamir Sapramer and Dr. G. D. Acharya (2015), "Test Rig Design for Measurement of Shock Absorber Characteristics", Proceeding of 3rd Afro - Asian International Conference on Science, Engineering & Technology AAICSET-2015, ISBN: 9-780993-909238, p: 126-130.
3) Hamir Sapramer, Dr. S. P. Bhatnagar and Dr. G. D. Acharya (2016), "A Study of MR Fluid Based Damper by Mathematical Model", International Journal of Engineering Science and Futuristic Technology, A Peer-reviewed journal, ISSN: 2454-1338(O), ISSN: 2454-1125(P), Volume 02 Issue 02, February 2016.
4) Hamir Sapramer, Dr. S. P. Bhatnagar and Dr. G. D. Acharya (2016), "Instrumentation of Shock Absorber Test Rig", International Journal of Engineering Science and Futuristic Technology, A Peer-reviewed journal, ISSN: 2454-1338(O), ISSN: 2454-1125(P), Volume 03 Issue 01, March 2016.
5) Hamir Sapramer, Dr. S. P. Bhatnagar and Dr. G. D. Acharya (2016), "Magnetic design of MR fluid based damper", International Journal of Mechanical Engineering and Futuristic Technology, A Peer-reviewed journal, ISSN: 2456-1266(O), Volume 01 Issue 02, September 2016.
6) Hamir Sapramer, Dr. S. P. Bhatnagar and Dr. G. D. Acharya (2016), "Experimental Investigations of Parameters Influence on Total Damping Force in MR Fluid Base Damper", 3rd International Conference on Multidisciplinary Research & Practice, ISSN 2321-2705, Volume IV, Issue I, page 54-61, December 2016.

Appendix B:
C Program Codes

```
#include <stdio.h>
#include <stdlib.h>
#include <string.h>

#define MAX_LINE_SIZE 50
#define MAX_STRING 30

main()
{

int a,avg_no, loop_count;
double tim, pos, lod;
double init_time, sum_pos, sum_load, avg_pos, avg_load, grp_time;
double max_pos, min_pos, center_pos;
char in_file[MAX_STRING],out_file[MAX_STRING],
fileline[MAX_LINE_SIZE];
FILE * fp_in;
FILE * fp_out;

printf("Enter the name of file you wish to process\n");
scanf("%s", in_file);
fp_in = fopen(in_file,"r"); // read mode
if( fp_in == NULL )
   {
      perror("Error while opening the file.\n");
      exit(EXIT_FAILURE);
   }

printf("Enter the name of file you wish to write to\n");
scanf("%s", out_file);
fp_out = fopen(out_file,"w+"); // read mode
fprintf(fp_out, "%s %s %s\n%s %s %s\n", "Time", "Displacement",
"Force", "Sec", "cm", "N");

/* number of points per average */
printf("How many points per average \n");
scanf("%d", &avg_no);

/* skip first two lines containing headers */
fgets( fileline, MAX_LINE_SIZE, fp_in);
fgets( fileline, MAX_LINE_SIZE, fp_in);

fgets( fileline, MAX_LINE_SIZE, fp_in);
sscanf(fileline,"%lf,%lf,%lf\n", &tim, &pos, &lod);

max_pos=pos;
min_pos=pos;
while(!feof(fp_in))
{
    fgets( fileline, MAX_LINE_SIZE, fp_in);
    sscanf(fileline,"%lf,%lf,%lf\n", &tim, &pos, &lod);
```

```
    if(pos > max_pos)
        max_pos = pos;

    if(pos < min_pos)
        min_pos = pos;
 }
 center_pos =  (max_pos + min_pos)/2 ;

printf("Max = %f, Min = %f, CP = %f\n", max_pos,
min_pos,center_pos);

rewind(fp_in);

/* Now do the averaging and other processing
skip first two lines containing headers */
fgets( fileline, MAX_LINE_SIZE, fp_in);
fgets( fileline, MAX_LINE_SIZE, fp_in);

loop_count = 0;
while(!feof(fp_in))
{
fgets( fileline, MAX_LINE_SIZE, fp_in);
sscanf(fileline,"%lf,%lf,%lf\n", &tim, &pos, &lod);
if (loop_count == 0)
    init_time = tim; /* only first time to be stored for zeroing
out*/
loop_count++;

grp_time=tim; /* initial time of avg_no readings */
sum_pos = pos;
sum_load = lod;

for (a =0; a<=avg_no-2; a++)
{
    fgets( fileline, MAX_LINE_SIZE, fp_in);
    sscanf(fileline,"%lf,%lf,%lf\n", &tim, &pos, &lod);
    sum_pos = sum_pos+ pos;
    sum_load = sum_load + lod;
}
    avg_pos = sum_pos / avg_no;
    avg_load = sum_load / avg_no;
fprintf(fp_out, "%f %f %f\n", (grp_time - init_time), ( center_pos
- avg_pos) *3.0, avg_load*500);
printf("%f,%f,%f\n", (grp_time - init_time), ( center_pos -
avg_pos) *3.0, avg_load*500);
}
fclose(fp_in);
fclose(fp_out);
}
```

Experimental Investigations of Parameters Influence on Total Damping Force in MR Fluid Base Damper

Hamir Sapramer, Dr. S. P. Bhatnagar, Dr. G. D. Acharya

Sir Bhavsinhaji Polytechnic Institute, Gujarat Technological University, Ahmedabad, India

***Abstract*— A magnetorheological fluid composition having a magnetisable carrier medium loaded with magnetisable particles to provide a magnetorheological fluid exhibiting enhance rheological properties. Also disclosed in a magnetic particle damper utilizing the magnetorheological fluid composition.**

Magnetorheological (MR) dampers are one of the most advantageous control devices for mechanical engineering applications due to many good features such as small power requirement, reliability, and low price to manufacture. The smart passive system (semi active control system) consists of an MR damper and an electromagnetic induction (EMI) system that uses a permanent magnet and a coil. According to the Faraday law of induction, the EMI system that is attached to the MR damper can produce electric energy and the produced energy is applied to the MR damper to vary the damping characteristics of the damper. Thus, the smart passive system does not require any power at all. Besides the output of electric energy is proportional to input loads due to vibration, which means the smart passive system has adaptability by itself without any controller or sensors.

In the present study, an attempt has been made to investigate the effect of velocity, amplitude and current on total damping force in MR fluid base damper developed at Physics Department, Shri M.K. Bhavnagar University. The experiments were conducted based on response surface methodology (RSM) and sequential approach using face cantered central composite design. The results show that all the factors (piston velocity, Amplitude and Current) has significant effect on Total Damping Force. A linear model best fits the variation of total damping force with velocity, amplitude and current. Current is the dominant contributor to the total damping force. A non-linear quadratic model best describes the variation of total damping force with major contribution of all parameters. The suggested models of total damping force adequately map within the limits of the parameters considered.

***Keywords*— DOE, MR fluid, Damper, Damping force, Dynamic range**

I. INTRODUCTION

Vibration suppression is considered as a key research field in engineering to ensure the safety and comfort of their occupants and users of mechanical structures. To reduce the system vibration, an effective vibration control with isolation is necessary. Vibration control techniques have classically been categorized into two areas, namely passive and active controls. For a long time, efforts were made to improve the effectiveness of the suspension system by optimizing its parameters, but due to the intrinsic limitations of a passive suspension system, improvements were effective only in a certain frequency range. Compared with passive suspensions, active suspensions can improve the performance of the suspension system over a wide range of frequencies. Semi-active suspensions were proposed in the early 1970s [1], and can be nearly as effective as active suspensions. When the control system fails, the semi-active suspension can still work under passive conditions. Compared with active and passive suspension systems, the semi-active suspension system combines the advantages of both active and passive suspensions because it provides better performance when compared with passive suspensions and is economical, safe and does not require either higher-power actuators or a large power supply as active suspensions do [2].

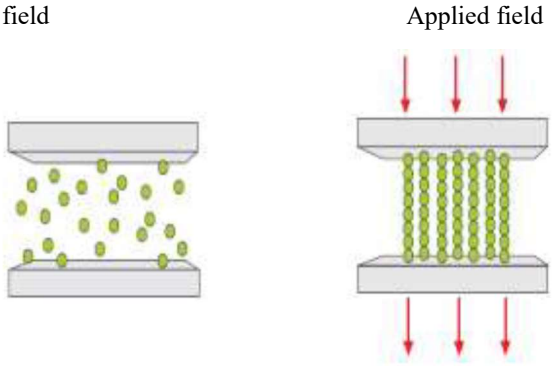

Figure 1: Chain-like structure formation in controllable fluids

The initial discovery and development of MR fluid can be credited to Jacob Rainbow at the US National Bureau of Standards in the late 1940s [6, 7]. These fluids are suspensions of micron-sized, magnetisable particles in an appropriate carrier liquid [8-12]. Normally, MR fluids are free flowing liquids having consistency similar to that of motor oil. However, in the presence of applied magnetic field, the iron particles acquire a dipole moment aligned with the external field which causes particles to form linear chains parallel to the field, as shown in Fig. 1. This phenomenon can solidify the suspended iron particles and restrict the fluid movement. Consequently, yield strength is developed within the fluid. The degree of change is related to the magnitude of the applied magnetic field, and can occur only in a few milliseconds. A typical MR fluid contains 20-40% [5] by volume of relatively pure, soft iron particles, e.g., carbonyl

iron. These particles are suspended in mineral oil, synthetic oil, water or glycol. A variety of proprietary additives similar to those found in commercial lubricant are commonly added to discourage gravitational settling and promote suspension, enhance lubricity, modify viscosity, and inhibit wear. Recently developed MR fluids appear to be attractive alternative for designing of semi active system (controllable fluid dampers) compared to other smart fluids. [6-12]. Magneto rheological (MR) fluids possess rheological properties, which can be changed in a controlled way. These rheological changes are reversible and dependent on the strength of excited magnetic field. MR fluids have potential beneficial applications when placed in various applied loading (shear, valve and squeeze) modes. The squeeze mode is a geometric arrangement where an MR fluid is sandwiched between two flat parallel solid surfaces facing each other. The distance between these two parallel surfaces is called the gap size. These surfaces are either pushed towards or pulled apart from each other by orthogonal magnetic-induced force.

The ultimate strength of an MR fluid depends on the square of the saturation magnetization of the suspended particles. The key to a strong MR fluid is to choose a particle with a large saturation magnetization. The best practical particles are simply pure iron, as they have saturation magnetization of 2.15 Tesla. Typically, the diameter of the magnetisable particles is 3 to 10 microns. Functional MR fluids may be made with larger particles; however, particle suspension becomes increasingly more difficult as the size increases. Smaller particles which are easier to suspend could be used, but the manufacturing of such particles is difficult. Due to the special behaviour of MR fluid, it is used for vast applications such as: dampers, shock absorbers, rotary brakes, clutches, prosthetic devices, polishing and grinding devices, etc. Among them, MR fluid dampers are widely used because of their mechanical simplicity, high dynamic range (Ratio of Controllable force to uncontrollable force), low power requirements, large force capacity and robustness. This class of device has shown to match well with application demands and constraints to offer an attractive means of protecting various engineering systems against interrupted force. MR dampers are being developed for a wide variety of applications where controllable damping is desired. MR damper which utilize the advantages of MR fluids, are semi-active control devices and is popular topic for researchers. A typical MR damper includes MR fluid, a pair of wires, housing, a piston, a magnetic coil and an accumulator as displayed in Fig. 2a. Here, the MR fluid is housed within the cylinder and flows through a small orifice. The magnetic coil is built in the piston or on the housing. When a current is supplied to the coil, the particles are aligned and the fluid changes from the liquid state to the semi-solid state within milliseconds. Consequently, the controllable damping force is produced. The force produced by a MR damper depends on magnetic field induced by the current in the damper coil and the piston velocity as in Fig. 2b.

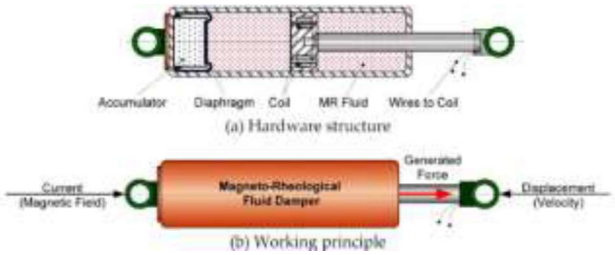

Figure 2. General configuration of a MR fluid damper.

It is capable of generating the force with magnitude sufficient for rapid response in large scale applications [13-15], with requirement only a battery for power [10]. Additionally, these devices offer highly reliable operations and their performance is relatively insensitive to temperature fluctuations or impurities in the fluid [9]. As a result, there has been active research and development of MR fluid dampers and their applications [6-18, 20-21].

The controllable force and the dynamic range are two of the most important parameters in evaluating the overall performance of the MR damper. As illustrated in Fig. 3, the total damper force can be decomposed into a controllable force F_τ due to controllable yield stress and an uncontrollable forceF_{uc}. The uncontrollable force includes a plastic viscous force F_η and a friction F_f. The dynamic range (D) is defined as the ratio between the damper controllable force F_τ and the uncontrollable force F_{uc} as follows:

$$D = \frac{F_\tau}{F_{uc}} = \frac{F_\tau}{F_\eta + F_f}$$

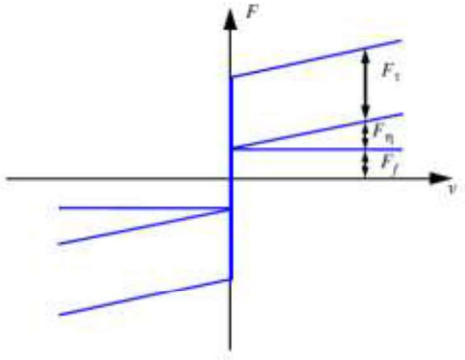

Figure 3: Conceptual design for the MR damper and the EMI part

Most of the experimental investigations on damping force have been conducted using two-level factorial design (2k) for studying influence of parameters on total damping forces. In two-level factorial design, one can identify and model linear relationships only. For studying the nonlinearity present in the output characteristics at least three levels of each factor are required (i.e. three-level factorial design, 3k). A central composite design which requires fewer experiments than alternative 3k design is usually better [19]. Again, sequential experimental approach in central composite design can be used to reduce the number of experiments required. Keeping

the foregoing in mind, the present work is focused on investigations of total damping force as a function of amplitude, velocity and current value using sequential approach in central composite design. The study was conducted on MR damper developed at physics department, Shri M. K. Bhavnagar University, Bhavnagar.

II. ENXPERIMENTAL DETAILS

The details of experimental conditions, instrumentations and measurements and the procedure adopted for the study are described in this section.

A. Magneto Rheological Fluid (MR Fluid)

The magneto rheological fluid developed in house was used in the prototype. The fluid is a suspension of a 10 micron diameter sized magnetically susceptible particles, in Castrol oil carrier fluid. According to the data available by testing this MR fluid on rheometer at this laboratory, the density of the liquid is around 3 g/cm^3 and off state viscosity of a 3.5 Pas. The maximum yield stress value is 15 kPa and it is achieved with the magnetic induction of 0.7 T. When exposed to a magnetic field, the rheology of the fluid reversibly and instantaneously changes from a free-flowing liquid to a semi-solid state with the controllable yield strength as a consequence of the sudden change in the particles arrangement. Figure 4 shows the detail relations of magnetic flux density, viscosity and shear stress available from rheometer.

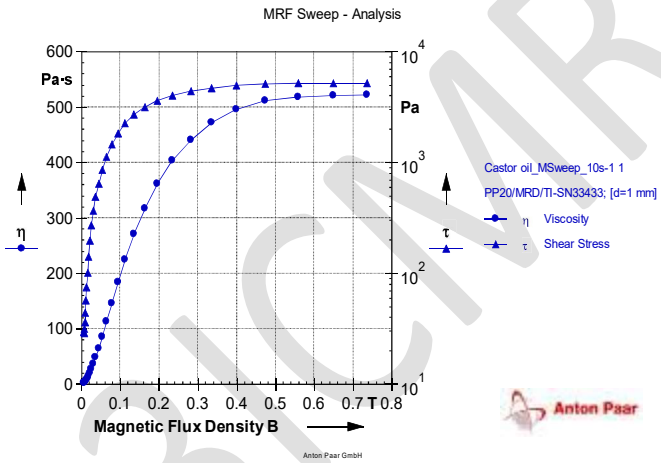

Figure 4. Relation between Magnetic flux density, Viscosity and Shear stress

B. MR Fluid base Damper

The damper is made up of two principal components: housing and piston. Housing contains a volume of magnetorheological (MR) fluid. One fluid which has shown itself to be particularly well-suited for this application consists of carbonyl iron particles suspended in castor oil. Housing is a cylindrical tube with a first closed end with an accumulator and attachment eye associated therewith. A second or open end of the cylinder is closed by upper end cap. A seal is provided to prevent fluid leakage from housing. Accumulator is necessary to accommodate fluid displaced by piston rod as well as to allow for thermal expansion of the fluid. Piston head is spool shaped having an upper outwardly extending flange and a lower outwardly extending flange. Coil is wound upon spool-shaped piston head between upper flange and lower flange. Piston head is made of a magnetically permeable material, in this case, low carbon steel. Guide rails are attached above and below side of piston to keep the piston in centring position to housing during operation. Piston head is formed with a smaller maximum diameter (in this case, D_{pole}) than the inner diameter, D_i of housing. The external surfaces of guides are contoured to engage the inner diameter Di of housing. Guides are made of non-magnetic material, in this case, bronze, and it maintains piston centred within gap 'g'. In this model, gap g (in conjunction with coil) functions as a valve to control the flow of MR fluid past piston. Electrical connection is made to coil through piston rod by lead wires. A first wire is connected to a first end of an electrically conductive rod which extends through piston rod to outside of damper. The second end of the windings of coil is attached to a "ground" connection on the outside of damper. The upper end of piston rod has threads formed thereon to permit attachment of damper, as depicted in figure. An external power supply, which provides a current in the range of 0-4 amps at a voltage of 12-24 volts, is connected to the leads. The outer surface of coil is coated with epoxy paint as a protective measure. The damper of this experiment functions as a Bingham type damper, i.e., this configuration approximates an ideal damper in which the force generated is independent of piston velocity and large forces can be generated with low or zero velocity. This independence improves controllability of the damper making the force a function of the magnetic field strength, which is a function of current flow in the circuit.

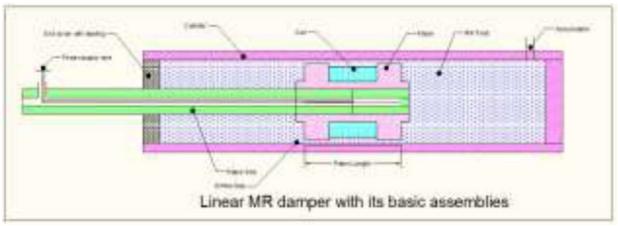

Figure 5. Basic assembly of proposed MR Damper

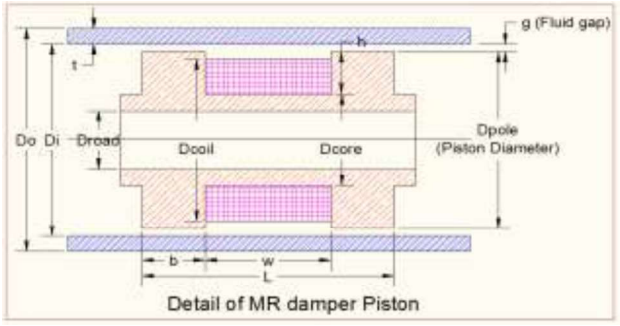

Figure 6. Details of proposed MR Damper Piston

The linear damper prototype is presented as a blueprint in Figure 5. Details of MR damper piston is shown in Figure 6.

C. Total Damping Force Measurement

The shock absorber is characterized by its instantaneous value of position velocity, acceleration, force, pressure, temperature etc. and various plots among these parameters. For the measurement of listed parameters of the shock absorber a test rig is designed and developed. An experiment on the test rig is carried out at different speeds and loads which lead to the output in terms of sinusoidal waveform on attached oscilloscope. The waveform is used to find out the characteristics at different load-speed combination. The results obtained are used to find out the behaviour of shock absorber at different speed and loads.

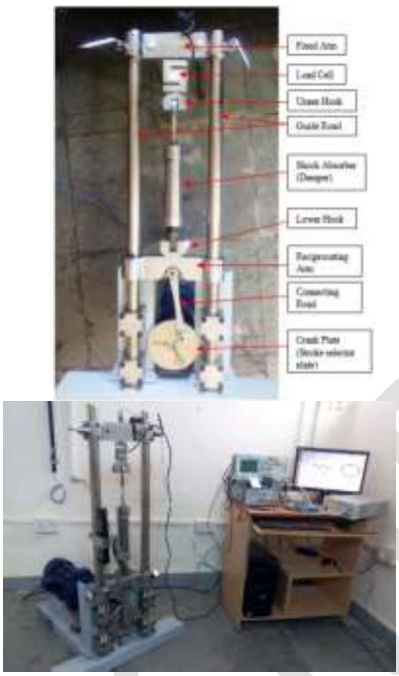

Figure 7. Shock absorber test rig

Figure 7 indicates details of shock absorber test rig setup. The setup consist of Piston and crank (Single Slider Crank Mechanism). This mechanism consists of a crank, connecting rod and piston (reciprocating arm). The crank plate has holes drilled to achieve different stroke lengths shown in figure 7. The advantage of this mechanism is its cost effectiveness because there is less high tolerance machining. The frequency is adjusted by using variable gear drive system based electric motor. The output from the motor is geared down using gearbox. The maximum output shaft speed is in the range of 350 to 400 RPM at full speed of motor having 1440 RPM. Variation

of stroke is possible by fixing the connecting road in appropriate hole made in crank plate, so the stroke is set to give the desired maximum speed within the limits of the damper and test apparatus. There are twelve screwed holes located over spiral shape; connecting rod can be fixed in suitable hole to select stroke length. The longer the stroke, the greater the power needed on motor to move the shock absorber

D. Experimental plan procedure

Thirty two experimental runs composed of 23 factorial points, four centre points and five axial points were carried out in block 1. Table 2 shows complete design matrix with responses to total damping force. In design matrix, the coded variables were arranged as follows: A: amplitude (A), B: angular speed (N) and C: current (I). F is the responses representing total damping force. The experiments were conducted randomly as shown in design matrix ('runs' column in Table 2). The design matrix also, shows the factorial points, centre points and axial points with coded and actual values.

Table 1 – Parameters and their levels

Factor	Unit	Low level (-1)	Centre level (0)	High level (1)
Amplitude	mm	5	10	15
Angular speed	RPM	60	90	120
Current	Amp	0	0.5	1.0

The Model F-value (Table-3) of 255.862 implies the model is significant. There is only a 0.01% chance that a "Model F-Value" this large could occur due to noise. Values of "Prob > F" less than 0.05 indicate model terms are significant. In this case A, B, C and AB are significant model terms. Values greater than 0.05 indicate the model terms are not significant. The "Pred R-Squared" of 0.976504 is in reasonable agreement with the "Adj R-Squared" of 0.986665. "Adeq Precision" measures the signal to noise ratio. A ratio greater than 4 is desirable. The ratio of 67.89797 indicates an adequate signal. This model can be used to navigate the design space.

Table 2 – Design matrix with responses (Total Damping Force)

Std	Run	Block	Type	A:A(mm)	B:N(rpm)	C:I(Amp)	A:A(mm)	B:N(rpm)	C:I(Amp)	F(N)
1	5	1	Axial	0	0	-1	10	90	0	805
2	16	1	Fact	-1	1	0	5	120	0.5	907
3	29	1	Centre	0	0	0	10	90	0.5	1080
4	14	1	Centre	0	0	0	10	90	0.5	1080

5	20	1	Fact	0	-1	1	10	60	1	1215
6	8	1	Fact	0	1	-1	10	120	0	960
7	12	1	Fact	1	-1	0	15	60	0.5	1124.5
8	13	1	Axial	-1	0	0	5	90	0.5	794
9	4	1	Fact	-1	0	-1	5	90	0	510
10	19	1	Fact	-1	-1	1	5	60	1	958
11	17	1	Axial	0	1	0	10	120	0.5	1205
12	27	1	Fact	1	1	1	15	120	1	2070
13	10	1	Fact	-1	-1	0	5	60	0.5	638
14	32	1	Centre	0	0	0	10	90	0.5	1080
15	7	1	Fact	-1	1	-1	5	120	0	616
16	30	1	Centre	0	0	0	10	90	0.5	1080
17	26	1	Fact	0	1	1	10	120	1	1492
18	18	1	Fact	1	1	0	15	120	0.5	1803
19	25	1	Fact	-1	1	1	5	120	1	1263
20	23	1	Fact	1	-1	1	10	90	1	1360
21	22	1	Fact	-1	0	1	5	90	1	1151
22	24	1	Fact	1	0	1	15	90	1	1669.5
23	11	1	Axial	0	-1	0	10	60	0.5	903
24	21	1	Fact	1	-1	1	15	60	1	1434.5
25	9	1	Fact	1	1	-1	15	120	0	1545
26	2	1	Fact	0	-1	-1	10	60	0	599
27	28	1	Fact	0	0	0	10	90	0.5	1080
28	6	1	Fact	1	0	-1	15	90	0	1155
29	1	1	Fact	-1	-1	-1	5	60	0	342
30	3	1	Fact	1	-1	-1	15	60	0	875
31	15	1	Axial	1	0	0	15	90	0.5	1397.5
32	31	1	Fact	0	0	0	10	90	0.5	1080

Table 3 – ANOVA (Partial sum of square) for total damping force (F)

Source	Sum of squares	d.f.	Mean square	F-value	Prob>F	Remark
Model	4365178	9	485019.7354	255.865	< 0.0001	Significant
A-A-Amplitude	1930613	1	1930612.5	1018.466	< 0.0001	Significant
B-B-RPM	790443.6	1	790443.5556	416.9868	< 0.0001	Significant
C-C-Current	1505691	1	1505690.889	794.3049	< 0.0001	Significant
AB	107541.3	1	107541.3333	56.73183	< 0.0001	Significant
AC	7752.083	1	7752.083333	4.089497	0.0555	
BC	638.0208	1	638.0208333	0.336578	0.5677	
A^2	17807.78	1	17807.77502	9.394227	0.0057	
B^2	2.640405	1	2.640405294	0.001393	0.9706	

C^2	874.9481	1	874.9480976	0.461566	0.5040	
Residual	41703.38	22	1895.60825			
Lack of Fit	41703.38	17	2453.140088			
Pure Error	0	5	0			
Cor Total	4406881	31				
Std. Dev.	43.53858		R-Squared	0.990537		
Mean	1102.25		Adj R-Squared	0.986665		
C.V. %	3.949974		Pred R-Squared	0.976504		
PRESS	103545.1		Adeq Precision	67.89797		

III. RNESULTS AND DISCUSSION

Table 2 shows all values of total damping force. The total damping force was obtained in the range of 342 N to 2070 N.

The increase in total damping force is due to

- Increasing of applied current value, which increases the shear stress of MR fluid.
- Increasing of angular speed, which increases the velocity of piston.
- Increasing of amplitude, this is also due to large displacement of fluid inside the piston cylinder assembly.

Fig. 8-10 shows relation between total damping force (measured force in N) with applied current values, angular speed and amplitude for different combinations. The rate of increasing in total damping force is higher for increasing the value of current compare to amplitude and velocity. Fig. 8 also shows that the total damping force is increased linearly with respect to increase in value of applied current. This observation agrees well with results reported by previous researchers. [13, 14, 15, 17, 20]

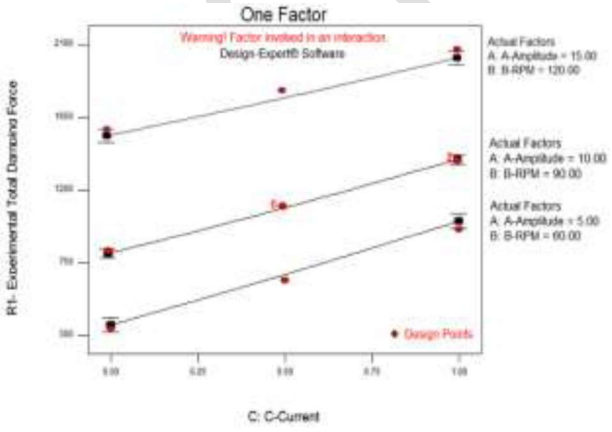

Fig. 8 – Total measured damping force vs. applied current at different values of amplitude and angular speed.

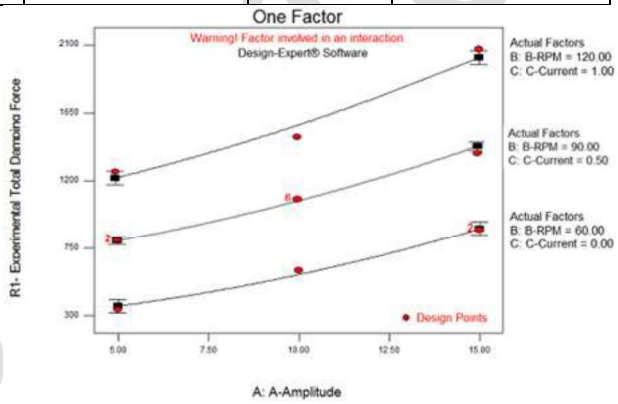

Fig. 9 – Total measured damping force vs. Amplitude at various angular speed and applied current.

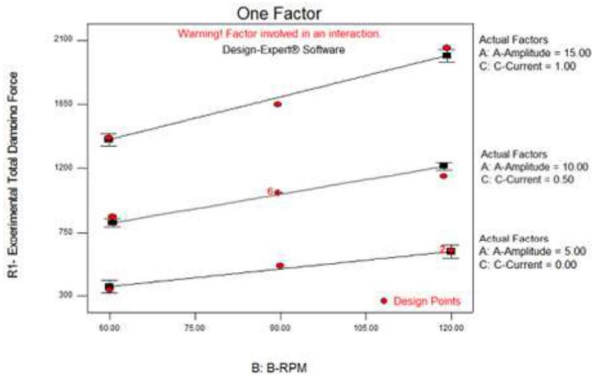

Fig. 10 – Total measured damping force vs. Angular velocity at various amplitude and applied current.

Furthermore, the results were analysed in Design Expert V6 software. The results of the block 1 experiments in the form of analysis of variance (ANOVA) are presented. An ANOVA summary table is commonly used to summarize the test of the regression model, test of the significance factors and their interaction and lack-of-fit test. If the value of 'Prob > F' in ANOVA table is less than 0.05 then the model, the factors, interaction of factors and curvature are said to be significant

Table 3 shows that the model is significant and amplitude (A), angular speed (B), applied current (C) and (A, B) are only the significant factors (terms) in the model. All other terms are insignificant. The contribution of factors, their interaction and curvature is also shown in Table 3.

The various R2 statistics (i.e. R2, adjusted R2 (R2 Adj) and predicted R2 (R2 Pred)) of the total damping force Table 3. The value of R2 = 0.990537 for total damping force indicates that 99.05% of the total variations are explained by the model. The adjusted R2 is a statistic that is adjusted for the "size" of the model; that is, the number of factors (terms). The value of the R2 Adj = 0.986665 indicates that 98.66% of the total variability is explained by the model after considering the significant factors. R2 Pred = 0.976504 is in good agreement with the R2 Adj and shows that the model would be expected to explain 97.65% of the variability in new data (Montgomery, 2001). 'C.V.' stands for the coefficient of variation of the model and it is the error expressed as a percentage of the mean ((S.D./Mean) ×100). Lower value of the coefficient of variation (C.V. = 3.9%) indicates improved precision and reliability of the conducted experiments. As curvature (nonlinearity) is not present in the model, additional experiments are not required to be performed. This is the main advantage of sequential approach in face cantered central composite design.

The normal probability plot of the residuals (i.e. error = predicted value from model−actual value) for Total damping Force is shown in Fig. 11, reveal that the residuals lie reasonably close to a straight line, giving support that terms mentioned in the model are the only significant (Montgomery, 2001).

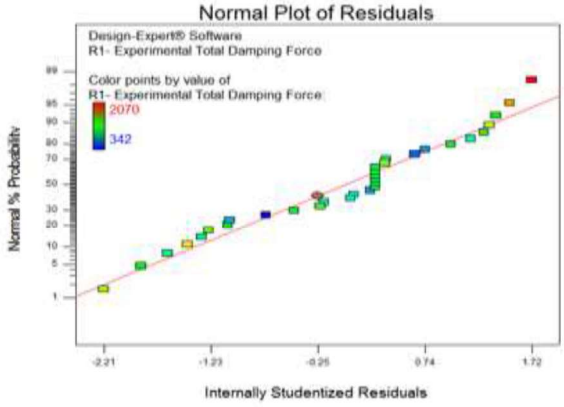

Fig. 11 Normal probability plot of residuals for Total Damping Force data.

After removing the insignificant factors, the response surface equations for Total damping Force is obtained in the actual values as follows:

Total Measured damping Force

$$F = -26.1306 * A + 1.038635 * B + 679.6246 + 0.631111 * A * B - 10.1667 * A * C - 0.48611 * B * C + 1.995699 * A^2 - 0.00068 * B^2 + 44.23656 * C^2 + 195.8705$$

Where

F = Total damping force in N
A = Amplitude value in mm
B = Angular Speed value in RPM
C = Applied Current value in Amp.

The predicted values from the model (equation value) and the actual (experimental) values are shown in Fig. 12.

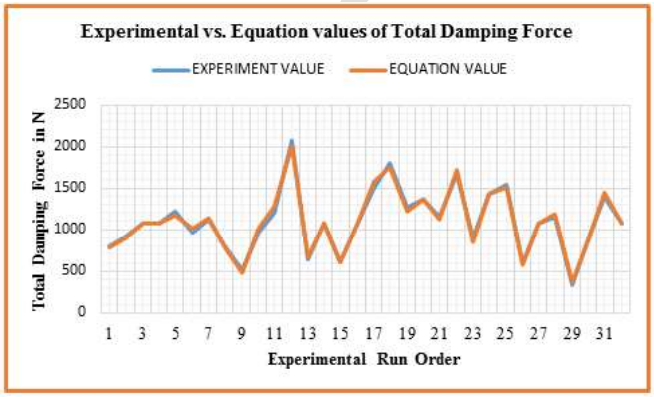

Fig. 12 – Actual vs. predicted values of total damping forces.

Since variable damping force is required for replacing the passive vibration control system to a semi-active vibration control system. The major focus of research is to find out total damping force for which desired damping coefficient can be achieved. Hence, the contour plots of the total damping force with relation in amplitude of vibration, angular velocity of vibrating device and applied current to MR damper are essential. The contour plot of the total damping force in angular velocity-amplitude at current value of 0.5 amp, current-amplitude at angular velocity value of 90 RPM, and current-angular velocity at amplitude value of 10 mm are shown in Figs 13-15, respectively. Figs. 13-15 clearly show that a good total damping force can be achieved for any level of amplitude and angular velocity, when current value is changed from low to high. In present research work, the MR fluid based semi-active damper is designed to achieve variable damping force by changing the current value.

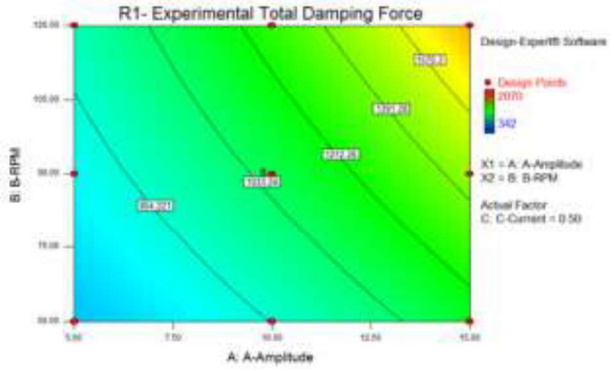

Fig. 13 – Measured Damping Force (N) contour in Angular speed (RPM) and Amplitude (mm) plane at current value of 0.5 Amp.

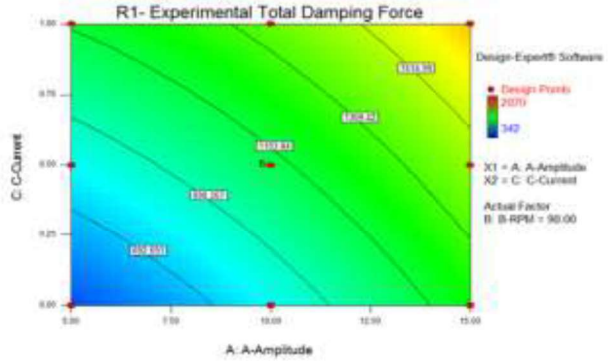

Fig. 14 – Measured Damping Force (N) contour in current (Amp) and Amplitude (mm) plane at Angular speed of 90 RPM.

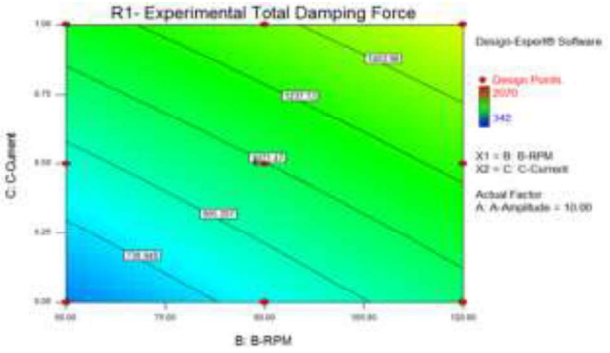

Fig. 15 – Measured Damping Force (N) contour in current (Amp) and Angular speed (RPM) plane at Amplitude of 10 mm.

IV. CONCLUSION

This paper presents the findings of an experimental investigation of the effect of velocity of damper piston, amplitude of damping system and applied current value to damper on the total damping force developed by damping system of developed MR fluid based damper for this research project and following conclusions are drawn. Sequential approach in central composite design is beneficial as it saves number of experimentations required. This was observed in total damping force analysis.

- Quadratic model is fitted for total damping force.
- All the factors (piston velocity, Amplitude and Current) has significant effect on Total Damping Force.
- The applied current is most significant factor, by which the value of total damping force can be adjusted according to system requirement. Thus the current provides primary contribution and influences most significantly on the total damping force. The interaction between amplitude and velocity provide secondary contribution to the model.
- High value of total damping force can be achieved when amplitude, velocity and current values are set nearer to their high level of the experimental range (15mm, 120 RPM and 1.0 A respectively).
- Contour plots can be used for selecting the parameters for providing the given desired total damping force.
- Experimental results of the developed damper are in good agreement with the predicted (equation) values.

REFERENCES

[1]. Karnopp D, Crosby M.J, Farwood R.A (1974) Vibration control using semi-active force generators. ASME j. eng. ind. 96(2): 619-626.
[2]. Yi K, Song B.S (1999) A new adaptive sky-hook control of vehicle semi-active suspensions. Proc. of IMechE, Part D: j. auto. eng. 213(3): 293-303.
[3]. Kawashima K, Unjoh S, Shimizu K (1992) Experiments on Dynamics Characteristics of Variable Damper. Proc. of the japan national symp. On structural response control, Tokyo, Japan: 121.
[4]. Mizuno T, Kobori T, Hirai J, Matsunaga Y, Niwa N (1992) Development of Adjustable Hydraulic Dampers for Seismic Response Control of Large Structure. ASME PVP conf.: 163-170.
[5]. Mark R Jolly, J David Carlson and Beth C Munoz (1996) A model of the behaviour of magnetorheological materials", Smart Mater. Struct. 5 (1996) 607–614.
[6]. Rabinow J (1948) Proceedings of the AIEE trans. 67: 1308-1315.
[7]. Rabinow J (1951) US Patent 2,575,360.
[8]. Carlson J.D, Chrzan M.J (1994) Magnetorheological Fluid Dampers. U.S. Patent 5277281.
[9]. Carlson J.D, Weiss K.D (1994) A growing attraction to magnetic fluids. J. Machine design 66(15): 61-64.
[10]. S.J Dyke, Spencer B.F. Jr, Sain M.K, Carlson J.D (1996) Modelling and control of magneto-rheological fluid dampers for seismic response reduction. Smart material and structures 5: 565-575.
[11]. Boelter R., Janocha H (1998) Performance of long-stroke and low-stroke MR fluid damper. Proc. of SPIE, smart structures and materials: passive damping and isolation, San Diego, CA: 303-313.
[12]. Carlson J.D, Jolly M.R (2000) MR fluid, foam and elastomer devices. Mechatronics 10: 555-569.
[13]. Hong S.R, Choi S.B, Choi Y.T, Wereley N.M (2005) Non-dimensional analysis and design of a magnetorheological damper. J. of sound vib. 288(4): 847-863.
[14]. Choi K.M, Jung H.J, Cho S.W, Lee I.W (2007) Application of smart passive damping system using MR damper to highway bridge structure. KSME Int. j. 21(6): 870-874.
[15]. Spelta C, Previdi F, Savaresi S.M, Fraternale G, Gaudiano N (2009) Control of magnetorheological dampers for vibration reduction in a washing machine. Mechatronics 19(3): 410-421.
[16]. Spencer B.F, Dyke S.J, Sain M.K, Carlson J.D (1996) Phenomenological Model of a Magneto-Rheological Damper. ASCE J. of eng. mech. 123(3): 230-238.
[17]. Choi S.B, Lee S.K (2001) A Hysteresis Model for the Field-dependent Damping Force of a Magneto-rheological Damper. J. of sound vib. 245(2): 375-383.
[18]. Dominguez A, Sedaghati R, Stiharu I (2004) Modelling the hysteresis phenomenon of magnetorheological dampers. Smart mat. struc. 13(6): 1351–1361.
[19]. D.I. Lalwani, N.K. Mehta, P.K. Jain (2007), Experimental investigations of cutting parameters influence on cutting forces and surface roughness in finish hard turning of MDN250 steel. Journal of materials processing technology (Elsevier) 206 (2008) 167–179
[20]. Heon-Jae Lee, Seok-Jun Moonb, Hyung-Jo Junga, Young-Cheol Huhb, Dong-Doo Janga –Korea(2008) Integrated Design Method of MR damper and Electromagnetic Induction System for Structural Control, Sensors and Smart Structures Technologies for Civil, Mechanical, and Aerospace Systems 2008, SPIE Vol. 6932 69320S-2

International Journal of
Engineering Science and Futuristic Technology
A Peer-reviewed journal

ISSN : 2454-1338(O), ISSN : 2454-1125(P)

IJESFT 15 (2016) 001-007

Instrumentation of Shock Absorber Test Rig

H. R. Sapramer [1*], Dr. S. P. Bhatnagar [2], Dr. G. D. Acharya [3]

[1] Mechanical Engineering Department, Sir Bhavsinhaji Polytechnic Institute - Bhavnagar, India

[2] Physics Department, M. K. Bhavnagar University - Bhavnagar, India

[3] Atmiya Institute of Science and Technology - Rajkot, India

A B S T R A C T : The shock absorber is characterized by its instantaneous value of position, velocity, acceleration, force, pressure, temperature etc and various plots among these parameters. For the measurement of listed parameters of the shock absorber a test rig is designed and developed with instrumentations. An experiment on the test rig is carried out at different speeds and loads which lead to the output in terms of sinusoidal waveform on attached oscilloscope. The waveform is used to find out the characteristics at different load-speed combination. The results obtained are used to find out the behavior of shock absorber at different speed and loads. Shock absorber test rig is a machine to test shocks and generate graphs for the shock characteristics. These graphs could be printed for the shocks or stored so user could develop a database of how each shock works under the test conditions. This machine replaces the trial and error approach into a reliable and efficient method to determine the shocks used during an operation.

Article History

Available online:
15/03/2016

Keywords: Damping, Shock Absorber, Shock Absorber Test Rig, Instrumentation

1. Introduction

The phenomenon of damping is found everywhere in today's society and plays a crucial role when it comes to safety, stability and fatigue in a product. Using dampers on a car or any other vehicle is just a tiny area where damping is used. The phenomenon and concept can be found on buildings, bridges, shoes and many other applications. Damping is an effect that reduces the amplitudes of oscillations in an oscillating system, such as the examples above. No matter what material something is built from or how stiff it is, it will always move due to different conditions, and will eventually become an oscillating system, if only for a tiny bit of time. If the oscillations within that system is not controlled or reduced, at some point the material and construction will break, or the system will become very unstable, with possible catastrophic consequences. Therefore, damping is needed to improve the fatigue and stability, as well as reduce the risk of failure and increase the performance.

The purpose of dampers is to dissipate any energy in the vertical motion of the body or wheels of a vehicle. This includes motion arisen from control inputs or from disturbance by rough roads or winds. When moving, a vehicle with their wheels constitutes a vibrating system that needs to be controlled by dampers to prevent response overshoots, and to minimize the influence of some unavoidable resonances.

Testing of theory is required to validate methods of analysis and to give confidence in theory for design work. This is likely to involve testing of individual parts or testing of complete shock absorber to relate damping characteristics, to investigate piston or rod seal friction effects, etc.

[*] Corresponding author e-mail: merhamir@yahoo.com
Tel.: +91 9426587197

Nomenclature

X	Position
V	Velocity
A	Acceleration
F	Force
P	Pressure
T	Temperature
LVDT	Linear Variable Differential Transformer

Performance testing is required to check that prototypes or samples of production dampers meet their specifications within tolerance, and are adequately consistent one to another. In competition, performance testing is required to check that a design gives the expected behavior and, again, that dampers are consistent and in matched pairs. Testing may therefore be used to select matched pairs or to refine manufacture and assembly to the necessary level.

Attempts have been made previously to find out various shock absorber properties by various approaches. Rao and Greenberg carried experiment for measurement of equivalent stiffness and damping properties of shock absorber [1]. Y. Ping studied dynamic behavior of an oil-air coupling shock absorber [2]. A K Samantray developed preloading mechanism for liquid spring /damper shock absorber and studied the shock isolation properties [3]. For nonlinear viscous damping device force transmissibility of multi degree of freedom is also studied by Peng and others [4]. Also simulation and experimental validation of vehicle dynamic characteristic for displacement sensitive shock absorber with fluid flow modeling [5,6].

Following are typical plots of interest for shock absorber to characterize it.

- Position vs Time;
- Velocity vs Time;
- Acceleration vs Time;
- Force vs Time;
- Force vs Position;
- Force vs Velocity;

For obtaining such parameters, test rig should be properly design and instrumented, which gives the parameters listed above in close tolerance.

2. Instrumentations

The basic parameters to be measured may include instantaneous values of
(1) Position
(2) Velocity
(3) Acceleration
(4) Force
(5) Pressure
(6) Temperature.

These need sensors, pulse data processing and suitable display. In addition the data stream will be processed to give items such as cyclic extremes of position and force.

The basic shock analyzer kit connections are shown in figure 1. Real setup of develop test rig with instrumentation is shown in figure 2.

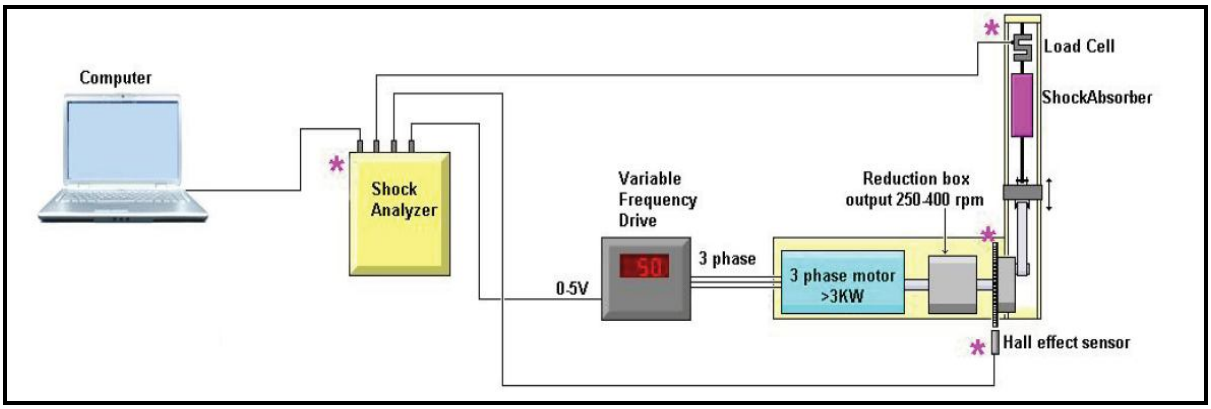

Fig.1 Shock analyzer kit connections.

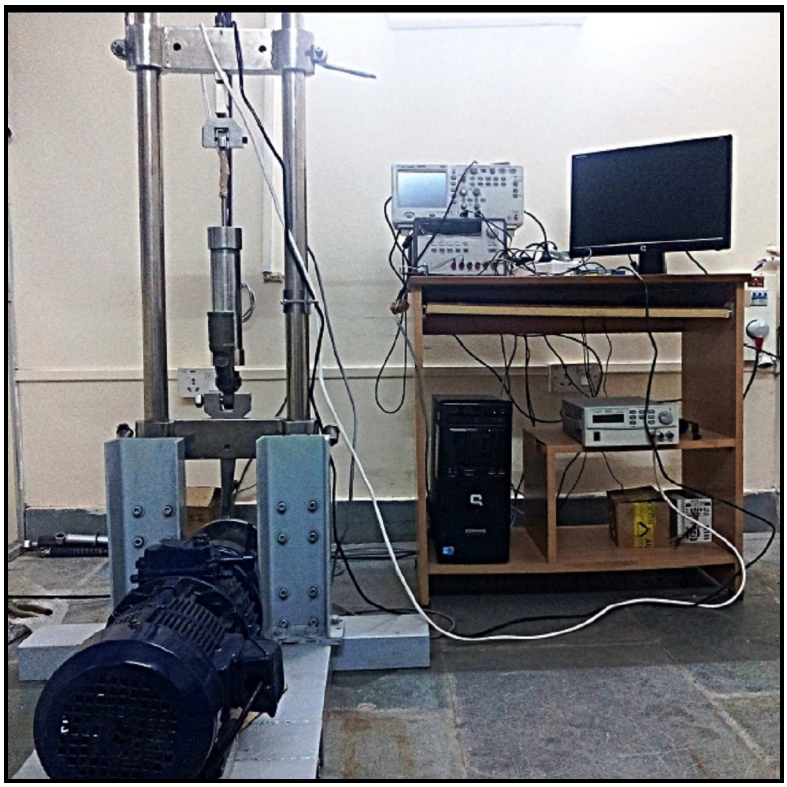

Fig. 2 Instrumented Shock Absorber Test Setup (Real Photo)

Following are various instruments required to achieve listed variables.

2.1 Oscilloscope

The raw data, change through the cycle, is usually presented on an oscilloscope. The storage type of oscilloscope is much superior in showing the cycle shape, such as force against position; F(X) will be attached with test rig.

2.2 Linear Variable Differential Transformer (LVDT)

LVDT is a position sensor, will be built into the ram. It will give a voltage output directly to computer by oscilloscope and it linearly related to the position, with a positional signal.

2.3 Velocity Sensor

Velocity of piston is derived from velocity sensor. Velocity is also obtained by electronic differentiation of the position signal obtained by LVDT.

2.4 Load cell

The damper force is measured by load cell. It is simply a slightly flexible beam supporting the static end of the damper, giving a small deflection, which can be measured to give an instantaneous load signal. The load signals in the form of voltage output transferred directly to computer by oscilloscope.

2.5 Accelerometer sensor

It gives instantaneous value of acceleration. Acceleration can be also obtained by differentiation of the velocity signal, but two stage of differentiation will greatly exaggerate any noise in the original position signal. Accelerometer sensor is basically just a load cell with a known mass, with acceleration derived from A = F/m. Velocity also could be integrated from the acceleration.

2.6 Pressure sensor

Damper liquid pressure is measured by pressure sensor. It is installed into damper body by welding or brazing of a tapped boss to accept a standard sensor. It is preferably positioned at the extreme ends of the damper so that the piston seals are not damaged by passing over the hole and so that welding distortion of the working tube does not cause the leakage.

2.7 Thermocouple sensor

It is used to measure temperature of damper body and damper fluid. The temperature value is affecting the performance, tending to reduce the damping forces at a given speed, required to measure it. The most suitable sensors are thin flexible insulated wires, and should be rated for a temperature up to 2000C or better. These are easily taped to the body of the damper.

3. Instrumented Shock Absorber Test Rig

The purpose of Shock Absorber Test Rig is to build a shock absorber dynamometer. Shock absorber dynamometer is a machine to test shocks and generate graphs for the shock characteristics. These graphs could be printed for the shocks or stored so user could develop a database of how each shock works under the test conditions. This machine replaces the trial and error approach into a reliable and efficient method to determine the shocks used during an operation.

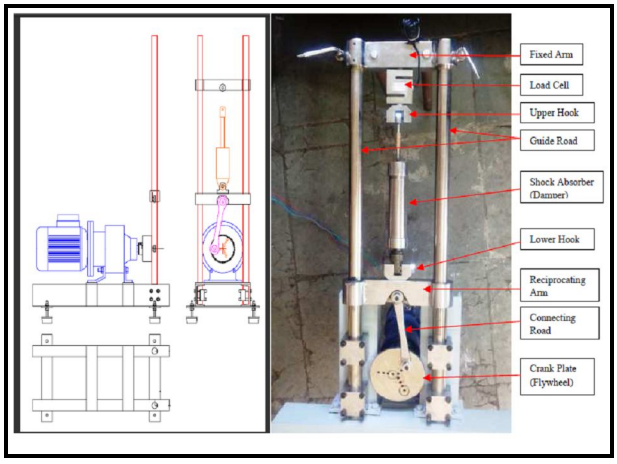

Fig. 3 Shock absorber Test rig

3.1 Mechanical

The Shock absorber Test rig consists of a metallic main structure, a motor with gear box to reduce motor speed, a piston-crank slider mechanism to cycle the shock, and a computer connected with Shock absorber Test rig by oscilloscope. The oscilloscope acquires data and displays the test graphs. It is also save individual test results and allows overlying a various tests to compare the performance. It is easy to build with industrial devices and it is simple to use. The structure consists of a strong steel frame with two vertical cylindrical beams. The two cylindrical beams tied together with a strong top beam, to which the load cell is bolted. The load cell has an adapter for bolting the shock to it. The main frame act as a mount for the motor, gear box and the two cylindrical shafts. A LVDT is mounted on any vertical beam, measure displacement with respect to time, gives velocity of the shock.

Basic characteristics of presented Shock absorber Test rig are

Stroke 5-100 mm
Speed 0-500 mm/s
Force (Load Cell) 1500 Kg (Output in terms of volt - 0 to 10 V
Cycle frequency 0 to 400 rpm
LVDT range 0 to 150 mm (Output is in terms of volt - 0 to 5 V)

3.2 Components

Following are the important component by which the shock absorber test rig is instrumented to retrieve data during test.

3.2.1 Electric Motor and Gear Box

Shock absorber Test rig is usually powered by 3-phase AC electric motors. The motors size and power is limited to its supply voltage. For applications up to 2hp, the motor can be powered by the usual mono-phase power source. Larger motors in the 2hp to 10hp range can be powered by 3-phase power source. The motor can be connect to a variable frequency drive or variable speed gear box to allow the user to cycle his shock at variable cycles/minute to test diverse speed range. Variable frequency drive usually allows connecting 3-phase motors to mono-phase mains supply.

This setup of Shock absorber Test rig powered by 3-phase, 2hp AC electric motor with variable speed gear box. The output from the motor is geared down, using gears. The maximum output shaft speed is in the 300 to 400 RPM range.

3.2.2 Mechanism

This mechanism consists of a flywheel (crank), connecting rod, and piston similar to the piston-crank mechanism in an internal combustion engine. The flywheel has holes drilled to achieve different stroke lengths. The disadvantage of using this mechanism is that it does not produce perfect sinusoidal motion in the piston, but having a longer connecting rod can compensate for this. Although it is not necessary to have sinusoidal motion, it does help reduce vibration. The advantage to this mechanism is its cost effectiveness because there is less high tolerance machining.

3.2.3 Load Cell

A load cell is a transducer that converts load acting on it into analog electrical signals. A load cell attached to the crossbeam is measure the force placed on the shock.

3.2.4 Shock temperature sensor

Shock temperature is measured using a thermocouple attached to the casing of the shock with a Velcro strap. Shock performance can vary dramatically at different temperatures. With the temperature monitoring system, it can be determine, how the shock is perform under various temperatures.

3.2.5 Stroke length selector

There are twelve screwed holes located over spiral shape in a plate, also working as a flywheel for the system as shown in figure 4. Connecting rod can be fixed in any hole to select stroke length. The longer the stoke, the greater the power needed on motor to move the shock absorber. At higher stroke, it is possible that the motor couldn't move the shock absorber, thus it is recommend starting at position 1 and increasing it step by step.

Fig. 4 Stroke length selector plate (Real photo)

Table 1. Hole position – Stroke length

Hole Position	Stroke Length
1	10 mm
2	20 mm
3	30 mm
4	40 mm
5	50 mm
6	60 mm
7	70 mm
8	80 mm
9	90 mm
10	100 mm
11	110 mm
12	120 mm

4. Working of Instrumented Shock Absorber Test Rig

Shocks are bolted into the test rig unit on the provided mounting locations. The stroke and motor speed is set to a chosen speed range. The computer is set up to receive the data from oscilloscope and the initial temperature is taken. The machine is then started and the shock is cycled into the chosen velocity range where the data is sent to the computer. The computer can then display the data in a graphical method that will allow the operator to adjust the shocks accordingly. For example, if a vehicle is coming out of the turns too tight the operator will run the shock on the test rig to check the setting. The shock is then rebuilt to loosen up the shock and run on the test rig again. With the proper expertise, the shock can be reinstalled on the system with the desired characteristics.

Conclusion

The principle mechanism for the basis of this test rig designed to measure the characteristics is single slider crank mechanism. This mechanism converts rotary motion of the circulating disc into the linear motion of the shock absorber. At various loads and speeds combinations the readings on the test rig is taken with the help of various sensors mounting on test rig and by using the data, characteristics of shock absorber is calculated. The final accuracy of shock absorbers performance is decided by experimental data collection through shock absorber test rig. Thus the shock absorber test rig design is very important for characteristics of shock absorber.

The authors is continues with predicted test rig in this paper for their future work related to design and development of shock absorber.

Reference

[1] Rao and Gruenberg, ”Measurement of equivalent stiffness and damping of shock absorbers” ,Michigan Technological University, pp. 1-3

[2] Y.Ping.”Experimental and mathematical evaluation of dynamic behaviour of an oil-air coupling shock absorber”, Elseveir, vol.17, Issue no.6,pp.1367-79,2003

[3] A.K.Samantray,”Modelling and analysis of preloaded liquid spring/damper shock absorber”, Simulation modelling practice and theory, vol.17,pp. 309-325,2009

[4] Peng et al., ”The force transmissibility of MDOF structures with a non linear viscous damping device”, International journal of non linear mechanics, Elsevier, vol.46, pp.1305-14,2011

[5] W.J.Hsueh.”Vibration transmissibility of a unidirectional multidegree of freedom system and multiple dynamic behaviour”, Journal of sound and vibration, vol.229, Issue no.4, pp793-05, 2000

[6] C.Lee, B.Y.Moon,”Simulation and experimental validation of vehicle dynamic characteristics for displacement sensitive shock absorber using fluid flow”, Sciencedirect, vol. 20,pp. 373-88,2006

[7] Lee,Kim,”A method of transmissibility design for dual chamber pneumatic vibration isolator”,Elseveir,vol.323, pp.66-92

[8] John C. Dixon,” The Shock Absorber Handbook”, John Wiley and Sons Ltd.,2007